Scaffolds for bone repair using computer aided design and manufacture

PHILIPPE TADEUSZ VADILLO

A Thesis submitted for the degree of Doctor of Philosophy

The University of Edinburgh

May 2008

Thesis Abstract

Defects in bone are a constant and serious problem. They occur as a result of high energy trauma, congenital conditions or are created surgically to treat bone tumours or infection. Currently the treatment for these conditions is awkward for the patient, takes a long time and has a high complication rate.

An elegant solution would be to mend the bone defect using the patient own cells; osteoblasts or mesenchymal stem cells seeded onto a supportive material scaffold. For successful regeneration of bone structures, a scaffold production technique has to be adopted that can precisely control porosity, internal pore architecture and fibre thickness, as well as maximising media diffusion and optimising scaffold mechanical properties so that the scaffold can withstand bone bearing pressures. It would also be beneficial if the scaffold uniformly distributed surface strain along the fibres throughout the entire scaffold as this would encourage more even cell proliferation/differentiation in the structure.

This was addressed by performing a series of finite element analyses on the computer aided design model where the mechanical properties of the natural or synthetic polymer used have been incorporated to yield an accurate strain profile of the entire scaffold. The process used here to generate the scaffolds is a Rapid Prototyping method that creates a three-dimensional object through the repetitive deposition of fibres in layers via extrusion. Due to the high accuracy and versatility of the extruder, the diameter of the pores can be precisely controlled to an accuracy of 10μm, in the manufactured scaffolds the pore size ranges from 100 to 300μm as that is what is found in trabecular bone. Natural and synthetic polymers were plotted which altered the biodegradability properties of the scaffold and the degrees of cell adhesion, proliferation and differentiation in the structure. Scaffolds were manufactured that demonstrated compatibility with cell adhesion, proliferation and osteogenic differentiation. On completion of the scaffolds, the latter were seeded with osteoblasts or marrow stromal cells and put into a mechanically stimulating bioreactor machine to induce a small strain in the scaffold; this was performed to encourage cell proliferation/differentiation. The structure was left until the osteoblasts or marrow stromal cells modified the scaffold through bone deposition. *In-vivo* experiments were then undertaken.

Preliminary data indicated an effect of mechanical stimulation of the cell/scaffold construct on the degree of mineralization of cell matrix generated by human osteogenic cells.

Declaration

I hereby declare that this thesis has been composed by myself and is the result of my own work. I have been assisted through the donation of cellular material, as clearly indicated throughout the text of the thesis. The *in vivo* study was undertaken by a team of scientists, in particular Dr Aimee Martin and Dr Jordi Tremoleda, part of the Musuloskeletal Tissue Engineering Collaboration (MTEC). This work has not been submitted for any other degree.

Philippe Tadeusz Vadillo

May 2008

Acknowledgements

I would like to firstly thank my primary supervisor Dr Brendon Noble without whose help, support and guidance, this thesis would never have been possible. I would also like to thank my second supervisor Prof. Hamish Simpson whose good advice and positive outlook helped me complete my PhD studies.

I am particularly grateful to Dr. Brendon Noble not only for his encouragement and guidance but also for his constructive criticism and valuable advice. I would also like to thank everybody at MTEC for their suggestions regarding my PhD, in particular Dr Val Mann for her help with the Zetos™ bioreactor, Dr Aimee Martin for her frank opinions and her valuable suggestions, Dr Jordi Tremoleda for his help with the *in vivo* experiment, Duncan for his enjoyable conversations and Popi whose support and energy made the PhD even more enjoyable.

I have also been very lucky in having a really loving and supportive family and friends who now can read what I have been doing for all these years. I would like to thank my parents and my brothers for their continual support.

Last, but by no means least, I would like to thank my fabulous girlfriend, Marion, for her encouragement, support and positive outlook throughout all these years.

To my Mother and Father,

brothers, Olivier and Alexander

and girlfriend Marion

Table of Contents

Figure Index

Table index

General Introduction

Tissue Engineering

The number of patients needing organ transplants far exceeds the number of organs available. In the UK, for the financial year 2005-06, approximately 8300 people were on the active waiting lists for an organ transplant which represents an increase of 9% on the same figures at the end of the previous year. 2,794 transplants occurred, which represents a 3% increase compared to last year, with 78% of those transplants being from a deceased donor (Figure 1). Unfortunately, 483 patients died while waiting for their transplant.

In addition 2,502 patients had their sight restored by a cornea transplant. Compared to last year, these figures represent a 5% increase in corneal transplants. With regards to cardiothoracic transplants, there has been a decrease of 9% in 2005-2006 with a decrease of 9% in the number of heart transplants and a 3% drop in the number of lung transplants. This is linked to the number of donors also falling from 238 to 216.

The number of liver transplants has fallen by 7% due to a decrease of 35 donors. With regards to renal transplantations, the number of kidney only transplants increased by 6% and the number of kidney and pancreas transplants increased to 107 which represents an increase of 35% on last year. (www.uktransplant.org.uk 2006).

In the United Kingdom, nearly 50,000 total hip replacements (arthroplasties) are performed each year. The operation is highly successful in reducing pain and disability of a damaged or a worn joint which involves replacing the acetubulum (the natural socket) and the femoral head with a prosthetic. Although the general success of the operation, 10% of hip replacements need revision surgery after ten years due to the loosening of the shaft of the prosthetic in the hollow of the femur.

Total knee replacements (total knee arthroplasties) are another common musculoskeletal operation with over 35,000 knee replacements carried out every year. Knee arthroplasties are routine operations that are performed on patients with knee pain and damaged knee joints mainly through osteoarthritis. Osteoarthritis occurs when the knee cartilage becomes thin and rough and can sometimes wear away totally. This results in the two ends of the bone to rub

which causes pain and in some cases inflammation. Patients that undergo a knee replacement are able to walk without discomfort after six months and in 90% of cases will last between ten and fifteen years, however in about 6% of cases, the knee fails within five years.

This lack of available organs and the need for artificial joints, has motivated the progress of tissue engineering. The concept proposed is that cells will be able to organise into tissues and ultimately replace failed organs if the appropriate three dimensional conditions are applied (Langer and Vacanti 1993). In order to create a three-dimensional environment, scaffolds need to be designed that enable cellular attachment, proliferation and differentiation (Lavik and Langer 2004).

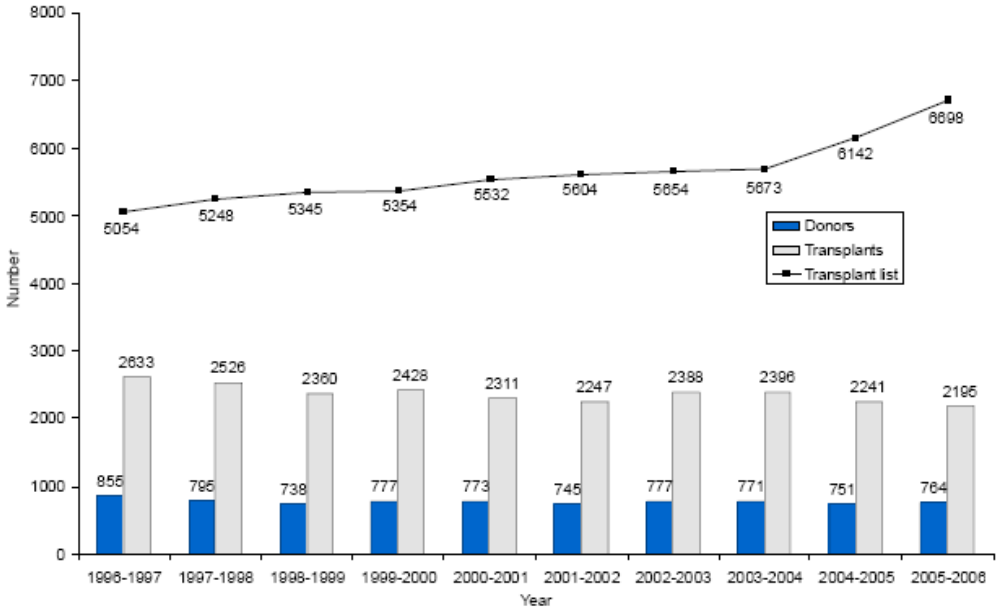

Figure 1: Number of deceased donors and transplants in the UK

Fully differentiated cells, progenitors and stem cells have shown potential in creating complex and functional tissues that might one day reduce the shortfall of tissues and organs. However there are several steps which must be addressed to exploit this potential. While stem

cells and progenitors have been shown to differentiate into a variety of cell types, the challenge of differentiating the cells in a controlled and reproducible manner still remains.

Tissue engineering is a cross-disciplinary field that involves the application of cell biology, engineering and material science to develop biological substitutes that restore, sustain or improve the tissues function. The aim of tissue engineering is to avoid having to use conventional solutions such as organ transplants and biomaterial implants, and create a supply of immunologically sound organs and tissues under laboratory conditions that can grow with the patient. Tissue engineering is being widely used in medicine to try and create, regenerate and aid tissue repair. Most major organs have been attempted for generation, e.g. the small intestine (Gupta et al. 2006), the trachea (Kobayashi et al. 2006a), smooth muscle (Rodriguez et al. 2006), liver and kidneys (Leclerc et al. 2006) and heart valves (Mendelson and Schoen 2006)

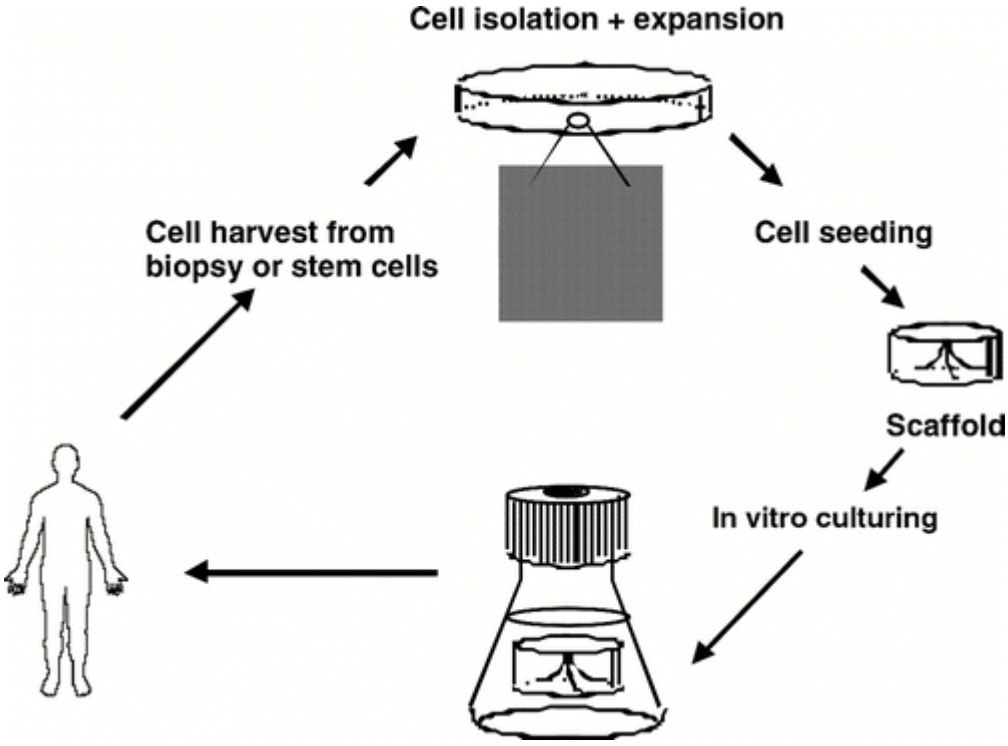

Figure 2: Principles of tissue engineering (Lu et al. 2003)

One of the principle strategies of tissue engineering involves growing relevant cells in vitro into a three dimensional (3D) arrangement. Unfortunately, many cells are not capable of growing in a 3D orientation without a scaffold. A notable exception are embryonic stem cells that grow in colonies (Tremoleda et al. 2008).Three dimensional growth of tissues can be achieved by seeding cells onto a scaffold to which the cells attach and colonise (Stock and Vacanti 2001). Thus the scaffold is potentially a very important part of tissue engineering.

There are several crucial requirements that need to be considered before the production of tissue engineering scaffolds can be undertaken:

- the scaffold should contain interconnecting pores of appropriate scale to favour tissue integration and vascularisation, which permits fluid and oxygen diffusion.
- be made from material where biodegradability and bioresorbability can be controlled, so that the scaffold will be replaced by the tissue at the required rate,
- have appropriate surface chemistry to favour cellular attachment, differentiation and proliferation,
- possess adequate mechanical properties to match the intended site of implantation,
- should not induce any adverse response
- should be easily fabricated into a variety of shapes and sizes. (Stock and Vacanti 2001)

Bearing these conditions in mind, several scaffold manufacturing techniques have been developed to try and create suitable scaffolds for tissue engineering.

Chapter 1.

Scaffold manufacturing and materials

1.1 Introduction

1.1.1 Scaffold manufacturing techniques

Numerous techniques have been adapted and developed to make use of synthetic and natural polymers to create scaffolds that may be used for tissue engineering. Besides basic material properties such as polymer biocompatibility with cells and the materials being non-toxic, a number of other scaffold properties are essential for cell growth and survival:

Pore interconnectivity and porosity: Scaffolds must have an open pore geometry with a very porous surface which will allow cell in-growth and organization in vitro and enable vascularisation from surrounding tissues. The degree of pore interconnectivity will have a direct affect on the diffusion of physiological nutrients and gases to the penetrated pores and also the removal of cellular waste (Vacanti et al. 1988).

Pore size: In bone regeneration in vitro, the quoted pore sizes that have been utilised range from 200 to 400μm (Dennis et al. 1992, Robinson et al. 1995). If the pores are too small, pore occlusion may occur and prevent cell infiltration within the scaffold.

Surface area: It has been proposed that high internal surface area to volume ratio is vital in order to accommodate the vast number of cells that are needed to replace or restore tissue (Leong et al. 2003).

A description of some of the scaffold manufacturing techniques will be provided. Some of the techniques cannot be mathematically modelled and thus the effect of strain and cell behaviour cannot be investigated. It would be beneficial in terms of our ability to design mechanically competent scaffolds if a manufacturing process had all aspects controlled and could be mathematically modelled.

1.1.1.1 Electrospinning

In 1934, a process was patented (Formhals 1934) in which an experimental setup was outlined for the production of polymer filaments using electrostatic force. When used to spin filaments this way, the term is called electrospinning.

The setup for electrospinning consists of a syringe with a metallic needle, a syringe pump and a high voltage supply. The desired polymer or polymer solution is loaded into the syringe and the polymer is forced to the needle tip by the syringe pump thus forming a droplet which is held in place at the tip by surface tension. When a voltage is applied to the needle, a mutual charge repulsion causes a force directly opposite to the surface tension of the droplet (Doshi and Reneker 1995) . As the intensity of the electric field is increased, the hemispherical surface of the solution at the tip of the needle elongates to form a conical shape known as the Taylor cone (Taylor 1964). When the electric field reaches a critical value at which the repulsive electric force overcomes the surface tension force, a charged jet of the solution is ejected from the tip of the Taylor cone. Since the jet is charged, its trajectory can be controlled by an electric field. As the jet travels in the air, the solvent evaporates leaving behind a charged polymer fibre which lays itself randomly on a collected metal screen (Figure 3).

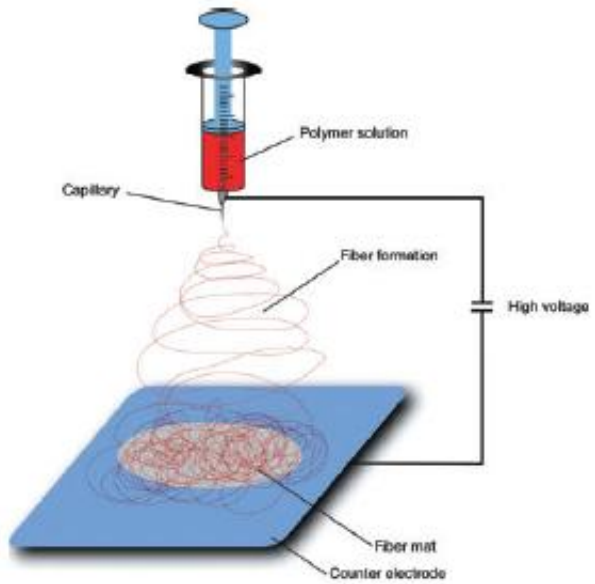

Figure 3: Schematic representation of electrospinning (Boudriot et al. 2006)

Several groups have used this technique to create scaffolds for tissue engineering i.e. to generate muscle tissue in vitro, briefly human muscle cells were seeded on a poly (L-lactide-co-epsilon-caprolactone) [P(LLA-CL)] (75:25) and analyzed after 7 days (Xu et al. 2004). To deliver plasmid DNA for therapeutic applications by incorporating the DNA in the polymer solution prior to electrospinning (Luu et al. 2003), create bone tissue (Sakai et al. 2006, Thomas et al. 2006), differentiate MSC to chondrocytes (Li et al. 2005) and to prevent post surgery abdominal adhesion by introducing a polycaprolactone electrospun sheet on the peritoneum of the abdominal wall (Bolgen et al. 2006). Electrospinning is a popular technique for tissue engineering but it involves a random deposition of fibres. This produces a scaffold with an interconnecting network of pores but the technique does not control the internal geometry of the produced scaffold. This makes it difficult to predict the strain distribution throughout the scaffold and due to the random orientation of the strands, difficult to distribute the strain within the scaffold evenly.

1.1.1.2 Freeze drying

There are various techniques for scaffold production that make use of freeze drying. One of the simplest scaffolds produced using this technique involves a natural or synthetic polymer which is dissolved in a solution and then placed into a mould, with the solution then being lyophilised (freeze dried) to yield a porous matrix. The pores are created by the formation of ice crystals in the initial freezing stage and then the removal of them in the freeze drying part. The pore size can be controlled by the freezing rate and by altering the pH; a fast freeze produces a smaller pores (Doillon et al. 1986). This is a fairly simple technique and has been extensively reported in the literature. It has been used with natural materials such as chitosan, alginate and collagen to create porous scaffolds that are then seeded with cells to generate cartilage (Li and Zhang 2005, Shi et al. 2005, Xia et al. 2004), to create artificial skin in vitro (Liu et al. 2004), to differentiate stromal cells (Oliveira et al. 2006). Lyophilising has also been performed on dissolved synthetic materials to remove solvents (Cao et al. 2006) and in combination with salt leaching to increase the pore connectivity (Hou et al. 2003). Freeze drying is an adequate method of generating pores in a polymer but there

is no control in defining the pore connectivity and the internal geometry of the scaffold. From the literature, the pore sizes in chitosan, ranges from approximately 80 ± 30μm to 720 ± 150μm depending on the freeze drying rates (Lee et al. 2004a). This demonstrates that there is a large variability in pore size.

1.1.1.3 Gas foaming

This scaffold manufacturing technique avoids the use of organic solvents which could have a toxic effect on cells and it is also an inexpensive and simple method. A synthetic polymer i.e. poly(lactide-co-glycolide) (PLGA) is placed in a mould and compressed into a disk. The latter is then saturated with carbon dioxide (CO_2) by exposing to high pressure CO_2 gas. The solubility of the gas in the polymer is then decreased very quickly by releasing the CO_2 pressure back to atmospheric level. This technique can yield scaffolds with a porosity of approximately 93% with pore sizes ranging from 100 to 500μm (Mooney et al. 1996). This scaffold manufacturing method is used to enhance osteoconductivity without the presence of cells in a critical size defect in rat skulls, in this case the implanted scaffold enhances bone regeneration (Kim et al. 2006a) and by using adult osteoblasts seeded on the scaffold and maintained in vitro (Kim et al. 2006b, Montjovent et al. 2005). It has also been reported that the gas foaming method was used for DNA delivery by incorporating the plasmid in PLGA before manufacturing the scaffold (Jang et al. 2005). The described technique is simple and several different polymers can be used, i.e. polylactic acid (PLA), poly(DL-lactide-co-glycolide) (PLGA) and chitosan. The main disadvantage is that the pores created are not completely connected and some of the pores remain in the polymer (Mathieu et al. 2006) which depending the chemicals used during manufacture of the scaffold, might release harmful substances that would affect cells and tissue. In addition, the pores created vary in size and their orientation is random, which would create a problem in determining the areas of strain throughout the scaffold.

1.1.1.4 Scaffold production by moulding

Moulds can be used to fabricate scaffolds indirectly; this increases the range of biopolymers for tissue engineering to include many materials that could not be processed using any of the previously mentioned methods. An example of this technique was described by Orton et al, where an epoxy negative mould of the required scaffold design was created by using 3D printing. A thermal-curable hydroxyapatite/acrylate suspension is cast into the epoxy mould and cured in low temperature oven (85^{o}C). The cured part is then placed into a furnace at high temperature to burn out the mould and the acrylate binder simultaneously. The hydroxyapatite body is then completely sintered into a 3D scaffold (Chu et al. 2002).

1.1.1.5 Woven scaffolds

This technique involves a microscale weaving technology (3Tex, 3Weave™ process) which generates three-dimensional (3D) structures. Weaving in this case is defined as the formation of a scaffold by the interlacing of two sets of yarns, the warp (x-direction) and the weft (y-direction) (or filling). A single filling yarn is inserted through an opening in a set o warp yarn. The principles of the 3Weave™ process is that two or more filling yarns are simultaneously from one or both sides, thus building the 3D scaffold. In the 3Weave process, a third set of yarns, called the Z-yarns, then integrates all sets of yarns (layers) of the scaffold (Figure 4). The 3D structure with fibres orientated in three orthogonal directions were specifically constructed to produce orthotropic, porous textile structures that have prescribed mechanical properties that can be controlled by the small diameter, biodegradable yarns (Mohamed et al. 2001). In contrast to standard weaving methods, this process eliminates fibre crimp and creates a 3D structure by interlocking multiple layers of two perpendicularly orientated sets of in-plane fibres with a third set of fibres that pass through the thickness of the scaffold structure.

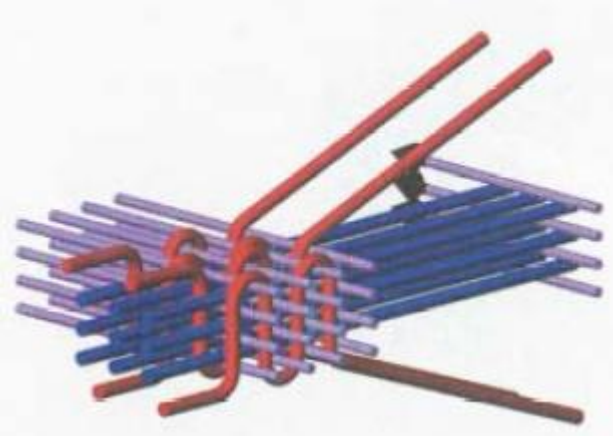

Figure 4: Illustration of 3Weave ™ multiple insertion process

The 3D scaffold was produced using 104μm diameter continuous multifilament polyglycolic acid yarn. The latter was woven into two different 3D structures with a combined total of 11 fibre layers; five layers orientated in the warp direction and six layers orientated 90° to the lengthwise fibres (weft direction). The resulting scaffold had interconnecting pores which had dimensions of 390μm x 320μm x 104μm, which yielded a total void volume of 70% (Moutos et al. 2007).

The scaffolds were then seeded with porcine articular chondrocytes in 2% agarose. Using this technique, it was reported that the scaffold was readily seeded with cells with a spatially uniform distribution with the cells maintaining a rounded morphology which is important in promoting a chondrogenic phenotype. The group did not go into any further detail about the survival or if there was any cartilage formation.

1.1.1.6 Solid free-form fabrication

The above scaffold manufacturing techniques described are extremely limited in the control over scaffold architecture. They all lack the ability to dictate geometry, and the control of the pore size is limited to the accuracy of the process involved (Woodfield et al. 2004). Due to these inadequacies, the field of tissue engineering has turned to solid free-form

fabrication (SFF) which is also commonly known as rapid prototyping (RP) techniques, for producing porous scaffolds. RP is a subset of a mechanical engineering process that allows complex structures to be created layer by layer in a reproducible fashion. Complex objects can be created using SFF techniques by generating data from a CAD (computer aided design) model or other computer based medical imaging modalities. The models are then sent digitally to a computer aided manufacture (CAM) system which interprets the data and manufactures the scaffold. The principal concept of SFF is layered manufacturing which involves a three-dimensional object being built up layer-by-layer.

The flexibility and the manufacturing ability of SFF and its enormous potential for creating complex and precise scaffolds is widely recognised and there has also been reports of replicas of human bones and other body organs (Leong et al. 2003).

The following section will describe the small number of SFF techniques that have been used successfully to create tissue engineering scaffolds.

1.1.1.6.1 Laser stereolithography

Lasers can be used to create polymer structures which can be achieved by photopolymerisation which uses light energy to initiate a chain reaction that solidifies a liquid polymer solution. The laser beam is focused onto a layer of liquid polymer which also contains a photoinitiator, when the light hits the surface it causes the polymer to solidify. The stage is then lowered covering the solid layer with a fresh layer of liquid polymer and the process is then repeated. This is shown schematically in figure 5.

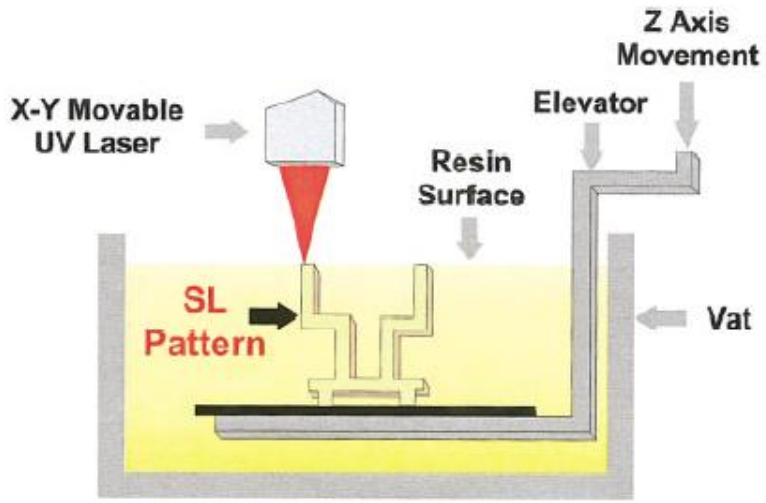

Figure 5: Stereolithography, laser is used to cross-link polymer (Cooke et al. 2003)

The desired structure is made up using a computer aided design (CAD) package which creates a virtual model. This CAD file is then processed and sliced data is generated which is sent to the computer that controls the stereolithography process and the structure is created layer by layer. This manufacturing technique has been used to create aortic valves (Gilon et al. 2002) and as a model for surgeons to visualize cleft lip (Kobayashi et al. 2006b).

1.1.1.6.2 Selective laser sintering

Selective laser sintering (SLS) uses a laser beam to sinter polymer or composites, i.e. polymer/ceramics (Tan et al. 2005b), to form material layers. The laser beam is directed onto the powder bed by a precise laser scanning system. The materials are fused and are stacked on top of one another to the CAD object's height. During manufacture, the object is supported and embedded by the surrounding unprocessed powder, on completion of the layer, rollers spread the fresh powder evenly across the top of the sintered layer. The created structure can either occur through the direct melting and solidification of the powder (direct laser sintering) or by the use of a binder which has a lower melting point and is mixed in with the desired material (indirect laser sintering). When indirect SLS is used, it is common for the

created part to undergo a further heat treatment to remove the binder material and to modify and further react the powder (Goodridge et al. 2006). This method of manufacture has a few limitations, since the powder is not compacted during the sintering, the objects are porous and this porosity might be difficult to control. Furthermore, the smallest feature is primarily governed by the powder particle size, the laser beam diameter and the heat transfer in the powder bed. Large particle sizes increase the roughness of the surface whereas small particles, less than 10μm, exhibit poor flow and spreading properties. Small particles also sinter faster which can lead to dimensional inaccuracies especially at the boundaries of the part. The commercially available SLS machines are normally fitted with a Gaussian CO_2 laser which has a maximum focused spot of 450μm which also limits the smallest feature that can be created. It also has been reported that the smallest pores that have been successfully created are 1.75 mm (Williams et al. 2005).

1.1.1.6.3 Adhesives used for scaffold production

Another approach to manufacturing scaffolds is to bind polymers by using solvents or adhesives. This eliminates any limitations of the biomaterial such as heat and dependence on a photoinitiator. One example of adhesive use for scaffold manufacture is three dimensional printing (3D-P). This involves the use of a binder solution which is deposited onto a biomaterial powder bed using ink jet printing technology. The versatility of 3D-P allows the processing of a wide range of powdered materials including polymers, metals and ceramics. The three-dimensional scaffold is created as the printer head dispenses liquid binder onto a thin layer of powder. The printer head is controlled by a computer which has a virtual model of the desired part. The repetitive stacking and printing of material layers recreates the desired structure (Figure 6) (Park et al. 1998). The finished object is embedded inside the unprocessed powder and is extracted by removing the loose powder.

The advantage of 3D-P is that complex scaffold designs with through channels and overhanging features may be manufactured; this is due to the unprocessed powder which provides the necessary support. It is also a simple and versatile technique which allows for

the processing of a wide range of biomaterials i.e. polymers, ceramics and metals. In addition it operates at room temperature so temperature sensitive materials may be used.

The limitations of 3D-P include the fact that the porosity of the scaffold is dependent on the size of the powder. In general, the smallest pore sizes available are limited to <50μm, which are well distributed throughout. Porogens such as salt (NaCl) and sucrose, can be added to generate more consistent pore sizes, however this may lead to the porogens not being completely removed through leaching (Kim et al. 1998). For processing polymers, 3D-P relies on the use of organic solvents as a binder which could remain in the scaffold and effect cells and tissue in-growth (Taboas et al. 2003).

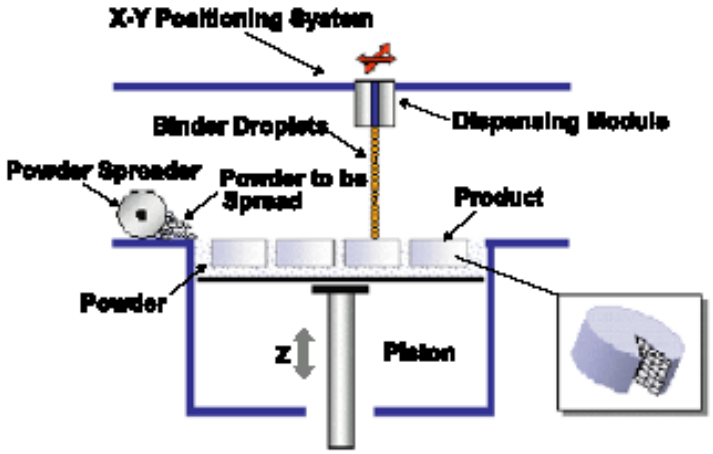

Figure 6: Three-dimensional printing

1.1.1.6.4 Fused deposition modelling and the Bioplotter

The principle of fused deposition modelling (FDM) is the continuous extrusion of molten polymer in a series of parallel fibres to form a layer. The polymer is fed and melted inside a heated syringe before being extruded through a needle. The pressure in the syringe is generated by a gas supply that is passed through the FDM machine. The machine can provide both a positive and a negative pressure allowing very accurate deposition. The negative pressure is very useful when low viscose polymers are used and tend to leak out from the needle tip. Once a layer is finished, the subsequent layers direction can be changed, which

creates a uniform structure and complete pore interconnectivity. This also allows the designer of the scaffold to alter the porosity, pore size and interconnectivity (Leong et al. 2003).

The Bioplotter (Envisiontec GmbH, Germany) which is a fused deposition device (Figure 7) also has several other advantages; it can extrude natural and synthetic polymers, it possesses a heating jacket that can melt a polymer and extrude it into a cooled medium to form a 3D structure. It is also capable of extruding at low pressures that limits the damage to cells whilst they are extruded in natural polymers such as alginate (Khalil et al. 2005a). Another natural polymer that has been plotted into a scaffold using FDM is a chitosan-hydroxyapatite mix, this yielded a good scaffold but there was a 31% shrinkage. There was good attachment between layers therefore providing good interconnected pore architecture. An in vitro experiment with human osteoblasts was carried out and good cell attachment was concluded (Ang et al. 2002). Another group (Malda et al. 2005), used a synthetic biodegradable polymer poly(ethylene glycol)-terephthalate/ poly(butylene terephthalate) (PEGT/PBT) to create a scaffold that was then seeded with chondrocytes to evaluate tissue formation. The results obtained were interesting as cartilage matrix formation was increased but further work needs to be done and the technique further developed in order to treat articular cartilage defects.

In general FDM is a more precise method of scaffold manufacture as it relies on fibres being deposited in a controlled and systematic way. There is also a complete pore interconnection which is not always the case with the non-free form fabrication methods. There are some limitations to this manufacturing technique. In order to generate overhangs, supports need to be in place a situation that is not easy to accomplish. In addition not all biologically appropriate materials can be used as some have inherent chemical properties which may not be controllable in FDM.

Figure 7: The Bioplotter has an X, Y and Z axis that can plot a scaffold layer by layer

1.1.2 Scaffold materials

1.1.2.1 Natural polymers

There has been a lot of work undertaken with natural polymers and most of them considered are used in form of hydrogels in the tissue engineering applications. The most widely used natural polymers are alginate, chitosan, collagen, fibrin, gelatin and hyaluronic acid.

1.1.2.1.1 Alginate

Alginate is a naturally occurring biopolymer that is finding increasing applications in the cell biology and tissue engineering. Alginate has been useful for many years in the food and beverage industry as a thickening agent, a gelling agent and a colloidal stabilizer. Alginate also has several inherent properties that permit it to be used as a matrix for cell entrapment and/ or delivery of various proteins, drugs and cells. These properties include: a) a relatively inert aqueous environment within the matrix; b) a mild room temperature encapsulation

process free of organic solvents; c) a high gel porosity which allows for high diffusion rates of macromolecules; d) the ability to control porosity by coating and e) dissolution and biodegradation of the system under normal physiological conditions (Wee and Gombotz 1998).

Alginates are random, anionic, linear polymers belonging to the group of polyanionic copolymers derived from brown sea algae and comprises 1,4-linked β-D-mannuronic (M) and α-L-guluronic (G) residues in varying proportions. The residues may vary widely in composition and sequence and are arranged in a pattern of blocks along the chain. Salts of alginate are formed when metal ions react with the guluronic or mannuronic acid residues. Alginate is soluble in aqueous solutions and forms stable gels at room temperature in the presence of certain divalent cations (i.e.: Sr^{2+}, Ba^{2+}, Ca^{2+}), whereas monovalent cations do not induce gelation. The gelation and crosslinking of alginate is mainly achieved by the exchange of sodium ions from the guluronic acids with the divalent cations, and the stacking of these guluronic groups to form the characteristic 'egg-box' structure shown in figure 8.

Figure 8 represents the alteration of random coils to crosslinked strip like structures which include arrays of Ca^{2+} ions. The lower diagram represents the determined stereochemistry of Ca^{2+} ion. The filled circles represent the oxygen atoms involved in the coordination sphere (Wee and Gombotz 1998).

The divalent cations bind to the α-L-guluronic acid blocks in a highly cooperative manner and the size of the cooperative unit is more than 20 monomers. Each alginate chain can dimerise to form junctions with many other chains and as a result gels networks are formed rather than insoluble precipitates (Wee and Gombotz 1998).

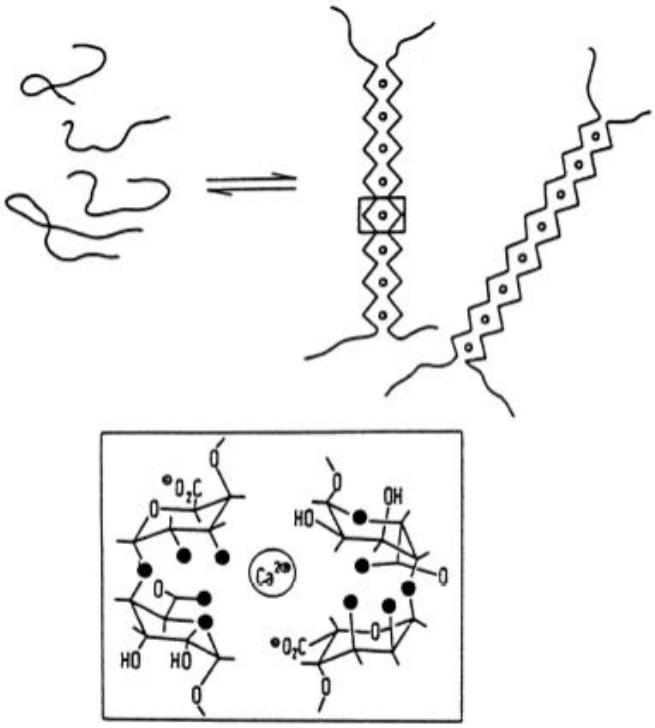

Figure 8: Schematic representation of the egg-box association of the poly-L-guluronate sequences of alginate crosslinked by calcium ions

1.1.2.1.2 Chitosan

Chitosan is obtained by deacetylation which involves removal of acetyl group from an organic compound, in this case of chitin. The latter is the primary structural polymer in arthropod exoskeletons. Chitosan is a natural, hydrophilic, non-toxic, biocompatible and biodegradable polysaccharide suitable for applications in medicine (Ang et al. 2002, Miyazaki et al. 1981).

Chitosan is a non-branched homopolymer formed by β-(1,4)-linked glucosamine units (Di Martino et al. 2005). Chitosan is insoluble in aqueous solutions above pH 7, yet in weak acidic conditions (pH <6), the molecule becomes soluble due to the protonation of the free amino group (Figure 9).

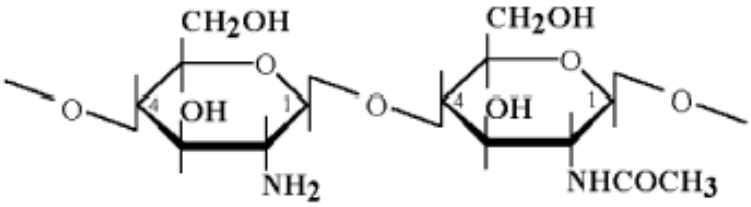

Figure 9: Chitosan molecular structure (Madihally and Matthew 1999)

Due to its polymeric nature, chitosan has been studied in many biomedical applications, these include wound dressing, drug delivery systems and for filling in spaces in implants, (Madihally and Matthew 1999).

1.1.2.1.3 Gelatin

Gelatin is a derivative of collagen created by breaking the natural triple helix structure of collagen into random single strand molecules. There are two types of gelatin, gelatin type A and type B. Gelatin type A is produced by acidic treatment before thermal denaturation, while gelatin type B is prepared by alkaline treatment that leads to a high carboxylic content (Lee and Mooney 2001). At temperatures of about 40°C, a gelatin aqueous solution is created and forms a physical thermoreversible gel on cooling. During gelling, the chains undergo a conformational change from a random to a orderly transition and tend to recover the triple helix structure (Bigi et al. 2001a). Gelatin is widely used in the pharmaceutical industry as well as the biomedical field in the form of porous scaffolds for tissue engineering (Kang et al. 1999), wound dressings (Lee et al. 2005, Liu et al. 2004, Otani et al. 1998), drug release (Yong et al. 2006) and capsules production (Digenis et al. 1994, Mei et al. 2006). However, the poor mechanical properties of gelatin limit its use as a biomaterial and a number of chemical modifications methods have been investigated to improve the mechanical properties (Bigi et al. 2001b, Bigi et al. 2004, Zhu et al. 2006). The main chemical crosslinking agent used is glutaraldehyde due to its high efficiency of collagenous material stabilization however transglutaminase (Bertoni et al. 2006, Chau et al. 2005, McDermott et al. 2004) and genipin

(Bigi et al. 2002, Chiono et al. 2007) have also been reported. During crosslinking of gelatin and other collagenous materials with glutaraldehyde, the free amino groups of lysine or hydroxylysine amino acid residues of polypeptide chains react with the aldehyde groups of glutaraldehyde (Olde Damink et al. 1995). Glutaraldehyde crosslinked gelatin microspheres have been successfully used as microcarriers for the growth and proliferation of fibroblasts and endothelial cells (Wissemann and Jacobson 1985), however if gluteraldehyde is released into the host due to biodegradation it is toxic (Olde Damink et al. 1995).

1.1.2.2 Synthetic materials

Aliphatic polyesters such as polyglycolic acid (PGA), polylactic acid (PLA), their copolymers i.e. PLGA and polycaprolactone (PCL) are by far the most widely used synthetic polymers for tissue engineering scaffold application. The degradation products (glycolic acid and lactic acid) of theses polymers are present in the body and therefore are easily removed by natural metabolic pathways and they are both FDA approved and appear in many medical in vivo devises. There are hundreds of other synthetic polymers including poly(ethylene oxide) (PEO), poly(vinyl alcohol) (PVA), poly(acrylic acid) (PAA) and polypeptides.

1.1.2.2.1 Poly(ε-caprolactone) (PCL)

Poly(ε-caprolactone) is made up by ring opening polymerization of ε-caprolactone (Figure 10) which yields a semicrystaline polymer with a melting point of 59-64°C. The homopolymer has a degradation time of approximately two years (Middleton and Tipton 2000). Copolymers of ε-caprolactone have been synthesised with DL-lactide to decrease the rate of degradation (Vandamme and Legras 1995).

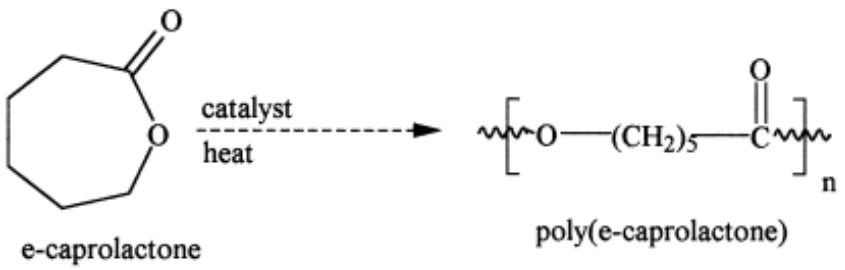

Figure 10: Synthesis of poly(ε-caprolactone)

1.1.2.2.2 Poly(lactide-co-glycolide acid) (PLGA)

PLGA is synthesized by means of random ring opening co-polymerization of two different monomers, the cyclic dimmers (1,4-dioxane-2,5-diones) of glycolic acid and lactic acid. The common catalysts used to achieve this polymer are Tin (II) 2-Ethylhexanoate, Tin (II) alkoxide or aluminium isopropoxide ($C_9H_{21}O_3Al$). During polymerization successive monomer units of glycolic acid and lactic acid are linked together to form PLGA by ester linkage hence producing an aliphatic polyester (Figure 11). Depending on the ratio of lactide to glycolide used for polymerisation, various forms of PLGA can be created, so PLGA 80:20 would mean that the composition is 80% lactic acid and 20% glycolic acid. All PLGA are amorphous (where molecules are not organised in a lattice pattern) and generally have a glass transition temperature of approximately 50^{o}C. PLGA degrades by hydrolysis of its ester linkages in the presence of water. Depending on the ratio of the two groups affects the time taken to degrade the polymer. The lower the content of the lactide units, the shorter the time required for degradation.

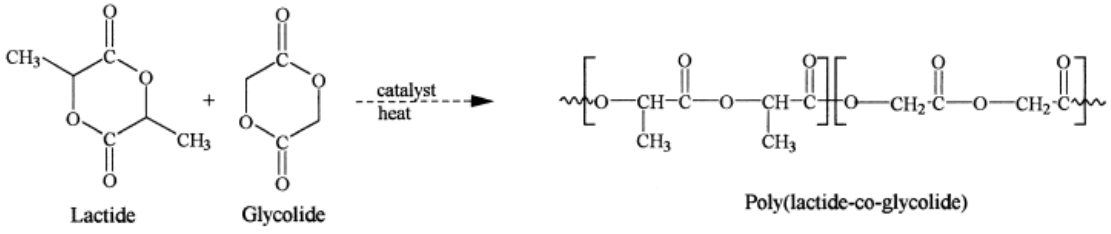

Figure 11: Synthesis of Poly(lactide-co-glycolide) (Middleton and Tipton 2000)

1.2 Methods

1.2.1 Bioplotter and accuracy

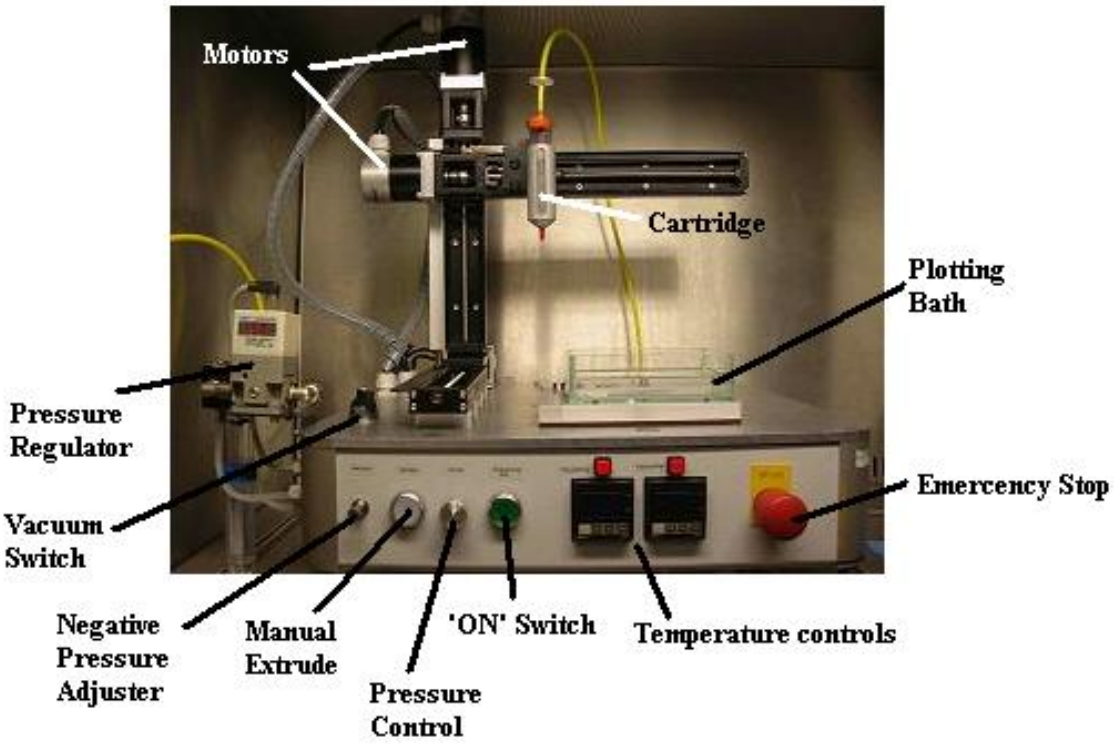

Figure 12: View of Bioplotter™

Before the initial use of the Bioplotter™ (Figure 12), the exact needle tip position was measured as all parameters such as layer thickness and initial starting plotting height were relative to the exact needle tip position. This was achieved by using the needle sensor which was located behind the plotting bath. This measurement was important. The needle tip position and length were measured by passing through two light barriers. The one measures the position in the x direction and the other sensor measures the tip position in the y and z direction (Figure 13). This measurement was performed before every scaffold manufacturing process.

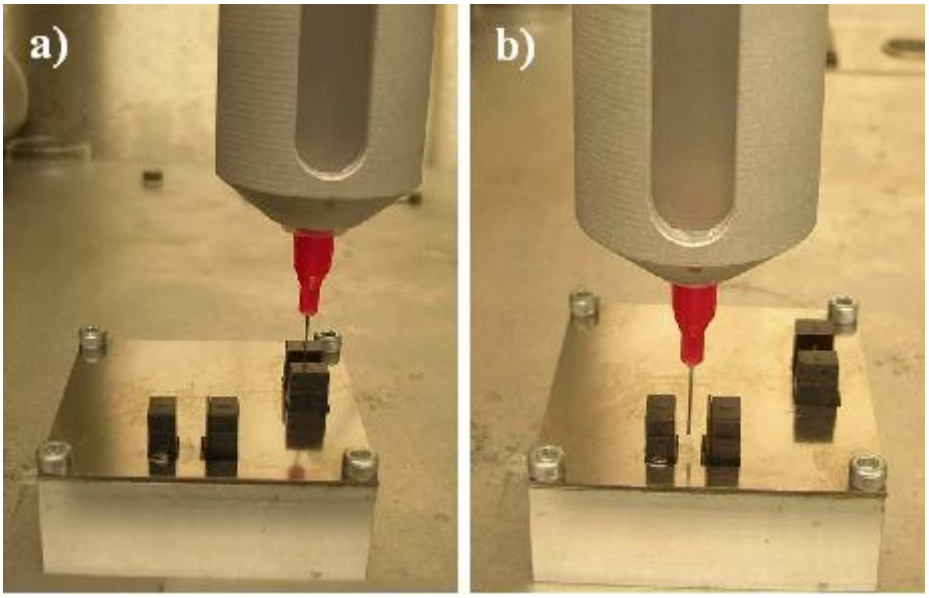

Figure 13: The needle sensor, a) x-position, b) y and z position

The software used to control the Bioplotter was comprised of three individual modules:

- The Mutronic machine driver
- The PrimCAM software that processes the data
- The PrimCNC software that controls the machine

The Mutronic machine driver forms the basis of the Bioplotter's activation system and operates in the background with no interference required from the user. The PrimCAM module enables one to import the 3D structure and set the manufacturing parameters (Figure 14).

Figure 14: PrimCAM, alteration of manufacturing parameters

PrimCNC modules was the main interface for manufacturing the scaffolds, where speed and initial plotting height was set and where the manufacturing process could be started and stopped (Figure 15). For standard operating procedure see appendix C.

Figure 15: PrimCNC screen shot

1.2.1.1 Accuracy of Bioplotter plotted geometries

The comparison of the inputted data versus the plotted strand was investigated. This was achieved by plotting a strand with various speeds and pressures and then capturing images using a Nikon E800 and camera and subsequent histomorphometric measurements were taken using the computer program BioQuant. The computer information was noted and the resulting measurements and distances were compared.

1.2.2 Scaffold Manufacture and *in vitro* experiments

For this study, alginate, chitosan and gelatin were chosen as examples of naturally derived polymers and the synthetic polymers considered were polycaprolactone (PCL) and poly(lactide-co-glycolide) (PLGA). In addition these polymers were chosen as they were readily available and inexpensive.

1.2.2.1 Chitosan scaffold manufacture

The use of chitosan as a scaffold material for tissue engineering has been reported in the literature (Ang et al. 2002, Madihally and Matthew 1999, Zhang and Zhang 2001). The authors Ang et al used chitosan in a dissolved form and generated scaffolds by using a 3D robotic dispenser, this paper formed the basis of my work regarding chitosan scaffolds. Chitosan is normally insoluble in aqueous solutions above pH 7 but in weak acids, chitosan becomes fully soluble which permits the chitosan to be extruded. The acidic solution of chitosan was then plotted into an alkaline solution of 1% w/v sodium hydroxide mixed in a ratio of 7:3 with 100% ethanol, which precipitates out the chitosan forming a hydrated gelatinous strand of chitosan.

A computer aided design model (CAD) first was created; this was achieved in Solid Works 2003. The initial model generated was a solid block with dimensions of 10 x 10 x 5mm. The model was then saved in a STL format. This is a format created by 3D systems and is used to export and import files by converting the CAD object so that only the surface geometry is represented by a set of triangles.

1.2.2.1.1 Bioplotter parameters

There are several Bioplotter parameters that can be controlled they include the pressure, dispensing velocity, the initial dispensing height, the layer thickness and the strand distance. For the scaffold production, the chosen values were: 1.20 bar, 120 mm/min, 500μm, 280μm and 630μm respectively and plotting was undertaken at room temperature. The needle tip (EFD International, UK) was a 25 gauge with internal diameter of 250μm. These initial parameters were obtained through trial and error. Firstly the syringe was loaded and a low pressure was applied (0.5 bar), the pressure was slowly increased until a slow and regular flow was achieved from the tip of the needle. This gave an initial starting point to determine the other parameters. The next step was to find the height above the substrate the needle was to start plotting, this was critical because if the needle was too low, the strand would be compressed and distort the geometry of the layer. On obtaining these two parameters, the speed of the plot was determined by starting with a low speed (100 mm/s) and gradually

increasing the speed until a well formed strand was plotted; this was fine tuned by also adjusting the pressure.

1.2.2.2 Dispensing material preparation

Various chitosan solutions were tested from 2% w/v, 3% w/v and 4% w/v, chitosan solution concentrations at 4% and above were very viscous and did not completely dissolve hence making them unsuitable for extruding. The selected concentration was prepared by dissolving 3% weight/volume chitosan (Sigma UK) in 2% v/v glacial acetic acid (Sigma UK) to form a hydrogel which completely dissolved and was sufficiently viscous to enable controlled scaffold manufacture. The dissolved hydrogel was then placed on mixing rollers and left to dissolve overnight at room temperature.

1.2.2.2.1 Dispensing medium preparation

The chitosan scaffolds were created by extruding a viscous chitosan solution into a bath mixture of sodium hydroxide (NaOH) solution and ethanol to yield a gel like precipitate. The concentration of NaOH determines the rate at which the gelation occurs. Three millilitres of chitosan solution was poured into a 30 centimetre cubed (cc) polypropylene barrel (EFD, UK) with a 25 Gauge (internal diameter 0.25mm) stainless steel tip (EFD, UK). The dispensing medium was made up of various concentrations (0.8 w/v – 1.5% w/v) of sodium hydroxide (Sigma, UK) but always maintaining a ratio of 7:3 with 100% ethanol (Fisher Scientific) and the choice of ratios were based on the work performed by Ang et al. The optimal concentration of NaOH was found to be 1% w/v.

1.2.2.2.2 Post-process

After the scaffold had been manufactured, it was gently removed from the bath and immersed in 100%, 70% and 50% ethanol for 5 minutes with a wash in distilled water after every ethanol immersion to remove the excess NaOH and the ethanol. The penultimate step

was to immerse the scaffold in 2% w/v pentasodium tripolyphosphate (PTT) for 10 minutes which further cross-links the chitosan (Anal et al. 2006, Dyer et al. 2002), with a final wash in distilled water for 30 minutes. The scaffold was then placed at -20°C for 8 hours to solidify the solvent and then the scaffold was freeze dried for 1 day at -60°C to remove the residual solvent through solid-liquid phase separation (Shu and Zhu 2002).

1.2.2.2.3 *In vitro* chitosan scaffolds experiment using MG63 an osteoblast cell line

The purpose of this experiment was to determine whether manufactured chitosan scaffolds with and without calcium phosphate incorporated in the chitosan mix were biocompatible and could support MG63 cells which are an osteosarcoma cell line (Sakai et al. 2006).

Chitosan scaffolds were manufactured as previously mentioned however two chitosan mixtures were created, the first was 3% w/v chitosan dissolved in 2% v/v acetic acid and the second chitosan mixture was a 3% w/v chitosan dissolved in 2% v/v acetic acid with 0.2% w/v calcium phosphate powder added. Calcium phosphate powder was added to attempt to introduce some mechanical strength to the plotted scaffolds.

Two chitosan scaffolds with added calcium phosphate and two chitosan scaffolds without calcium phosphate were cut into four using a scalpel (Morton-Swann, UK) into 10mm x 10mm squares and autoclaved. All subsequent manipulations were carried out under sterile conditions. The 16 (8 chitosan scaffolds with calcium phosphate and 8 without calcium phosphate) scaffolds were then placed in a 24 well plate and hydrated in growth media for 15 minutes. The growth medium used was made with Dulbecco's modified eagle's medium (Sigma, UK) supplemented with 10% fetal calf serum (Gibco-Invitrogen, UK) which supplies the cells with nutrients to promote growth, 1% penicillin/streptomycin (Gibco-Invitrogen, UK) which acts as an antibiotic and 1% L-Glutamine (Gibco-Invitrogen, UK) which is the cells energy source and reduces protein degradation in cells. During the hydration of the chitosan scaffolds, the flasks containing the cells were washed thrice with PBS, washed with 1ml of trypsin concentration 0.25% followed by an incubation in 1 ml of trypsin added to the

cells. After approximately 5 minutes the cells were detached from the surface of the flask and the trypsin was then neutralised with 9ml of growth media to stop the effect of the enzyme. The MG63 cells were then transferred to a universal tube and a cell count was performed using a haemocytometer. The cells were then centrifuged at 2000 rpm at 4°C for 5 minutes to obtain a cell pellet and the media was then carefully removed. The cells were then re-suspended in growth media to obtain a final cell concentration of $4.2x10^6$ cells/ml. The cells were statically seeded at a concentration of 250,000 cells/scaffold. This involved pipetting the cells directly onto the scaffold and allowing the cells to adhere to the scaffold for four hours. The wells were then filled with 500µl of growth media and left for seven days with media changes every 2 days.

1.2.2.2.4 Analysis

At the end of the experiment, the scaffolds were removed and fixed for 10 minutes using 4% w/v paraformaldehyde (PFA) dissolved in phosphate buffer solution (PBS) for 10 minutes. The fixed scaffolds were then stained with 4'-6-Diamidino-2-phenylindole (DAPI) which is a fluorescent stain that binds strongly to deoxyribonucleic acid (DNA). DAPI can pass through an intact cell membrane and can be used to stain live and fixed cells and fluoresces bright blue.

1.2.2.3 Alginate scaffold manufacture

As has been stated in section 1.1.2.1., alginate has been used as a biomaterial and has properties that make it good for scaffold manufacture using the Bioplotter (Khalil et al. 2005b). For scaffold manufacture, the alginate was first dissolved in sterile 0.9% w/v saline solution and then extruded into a 0.09% w/v calcium chloride solution that precipitates out the alginate creating a hydrogel scaffold. These basic principles were used and adapted from the work done by Khalil et al.

1.2.2.3.1 Bioplotter parameters

For alginate, the manufacturing parameters found to yield the best scaffolds were, extruding pressure set at 1 bar, speed of plotting at 100 mm/min, layer thickness at 230μm and the strand distance set at 1.2 mm. The needle to extrude was a 27 gauge with internal diameter of 200 μm (EFD, UK). These initial parameters were obtained through iterative work. Firstly the syringe was loaded and a low pressure was applied (0.5 bar), the pressure was slowly increased until a slow and regular flow was achieved from the tip of the needle. This gave an initial starting point to determine the other parameters. The next step was to find the height above the substrate the needle was to start plotting, this was critical because if the needle was too low, the strand would be compressed and distort the geometry of the layer. On obtaining these two parameters, the speed of the plot was determined by starting with a low speed (60 mm/s) and gradually increasing the speed until a well formed strand was plotted; this was fine tuned by also adjusting the pressure.

1.2.2.3.2 Dispensing material preparation

Various concentrations of alginate were made, ranging between 1%, 2%, 3%, 4%, 5% and 6% w/v. These solutions of alginate (Sigma, UK) were made up at room temperature by dissolving in sterile 0.9% w/v saline water. To enhance dissolution, the solution was placed in an orbital shaker for three hours until completely dissolved. The resulting solution was then autoclaved to sterilise it.

1.2.2.3.3 Dispensing solution preparation

The dispensing solution precipitates out the alginate in the form of a viscous gel. It was made by dissolving calcium chloride ($CaCl_2$) (Sigma, UK) in sterile distilled water. The concentration of calcium chloride required for gelation was 0.09% w/v but numerous other concentrations were experimented with ranging from 0.08%, 0.85%, 0.9%, 0.95%, 1%, 1.5%,

2%, 3%, 4% and 5% w/v. The dissolved solution was then filter sterilized using a 0.22μm filter (Millipore, UK).

1.2.2.3.4 Post-process

After the scaffold was manufactured, it required a further step to cross-link the alginate fully this was achieved by removing the dispensing solution from the bath and replacing it with a 1% w/v calcium chloride solution until the scaffold was submerged. This more concentrated solution further cross-links the alginate. The scaffold was left immersed at room temperature for thirty minutes and then removed and washed twice in sterile 5% w/v phosphate buffer saline (PBS) to remove any residual calcium chloride.

1.2.2.3.5 Alginate bead and marrow stromal cells (MSC) experiment

Alginate was made up at concentrations of 2% w/v, 3% w/v (Sigma UK). A 5 % w/v stock solution of alginate was made and then diluted down to the required concentration, so ratios of 1:1.5, 1:0.67 with sterile 0.9% w/v saline water were used to create a final concentration of 3% w/v and 2% w/v alginate solutions.

1.2.2.3.5.1 Cell collection and culture

Marrow stromal cells (MSC), which contain a sub population of mesenchymal stem cells (Kuznetsov et al. 1997), were harvested from the femoral head tissue that was obtained, with written informed consent and with the approval of the local ethical committee, from patients undergoing elective arthroplasty. All subsequent manipulations were carried out under sterile conditions. The trabecular bone and marrow from inside the femoral head was removed and placed in 5ml of growth media. The growth medium used was made with Dulbecco's modified eagle's medium (Gibco, UK) supplemented with 10% fetal calf serum (Autogen, Bioclear) which supplies the cells with nutrients to promote growth, 1%

penicillin/streptomycin (Gibco-Invitrogen, UK) which acts as an antibiotic and 1% L-Glutamine (Gibco-Invitrogen, UK) which is the cells energy source and reduces protein degradation in cells. The media and trabecular bone mix were then shaken by hand for 1 minute in order to dislodge the MSCs. The media containing cells was then carefully decanted to avoid the presence of bone fragments and placed in a tissue culture treated T25 flask ($25cm^2$ represents the surface area of the flask) (Corning, UK). The media and cells were left for four days and after that period the cells that had attached to the plastic culture flask were cultured. The media was then removed and the cells washed with PBS before being fed with cell culture media. Once the cells in the flask were 80% confluent, the cells were passaged into a T75 flasks. This was accomplished by first removing the media which was transferred into another T25 flask so that a second harvest could be obtained. The cells were washed thrice with PBS and washed with 1ml of trypsin followed by incubation in 1 ml of trypsin. After approximately 5 minutes the cells were detached from the surface of the flask and the trypsin was then neutralised with 9ml of growth media to stop the effect of the enzyme. The cells were then transferred to a universal tube and centrifuged to obtain a cell pellet and the media was then carefully removed. 12ml of cell culture media was added to the cell pellet and the cell suspension was then transferred to a T75 flask. The cells were grown for approximately four weeks until cell were approximately 80% confluent (See appendix A).

Alginate beads were created using a blunt 19 gauge needle. Firstly a known volume of alginate solution was loaded into a syringe, in this case 400µl and as many beads were created as possible. With this fixed volume, twenty beads were produced which then enabled the volume of one bead to be calculated. For the experiment a total of 10 million cells were required but it was not possible to obtain this number from a single patient therefore the cells were pooled together from two patients. The aim of the experiment was to determine the effects of different concentrations of alginate different calcium chloride concentrations for gelling of beads on cell survival. Prior to starting the experiment, the following was prepared:

Alginate types required for experiment:

- 2% Sigma Alginate (w/v in sterile 0.9% w/v saline water)
- 3% Sigma Alginate (w/v in sterile 0.9% w/v saline water)

Calcium Chloride solutions required for experiment:

- 1% w/v $CaCl_2$
- 0.09% w/v $CaCl_2$

For this experiment, the alginate solutions that were used were: 2% and 3% w/v dissolved in 0.9% saline solution. The beads were formed in the 0.09% w/v $CaCl_2$ and left for 10 min then the $CaCl_2$ was removed and replaced by 1% $CaCl_2$ and left for 5 min at room temperature.

Alginate bead production:

Firstly the alginate solutions and the two (1% and 0.09% w/v) calcium chloride solutions were made up and filter sterilised using a 0.22μm filter (Millipore, UK). Once the cells in the flask were 80% confluent, they were prepared by removing them from the flask. This was accomplished by first removing the media. The cells were washed thrice with PBS and washed with 1ml of trypsin followed by 1 ml of trypsin added to the cells. After approximately 5 minutes the cells were detached from the surface of the flask and the trypsin was then neutralised with 9ml of growth media to stop the effect of the enzyme. The cells were then transferred to two universal tubes and a cell count was performed using a haemocytometer. The cells were then centrifuged at 2000 rpm at 4°C for 5 min to obtain a cell pellet and the media was then carefully removed. The cells were then re-suspended in 0.2ml of growth media and an appropriate volume of 2% and 3% alginate mixture was added so that the final cell density was 2×10^6 cells/ml.

The cell suspension was then carefully pipetted into a barrel of a 1 ml syringe fitted with a 19 gauge needle. The alginate/cell mixture was then placed drop-wise into the 0.09% w/v or calcium chloride solutions to create beads. Ten wells with calcium chloride were available this permitted one bead in each well to be created before the second and third bead was added. The beads were then left in the 0.09% w/v for 10 minutes at room temperature. After the time had elapsed the calcium chloride was carefully removed as not to damage the beads and replaced with 1% calcium chloride and allowed to further cross-link for 5 minutes at

room temperature. The calcium chloride was then carefully removed and washed twice with 5% PBS and finally 500µl of growth media was added to each well and was changed every 2 days for 21 days. Complete cell culture media consisted of Dulbecco's modified Eagle Medium (DMEM) supplemented with 10% Foetal calf serum (FCS) (Autogen, Bioclear), penicillin (50IU/ml), streptomycin (50µg/ml), l-glutamine (2mM). For this experiment, five time points were created, day 0 (T_0), day 2 (T_2), day 7 (T_7), day 14 (T_{14}) and day 21 (T_{21}). At each time point, 6 alginate beads were removed from the 2% alginate group and 6 beads were removed from the 3% alginate group. On removal, 3 of the beads from each group were stained for 5 minutes with 4'-6-Diamidino-2-phenylindole (DAPI) which is a fluorescent stain that binds strongly to deoxyribonucleic acid (DNA) and stained with Propidium iodide (PI), which stains DNA but cannot penetrate an intact cell membrane therefore only marking necrotic and late apoptotic cells and un-affecting the viable ones. The beads were then examined using a fluorescent microscope (Nikon, Eclipse E800) and the number of DAPI stained and PI stained cells counted. The other three remaining beads were prepared for sectioning (further details in following paragraph).

1.2.2.3.6 Fixing and sectioning of alginate beads for analysis

The remaining 3 beads from the 2% w/v alginate group and the remaining beads from the 3% alginate group were washed in PBS and then left in 1 ml of fixing solution made up of 250µl of 80% gluteraldehyde, 750µl of 0.1M sodium cacodylate and 1µl of 1M calcium chloride for 3 hours. The beads were then removed and incubated in 1ml of 20% w/v sucrose dissolved in sterile water and 1 µl of 1 M calcium chloride for 24 hours. The beads were then immersed in polyvinyl alcohol (PVA) and snap frozen in a hexane chilled bath and then stored at -80°C. The samples were then mounted on bronze chucks and sectioned using a cryotome; sections were cut at 10µm thickness onto tape to facilitate the removal of the section from the cryostat blade. Sections obtained using the cryostat method were poor as the alginate did not adhere to the tape therefore another method of obtaining sections was then subsequently investigated.

Plastic-resin sections were obtained using a Technovit 9100 (Heraeus Kulzer GmbH, Germany) process. The samples were embedded in a methyl methacrylate plastic. This required a destabilised Technovit 9100 basic solution which was prepared by pouring the stabilised Technovit 9100 basic solution into a chromatography column with 50g of aluminium oxide (Al_2O_3) (Sigma, UK) and allowed to flow slowly through it. When the Technovit 9100 destabilised solution had been prepared, it was stored in a dark glass bottle at 4ºC to prolong the life of the solution, for full protocol see appendix A.

1.2.2.4 Gelatin scaffold manufacture

Gelatin (Sigma, UK) was dissolved in sterile distilled water at various concentrations ranging from 10%, 20%, 30%, 40%, 50% and 60% w/v. The solution was stirred and heated for approximately 10 minutes at 50°C until the gelatin had completely dissolved. The liquid solution was then transferred to a glass syringe that was compatible with the Bioplotter™. The syringe was placed in a heating jacket that was mounted on the Bioplotter™ and was set at 45°C to maintain the liquid state of the gelatin. A 25 gauge needle tip (EFD, UK) was fastened to the syringe via a luer lock and the extrusion of the liquid was ready to begin.

1.2.2.4.1 Gelatin scaffold Bioplotter parameters

For 20% w/v gelatin solution, the plotting speed was 250 mm/min, pressure 1bar and a layer thickness of 210μm. For greater concentrations of gelatin solution, the pressure was increased. During the manufacture of gelatin scaffolds, the tip of the needle was sometimes blocked which inhibited the flow of the plotting medium. This occurred because of the cooling of the gelatin and hence its solidification while still inside the needle. This problem was overcome by heating the needle tip by ‘resistance wire heating’: a known length of enamel coated copper wire (RS, UK) of diameter 132μm, standard wire gauge (SWG) 39, was wrapped round the needle tip and a current was passed through which heated up the wire which in turn heated the needle tip. The resistance of the wire and the connecting wire was

measured using an ohmmeter. The electric power was then calculated using the following formula:

$$P = I^2 \times R$$

where I denotes current in amps (A) and R denotes resistance in ohms (Ω).

A graph (Figure 16) was obtained of electric power versus released temperature which was measured using a thermocouple; the experiment was carried out at room temperature.

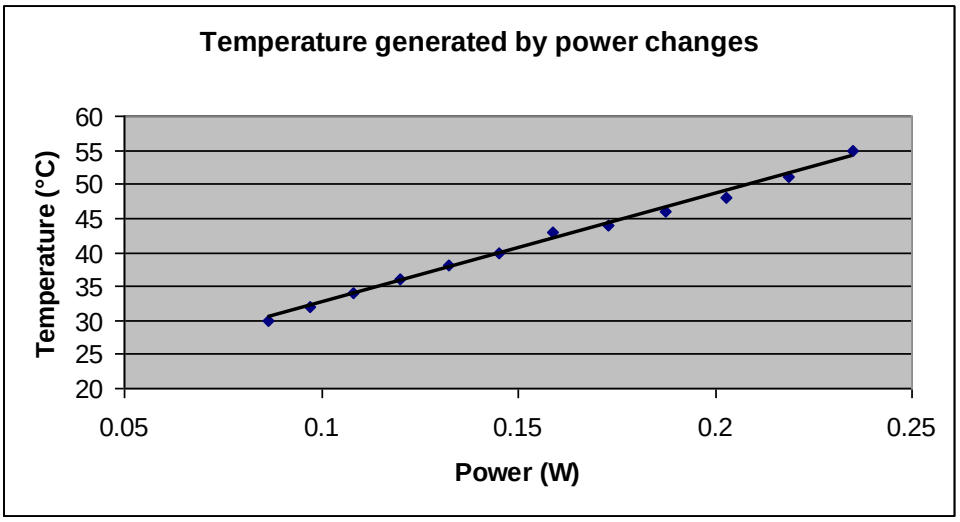

Figure 16: Temperature generated by changes in power

1.2.2.4.2 Gelatin cross-linking and cell toxicity

Gelatin scaffolds were difficult to create by cooling of the polymer alone, so cross-linking of the gelatin was attempted. Gluteraldehyde and the enzyme transglutaminase were considered. Two concentrations of gluteraldehyde were made, 0.25% v/v and 2.5% v/v (Yang and Ou 2005) and the two transglutaminase concentrations used were 5U/g and 50U/g (Fuchsbauer et al. 1996). These solutions were assessed to determine which was more effective in cross-linking gelatin and which concentration was less toxic to the cells. Scaffolds were then manufactured in 2.5% v/v transglutaminase by heating the gelatin and

extruding it through a heated needle tip into a bath of cross-linking agent with the plotting speed 250 mm/min, pressure 1bar and the layer thickness of 210μm.

All subsequent manipulations were carried out under sterile conditions. The 20% w/v gelatin solution was added to 12 wells of a 24 well plate with each of the four cross-linking agents added to three of the wells. The plate was incubated at 37ºC for 5 hours then washed thrice in PBS and the MG63s, an osteosarcoma cell line (Sakai et al. 2006), were statically seeded onto the gelatin. The concentration of cells was 24,000 cells/ml. Each well received 0.5ml of cell suspension (i.e. 12,000 cells suspended in growth media). The culture media was changed every two days for six days with growth media.

After seven days, the cells were fixed with 4% paraformaldehyde (PFA) for 10 minutes and stained with DAPI (1μg/ml) and propidium iodide (PI) (1μg/ml).

1.2.2.5 Poly (lactic-co-glycolic acid) scaffold manufacture

Unless otherwise indicated, all reagents were purchased from Sigma, UK

1.2.2.5.1 Dispensing material and solution preparation

Poly (lactic-co-glycolic acid) (PLGA) in a 75:25 ratio of lactide to glycolide was dissolved in various solvents including acetone, chloroform and glacial acetic acid. This technique of processing the PLGA and manufacturing scaffolds was adopted as previous attempts of creating scaffolds via heat extrusion, namely gelatine scaffolds, proved difficult and would require modifications to the Bioplotter™ that would need to be approved by the Health and Safety department. The solvent and precipitation method has been described in the literature (Kulkarni et al. 1966, Nelson et al. 2003). It is a safer manufacturing method with no Bioplotter™ modifications required. The concentration of PLGA used to manufacture scaffolds was 30% w/v dissolved in acetic acid however 10% w/v and 20% w/v concentrations in different solvents were also tested. The PLGA solution was in a sealed universal (Corning, UK) and left overnight in a heated orbital shaker with the temperature set to 35ºC until it had completely dissolved.

A number of different solutions were used to precipitate the PLGA from the solvent which included isopropanol (C_3H_8O), ethanol (C_2H_6O) and industrial methylated spirit (IMS) which is typically 95% ethanol mixed with 5% wood naphtha.

1.2.2.5.2 Bioplotter parameters, plotting techniques and post-processing

The initial test involving PLGA was inspired by the work undertaken by Nelson *et al* where fibres of PLGA were manufactured by a wet-spinning technique which creates a structure with random deposition of fibres (Nelson et al. 2003).

Scaffolds involving PLGA were created by dissolving the polymer in solvents that included chloroform and acetic acid to create a solution. The dissolved polymer was extruded in a coagulation bath that consisted of several different liquids to determine which one performed best. The tested liquids were isopropyl alcohol and industrial methylated spirit (IMS). Due to the price of PLGA a lot of techniques learnt from the manufacture of the polycaprolactone scaffold were transferred and used to manufacture the PLGA scaffolds. After some iterative work, it was deduced that the most adequate solvent for dissolving the PLGA was acetic acid and the best liquid to precipitation the PLGA was IMS.

Once the 30% w/v PLGA solution had completely dissolved IMS, it was transferred to a 50ml syringe which was fitted with a 25 gauge blunt needle (EFD, UK). The syringe was then placed in the Bioplotter™. The plotting parameters were set as follows: pressure of 0.27 bar, layer thickness 0.15mm, strand thickness 0.6mm with a 0.3mm offset, the plotting speed was set at 163 mm/min. The scaffolds were plotted on a polycarbonate substrate to which the precipitated polymer was able to adhere to. The size and dimensions of the scaffolds could be controlled and were generally manufactured as 20mm x 20mm blocks.

On completion of the scaffold, the polycarbonate substrate with the adhered scaffold was removed from the bath containing the precipitating solvent. The scaffolds were carefully peeled off the substrate and washed to remove the solvents by immersing in sterile distilled water for an hour and repeating the washing step with fresh distilled water. The scaffolds were then removed from the water and refrigerated at -20ºC until required.

The PLGA scaffolds were then examined using a scanning electron microscope (SEM) to investigate the characteristics of the scaffold. An SEM is a type of electron microscope capable of producing high definition images of sample surfaces. The SEM electrons are emitted thermionically from a tungsten or lanthanum hexaboride (LaB_6) cathode and are accelerated towards an anode. The electron beam is focused by a condenser lens into a very fine spot sized 1nm to 5nm. The beam then passes through an objective lens which deflects the beam in a raster fashion over a rectangular surface of the sample. Electrons are emitted through the scattering of the beam which is detected to form an image. Thus the scaffolds were examined under the SEM in order to obtain high definition images of the scaffold surfaces, the bonding of the layers and the scaffold geometry

1.2.2.5.3 PLGA scaffold degradation experiment

The aim of the degradation experiment was to determine whether manufactured PLGA scaffolds in 5% PBS would show a sign of degradation within 21 days.

The PLGA scaffolds manufactured were double layered with offset and created in small 20mm by 20 mm sheets and 2 mm high which were cut into smaller scaffolds 4mm by 4mm using a surgical scalpel (Morton-Swann, UK). The scaffolds were then placed into individual bijous with 2.5 ml of 5% w/v PBS. The bijous were placed in an incubator at 37°C for 21 days with five of the scaffolds being removed at T_0, T_1, T_3, T_6, T_9, T_{15} and T_{21}. The scaffolds were weighed using a weighting scale with an accuracy of 0.1mg (ADAM, model AFA-120LC, UK) and the data recorded to determine if there was a change in mass which would indicate degradation.

1.2.2.5.4 PLGA scaffold and *in vitro* MSC experiment

Before marrow stromal cells that contained a sub population of mesenchymal stem cells (Kuznetsov et al. 1997) were seeded on the PLGA scaffold, it was decided that a coating would be used to promote cell adhesion to the surface of the scaffold. Coatings used to

increase the cell adhesion potential of scaffolds have been widely used, either in the form of hydroxyapatite (Ciapetti et al. 2003, Tencer et al. 1987), polylactic acid (Tencer et al. 1988) or gelatin (Zhu et al. 2003). Gelatin was used due to its availability and the reported success in the literature as a coating agent (Pankajakshan et al. 2007, Shen et al. 2007).

An experiment was devised to determine the concentration of gelatin that would best improve the adhesion of cells to the PLGA scaffold. The gelatin (Sigma, UK) was made up in a universal flask (Corning, UK) to 0.1% and 0.2% w/v in sterile distilled water and allowed 20 minutes to completely dissolve in an orbital shaker (Stuart SI50, UK) at 35ºC. All subsequent manipulations were carried out under sterile conditions. Once dissolved, the two different gelatin solutions were filter sterilised using a 0.22µm filter (Millipore, UK) and 200µl of each gelatin solution was pipetted into 8 wells of an ultra-low binding 24 well plate (Corning, UK) for 15 minutes in a tissue culture hood (Figure 17). These multiwell plates have a covalently attached hydrogen layer on the surface of the plastic which is non-toxic, biologically inert and effectively inhibits cell attachment therefore the coating that counter acts the low binding effect will be the coating with the greatest cellular attachment potential. During the coating of the wells, the cells were prepared as previously mentioned in paragraph 1.2.2.3 and a cell suspension of 6,000 cells per well was created i.e. 12,000 cells/ml.

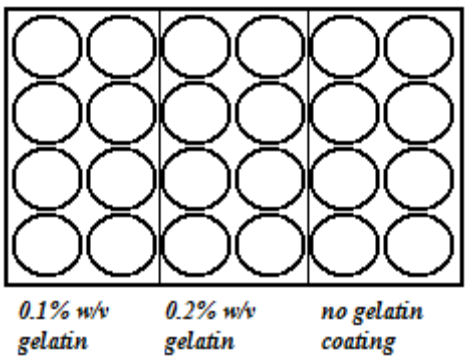

Figure 17: Gelatin coating of ultra-low tissue culture well

The gelatin solutions were then removed using a pipette and allowed to dry for 5 minutes in the tissue culture hood at room temperature. The cell suspension was then added to the

wells and placed into an incubator at 37ºC with 5% carbon dioxide (CO_2). After 24 hours, the media was removed using a pipette and the cells fixed for 5 minutes using 4% w/v paraformaldehyde dissolved in PBS. The cells were then stained with 4'-6-Diamidino-2-phenylindole (DAPI) which is a fluorescent stain that binds strongly to deoxyribonucleic acid (DNA) and fluoresces bright blue. The wells were then examined using a fluorescent microscope (Nikon, Eclipse E800) and the number of cells counted. The cell number was recorded and a graph plotted to determine the gelatin concentration that enabled the greatest number of cell attachment.

On obtaining the results of the gelatin coating, the aim of the following experiment was to determine whether cells seeded on the plotted PLGA scaffolds and PCL scaffolds (see section 1.2.2.6) are capable of adherence and survival. For this experiment, four PLGA and four PCL scaffolds were created two layers high and marrow stem cells were used that contained a mesenchymal stem cell population. MSC were cultured as previously mentioned in paragraph 1.2.2.3. On completion of the scaffolds, they were washed thrice in distilled water and then coated in 0.2% gelatin solution. The coating was achieved by allowing the scaffolds to soak in the gelatin solution for 30 minutes. During the coating of the scaffolds the cells were removed from their flasks using the enzyme trypsin and a cell concentration of 24,000 cells / ml was made up. After 30 minutes, the scaffolds were removed and placed on some sterile gauze to absorb any excess gelatin solution then placed into a 24 well plate. 500µl of the cells suspension was then gently pipetted on the scaffolds i.e. 12,000 cells / scaffold, and a further 4 empty wells were filled with the cell suspension which acted as control groups. The plate was then placed in an incubator at 37ºC and left for 24h.

After 24h, the scaffolds were removed and flash frozen using hexane at -80°C, the plates were then drained of media by placing on an absorbent paper towel and placed in a -80°C freezer. DNA assay was then performed on the plates to quantify the number of cells present in the wells which in turn will provide information on the number of cell attached on the scaffolds.

1.2.2.5.4.1 DNA assay

The assay used was based on a combination of an existing in house protocol and work done by Rago *et al* (Rago et al. 1990). Firstly the standard DNA curve was created by serial dilutions of the stock herring testis DNA (200µg / ml) solution were made in water. 200µl of the stock was pipetted into three wells of a 96 well plate then 100µl was removed and pipetted out into the following well with 100µl of water added. This process was then repeated until a final concentration of 3.125µl / ml was achieved. Then a solution of Hoechst 33258 was made up by diluting the stock at a concentration 1µg / µl, 1:5000 in 100mM NaCl and 10 mM Tris pH 7, which gave a final Hoechst 33258 concentration of 200ng / ml. The plates that were stored at -80°C were removed and 100 µl of distilled water was added to the wells and the plates were incubated at 37°C for 30 minutes. The plates were then frozen at -80°C for 1 hour and thawed until reaching room temperature, this freeze thaw step was performed so that the cells burst and release their DNA. The 100 µl of DNA solution was removed and pipetted into the 96 well plate (Corning, UK) with the standard curve. Then 100 µl of the Hoechst 33258 solution was added to each of the wells (the serial dilution and the burst cell's DNA). The plate was shaken to evenly distribute the mixtures and the fluorescence was then measured on an automated 96 well plate reader (Cytofluor multiwall reader, Series 4000). The plate reader excited at wavelength (λ) 350 nm and measured emission at λ 455 nm. The values obtained were then normalised by subtracting the values obtained from a solution made as described without DNA present.

1.2.2.6 Polycaprolactone scaffold manufacture

Unless indicated otherwise, all reagents were purchased from Sigma, UK.

1.2.2.6.1 Dispensing material and solution preparation

Polycaprolactone (PCL) with three different 'number average molecular weights' (M_n) of 10000, 42500 and 80000 was used in scaffold manufacture. This was so that scaffolds could be created with PCL of different molecular weights and the most suitable type could be

determined. The first attempt using this polymer was to melt the polymer in a heated syringe; the PCL was then extruded to plot the scaffold. Due to the problematic temperature control in the syringe delivery needle, this was not successful and therefore the solvent-precipitate technique was evaluated. The various molecular weights of PCL were dissolved to obtain a 20% and 30% w/v solution in different solvents such as chloroform ($CHCl_3$), acetone (CH_3COCH_3) and glacial acetic acid (CH_3COOH_3). The dissolved polymer was then extruded into a bath that would precipitate out PCL. The content of the precipitation bath was a solvent in which the PCL was insoluble but in which the dissolving solvent was fully miscible. The miscible solvents tested were isopropyl alcohol, methanol, ethanol, water, glycerine, industrial methylated spirit (IMS).The PCL solutions were produced in a sealed universal that was placed in an orbital shaker at 35ºC for 12 hours. Once the polymer had completely dissolved, it was left for 1 hour to cool down to room temperature and it was transferred to a syringe fitted with a 25 gauge (internal diameter 0.25mm) blunt needle.

1.2.2.6.2 Bioplotter parameters and manufacturing techniques

The Bioplotter is controlled by a computer programme called PrimCam (Primus Data, Switzerland) and the combination of these two items constitute technology that can undertake computer aided manufacturing (CAM). In this programme, plotting parameters such as the layer thickness, strand distance, height at the start of plotting, speed of plotting and the plotting geometry i.e. double or single strand, can be controlled and set. Other parameters such as strand thickness which depends on the needle gauge and the pressure were controlled manually. The programme permitted the user to alter the speed and the pressure while the scaffold was being created thus enabling fine tuning.

After a considerable amount of iterative work, the following parameters were regarded as the most appropriate: PCL with M_n 42,500 was dissolved in glacial acetic acid to create a 30% w/v solution, the pressure used for extrusion was 0.71 bar, the plotting speed 120 mm/min, the layer thickness 0.14 mm, the strand distance 0.6 mm with a 0.3 mm offset. The scaffolds were plotted on a polycarbonate substrate that was coated with a thin layer of Vaseline to avoid the strands adhering to the substrate.

On completion, the substrate with the scaffold attached to it, was removed and the scaffold was peeled off with care. The scaffold was then transferred to a universal tube with sterile distilled water and left for 15 minutes, this was repeated thrice however with the final wash, the scaffold was left in the water for 1 hour to remove as much of the solvent as possible before it was transferred to refrigeration at -20ºC.

1.2.2.6.3 Mechanical testing of scaffolds

Eight different scaffold geometries were created using the Bioplotter™ with all the plotting parameters the same in order to eliminate any discontinuities. The scaffold geometries manufactured included:

Double strand offset (DSO) (Figure 18)

Double strand offset with a 45º rotation (DSO45) (Figure 19)

Double strand no offset (DSNO)

Double strand no offset with a 45º rotation (DSNO45)

Single strand offset (SSO)

Single strand offset with a 45º rotation (SSO45)

Single strand no offset (SSNO)

Single strand no offset with a 45º rotation (SSNO45)

The scaffolds were cut into blocks of approximately 5 x 5 x 5 mm and compressed using a mechanical compression machine (Dartec, UK). The scaffold blocks were measured with callipers to ensure the exact measurements were obtained. A 10kN load cell was used and 3 scaffolds of the same geometry were tested until failure. Stress versus strain curves were plotted for each scaffold and the Young's modulus derived from the gradient of the graph. A specially designed aluminium platen (Figure 20) was manufactured to accommodate the

scaffold in the mechanical testing machine. Aluminium was selected as it was an easy material to manufacture with and was tough enough to compress polycaprolactone scaffolds without yielding.

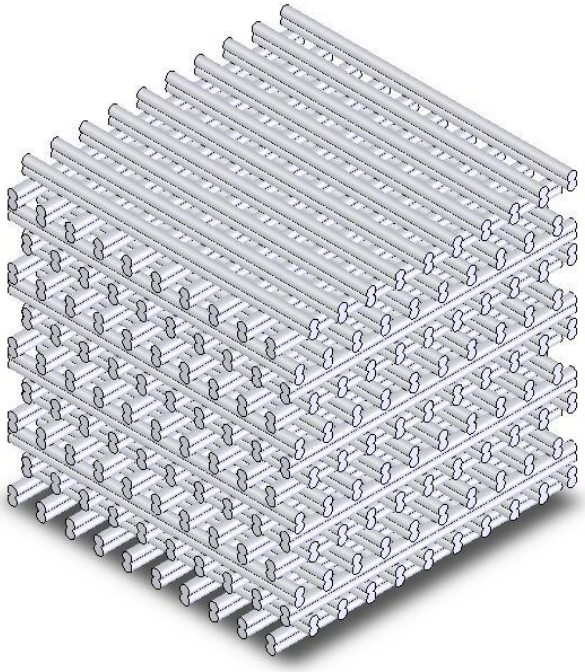

Figure 18: Double Strand with offset

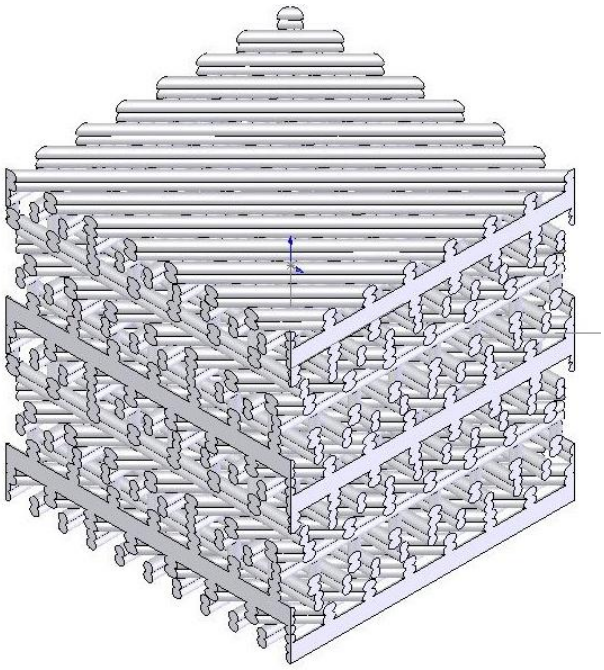

Figure 19: Double Strand with Offset and 45º rotation

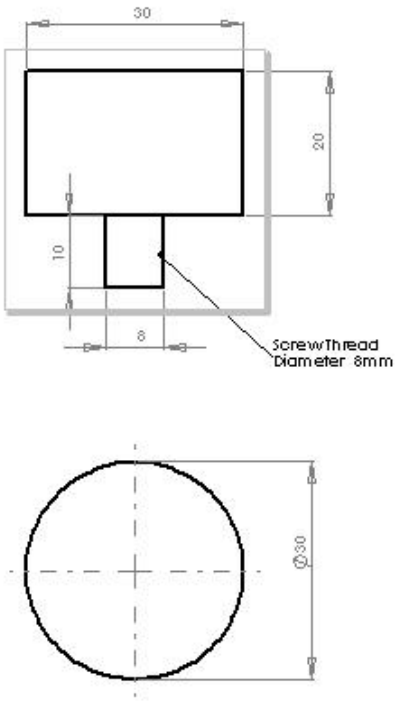

Figure 20: Mechanical device manufactured to compress scaffolds

1.2.2.6.4 *In vitro* assessment of polycaprolactone scaffolds with marrow stromal cells

The aim of this experiment was to determine whether in static conditions MSCs seeded on manufactured polycaprolactone scaffolds in osteogenic differentiation media were capable differentiating into osteoblasts and creating calcium deposits.

Before the marrow stromal cells could be seeded on the polycaprolactone scaffolds, the latter had to undergo several preparation steps. PCL scaffolds were removed from the -20ºC freezer and thawed by immersing in sterile distilled water for 40 minutes at room temperature. All subsequent manipulations were carried out under sterile conditions. The scaffolds were then transferred to a sterile tissue culture hood and six smaller scaffolds were then cored out using a 5 mm diameter biopsy punch (Miltex, Ø 5 mm) and placed in 100% industrial methylated spirit (IMS) (Sigma, UK) for 15 minutes to sterilise the scaffold. The scaffolds were then removed and washed thrice in sterile distilled water to remove any excess IMS. Scaffolds were then transferred, for 30 minutes, to a sterile universal containing previously prepared 0.2% w/v gelatin (Sigma, UK) which was dissolved in distilled water and filter sterilised using a 0.22 μm filter (Millipore, UK) to allow the coating process of the PCL scaffolds to occur. During the coating process, T75 flasks (Corning, UK) containing the marrow stromal cells were removed from the incubator and the media from the flasks aspirated using a pipette. The cells were then washed for 5 seconds with 1 ml of the enzyme trypsin which is used to detach cells from the flask. Another millilitre of trypsin was added to the flask for 5 minutes, the flask was occasionally tapped to encourage cell detachment. The trypsin was then neutralised using 9 ml of growth media to the flask. The growth media consisted of Dulbecco's Modified Eagle Medium (DMEM) (Gibco, UK) supplemented with 10% Foetal Calf Serum (FCS) (Autogen, Bioclear), L-Glutamine (2mM), penicillin (50 IU/ml) and streptomycin (50 μg/ml). Ten micro-litres on the cell suspension was then removed and pipetted onto a haemocytometer to determine the cell number. Growth media was added to the cell suspension to obtain a final cell concentration of 4.2 million cells/ml. After 30 minutes, the scaffolds were removed from the 0.2% w/v gelatin and placed on some sterile gauze to absorb any excess gelatin solution and placed using sterile forceps into a large cell culture dish (Corning, 150 mm x 25 mm). The PCL scaffolds were then seeded with 60μl of the cell suspension which contained 250,000 cells. The seeded scaffolds were then flipped

every 30 minutes for 4 hours to obtain a uniform cell distribution throughout the scaffold and then 45ml of growth media was added to the cell culture dish until the scaffolds were submerged. The culture dish was then placed in an incubator at 37ºC and left overnight. The three scaffolds seeded with cells and the three un-seeded scaffolds were then transferred to an ultra-low binding 48 well plate (Corning, UK) to encourage the cells to remain on the scaffold and 500 µl of growth media was added to each well containing a scaffold and the plate was then returned to an incubator at 37ºC for 3 days. Osteogenic differentiation media was then added to the three scaffolds seeded with MSCs and three scaffolds with no cells. The osteogenic differentiation media was made with growth media supplemented with β-glycerophosphate (Sigma, UK) (10mM/l), l-ascorbic acid-2- phosphate (Sigma, UK) (50µM/l) and dexamethasone (0.1µM/l). The media was then changed every two days for two weeks.

At the end of the experiment, the scaffolds were fixed with 4% w/v paraformaldehyde and cut in half with a scalpel (Swann-Morton). Half of the scaffold was then stained with DAPI to determine whether cells were present and the other half was sectioned by dipping in OCT embedding matrix (Raymond A Lamb) before being flash frozen in super cooled hexane at -80ºC. The samples were then placed in bijous and labelled and refrigerated and stored at -80ºC.

The embedded samples were then mounted on a bronze chuck and cryostat sectioned with sections 10µm thick. The section was cut onto tape to facilitate the removal of the section from the cryostat blade and to maximise the integrity and quality of the section. The sections were then stained with DAPI which binds with cellular DNA and stained using the Von Kossa technique which involves fixing the samples with 4% PFA (Sigma, UK) then washed thrice in distilled water followed by incubation under a strong light at room temperature in 5% silver nitrate ($AgNO_3$) for 1 hour. The sample was then washed thoroughly in water and incubated in 5% sodium thiosulphate ($Na_2S_2O_3$) for 5 minutes to neutralise the remaining excess silver nitrate. The Von Kossa technique stains calcium deposits dark brown that can be viewed using a microscope. The stained sections were then viewed and images captured with a DXM1200 camera mounted on a Nikon microscope (Eclipse E800) using a 20x/0.50 ∞/1.17 magnification lens.

1.2.2.6.5 *In vivo* assessment of polycaprolactone scaffolds

The aim of this experiment was to determine whether implanted polycaprolactone scaffolds seeded with marrow stromal cells were capable of aiding bone growth of a critical sized circular incision in a mouse skull.

The *in vivo* experiment was undertaken by a team of scientists within the musculoskeletal tissue engineering collaboration (MTEC). The experiment was designed and analysed by Dr Aimee Martin and the veterinary work performed by Dr J. Tremoleda and their help is kindly acknowledged. All animals were maintained under the guidelines by institutional Animal Care and Ethical Committee at the University of Edinburgh, and the surgical procedures were all performed in accordance to specification approved under a UK Home Office license (PP L60/3396).

Thin PCL scaffolds were manufactured using the single strand offset (SSO) geometry. The scaffolds were 500μm thick and were manufactured using the same parameters as previously described. The scaffolds were then cored out with a 3mm biopsy punch (Miltex, Ø 3mm) and sterilised in IMS and washed thrice in sterile distilled water. From this point on, the experiment was undertaken by Dr Aimee Martin and the scaffolds were then coated using a proprietary technology developed by Dr Aimee Martin. The scaffolds were then seeded with hMSC and the cells were allowed to proliferate for 2 days before implanting.

On delivery of the 6 – 8 week old NOD/SCID male mice, the animals were given a week to acclimatise to the animal house. On the day of the experiment, the animals were anaesthetised using an injectable anaesthesia which was made up of Ketamine (Vetalar) and medetomidine (Domitor). The dose used was 75mg/kg Ketamine and 1mg/kg of medetomidine. After a two minute wait, so that one could be certain that the anaesthetic has taken effect, the hair was removed from the top of the head. The animal was then transferred into a hood with a warming pad at approximately 32ºC and the skin around the surgical site was disinfected and analgesia (Vetergesic) was injected subcutaneously at a dose of 0.05mg/kg prior to surgery. A single skin cut was performed from the area behind the eyes to the back of the head exposing the skull. A 3mm diameter trephine attached to a micro-drill was used to create a circular bone incision and the site was irrigated with cold saline water

irrigation to prevent damage to the sectioned bone. On completion of the incision, the bone flap was carefully removed with forceps to avoid any bleeding. The scaffold with cells and the scaffold alone was then implanted and then sealed with fibrin glue (Tisseel®, Baxter healthcare Ltd). The wound was stitched with prolene 6/0 sutures and protected from animal bites with superglue. The animal was maintained during anaesthesia in 2 l/min O_2 this could be achieved by placing the nozzle close to the animals head. The animal was then injected with 0.9% warm saline and the eyes were then treated with Lacrimogel. After 10 minutes, 0.1ml of reversible anaesthesia Atipamezole (Antisedan) was injected subcutaneously while constantly maintaining the animal on the warming pad. Once the animal started to regain consciousness, it was placed back into its cage with the warming pad. After the three month implantation period, the animals were euthanized and the calvarial area collected using a micro-saw. Cryosections were then obtained of the calvarial defects and stained using the Von Kossa technique which involves fixing the samples with 4% PFA (Sigma, UK) then washed thrice in distilled water followed by incubation under a strong light at room temperature in 5% silver nitrate ($AgNO_3$) for 1 hour. The sections were then washed thoroughly in water and incubated in 5% sodium thiosulphate ($Na_2S_2O_3$) for 5 minutes to neutralise the remaining excess silver nitrate. The Von Kossa technique stains calcium deposits dark brown that can be viewed using a microscope. The sections were then stained with DAPI (1μg/ml) which binds strongly with DNA. The stained sections were then viewed and images captured with a DXM1200 camera mounted on a Nikon microscope (Eclipse E800) using a 10x/0.30 ∞/1.2 magnification lens.

1.2.3 Statistical analysis

All statistical analysis was performed using quantative data analysis with SPSS release 16 for Windows. Data was checked for normal distribution by applying the Kolmogorov-Smirnov test. In cases where the randomly selected data were shown to have normal (Gaussian) distribution, i.e. where 95% of the data fell within plus or minus 1.96 standard deviations from the mean, parametric statistical tests such as two-tailed Analysis of Variance (ANOVA) and the post-hoc Tukey-Kramer test were performed directly to determine

statistical significance between the groups. When the *p* value of the ANOVA test was $p<0.05$, the use of the Tukey-Kramer post-hoc test allowed comparison of more than two means at once without introducing the type I error associated with multiple t-tests (Fielding and Gilbert 2000, Zar 1984). Results are expressed as means ± S.E. $p < 0.05$ was considered to be statistical significance.

1.3 Results

1.3.1 Bioplotter accuracy of plotted geometries

The accuracy of the Bioplotter™ was determined by extruding four layers of the polycaprolactone polymer dissolved in acetic acid. The aim of the experiment was to observe the accuracy of the Bioplotter™. The parameter that was controlled by the Bioplotter™ was the strand distance, which was the distance from the centre of a strand to the centre of the neighbouring strand on the same layer.

Briefly the pressure and the speed were fixed with alterations only made to the CAM program to change the distance between the centres of the parallel strands (strand distance) on the same plotted layer. Four arbitrary strand distances were chosen 500, 600, 700 and 800µm. The strand distance was measured using a histomorphometry program (BioQuant) which enables measurements of microscope images to be measured accurately (Table 1). A graph was plotted of measured strand distances versus inputted strand distances in both the x- and y- directions (Figure 21) with pictures to show the results (Figure 22-25).

As can be seen from the two graphs below (Figure 21), statistical significance was observed between each strand distance in both the x- and y- directions. It can also be observed that the standard error was small which indicates that the strand distance does not differ much with respect to the mean. The measured strand distances were on average 2% lower compared to the inputted strand distance. This was because when the polycaprolactone strand was extruded, it contracted in both the x- and y- directions. It can also be observed that there tends to be less shrinkage in the y- direction.

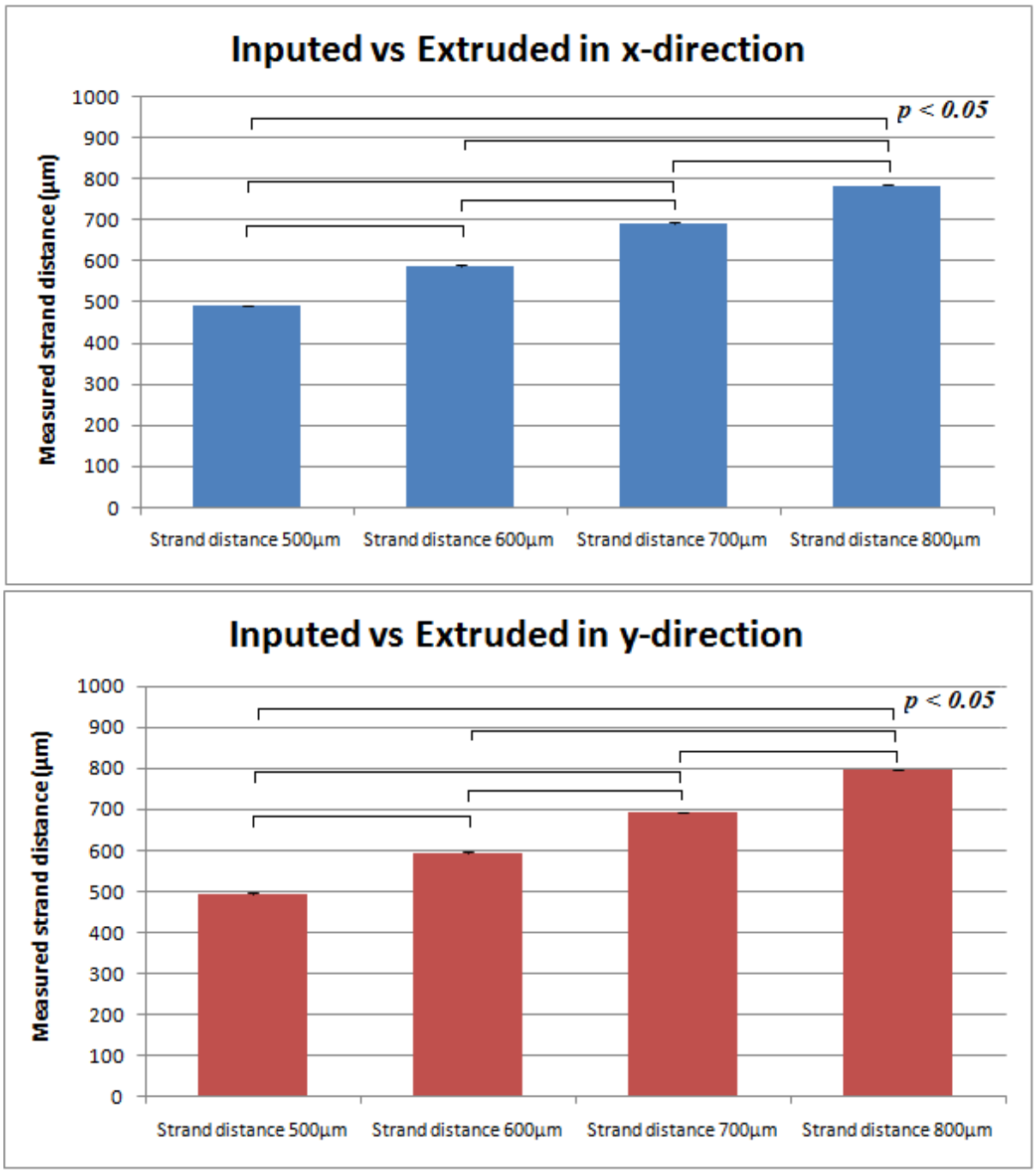

Figure 21: Inputted versus extruded strand distance, in the x-direction (top graph) and in the y-direction (bottom graph)

	Strand distance 500µm		Strand distance 600µm		Strand distance 700µm		Strand distance 800µm	
	x-direc	y-direc	x-direc	y-direc	x-direc	y-direc	x-direc	y-direc
	493.97	493.27	582.95	592.43	697.3	698.87	786.52	791.47
	494.38	508.97	594.16	602.24	703.37	678.64	795.77	798.19
	489.88	504.5	604.07	603.17	693.76	689.66	794.18	795.95
	485.39	495.51	589.68	591.01	674.16	692.44	777.53	779.08
	474.16	491.02	578.47	587.44	687.64	690.57	777.53	804.92
	494.38	504.48	586.13	593.25	687.64	697.3	795.5	794.64
	492.13	477.57	578.47	596.16	698.87	686.09	780	784.75
	485.39	479.82	603.13	593.25	692.13	692.82	764.04	800.44
	501.65	488.8	585.2	591.01	694.38	697.3	793.66	807.17
Aver	490.00	494.00	589.14	594.44	692.14	691.52	784.97	795.18
Stand. error	2.60	3.64	3.17	1.75	2.81	2.12	3.66	3.02

Table 1: Inputted versus plotted strand distance

A Nikon Eclipse E800 upright microscope was used to gather pictures of the scaffolds. Some examples of the pictures can be seen in figures 22 - 25. Histomorphometry was then performed using the BioQuant programme on the pictures and the strand distances were measured.

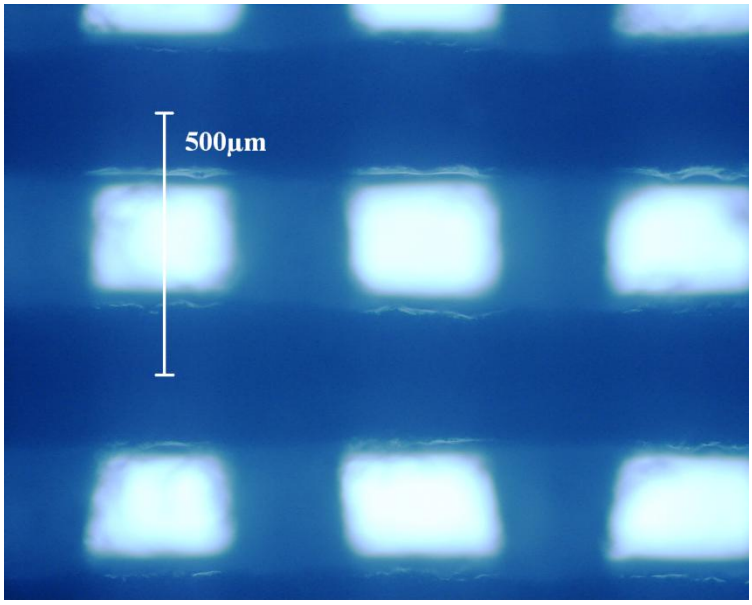

Figure 22: Scaffold with 500 µm strand distance, x10 magnification

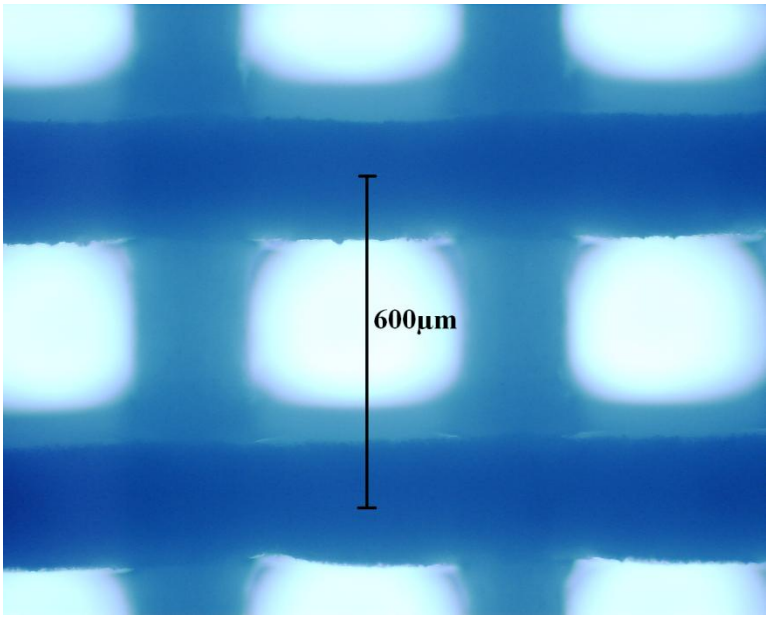

Figure 23: Scaffold with 600 µm strand distance, x10 magnification

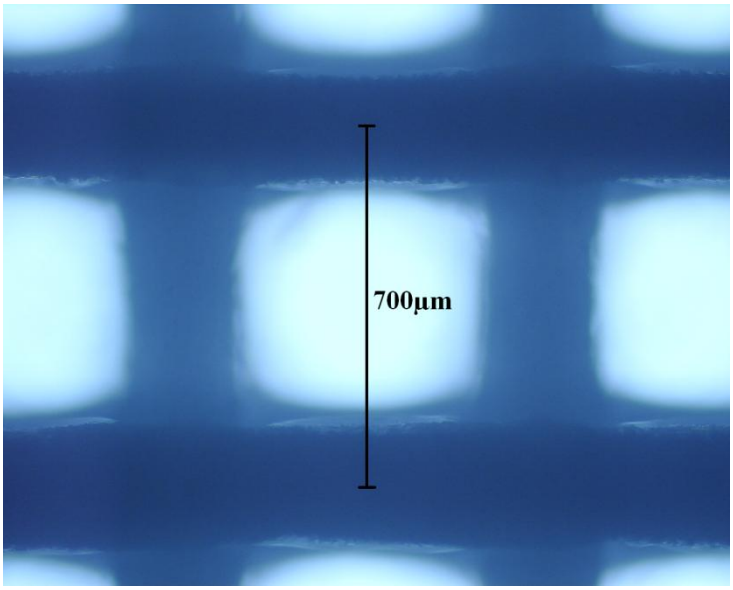

Figure 24: Scaffold with 700 µm strand distance, x10 magnification

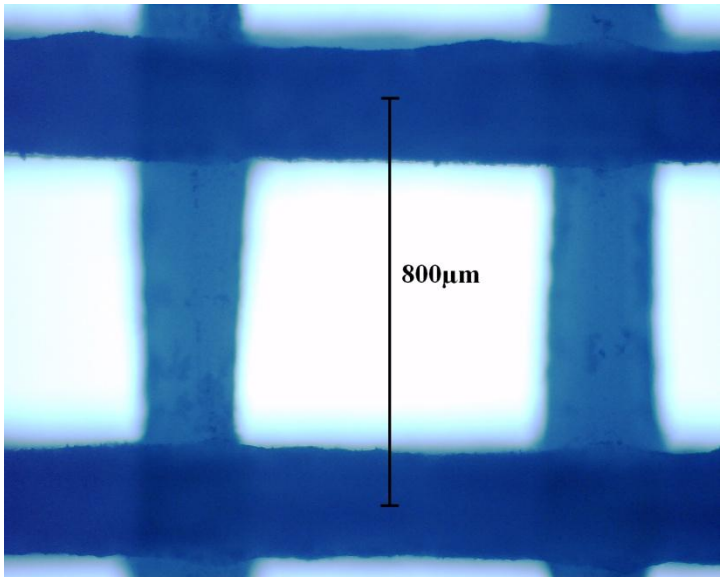

Figure 25: Scaffold with 800 µm strand distance, x10 magnification

1.3.2 Chitosan scaffold

1.3.2.1 Chitosan scaffold manufacture and Bioplotter parameters

Briefly, 3% w/v chitosan solution was created by dissolving in 2% acetic acid. The plotting medium was made with a 1% w/v NaOH and ethanol in a 7:3 ratio. The needle used to plot the chitosan solution was a 25 gauge (250 µm internal diameter) (EFD, UK). An initial arbitrary pressure was chosen by having the syringe in an idle position and the pressure increased until a flow of chitosan was observed, this pressure was 1.60 bar. The plotting speed was set at 100 mm/min and the strand distance 500 µm. The result of this combination of parameters can be observed in figure 26.

As can be observed from figure 26, a poor scaffold was created as all that can be observed was a pool of chitosan; this was due to the pressure being too high and the plotting speed too low.

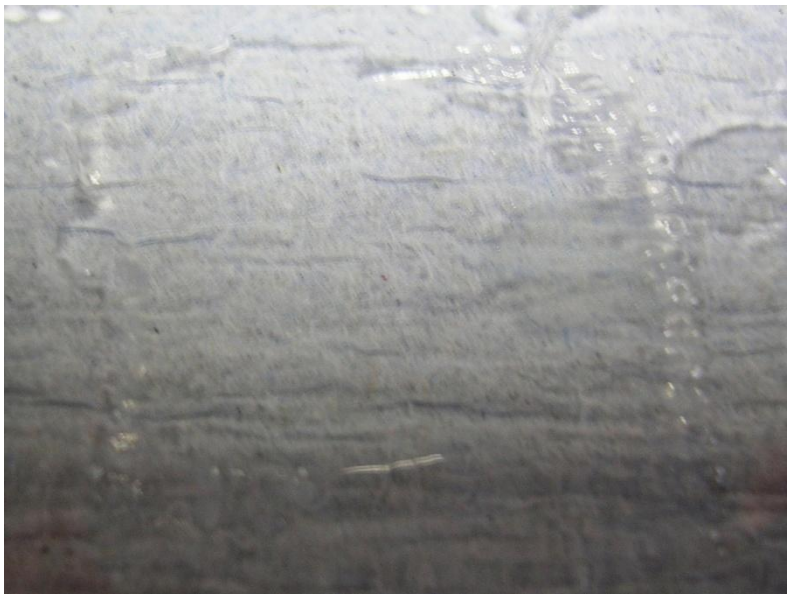

Figure 26: Attempt at creating a chitosan scaffold

The following scaffold was manufactured by increasing the plotting speed to 120 mm/min, this was performed to try and eliminate the pooling of the chitosan and the result of this can be seen in figure 27.

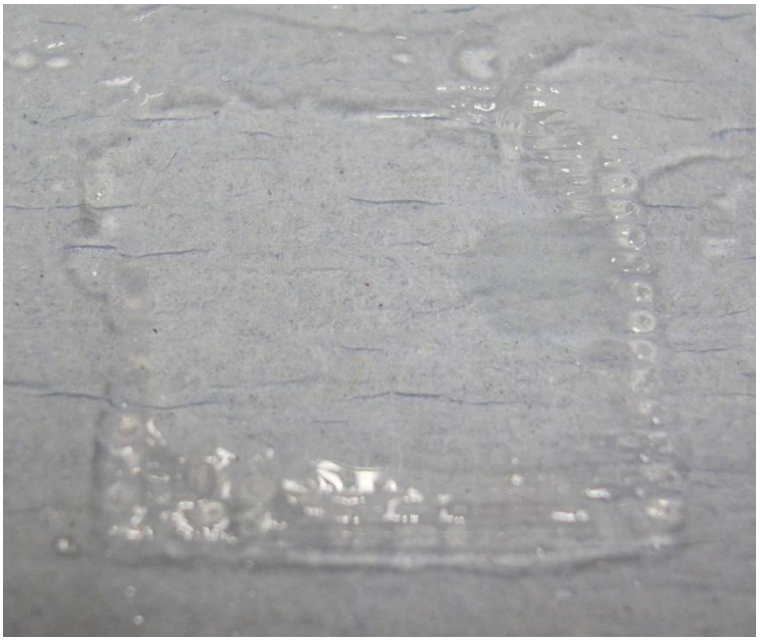

Figure 27: Chitosan scaffold with increased plotting speed to 120 mm/min

The increased plotting speed positively affected the scaffold manufacture as it can be observed that at the bottom of figure 27 a reduction of the pooling effect was witnessed and strands can be seen.

The following attempt consisted of further reducing the pressure to 1.40 bar to minimise the pooling effect further, in doing so, the plotting speed was also reduced to 114 mm/min so that during extrusion the plotted strand would not break an hence create a continuous strand, the results of these changes can be seen in figure 28. During the manufacture and as the first layer was plotted successfully, it was decided that a second layer would be created and the layer thickness was set at 280 µm.

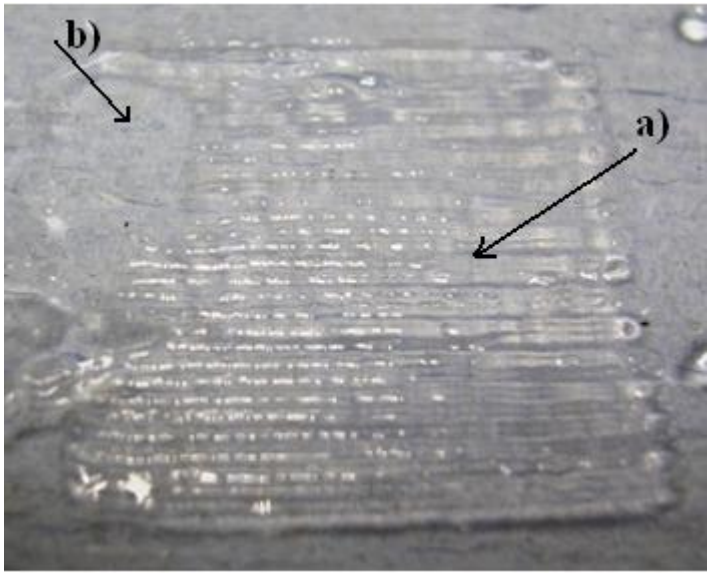

Figure 28: Attempt at two chitosan layers, pressure 1.4 bar and speed 114 mm/min, a) first layer, b) start of second layer.

It was observed that the first layer was successfully plotted but the second was poorly plotted (Figure 28b). This was due to the layer thickness being set too high and as the second layer was being extruded, the strands did not attach to the foundation layer and were dragged along creating a pool of liquid of non gelatinous chitosan.

The layer thickness was then lowered to 250μm and a five layer scaffold was created.On completion, the scaffold was allowed to cure completely in the bath for a further ten minutes. The scaffold was then removed and washed in 70% v/v, 50% v/v and 100% ethanol for five minutes in each. The scaffolds were then divided into two groups with one group being untreated and the other group treated with pentasodium tripolyphosphate (TPP) for ten minutes to further cross-link the chitosan (Anal et al. 2006, Dyer et al. 2002, Shu and Zhu 2002). The scaffolds were then given a final wash with distilled water and then refrigerated at -20ºC for at 8 hours so that the scaffold was completely frozen. The frozen chitosan scaffold was then removed and lyophilised for 24 hours. The resultant scaffolds treated with TPP and not treated and with offset and without, can be seen in figures 29 – 31. From these images it can be seen that the chitosan scaffolds treated with TPP appear to be more defined and the

pores clearly visible (Figure 29 and 30) compared to the non-TPP treated chitosan scaffold (Figure 31).

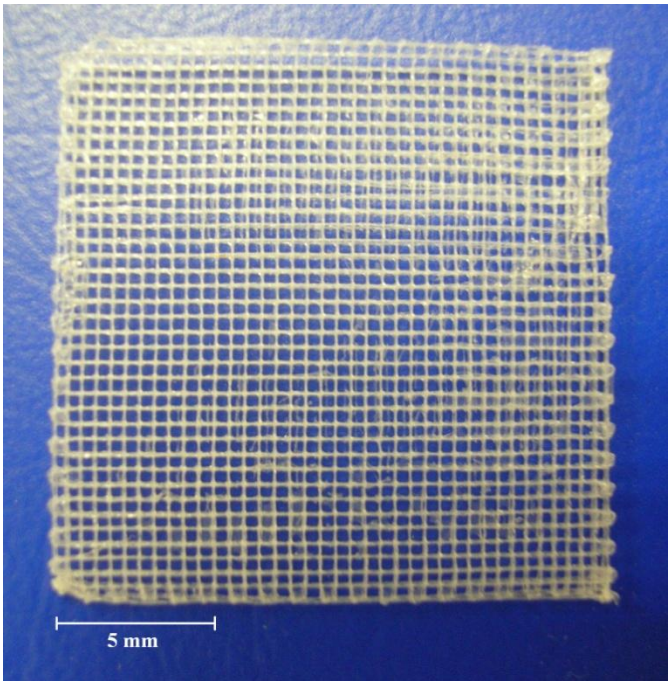

Figure 29: Chitosan scaffold treated with PTT, no strand offset

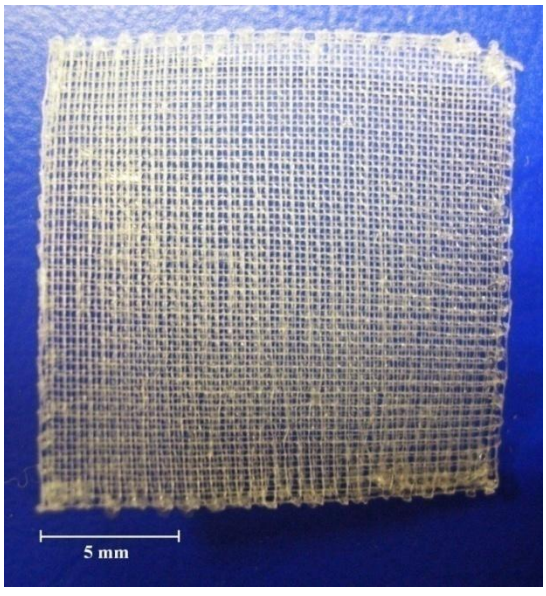

Figure 30: Chitosan scaffold treated with PTT with offset

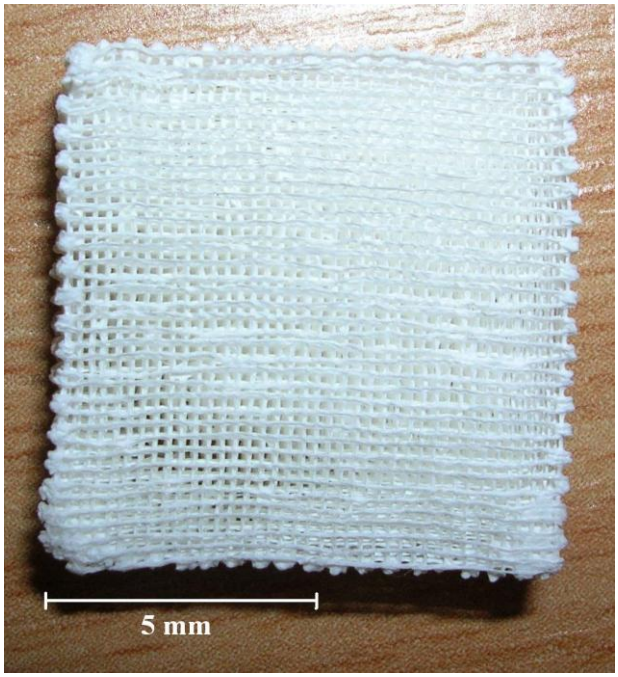

Figure 31: Chitosan scaffold not treated with PPT

1.3.2.2 Chitosan scaffold and cells *in vitro*

Briefly two different types of scaffolds were created i.e. with 0.2% w/v calcium phosphate powder and without and were prepared for static seeding with MG63 an osteoblast-like cells line. The scaffolds were plasma sterilised and then cut using a scalpel into smaller 10mm x 10mm scaffolds. The cut down scaffolds were then placed into a 24 well non tissue culture plastic plate and re-hydrated with growth media for 15 minutes. The media was removed and a cell suspension of 250,000 cells/ml was pipetted onto the scaffold and left in an incubator at 37ºC for 4 hours before 500µl of growth media was added. The scaffolds were left for 7 days with media changes every 2 days. At the end of the experiment, the media was removed and the scaffolds were stained with DAPI to determine whether the cells were still present on the scaffolds after 7 days, this can be seen in the following figures (Figures 32 - 34).

It can be observed from figures 32 and 33 that after the 7 day period, cells were still present on the scaffold which is shown by the blue (DAPI) stained cell nuclei. This demonstrated that the two types of chitosan scaffolds were capable of accommodating the MG63 osteoblast-like cell line. The staining performed on the chitosan scaffolds without cells (Figure 34) demonstrated that the staining obtained in the previous figures were stained cell nuclei. The presence of cells was a positive outcome and demonstrated the biocompatibility of the chitosan scaffold which was also reported by Ang *et al* (Ang et al. 2002) however the scaffolds lacked any mechanical strength after the 7 day period which made it impossible to move or transfer them which rendered chitosan scaffolds useless as load bearing tissue engineering scaffolds.

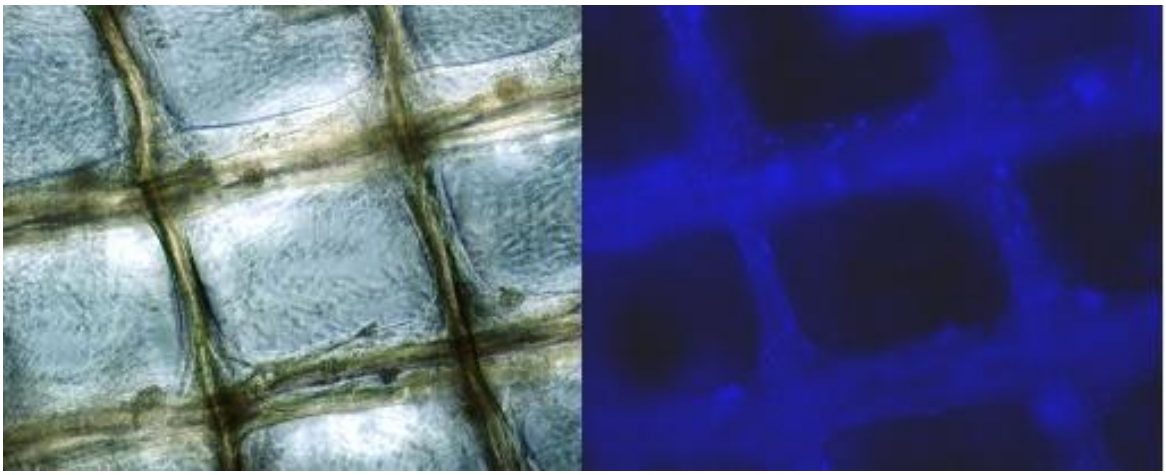

Figure 32: Chitosan scaffold seeded with MG63, Normal light (left) Fluorescence with DAPI (right)

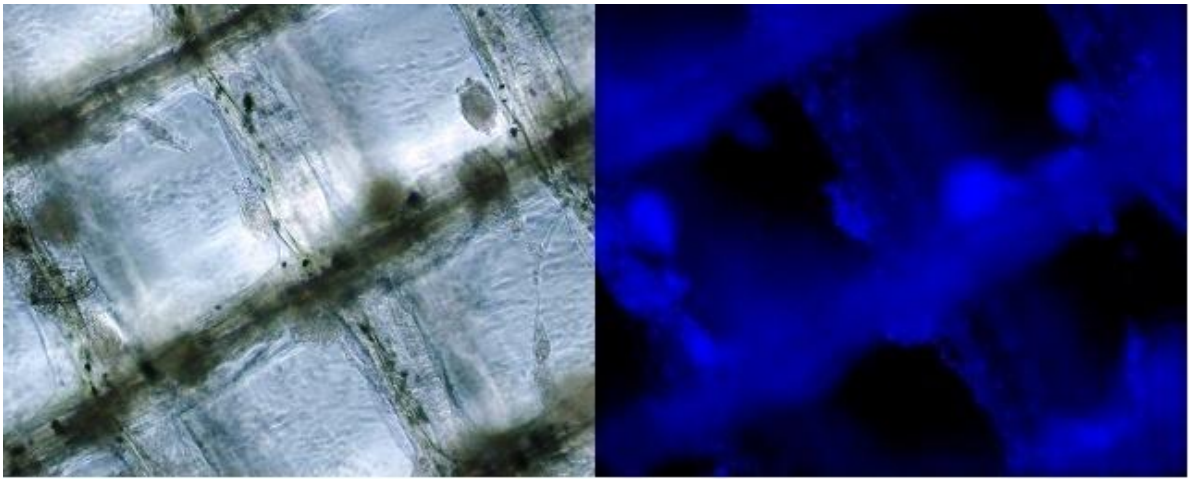

Figure 33: Chitosan scaffold with calcium phosphate seeded with MG63, Normal light (left), DAPI stained (right)

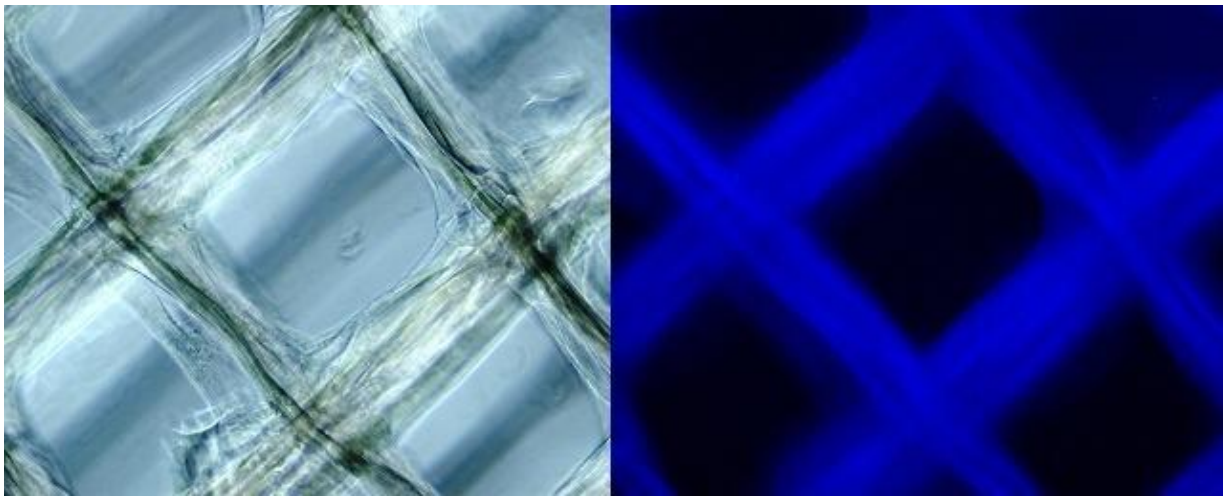

Figure 34: Chitosan scaffold with no cells

1.3.3 Alginate scaffold

1.3.3.1 Alginate scaffold manufacture and Bioplotter parameters

Briefly, 3% w/v alginate solution was made by dissolving the alginate in sterile 0.9% w/v saline water sterile distilled water. The solution was left to dissolve and then transferred to a syringe barrel. An iterative process was used where a low pressure was chosen (0.7 bar) and gradually increased until a flow of solution was observed from the blunt needle, the selected pressure was 1.4 bar. The manufacture of the first layer was then attempted by starting with a low plotting speed (60 mm/min) and then gradually increasing it until a distinguishable and defined strand was created.

As can be seen from figure 35, the pressure was too high and in combination with a low plotting speed a non uniform scaffold was created that closely resembled a pool of alginate. The following attempt involved reducing the pressure to 1 bar and changing the plotting speed to 100 mm/min. The layer thickness was set to 230µm and the strand distance set to 1.2 mm. The resultant scaffold can be observed in figure 36.

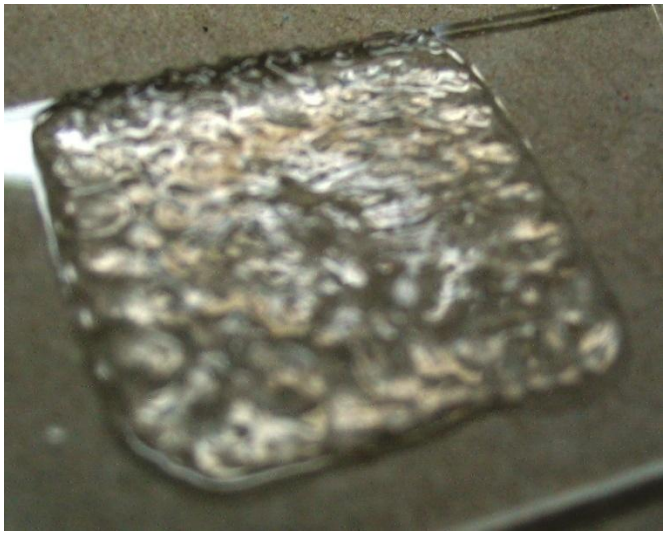

Figure 35: First layer of alginate scaffold

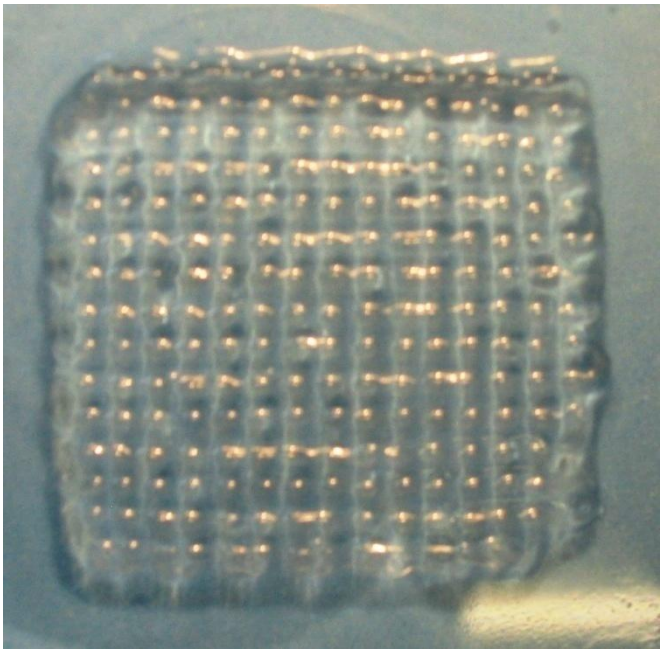

Figure 36: Alginate scaffold, plotted at 1 bar and plotting speed 100 mm/min

1.3.3.2 Alginate beads and marrow stromal cells

Briefly, MSCs were introduced in the alginate solution and beads were created. The beads were then stained with DAPI which stains cell nuclei and PI which stains dead or leaky cells, an example of this can be seen in figure 37. All the beads were stained and a cell count was performed to determine the number of live cells per field of the 2% w/v alginate and the 3% w/v alginate (Figure 38). A table with the number of live cells in the two different alginate concentrations can be observed in table 2 and a graph representing this data was then created (Figure 38).

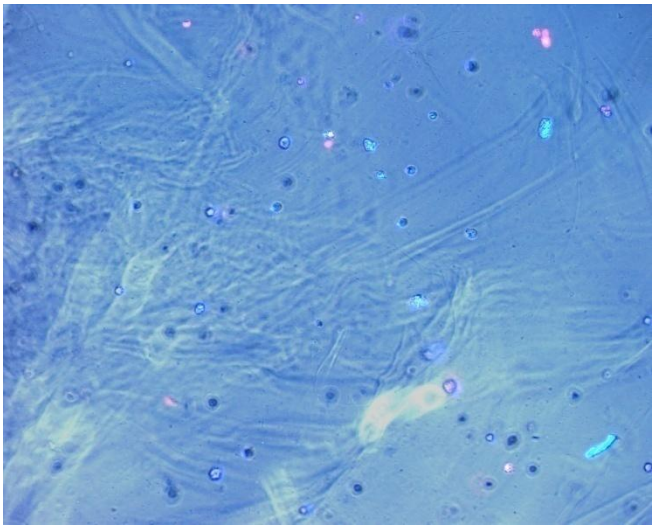

Figure 37: Alginate scaffold embedded with MSC and stained with DAPI (blue) to demonstrate all cell nuclei and PI (red) to demonstrate dead cells

	Percentage of Live cells (MSC)				
	Day 0	Day 2	Day 7	Day 14	Day 21
2% Alginate	99.2	89.4	82.1	78.6	66.7
Standard error	0.752	0.850	0.562	1.922	2.452
3% Alginate	93.3	87.5	83.0	75.6	64.1
Standard error	2.348	6.915	4.188	6.687	7.512

Table 2: Percentage of live cells in alginate scaffold

It can be observed from figure 38 that in the 2% w/v alginate beads, statistical significance was observed between day 0 and day 2, day 7, day 14 and day 21. This means that there was a significant drop of live cells at each time point compared to day 0 however in the 3% w/v alginate beads, no statistical significance was observed between any of the time points. This result means that the number of live cells does not statistically decrease during

the 21 days which would imply that the 3% w/v alginate beads were more biocompatible than the 2% w/v alginate.

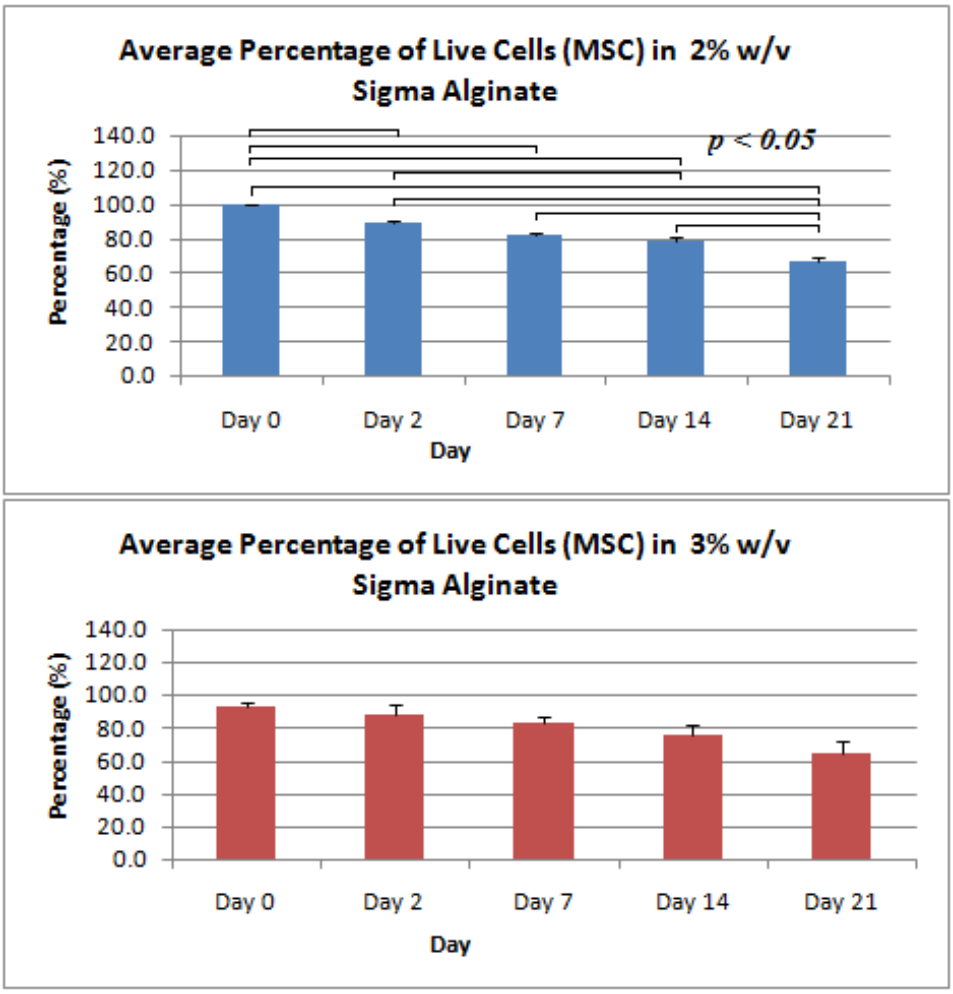

Figure 38: Average percentage of live cells over a 21 days period in 2% w/v Sigma alginate (top graph) and 3% w/v Sigma alginate (lower graph). Results are expressed as the mean percentage of live cells. Connecting lines denotes a statistical difference with $p < 0.05$

1.3.4 Gelatin scaffold

1.3.4.1 Gelatin scaffold and Bioplotter parameters

Briefly, various gelatin concentrations were experimented with, ranging from 10% w/v to 60% w/v. The 10% w/v - 20% w/v gelatin needed to be heated in order to dissolve them completely. The higher concentrations, 30%-60% w/v gelatin, never completely dissolved even with heating and so were discarded. The 20% w/v gelatin solution was used as it completely dissolved when heated and once in a dissolved state, was viscous enough so that flow rate was controllable. During the initial scaffold manufacture, the needle tip was not heated and due to this the gelatin would solidify inside the needle and block the flow. This problem was dealt with by using an in house wire heater coiled round the needle tip to keep the gelatin liquid (figure 39) however this had some limitations as the exact temperature was not measured and was only controlled by referring to the temperature vs power graph (Figure 16). As the wire needed to be coiled all the way down the needle tip, the gelatin was occasionally deposited directly onto the wire which solidified the gelatin and disrupted the flow of the liquid gelatin being extruded. This was avoided by moving the wire and exposing approximately 500μm of needle tip which improved the flow of the liquid gelatin. This enabled one to create the first layer of the scaffold however when a second layer was extruded on top, it would collapse into the channels created by the previous layer (figure 40). This could be avoided by introducing a liquid with a relative density similar to that of the gelatin being extruded to provide support for the strand. It was also decided that a cross linking agent could be added to further strengthen the gelatin which would provide increased mechanical strength. From the literature it was determined that gluteraldehyde (Yang and Ou 2005) and transglutaminase (Fuchsbauer et al. 1996) were used to cross-link and hence strengthen gelatin.

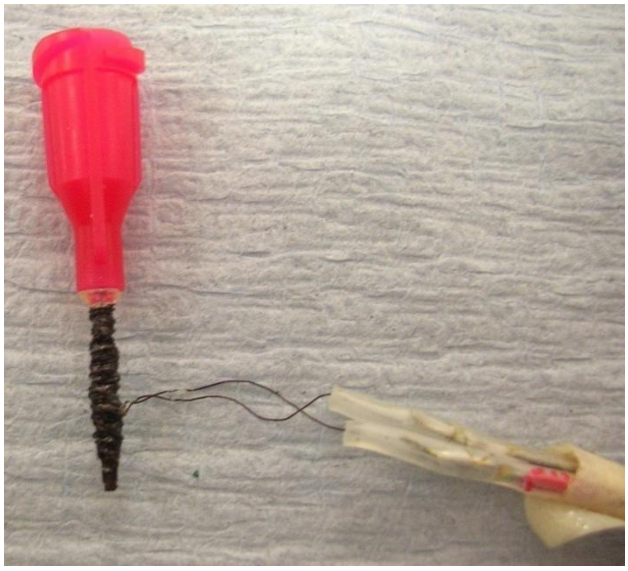

Figure 39: In house manufactured wire heater for blunt needle

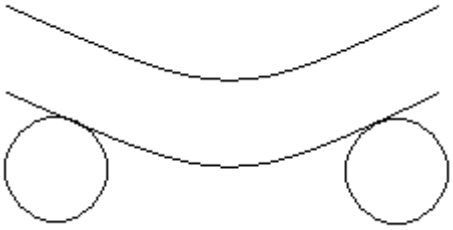

Figure 40: Cross-sectional representation of plotted strand collapsing between previously plotted layer

1.3.4.2 Gelatin cross-linking and cells

Briefly, as described in paragraph 1.2.2.4., the two cross-linking agents were made up to two different concentrations to determine which on was the least toxic to cells. The two gluteraldehyde concentrations were 0.25% and 2.5% and the two transglutaminase concentrations were 5U/g and 50U/g. The gelatin was added to the wells and then cross-linked with the appropriate cross-linking agent. After 7 days the cells were fixed with paraformaldehyde and stained with DAPI which is a fluorescent stain that binds strongly to

DNA. DAPI can pass through an intact cell membrane and can be used to stain live and fixed cells and fluoresces bright blue. In each field the number of cells was recorded by counting the total number of cells which were stained with DAPI (Figure 41).

As can be seen from figure 41, no statistical significance was observed between the two different concentrations of transglutaminase however statistical significance was observed between the 5U transglutaminase and both the gluteraldehyde groups.

An attempt was then made to manufacture gelatin scaffold into a bath of 5U transglutaminase however, the desired supporting effect of the solution was not observed during strand extrusion. Cross-linking of the gelatin strands was observed however this occurred after 2-3 minutes which was too lengthy as the manufacture of the second layer had already commenced.

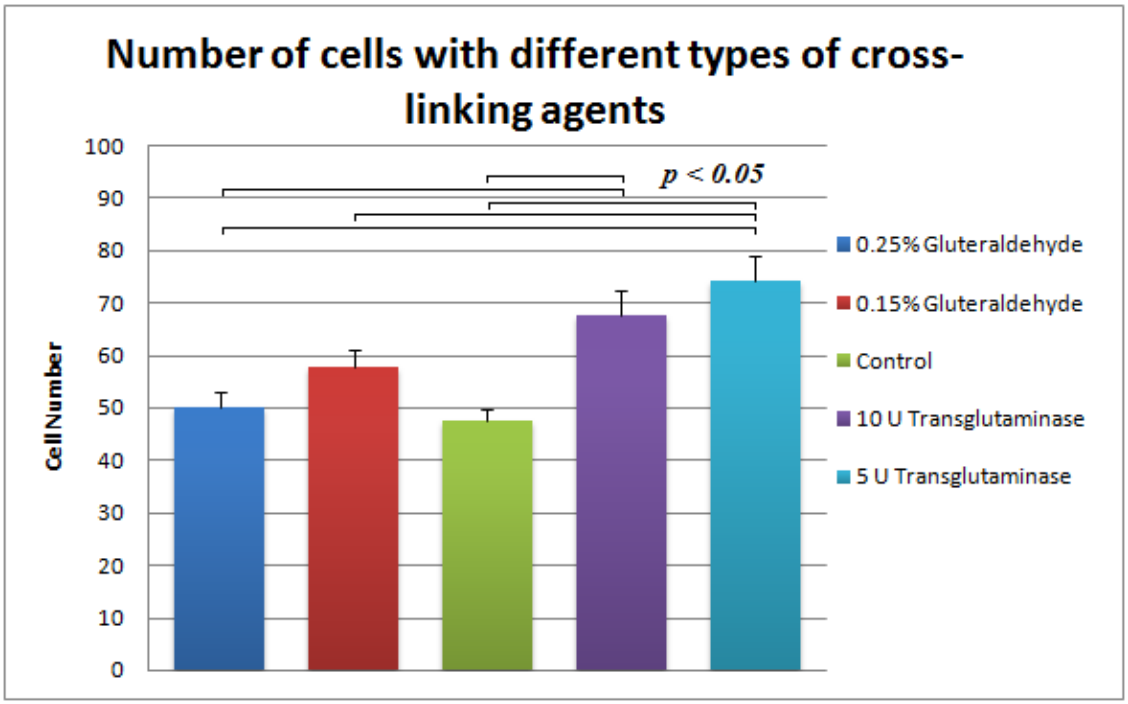

Figure 41: Cell number and various cross-linking agents

1.3.5 Poly (lactide-co-glycolic acid) (PLGA) scaffold

1.3.5.1 PLGA scaffold manufacture and Bioplotter parameters

Briefly, PLGA was dissolved in chloroform to a 20% w/v concentration and extruded into a coagulation bath of isopropyl alcohol. Numerous different plotting speeds and pressures were attempted ranging from 150 mm/min to 300 mm/min and 0.2 to 0.6 bar however after several iterations the plotting speed and plotting pressure that yielded the best results were 250 mm/min and 0.22 bar respectively. These parameters were chosen as the plotting medium was non-viscous and hence in order to create adequate strands a high plotting speed and low pressure were required (Figure 42). This yielded a satisfactory first layer but subsequent layers did not plot correctly as the PLGA did not solidify fast enough and hence the strand collapsed into the gaps before solidifying. The next step was to increase the concentration of the PLGA to 30% in order to increase the viscosity and therefore retains the strand morphology which would enable the manufacture of a second layer without collapsing into the gaps between strands. However, this was unsuccessful as the increased viscosity required and increased plotting speed that then meant the first layer was completed more rapidly and therefore did not have time to completely solidify. During scaffold manufacturing it was observed that the chemical reaction between the PLGA dissolved in chloroform with the isopropyl solvent coagulation bath were not a satisfactory combination and hence would not be appropriate for scaffold manufacture.

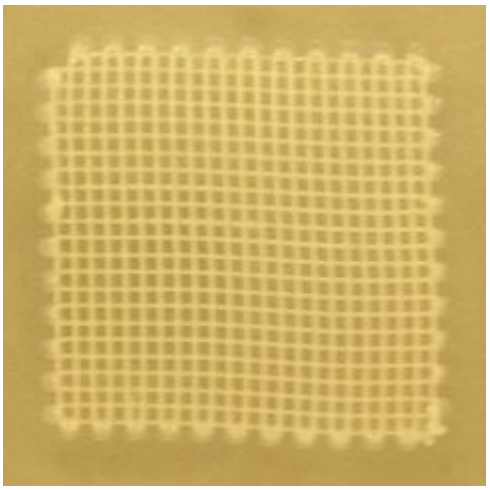

Figure 42: 20% PLGA where layers collapsed and formed a sheet

As the previously mentioned combination of solvent and coagulation bath had limited success, PLGA was dissolved in acetic acid to a 20% w/v solution and extruding into different coagulation reagents. Firstly isopropyl was used to precipitate the PLGA but this yielded a similar result as with the PLGA dissolved in chloroform. Industrial methylated spirit (IMS) was then employed which generated promising results as the strands would not collapse due to the increased precipitation rate of the PLGA. The scaffolds which maintained their geometry and did not experience layer collapse were generated with a plotting pressure of 0.05bar and a plotting speed of 202 mm/min and were obtained after substantial iterative work and the results can be seen in figure 43.

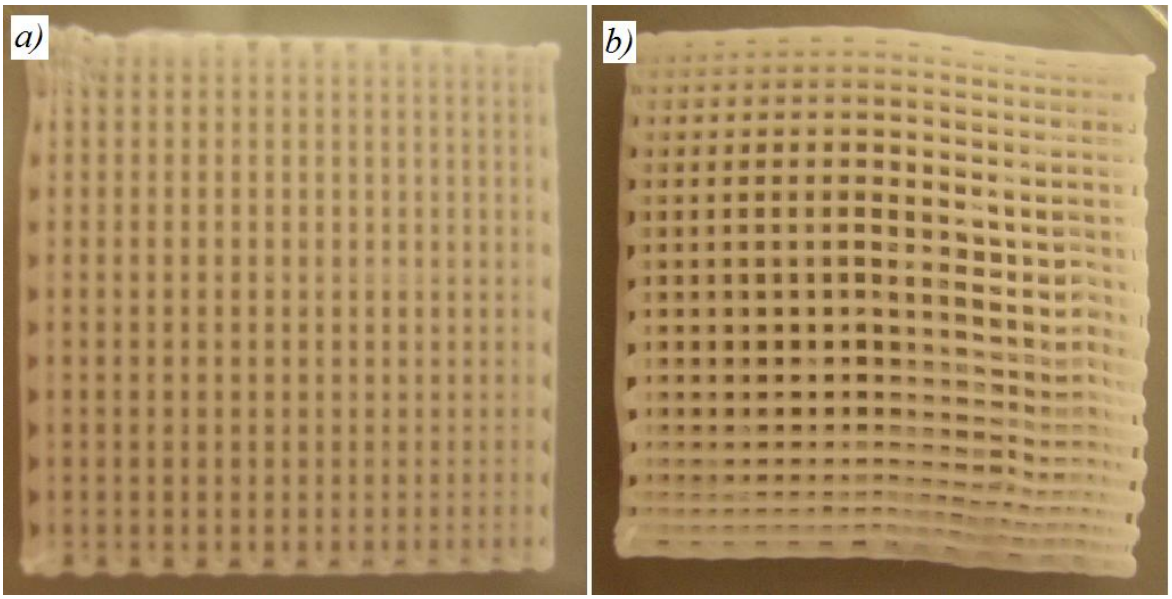

Figure 43: 20% PLGA scaffolds, a) and b) manufactured with the same plotting pressure of 0.05bar and plotting speed of 202 mm/min and four layers high, however a) was plotted on a polycarbonate substrate with no Vaseline™ and b) was with a polycarbonate substrate with a thin film of Vaseline™ to aid removal of the PLGA scaffold

Once an appropriate plotting speed, pressure, solvent and extruding medium was determined, the concentration of the PLGA solution was increased to 30% w/v. This was

performed to further increase the viscosity of the extruded solution which would render the extrusion process more controllable and also to have comparable solution concentrations with the polycaprolactone scaffolds. The increased viscosity created problems as a new plotting speed and pressure were required as scaffold manufacture using the same plotting parameters as the lower concentration yielded inadequate results (Figure 44). After several adjustments scaffolds which maintained their layer structure and the geometry were created and can be observed in figure 45. After the completion of the scaffolds, they were carefully removed from the substrate which was thinly covered with Vaseline™ which aided in its removal and immersed in water for 30 minutes to remove any solvent from the scaffold. The scaffolds were then placed into a small Petri dish for storage and kept refrigerated at -20ºC until required for experiments.

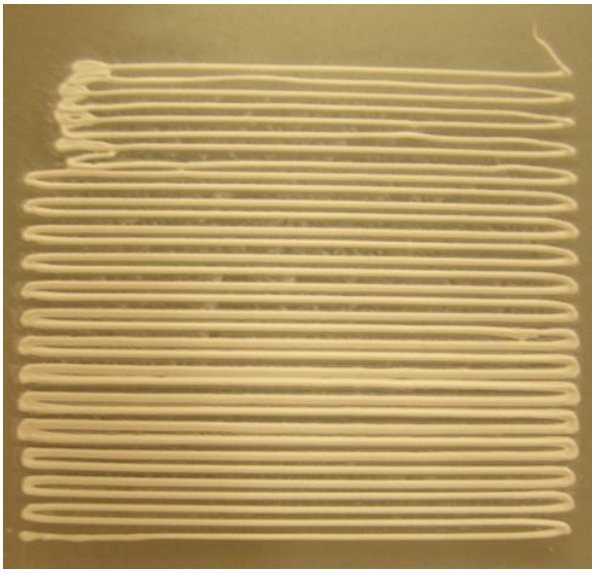

Figure 44: Initial attempt with 30% w/v PLGA solution

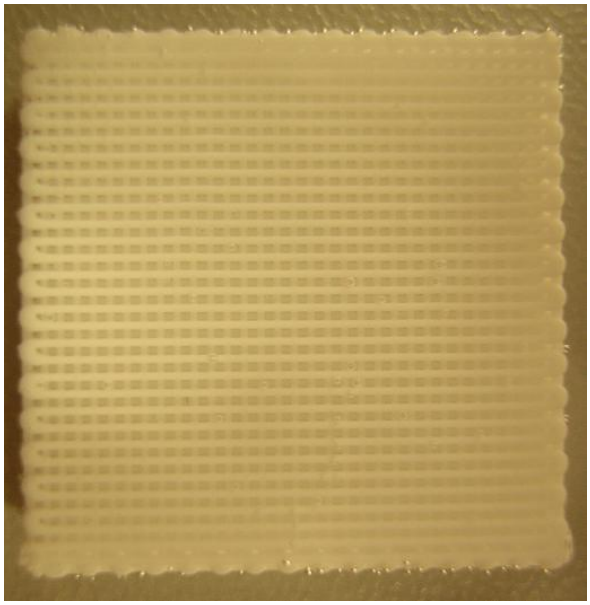

Figure 45: PLGA manufactured to 2mm in height and no collapse of created layers. Extruding pressure: 0.27 bar, plotting speed: 163 mm/min

Images of the scaffolds were then taken using the scanning electron microscope (SEM) to determine the scaffold geometry (Figure 46). From the SEM images (Figure 46 a) and b)) it can be observed that there is good geometry with even spacing between strands and that the layers maintain their structure and do not collapse. Figure 46b, also shows small anomalies between the perpendicular layers which appear to look like small bubbles which may have been caused during the fusion on the layers. Figure 46c shows the smooth surface of the strands.

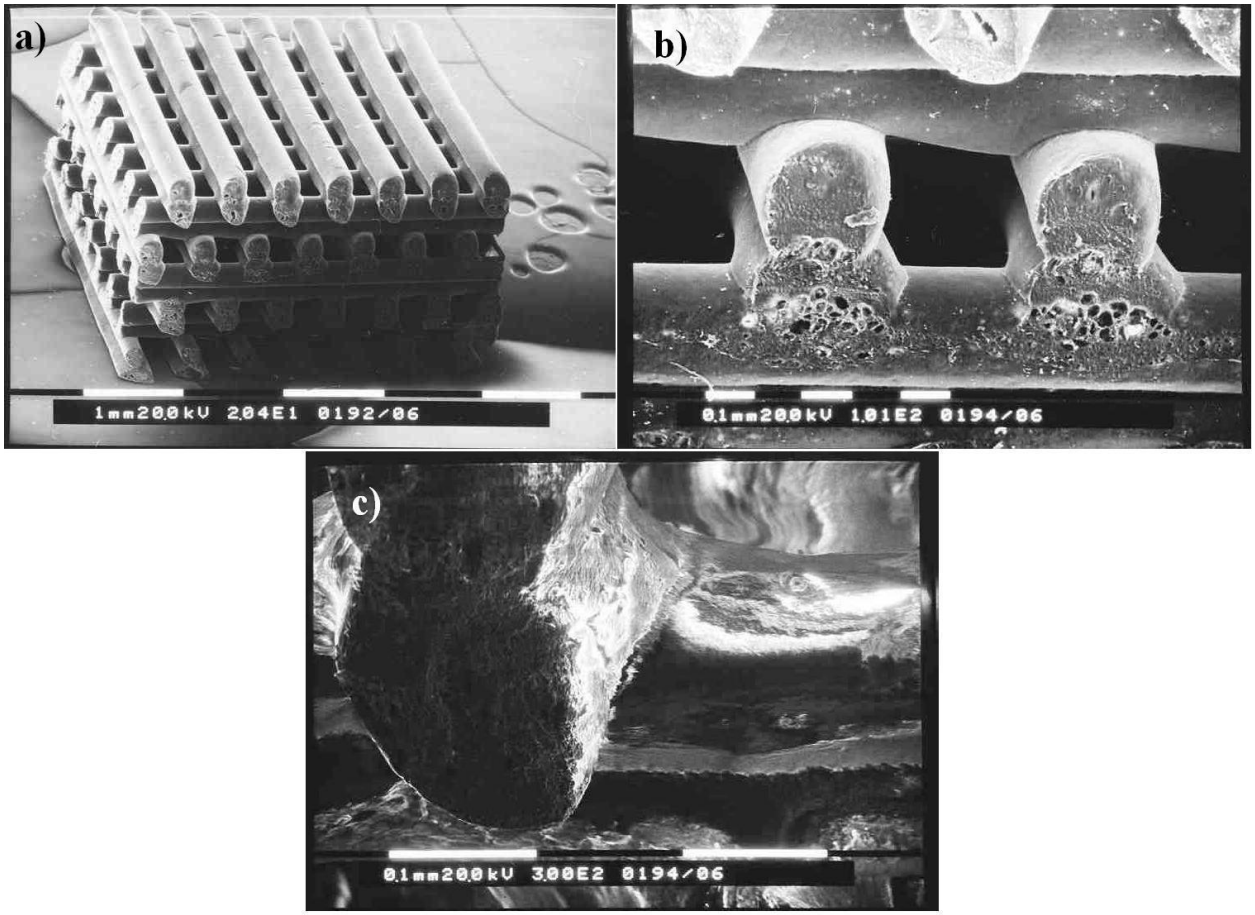

Figure 46: SEM image of PLGA scaffold

1.3.5.2 PLGA scaffold degradation

Briefly, PLGA scaffolds were created as mentioned in 1.3.5. and then cut with a scalpel (Morton-Swann, UK) to smaller scaffolds with dimensions approximately 4mm x 4mm. Thirty five scaffolds were cut so that at the seven different time points (T_0, T_1, T_3, T_6, T_9, T_{15} and T_{21}), five scaffolds were removed and weighed to determine if there was any weight loss which would indicate degradation. The table below (Table 3) shows the weights of the scaffolds and figure 47 demonstrate the data graphically.

	Weight of scaffold (mg)						
Time	**A**	**B**	**C**	**D**	**E**	**Average weight (mg)**	**Standard error**
Day 0	6.2	6.3	5.8	7.1	6.5	6.38	0.21
Day 1	5.8	6.1	5.8	6.3	6.1	6.02	0.10
Day 3	6.0	5.3	5.4	5.9	6.2	5.76	0.17
Day 6	5.8	5.8	6.0	5.0	6.2	5.76	0.20
Day 9	6.3	5.9	5.4	6.0	6.2	5.96	0.16
Day 15	5.5	6.1	5.3	6.8	5.9	5.92	0.26
Day 21	5.4	6.6	6.9	6.8	5.9	6.32	0.29

Table 3: Weights of PLGA scaffolds at various time points

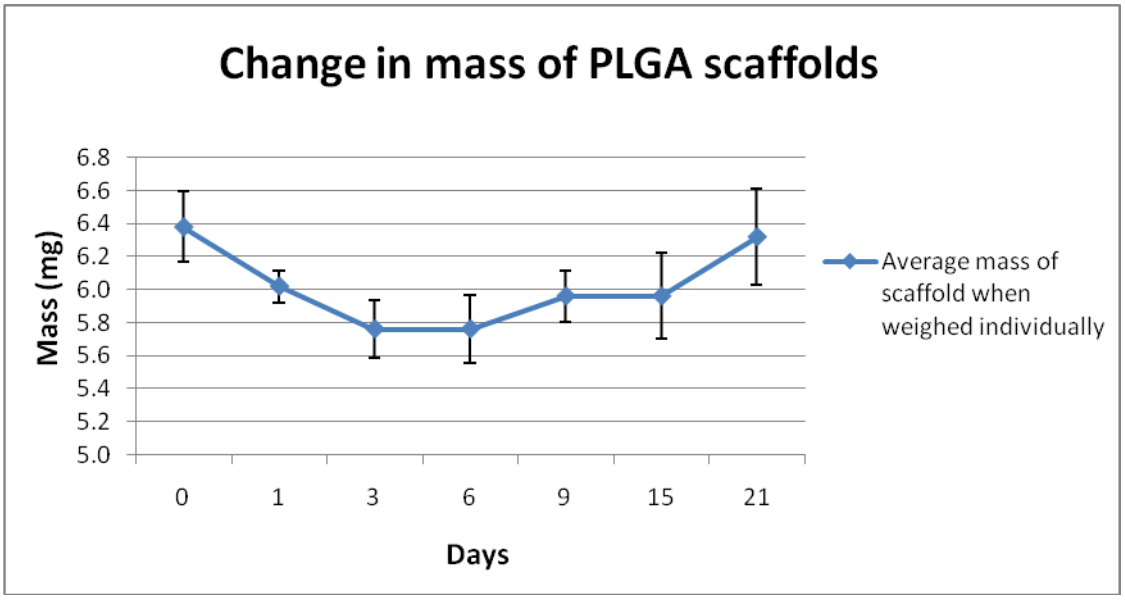

Figure 47: PLGA scaffold degradation (no statistical significance between time points)

1.3.5.3 Gelatin coating to enhance cellular attachment to scaffold

Briefly, an ultra-low binding tissue culture plate was coated with 2 different gelatin concentrations (0.1% w/v and 0.2%w/v) in order to determine which coating would increase the adhesion of marrow stromal stem cell to the manufactured scaffolds. The wells were then examined and the number of cells per field counted which yielded figure 48. Images were digitally stored and representative images can be observed in figure 49.

As can be seen from figure 48, there was a significant difference between the number of cells attached to the low-binding tissue culture plate coated with 0.2% w/v gelatin and the other two treatments. It can also be seen that there was a significant difference between the 0.1% w/v gelatin and the non coated plastic. This demonstrates that in coating the low-binding tissue culture wells with gelatin, significantly increased the number of cells that attached to the plastic. This experiment demonstrated that the 0.2% w/v gelatin coating significantly increase cell adhesion and therefore would be used to coat scaffolds prior to seeding with cells.

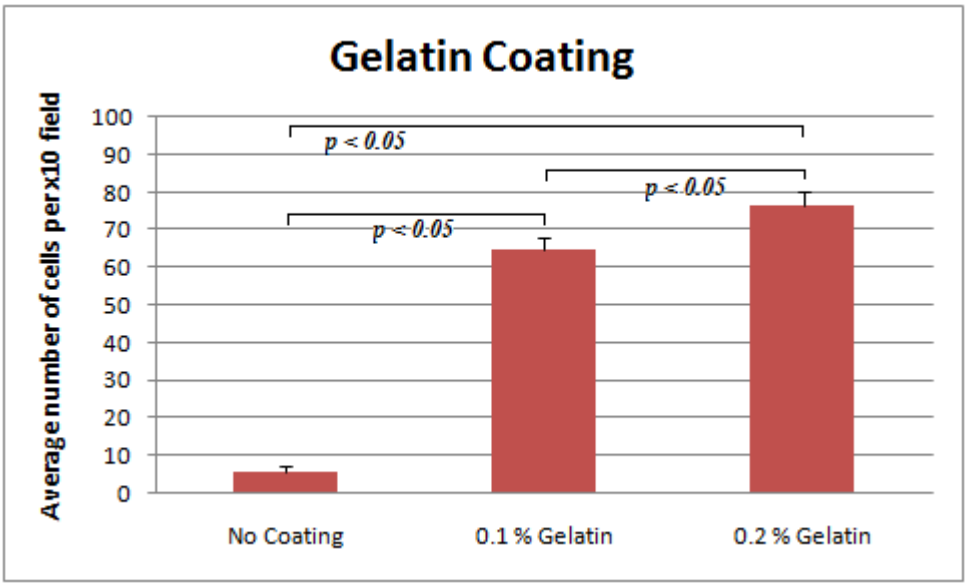

Figure 48: Average cell number against different concentrations of gelatin coating

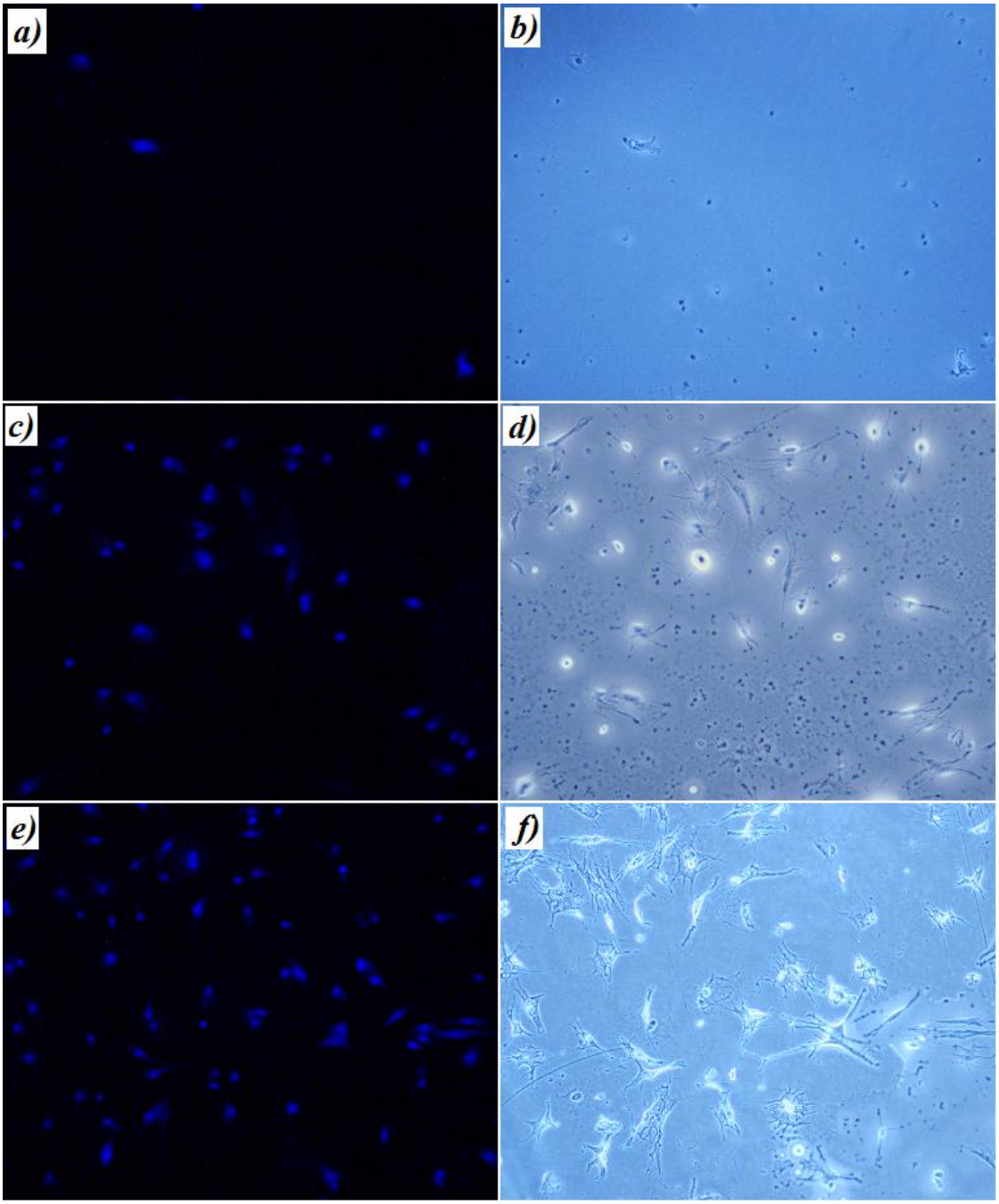

Figure 49: Representative images of DAPI stained MSC with different gelatin coatings, a) DAPI stained MSCs with no gelatin coating, b) bright field image of MSCs with no gelatin coating, c) DAPI stained MSCs with 0.1% gelatin coating, d) bright field image of MSCs with 0.1% gelatin coating, e)DAPI stained MSCs with 0.2% gelatin coating, f) bright field image of MSCs with 0.2% gelatin coating

1.3.5.4 PLGA and PCL with marrow stromal cells

All data points represented in the standard curve represent the average of 3 wells. The standard curve was created from serial dilutions of DNA from herring testis which demonstrated a linear relationship between concentration of DNA and fluorescence and yielded a linear equation (Figure 50). Using the linear equation obtained from the standard curve, measurements of the adhered cell cultures seeded onto the scaffolds and the wells were performed using the fluorescence values. This calculation yielded the relationship between the cell numbers. Florescence results obtained from the measurements of cultures containing the scaffolds were then compared to the known cell number curve which allowed the cell number to be determined (Figure 51).

It can be observed that at the end of the experiment, there were fewer cells in the wells where the PCL scaffold was present compared to the wells with the PLGA scaffolds. This was because there were a greater number of cells that attached to the PCL scaffold rather the PLGA scaffolds.

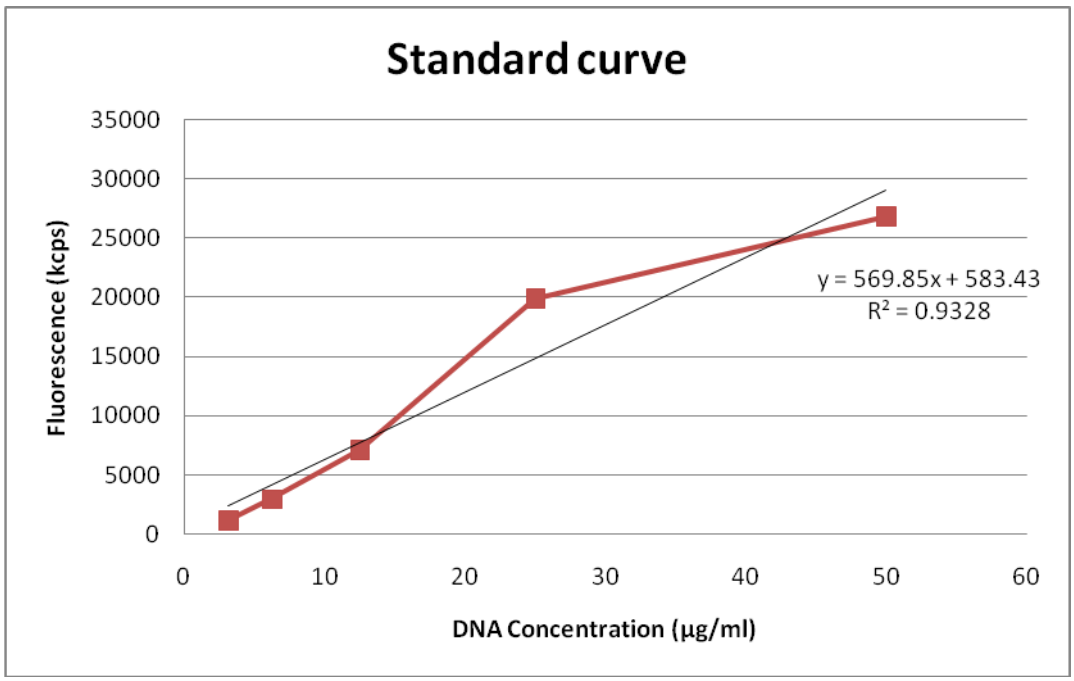

Figure 50: Standard curve for DNA from herring testis using Hoechst 33258

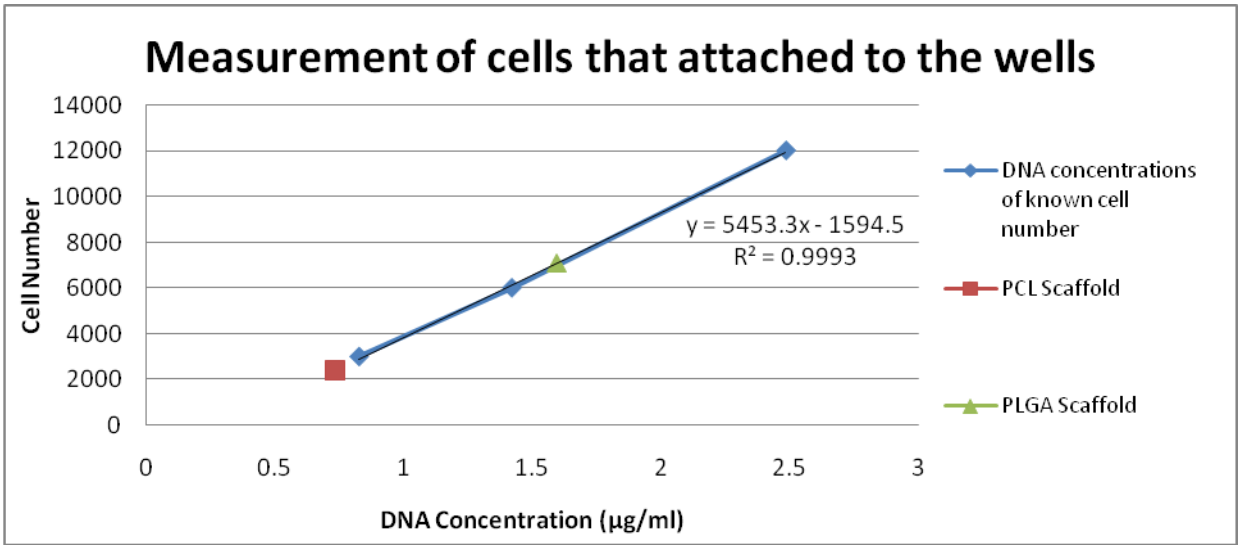

Figure 51: Cell assay for MSCs seeded on PLGA and PCL scaffolds

1.3.6 Polycaprolactone scaffold

1.3.6.1 Polycaprolactone scaffold manufacture and Bioplotter parameters

Briefly, polycaprolactone scaffolds were created by dissolving the polymer in a solvent. Various solvents were available hence several needed to be tested to determine which performed best. The pure solvents tested were: chloroform, dichloromethane, acetone and acetic acid. The dissolved polymer (25 and 30% w/v were tested) was then extruded into a bath that would precipitate out PCL. The content of the precipitation bath was a solvent in which the PCL was insoluble but in which the dissolving solvent was fully miscible. The miscible solvents tested were isopropyl alcohol, methanol, ethanol, water, glycerine, industrial methylated spirit (IMS).

Various concentrations were tested starting at 20% w/v and increasing the concentration so that the PCL stayed soluble at room temperature, with different concentrations being achieved with different solvents, the highest successful concentration occurred at 30% w/v with acetic acid.

The first test was performed using chloroform as the solvent and polycaprolactone (M_n 80,000) as the polymer. The PCL was dissolved to a 30% w/v concentration and extruded into isopropyl alcohol onto a glass slide, the results of these combinations can be seen in figure 52 accompanied by table 4. The inputted scaffold dimensions were 15mm x 15mm but due to the contraction of the polymer, the actual dimensions of the scaffold were 12.5mm x 12.5mm.

Scaffold	Pressure (bar)	Speed (mm/min)	Layer thickness (mm)	Notes
a	2.81	170	0.08	6 layers
b	3.15	150	0.08	5 layers
c	3.15	105	0.10	8 layers
d	3.15	115	0.08	8 layers, 0.3 mm offset
e	3.15	110	0.08	4 layers, 0.3 mm offset
f	3.20	115	0.08	12 layers, 0.3 mm offset

Table 4: PCL scaffold parameters for figure 52

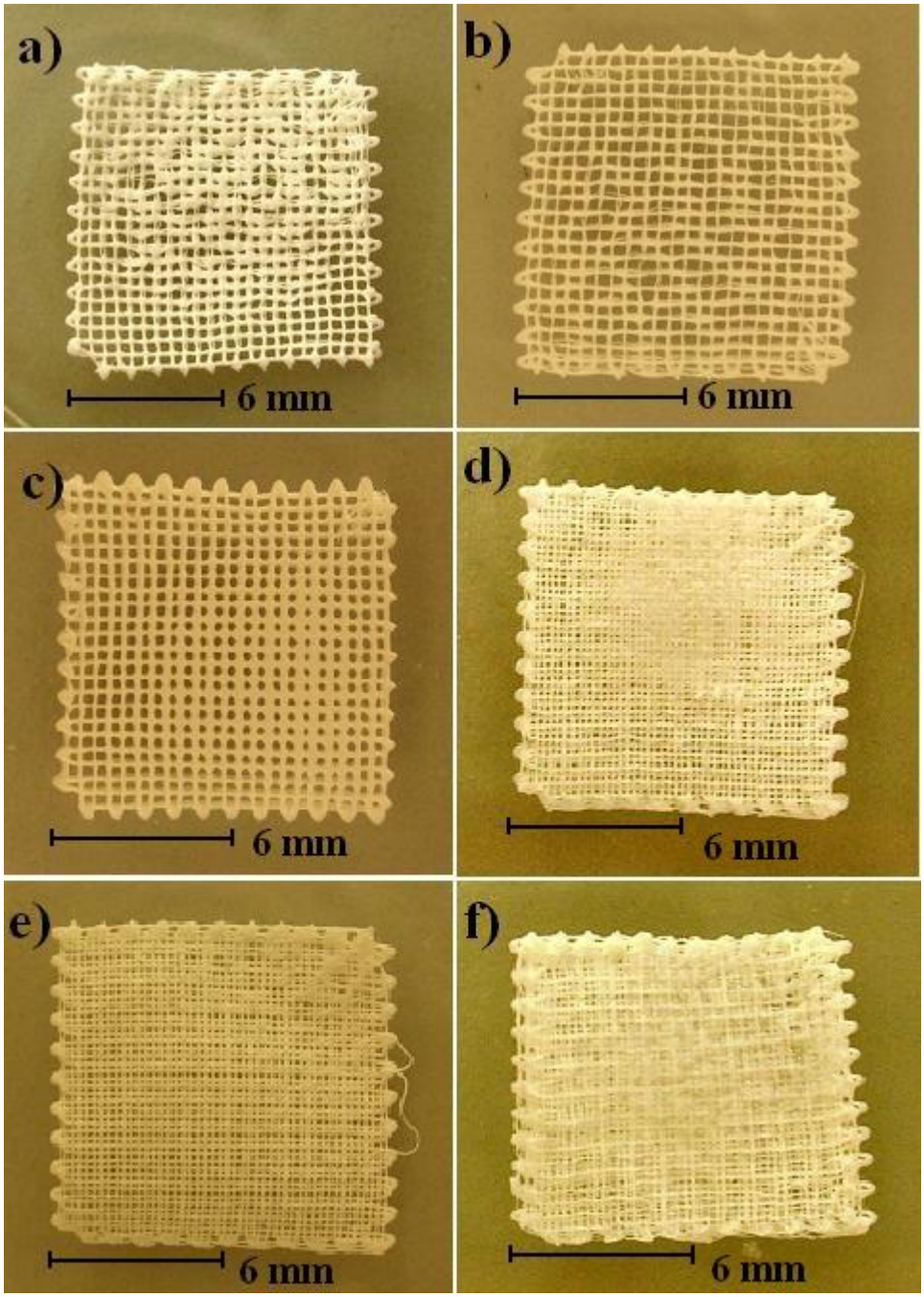

Figure 52: First test with 30% PCL M_n 80,000 dissolved in chloroform and extruded in isopropyl alcohol

The next set of scaffolds were plotted using a 25% concentration of PCL, the lower concentration was tested as it was thought that this might avoid the areas where the PCL did

not have time to solidify and eliminate the regions where structure was lost, results can be seen in figure 53 and table 5.

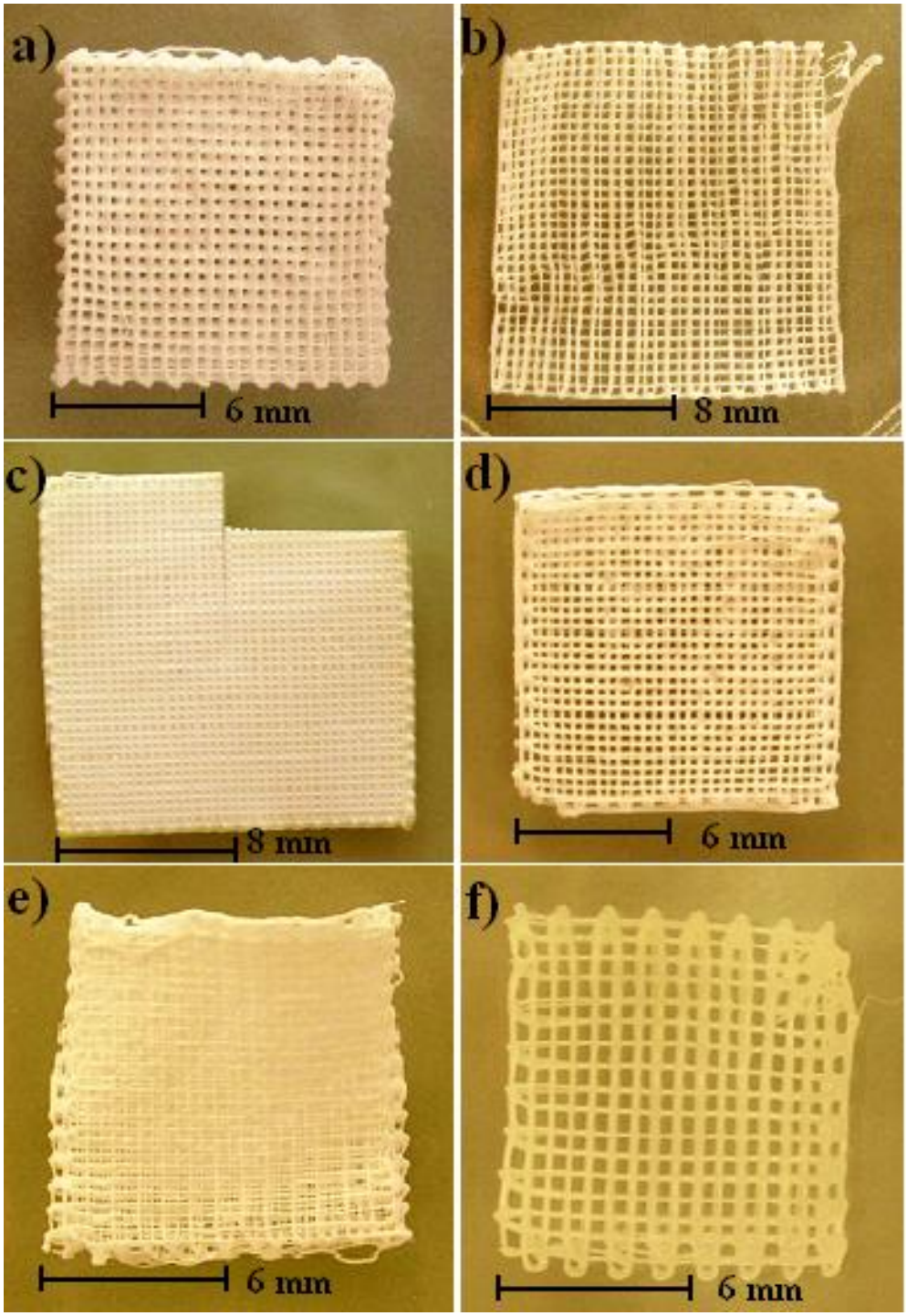

Figure 53: 25% PCL M_n 80,000 dissolved in chloroform and plotted into isopropyl alcohol

Scaffold	Pressure (bar)	Speed (mm/min)	Layer thickness (mm)	Notes
a	3.53	125	0.1	10 layers, Isopropyl was added while plotting and stirred, strand distance 0.6 mm
b	3.10	115	0.1	3 layers, peeled off at side, Isopropyl added + stirring, strand distance 0.6 mm
c	3.53	125	0.12	5 layers, Isopropyl added + stirring, strand distance 0.5 mm
d	3.55	125	0.15	5 layers, 2 drops of Isopropyl added during every layer + stirring, strand distance 0.5 mm, left in Isopropyl for 3 min after finished plotting
e	3.57	125	0.15	5 layers, 1 drop of Isopropyl added whilst plotting on scaffold, strand distance 0.5 mm
f	2.84	125	0.18	4 layers, on completion left to cure in water, 0.3 mm i/d needle

Table 5: Scaffold manufacturing parameters for figure 53

As can be observed from figure 53, the created scaffolds were still lacking accurate strand deposition and a defined geometry. It was then decided to test a different molecular number (M_n 42,500) of polycaprolactone to determine if this change would improve the scaffold geometry the scaffold attempts can be seen in figure 54 and table 6.

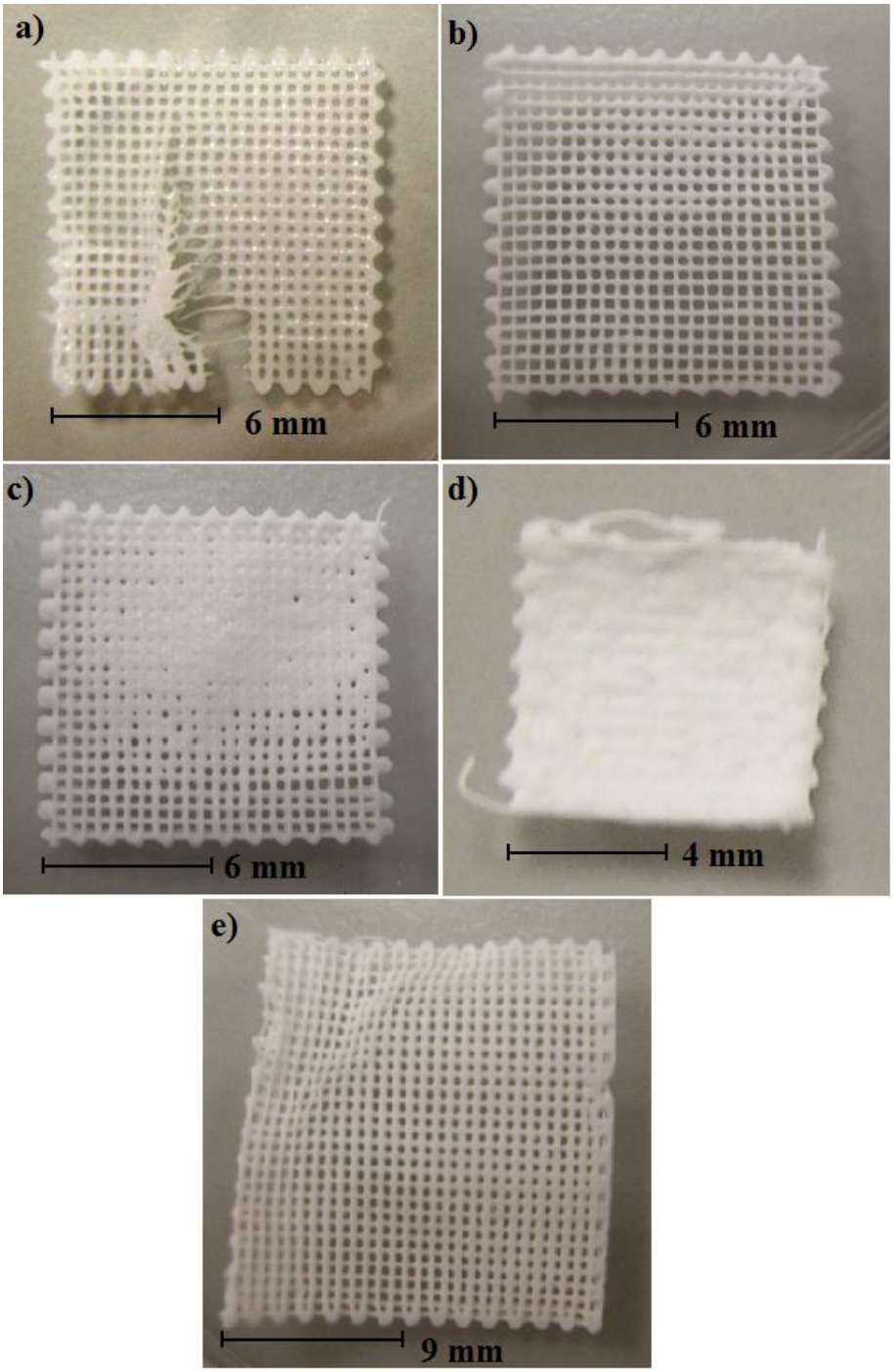

Figure 54: 30% PCL M_n 42,500 dissolved in chloroform, plotted in isopropyl

Scaffold	Pressure (bar)	Speed (mm/min)	Layer Thickness (mm)	Notes
a	3.0	100	0.13	4 layers, did not fully solidify in middle, started peeling of substrate and ripped
b	3.1	115	0.13	5 layers, centre and top right corner loss of strand definition, peeling off substrate at tope left corner
c	3.1	115	0.15	6 layers, top right and centre of scaffold fused together no strand definition
d	3.1	115	0.15	4 layers, 8x8 scaffold, no scaffold definition
e	3.1	121	0.15	4 layers, 18x18 scaffold, better definition, peeled off at corner

Table 6: Scaffold parameters for figure 54

From these attempts, the main problems were that the extruded strands did not solidify fast enough and therefore fused with the previous layer which resulted in the zones where there is no strand definition (Figure 54 b, c, d). The other problem was that the scaffolds did not adhere to the substrate and peeled off which meant that the scaffold could not be manufactured to more than 5 or 6 layers. It was decided to solve the accuracy of scaffold manufacture by using different solvents and precipitation baths. Adherence of the scaffold was solved by using different substrates and coatings.

For the following tests, a 20% PCL (M_n 80,000) was dissolved in acetone and plotted in various precipitation baths, the results and parameters can be seen in figure 55 and table 7 respectively.

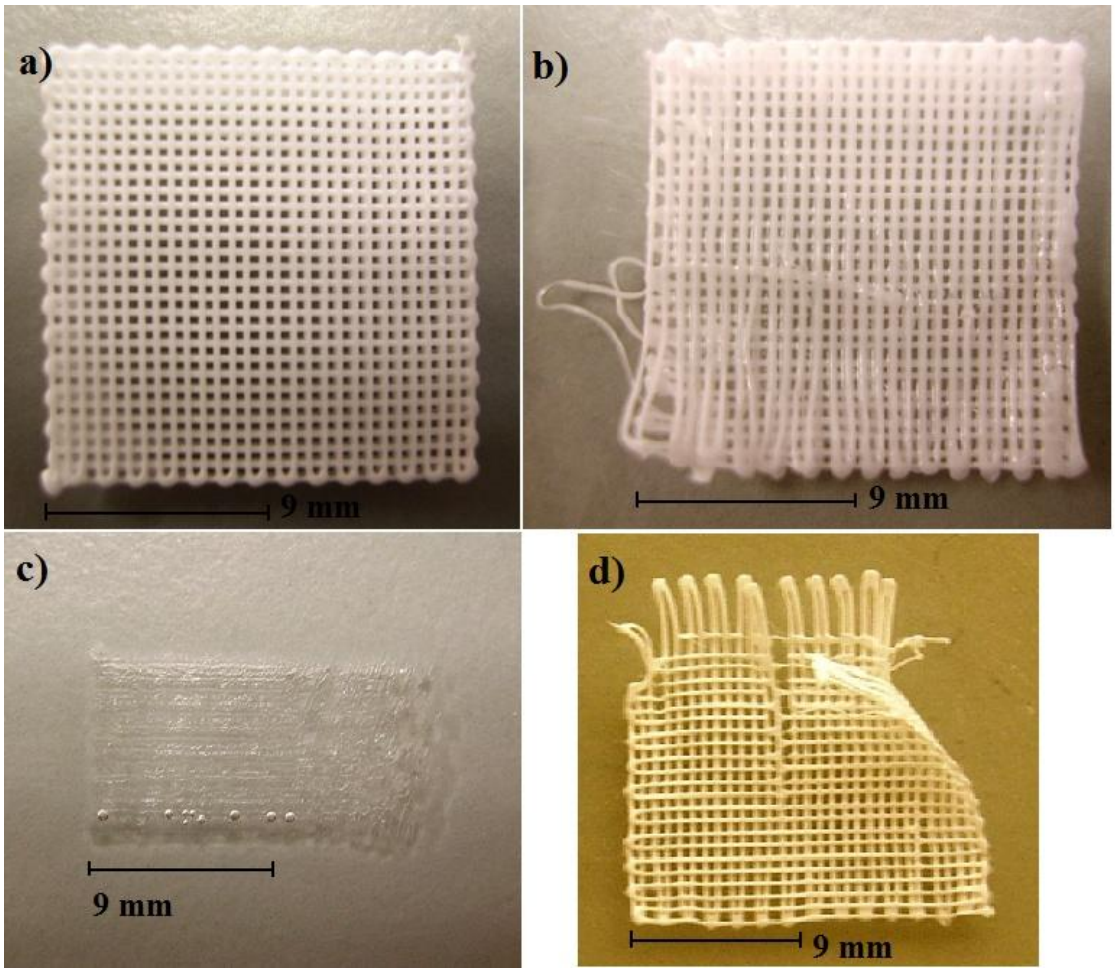

Figure 55: 20% PCL (M_n 80,000) dissolved in acetone

Scaffold	Pressure (bar)	Speed (mm/min)	Layer thickness (mm)	Notes
a	0.6	116	0.1	12 layers, plotted in 100% ethanol, Petri dish coated with Vaseline, washed in water on completion
b	0.6	116	0.1	4 layers, plotted in methanol, Petri dish coated with Vaseline
c	0.6	116	0.1	1 layer, plotted in glycerine, no strand definition
d	0.62	116	0.1	2 layers, plotted in ethanol, Petri dish coated with too much Vaseline hence peeling of scaffold

Table 7: Scaffold manufacturing parameters and notes for figure 55

After numerous iterations using acetone as the solvent, it was decided that a different solvent for the PCL should be tested as the combination of acetone and the various different coagulation baths were not going to yield a satisfactory scaffold.

Acetic acid was then used as the solvent for PCL polymer with the same reagents as previously described in the coagulation baths. The initial test was performed with 20% w/v PCL (M_n 10,000) dissolved in acetic acid and extruded in isopropyl (Figure 56a), table 8 contains additional notes. This produced inaccurate strand deposition and therefore IMS was tested as the coagulation agent (Figure 56b). It can be seen from the image that the geometry of the deposited strand was more accurate but once the four layers were completed, and the IMS drained, removal of the scaffold was unsuccessful as the polymer was extremely brittle (Figure 56c).

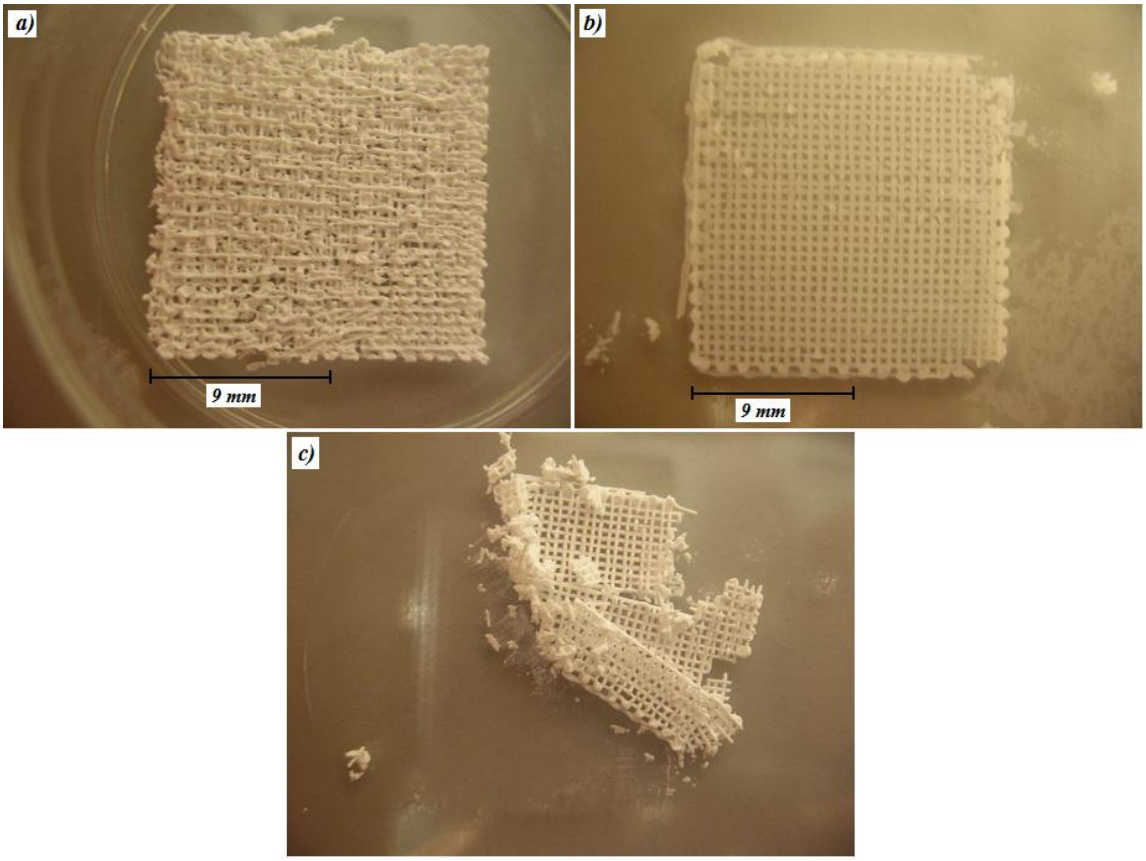

Figure 56: 20% w/v PCL (M_n 10,000) dissolved in acetic acid and extruded in a) isopropyl alcohol, b) in IMS c) attempt to remove scaffold in image b)

Scaffold	Pressure (bar)	Speed (mm/min)	Layer thickness (mm)	Notes
a	0.22	130	0.15	First layer successfully plotted, second layer unsuccessful. Extruded in Isopropyl alcohol. Very brittle
b	0.36	130	0.13	4 layer, total height of 0.56mm. Extruded in IMS
c	0.6	100	0.13	Attempt to remove scaffold from substrate. Too brittle

Table 8: Scaffold manufacturing parameters for 2% w/v PCL dissolved in acetic acid, additional notes for figure 56

The next test involved the highest average molecular number weight of PCL (M_n 80,000). The polymer was dissolved in acetic acid at a concentration of 20% w/v and extruded in isopropyl, methanol and 80% ethanol. Results can be observed in figure 57 and table 9 supplies additional notes.

For figure 57, it can be seen that the new tested solvent acetic acid, improved the strand geometry and therefore scaffold manufacture. This demonstrated that acetic acid was the solvent that future scaffold manufacturing processes should employ. However the reagents used to solidify the PCL were unsatisfactory. In figure 57e) and f), the manufactured scaffolds are well created and no layer collapse or un-solidified strands were observed however the removal of the scaffolds from the substrate proved to be difficult. The Vaseline™ coating on the substrate had no effect in easing the adhesion of the scaffold to the substrate and therefore damage to the scaffold was caused on removal. Due to this IMS was used which did not affect the Vaseline™ coating facilitating the removal of the PCL scaffold.

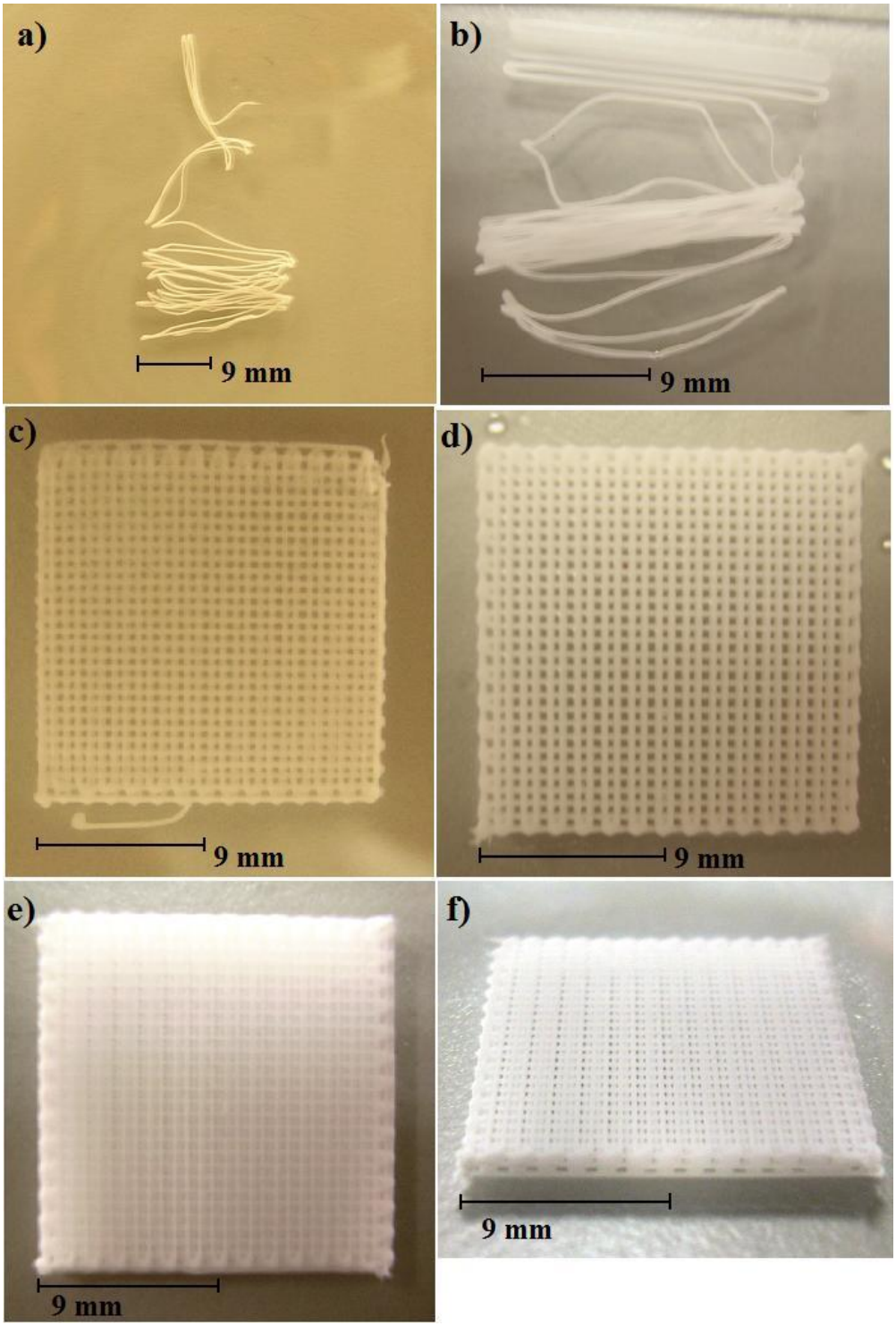

Figure 57: 20% w/v PCL (M_n 80,000) dissolved in acetic acid

Scaffold	Pressure (bar)	Speed (mm/min)	Layer thickness (mm)	Notes
a	0.7	106	0.13	1 layer, plotted in water in a glass slide, peeled off
b	0.7	100	0.13	1 layer, plotted in isopropyl alcohol on a glass slide, did not stick to glass
c	0.6	100	0.13	4 layers, plotted in isopropyl alcohol directly onto Petri dish, fused to Petri dish and could not take off scaffold
d	0.6	113	0.13	5 layers, plotted in 80% ethanol, washed in water after completion of scaffold
e	0.6	116	0.14	8 layers, plotted in methanol, PCL solidified quickly
f	0.6	116	0.14	Scaffold e) to demonstrate thickness of 1.04 mm

Table 9: Scaffold manufacturing parameters and additional notes for figure 57

The PCL concentration was then increased to 30% w/v which made the extrusion process even more controllable and the type of PCL changed to M_n 42,500. The pressure was then increased to 0.71bar and the plotting speed to 120 mm/min, the layer thickness was set at 0.14 mm, the strand distance 0.6 mm with an offset of 0.3 mm. These plotting parameters created the scaffolds that were then used for all the experiments involving PCL scaffolds. The resultant scaffolds can be seen in figure 58.

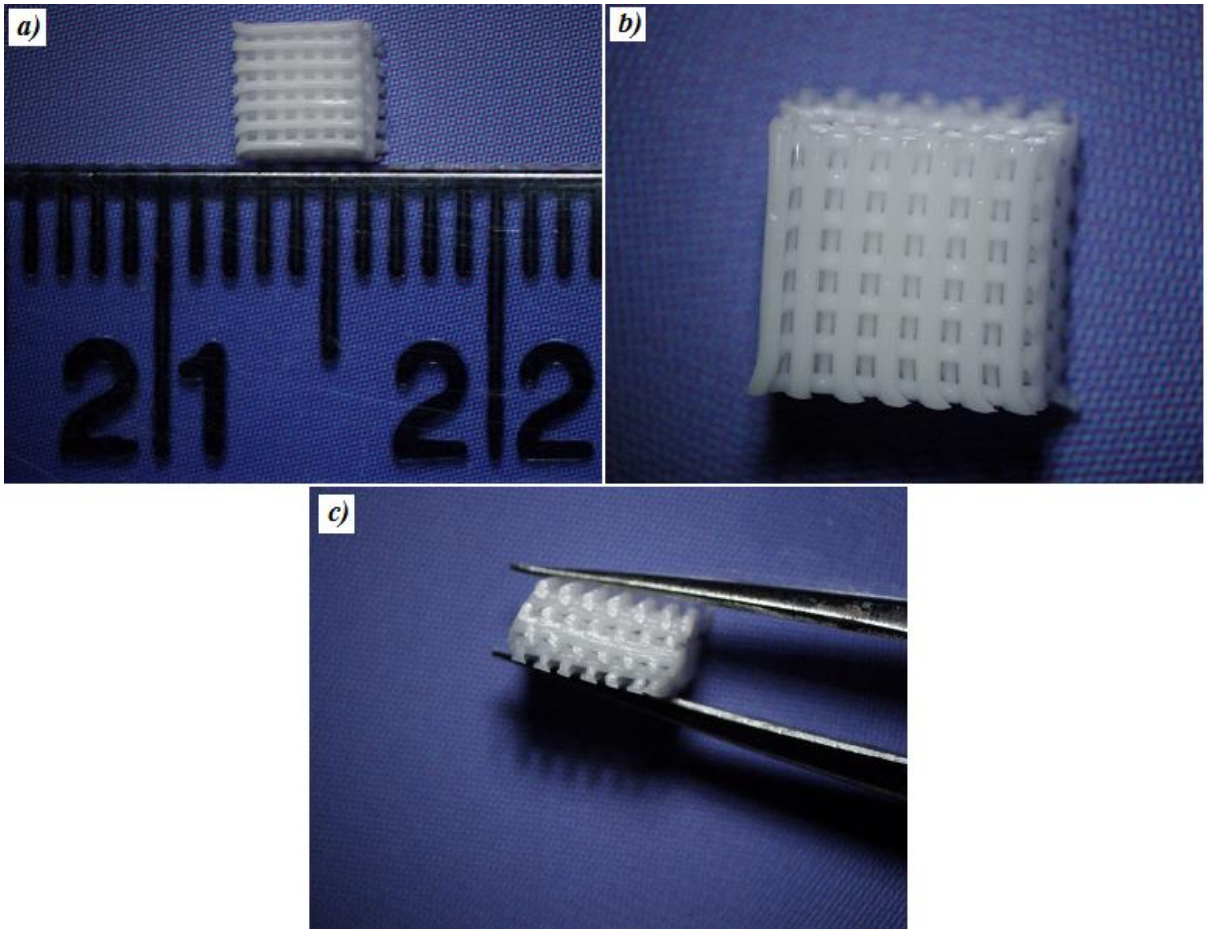

Figure 58: a) PCL scaffold, b) view from the top, c) side view

Once PCL scaffolds were created they were then scanned using an SEM and images taken (Figure 59). It can be observed that the layers do not collapse and that there seems to be satisfactory fusion between layers. The surface of the PCL has a slightly rough appearance compared to the PLGA scaffolds viewed under SEM.

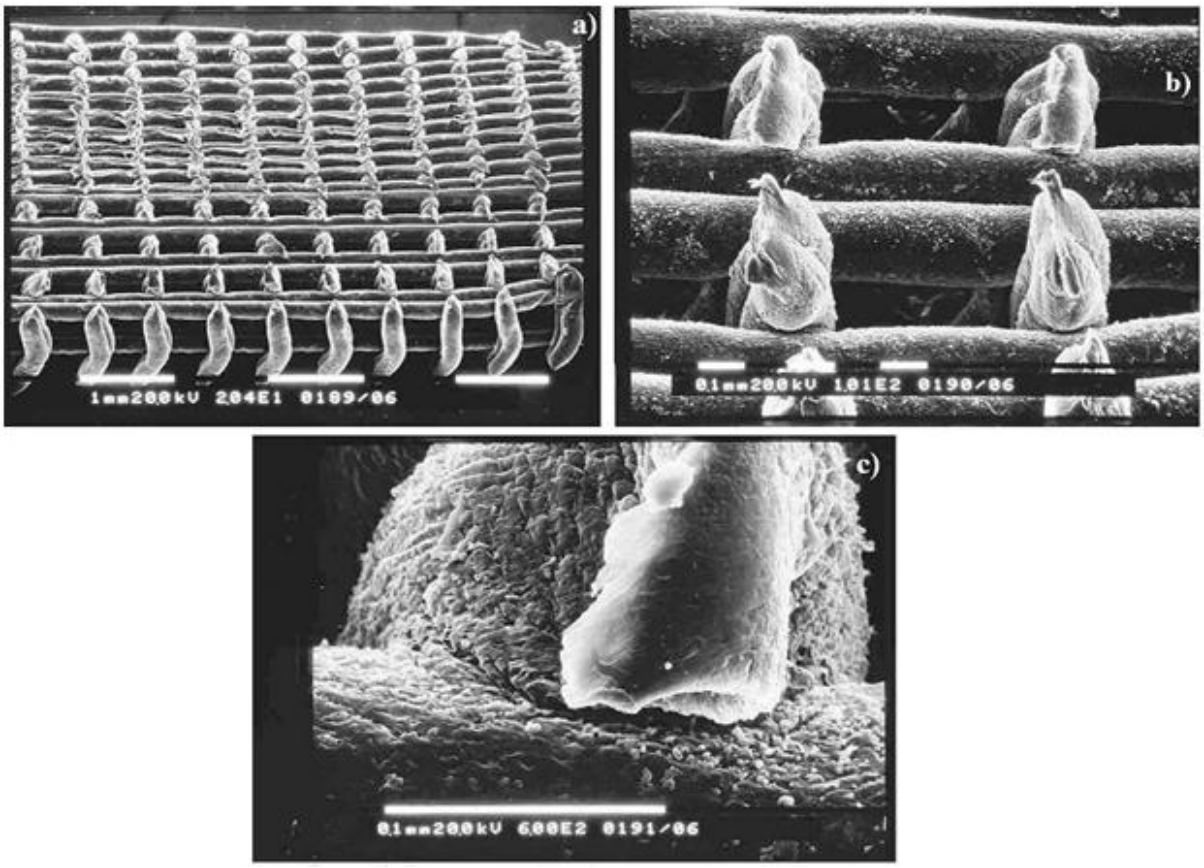

Figure 59: SEM images of PCL scaffolds, a) Double and single layer scaffold, b) Close-up of double layer, c) junction of two layers

Summary of results for scaffold manufacturing and cell type

	Chitosan	**Alginate**	**Gelatin**	**PLGA**	**PCL**
Concentration	3% w/v	3%, 2% w/v	20% w/v	30% w/v	30%
Dissolved in	2% v/v acetic	0.9% saline	Water	Acetic acid	Acetic acid
Extruded in	1% w/v NaOH + ethanol	0.09% $CaCl_2$	Air	IMS	IMS
Cell type used	MG63	MG63	MG63	MG63, MSC	MG63, MSC
Zetos™ bioreactor	No	No	No	No	Yes

Table 10: Summary of results for scaffold manufacture

1.3.6.2 Mechanical testing of Polycaprolactone scaffolds

As can be seen from figure 60, the DSNO had the highest Young's modulus and was significantly different compared to the DSNO45 and the DSO45 scaffolds. This result was expected as the Double Stranded No Offset (DSNO) creates 'columns' throughout the scaffold which bears the load and therefore rendered the scaffold mechanically stronger in the longitudinal direction which in turn increases the Young's modulus. It can also be observed that the scaffolds without the 45º rotation of the layer had lower Young's modulii than scaffolds with a 45º rotation of the layer.

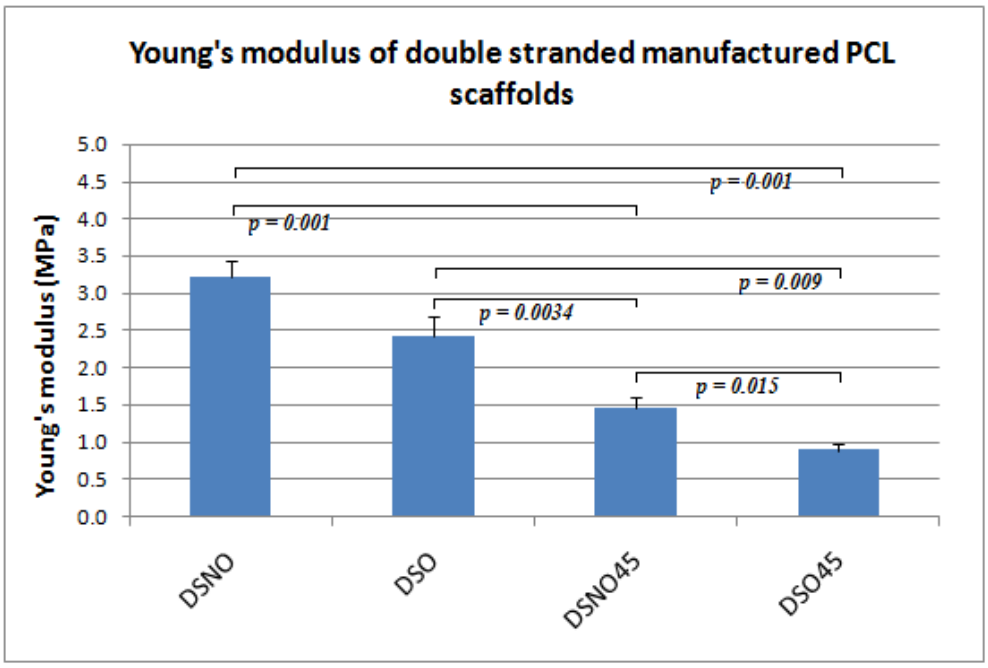

Figure 60: Young's modulus of double stranded manufactured polycaprolactone scaffolds of different geometries

In figure 61, it can be observed that the Single Stranded No Offset (SSNO) had the largest Young's Modulus for the same reasons as mentioned for the double stranded scaffolds. It can also be observed that the SSO had the lowest Young's modulus and the

SSO45 had the second largest. This result is opposite to what occurred in the double stranded scaffold.

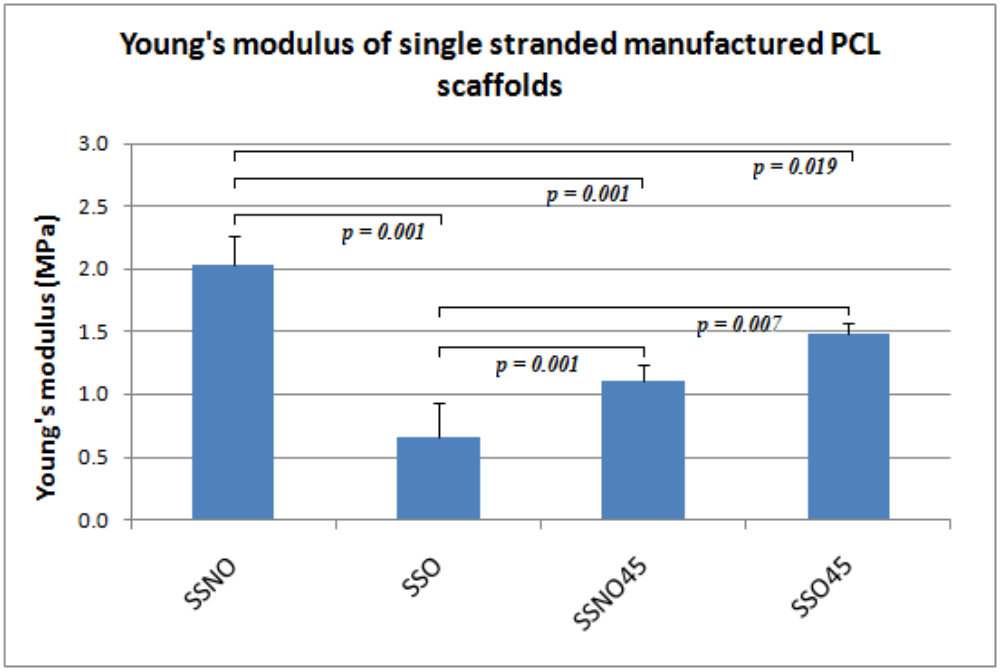

Figure 61: Young's modulus of single stranded manufactured polycaprolactone scaffolds with different scaffold geometries

1.3.6.3 *In vitro* assessment of polycaprolactone scaffolds and marrow stromal cells

As can be observed from figure 62a, Von Kossa staining can clearly be seen which would indicate that under static conditions and in osteogenic differentiation media, MSC are capable of producing calcium deposits. It can also be seen from figure 62b, that cells have been also stained with DAPI which would indicate that some cells were present at the end of the experiment. Figure 62c and 62d, demonstrate that the calcium deposits stained in figure 62a are in fact created by the cells and are not some product of other factors i.e. the gelatin coated PCL scaffold chemically reacting with the osteogenic differentiation media and spontaneously depositing calcium.

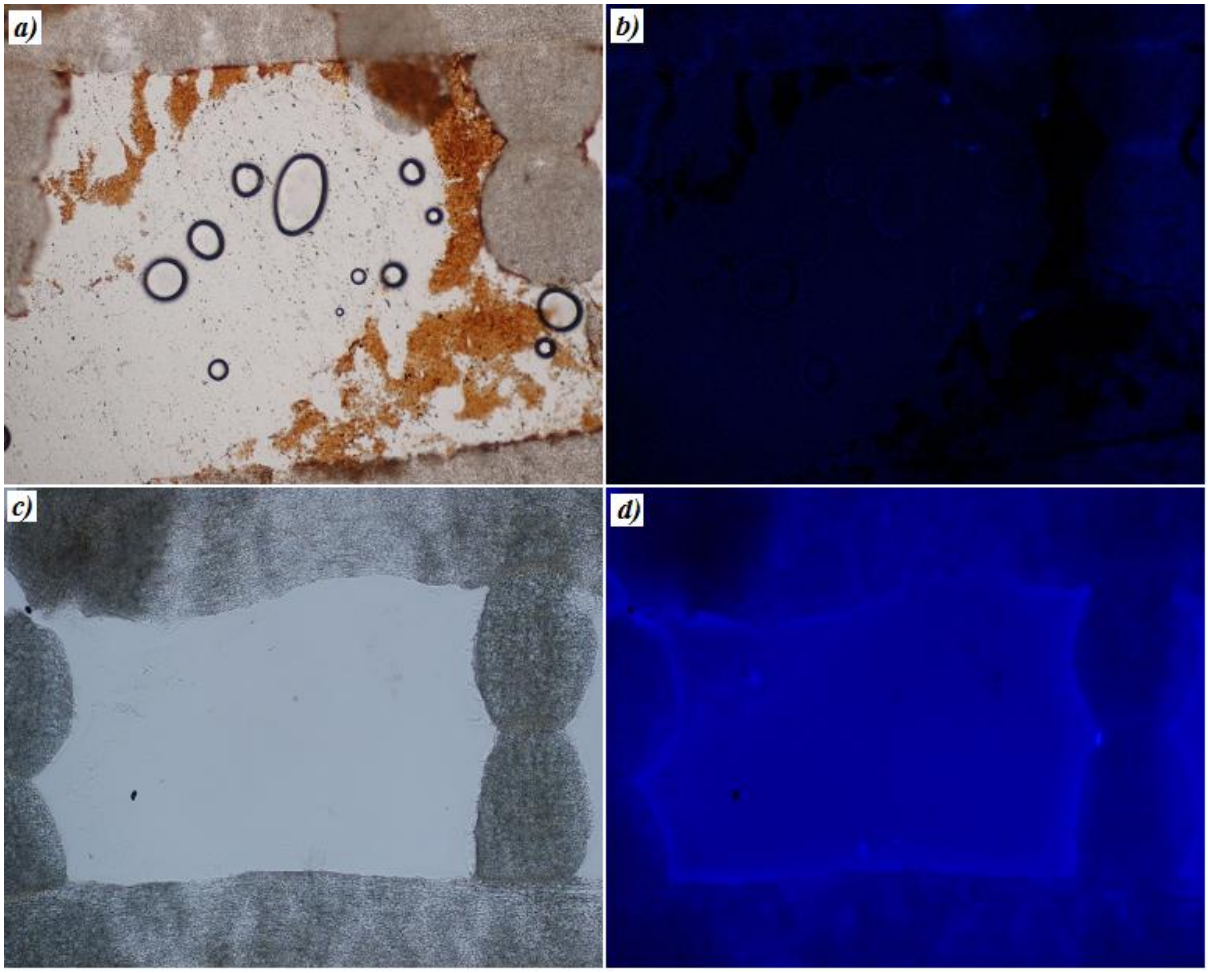

Figure 62: Representative images taken at x20 of MSCs seeded on PCL scaffolds in osteogenic differentiation media stained with a) Von Kossa and b) with DAPI. PCL scaffold not seeded with cells in osteogenic differentiation media stained with c) Von Kossa and d) with DAPI

1.3.6.4 *In vivo* assessment of polycaprolactone scaffolds

As can be seen in figure 63, the scaffolds that were implanted in the calvarial defect and seeded with marrow stromal cells produced calcium deposits which can be seen from the Von Kossa stain visible as brown in figure 63a. The stained calcium was in direct contact with the PCL scaffold visible as the circular shapes. In Figure 63b it can be observed that at the end of the experiment, cells were present around the scaffold which implied that after the three

month experiment *in vivo*, no toxic by-product was leached out of the scaffold. This could entail that further *in vivo* work could take place.

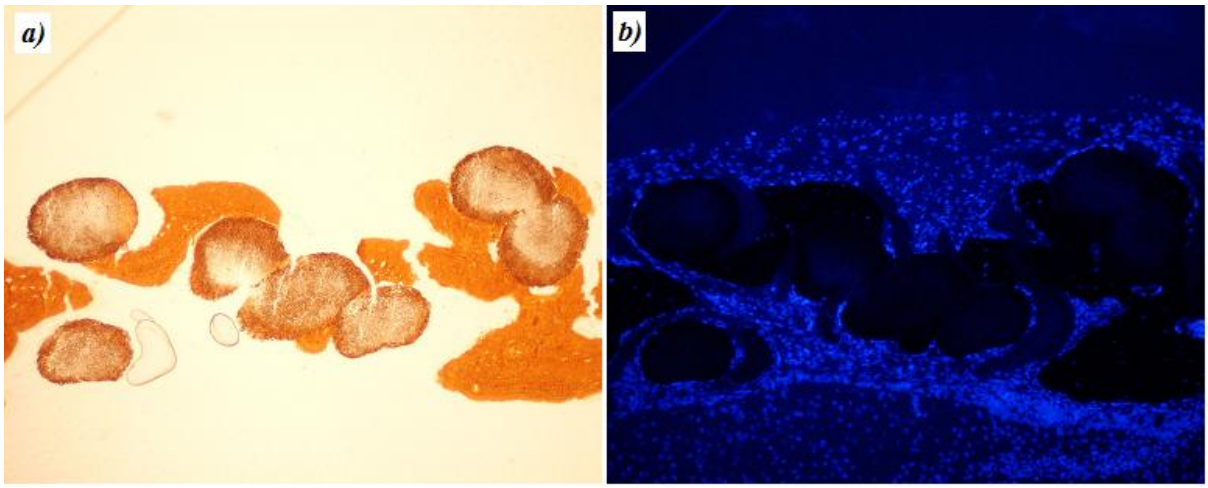

Figure 63: Representative images of polycaprolactone scaffold filling in calvarial defect, a) Von Kossa stain of section, b) DAPI stain of section

1.4 Discussion

1.4.1 Bioplotter accuracy of plotted geometries

Data presented in chapter 1.3.1 demonstrated that the extruded strands created by the Bioplotter are slightly smaller than the inputted values with an average of 2% difference. This shrinkage was likely due to the contraction of the polycaprolactone on solidification. Another factor which may have contributed to the discrepancy of the measurements and the inputted data may have been the measurements of distances using the histomorph programme. The measurements were obtained manually which involved some inaccuracies when measuring the distance between the centre of one strand and the centre of the other. This measuring inaccuracy could be avoided it the histomorphometry programme had an option of creating a straight line between two points. Furthermore, as the plotted strands were three dimensional, obtaining clear and focused pictures on the microscope sometimes proved difficult and may have influenced the quality of the measurements. For these reasons, numerous readings were taken to try and eliminate these possible errors that would affect the measurements of the strand distance and therefore the estimate of the plotting accuracy.

In work performed by other groups where scaffolds were manufactured using a fibre deposition technique similar to the Bioplotter™, accuracy of the extruded strand dimension was also investigated (Malda et al. 2005, Moroni et al. 2005, Woodfield et al. 2004). Woodfield *et al* reported manufacturing scaffolds with theoretical strand distances of 500µm, 1000µm and 2000µm which was the inputted value in the computer aided manufacture (CAM) programme. There was no noted discrepancy between the extruded and inputted values (Woodfield et al. 2004). Work performed by Moroni *et al* and Malda *et al* also reported high accuracy of the distances between the extruded strands (Malda et al. 2005, Moroni et al. 2005). The plotted material poly(ethylene glycol) terephthalate – poly(butelene glycol) terephphalate) (PEGT/PBT) co-polymer used by Woodfield *et at* and Malda *et al*, was not reported to experience shrinkage during extrusion as the polymer used for extrusion was heated and extruded in a viscous liquid form (Malda et al. 2005, Woodfield et al. 2004). In the reported experiments the plotting was not performed in a liquid with the scaffolds manufactured on a glass substrate in air and the extrude polymer was heated. However in

work undertaken by Nelson *et al* where the dissolved polymer PLGA was extruded in a coagulation bath to precipitate out the polymer, reports of reduced cross-sectional area were reported (Nelson et al. 2003).

1.4.2 Chitosan scaffolds

1.4.2.1 Chitosan scaffold manufacture

As can be seen from chapter 1.3.2, chitosan scaffolds were successfully created after a considerable number of trials and after achieving a balance between the extruding pressure and the plotting speed and obtaining a correct concentration of the dispensing material and the dispensing medium.

Three chitosan concentrations were tested, 2% w/v, 3% w/v and 4% w/v dissolved in 2% v/v acetic acid. The 4% w/v concentration of chitosan was too high and the chitosan did not completely dissolve which made it inadequate for extrusion. The remaining two concentrations both completely dissolved and hence were suitable for extrusion but the 3% w/v being more viscous was chosen as it was easier to control the flow of the dissolved chitosan during extrusion. The successful use of 3% w/v chitosan concentration is in agreement with the work done by Ang *et al* as it was the same concentration used (Ang et al. 2002).

The dispensing medium used to neutralise and hence create a gelatinous precipitate of chitosan was made up using a mixture of sodium hydroxide (NaOH) and pure ethanol mixed in a ratio of 7:3. Through a series of smaller tests, the concentration of sodium hydroxide required to yield an effective scaffold was found to be 1% w/v. Higher concentrations such as 2% w/v and 1.5% w/v were tested but they precipitated the chitosan out of solution too quickly and too effectively not allowing subsequent layers to adhere to the already deposited chitosan layer. Lower concentrations of 0.5% w/v and 0.75% w/v were also tested however they produced the opposite effect of the higher concentrations and did not solidifying fast enough resulting in a distorted and non-uniform scaffold. These observations were also reported by Ang *et al* and the sodium hydroxide concentration used was not specified

however was within a range of 0.75 % w/v and 1.5 % w/v (Ang et al. 2002). These findings reinforced the results generated by the experiments discussed in this thesis. The only other paper that has reported this chitosan manufacturing technique was Ng *et al* who seeded the scaffolds with human dermal fibroblasts (Ng et al. 2004a), however this was part of the same team as Ang *et al.*

The final parameters used to create a scaffold with a 250 µm needle were dispensing pressure of 1.20 bar, dispensing speed 120 mm/min, initial dispensing height of 500 µm, layer thickness of 280 µm and strand distance of 630 µm. The parameters used by Ang *et al* were dispensing pressure 3 bar, dispensing speed 360 mm/min and initial dispensing height of 200 µm but these differences were expected as the extruding needle used by Ang *et al* was a 30 gauge needle which represents a 150 µm internal diameter. The finer needle tip explains the reason for the need of a higher extruding pressure which directly influences the dispensing speed. Due to the finer strand being extruded, the starting height was also lower.

Several papers reported in the literature manufactured chitosan beads cross-linked with TPP also reported that this cross-linking agent was more effective in retaining the shape of the bead upon manufacture (Durkut et al. 2006, Shu and Zhu 2002, Zhang et al. 2002). In the work produced by Shu and Zhu, it was reported that the TPP treated beads exhibited increased mechanical strength compared to the other cross-linked beads after being lyophilised. This was observed in the manufactured chitosan scaffolds however was not investigated further as the scaffolds would not be used dry but in a wet state. It was discovered from the in vitro work (see paragraph 1.3.2.2.) that chitosan scaffolds cross-linked with TPP in cell culture media lost all mechanical strength after 14 days and therefore would render them useless as load bearing scaffolds. In the literature involving chitosan crosslinked with TPP, no reference to the mechanical strength was reported once the chitosan had been in a wet state furthermore the main application of the chitosan treated with TPP was as a drug delivery system (Dung et al. 2007, Shu and Zhu 2002, Vodna et al. 2007). This would imply that scaffolds manufactured using chitosan treated with TPP are not capable of being manufactured into load bearing structures, however there have been studies where chitosan has been used in combination with hydroxyapatite (Oliveira et al. 2006), calcium phosphate

(Zhang and Zhang 2001), gelatin (Liu et al. 2004, Xia et al. 2004) and poly(vinyl alcohol) (Park and Kim 2006) to increase the mechanical properties of the structure.

1.4.2.2 *In vitro* chitosan scaffold and MG63 cells

The MG63 cells were seeded statically at a density of 250,000 cells per scaffold. As can be seen from chapter 1.3.2., cell adhesion to the scaffold was observed as shown by the DAPI stained nuclei. This indicated that there was potential for cells survival on the chitosan scaffold and therefore possible cell differentiation. Several studies by other groups have also demonstrated that cells are capable of adhesion (Ang et al. 2002, Di Martino et al. 2005) and proliferation on chitosan (Nettles et al. 2002, Xia et al. 2004). Cell attachment was reported by Ang *et al* who had seeded human osteoblasts onto the manufactured chitosan scaffolds and observed the presence and adhesion of cells after four weeks on the scaffold using a scanning electron microscope. However interestingly in the study undertaken by *Ng et al*, very few dermal fibroblasts cells were present at the end of the 3 week experiment (Ng et al. 2004b).

The demonstration of cellular adhesion to the scaffold was a positive outcome however after seven days, when an attempt was made to transfer the scaffold to a Petri dish for staining; the chitosan scaffold fell apart and had lost all of its structural strength that was present at the start of the experiment. Even the scaffolds that were treated with pentasodium tripolyphosphate also lacked any structural strength. The scaffolds were then stained in the wells after removal of the cell culture media. This ruled out any future work with chitosan as a scaffold material to create a load bearing structure using the scaffold manufacturing method described in chapter 1.2.2.

1.4.3 Alginate scaffolds

1.4.3.1 Alginate scaffold manufacture

As can be seen from chapter 1.3.3., alginate was successfully used to manufacture a scaffold. The paper that the work was based on was performed by Khalil *et al* (Khalil et al.

2005) and is to the author's knowledge, the only paper where alginate has been extruded to produce a 3D scaffold. The sodium alginate was dissolved using sterile distilled water in several different concentrations from 2% w/v, 3% w/v and 4% w/v however the 3% w/v alginate solution was used for scaffold manufacture as it was more viscous and therefore would render the extrusion process more controllable. The same concentration was used by Khalil *et al* for alginate scaffold manufacture (Khalil et al. 2005). The optimal dispensing solution was created by testing various calcium chloride concentrations that ranged from 0.09% w/v to 5% w/v by attempting to plot a scaffold. Higher concentrations i.e. 2% w/v to 5% w/v solidified the alginate too quickly and also had a secondary effect where the solidified strand would float to the surface of the bath however this was not reported by the work performed by Khalil *et al*. The calcium chloride concentration was then lowered to 0.09% w/v and 1% w/v to observe the consequences that this would have on the solidification rate and the floating effect of the strands. Reducing the calcium chloride concentration helped in several ways to reduce the solidification rate and enabled a second layer to be plotted and also delayed the floating effect, which also allowed a second layer to be plotted but when a third layer was plotted, the scaffold again detached from the substrate and floated to the surface. This problem was investigated further by attempting to anchor the strands to the substrate by changing the material of the substrate. Several materials were tested including Petri dish plastic, a glass slide, aluminium and polycarbonate but these attempts were unsuccessful. The substrates were then coated with Vaseline™ which would roughen the surface and aid strand adherence but this did not improve anchorage of the initial strand. The problem was finally overcome by developing a plotting technique that was named the 'shallow bath' technique. This process involved having the plotted strand solidifying at the surface of the bath and when the layer was finished and the next was to be created, a few drops of calcium chloride were added so that this layer was being solidified at the surface. This technique was then repeated for every new layer. The three different alginate concentrations were successfully plotted into scaffolds using the 'shallow bath' technique. After several intermediate experiments, the concentration of calcium chloride used was 0.09% w/v as it would solidify the strands slow enough to enable the layers to fuse and also the scaffold could be built up to five layers high before it started detaching from the substrate.

Once the scaffolds were completed, they were transferred to a 1% w/v calcium chloride bath for further solidification.

In the study performed by Khalil *et al* and the scaffold manufacturing parameters reported in section 1.2.2.3, several similarities were observed. The alginate concentration used for extrusion (3% w/v alginate aqueous solution) and the needle internal diameter (200μm) were the same, however the calcium chloride concentration used to cross-link the alginate was 5% w/v (Khalil et al. 2005) compared to 0.09% w/v reported in 1.2.2.3. This large difference in calcium chloride concentrations suggests that the chemical composition of the alginate used in the study performed by Khalil *et al* was different to the alginate supplied by Sigma, UK.

1.4.3.2 Alginate beads and marrow stromal cells

Alginate beads were created that contained marrow stromal cells. The cells present in the scaffolds were stained with DAPI and PI and a cell count was performed to determine whether there is a difference between 2% w/v and 3% w/v alginate. From section 1.3.3 it was observed that in the 2% w/v alginate beads, statistical significance was observed between day 0 and day 2, day 7, day 14 and day 21. This implied that there was a significant drop of live cells at each time point compared to day 0 however in the 3% w/v alginate beads, no statistical significance was observed between any of the time points. This result suggests that the number of live cells does not statistically decrease during the 21 days which would imply that the cells encapsulated in the 3% w/v alginate beads had a better survival rate than in the 2% w/v alginate. This was supported by other work in the literature where 3% w/v alginate was used. In work performed by Khalil *et al* where human fibroblast cells were encapsulated and extruded in the alginate, cell survival was reported to be at 85% after 7 days encapsulation (Khalil et al. 2005). This concentration was also used in work performed by Wang et al, where murine bone marrow cells survived after 12 days encapsulation (Wang et al. 2003b). However the main difference was that the alginate used in both reported cases was an ultra pure form supplied by ProNova Biomedical. In other work reported in the literature, 2% w/v, 3% w/v and 5% w/v alginate were compared and it was determined that they had the

2% w/v and 3% w/v had similar properties when cells were encapsulated with 85% cell viability at the end of the experiment compared with 70% cell viability in the 5% w/v alginate (Wang et al. 2003a). In other studies, 2% w/v alginate concentration was used and a good cell survival was reported (Kong et al. 2003, Simmons et al. 2004) however the alginate underwent an irradiation step to reduce the molecular weight and the alginate used was of a purer grade. The alginate beads were not sectioned due to technical reasons.

1.4.4 Gelatin scaffold

1.4.4.1 Gelatin scaffold manufacture

Gelatin scaffolds were not successfully manufactured by extrusion due to several factors. Firstly gelatin was dissolved in sterile distilled water at various concentrations ranging from 10% w/v to 60% w/v. At concentrations between 30% w/v and 60% w/v the gelatin never completely dissolved rendering it inadequate for extrusion. Concentrations below that range did eventually dissolve when heated but when allowed to reach room temperature, the gelatin would solidify. This meant that the gelatin needed to be heated using the syringe heating jacket to keep the gelatin in a liquid state which occurred at around 40ºC. Once the gelatin reached its liquid state a dispensing needle was fastened via a luer lock to the syringe body and the gelatin was ready to extrude. The 10% w/v and 15% w/v concentrations were heated to their melting points however the gelatin solution became very liquid and therefore exited the needle tip without any pressure being used. The concentration was increased to 20% w/v gelatin which was viscous enough not to exit the syringe under its own weight and hence was viscous enough to be controlled while plotting. During the extrusion of the gelatin strand, the gelatin as it was being forced out of the needle tip would cool down and solidify in the needle which blocked the flow of the extruding material. This was dealt with by producing a wire heater around the needle tip (see chapter 3.4.1). This helped with the fluidity of the gelatin but created other problems that involved the liquid gelatin solution on extrusion being in direct contact with the heating wire which evaporated the water leaving solid gelatin that disrupted the flow. Various attempts were tested to minimise this effect by raising the needle heating coil but this then caused the gelatin to solidify in the needle tip. Heating gelatin and

extrusion was then disregarded as a viable method of manufacturing a gelatin scaffold and to the author's knowledge, no scaffolds have been created by extrusion of heated gelatin in the literature, however other gelatin scaffold fabrication methods were observed. The two mainly discussed techniques for gelatin scaffold manufacture in the literature were electrospinning (Thomas et al. 2007, Venugopal et al. 2008) and gelatin sponges (Hong et al. 2005, Kang et al. 2006, Rohanizadeh et al. 2008) however, scaffolds manufactured using the electrospinning technique used a polymer-gelatin blend, such as polycaprolactone (Chong et al. 2007, Venugopal et al. 2008), polyglyconate (Thomas et al. 2007), poly(lactide-co-glycolide) (Li et al. 2006) to increase the mechanical properties. In work performed by Hong *et al* and Rohanizadeh *et al*, the gelatin sponges used were commercial products (Gelfoam) and not manufactured by the groups however in Kang et al, gelatin scaffolds were manufactured using the particle leaching technique (Kang et al. 2006). This demonstrates that in order to manufacture gelatin scaffolds, electrospinning or particle leaching technique could be used however heated gelatin extrusion technique was unsuccessful.

The next technique considered was to extrude a lower concentration of liquid gelatin into a cross-linking solution such as glutaraldehyde or transglutaminase (McDermott et al. 2004). This was first attempted by manufacturing gelatin scaffold into a bath of 5U transglutaminase however, the desired supporting effect of the solution was not observed during strand extrusion. Cross-linking of the gelatin strands was observed however this started occurred after 4 minutes (Bertoni et al. 2006) which was too lengthy as the manufacture of the second layer had already commenced. Glutaraldehyde was also considered however this was deemed toxic to cells (Khor 1997) and due to its toxic nature considerable improvements to the Bioplotter™ would be required and a fume extractor for the gluteraldehyde fumes would need to be installed.

1.4.4.2 Gelatin cross-linking and cells

Data presented in section 1.3.4.2, demonstrated that significantly more cells were present on the transglutaminase cross-linked gelatin compared to the gluteraldehyde crosslinked gelatin which was due to the toxicity of the latter cross-linking agent.

The different effects between the two cross-linking agents was also reported in a study investigating the cellular effects of transglutaminase and gluteraldehyde (Bertoni et al. 2006, Chau et al. 2005, Yung et al. 2007). This result was not surprising as gluteraldehyde is a fixative and toxic to cells in high concentration (Bertoni et al. 2006). It can also be observed that the gelatin treated with transglutaminase had a higher cell count than the non cross-linked control group this may have been associated with a higher proliferation rate during the experiment. Work undertaken by Chau *et al* demonstrated that human osteoblasts seeded on transglutaminase treated gelatin had an increased rate of proliferation compared to non-treated gelatin. From these results, it can be concluded that 5U transglutaminase was a less toxic cross-linking agent as statistical significance was observed between the 5U transglutaminase group and the two concentrations of gluteraldehyde and the control. However work produced by Ito et al, compared three different concentrations of transglutaminase (0.5U, 1U and 2U) and reported that 1U transglutaminase was the optimum concentration to cross-link 5% w/v gelatin to increase fibroblast proliferation (Ito et al. 2003).

1.4.5 Poly (lactide-co-glycolic) acid (PLGA) scaffolds

1.4.5.1 PLGA scaffold manufacture

PLGA scaffolds were successfully created by dissolving the polymer in glacial acetic acid and creating a 30% w/v solution and extruding it in a bath of industrial methylated spirit (IMS). Several different solvents were used to dissolve the PLGA including chloroform (Nelson et al. 2003), acetone (Williamson and Coombes 2004) and acetic acid (Blanco-Prieto et al. 2000, Godbee et al. 2004, Notin et al. 2006) and coagulation baths were also tested as can be seen in chapter 1.3.5. In work presented by Nelson *et al*, fibres were created using a wet spinning technique where PLGA was dissolved in chloroform at a concentration of 20% w/v and extruded into a tube containing the coagulation agent isopropyl. When scaffolds were manufactured using the same solvent and coagulation bath, strands were created which was also obtained in Nelson *et al* however when attempts were made to extrude a second layer, the latter collapsed into the gaps of the initial layer. In view of this, PLGA was then dissolved in acetic acid (Blanco-Prieto et al. 2000) and extruded into IMS which produced

structurally sound scaffolds. The SEM pictures also demonstrated that the created scaffold had good geometry, it also showed that there was good fusion between layers and that the surface of the PLGA scaffold strands were smooth which was also observed by Nelson *et al* even though a different solvent and coagulation bath reagent was used (Nelson et al. 2003).

The degradation of PLGA scaffolds as seen in chapter 1.3.5 conformed with other work in the literature (Chen et al. 2004, Lu et al. 2000). The experiment performed in this thesis lasted 3 weeks however in previous studies degradation of PLGA was not observed until week 10 (Chen et al. 2004, Lu et al. 2000). This explains why no significant decrease in weight was observed during the three week long experiment. An issue with the experiment was that when the scaffolds were cut down to size, the smaller scaffolds were not identical. This explains why the mean weight of the scaffolds at day 21 where greater that at any other time point except day 0.

This experiment showed that there was no degradation during the 21day experiment and in order to witness degradation, the experiment would have to last a minimum of 10 weeks as was reported in the literature.

1.4.5.2 PLGA and marrow stromal cells

As seen in paragraph 1.3.5.4, the standard curve generated by using DNA from herring testis yielding a linear curve which was what previous literature suggested (Rago et al. 1990). Freezing cell cultures after incubation yielded a linear relationship between fluorescence and cell number. The freeze – thaw technique did not require any mixing as the cells are lysed and created a crude cellular homogenate (Schirmer et al. 2004). The processing time was minimal and the reactions did not require any dangerous reagents. The tissue culture plates were stored in -80ºC and therefore experiments can be batched and analysis performed simultaneously eliminating any inaccuracies that may occur between experiment analyses (Rago et al. 1990). The cell adhesion and viability comparison of the two scaffold materials yielded different results. From the DNA assay, the number of cells that remained attached to the well was greater with the PLGA scaffold compared with the PCL scaffold. This could

mean that more cells were attached to the PCL scaffold compared to the PLGA scaffold. This was an interesting and positive outcome regarding the cell adhesion to polycaprolactone coated with gelatin. In work performed by Chastain *et al* where the osteogenic potential of PLGA and PCL was compared, marrow stromal cells seeded on PLGA scaffolds were reported to significantly upregulate osteocalcin gene expression levels (noncollagenous protein found in bone and dentin and secreted by osteoblasts) and in contrast osteocalcin was markedly downregulated in the PCL scaffold (Chastain et al. 2006), however no significant difference was observed on the number of cells that attached to the two different scaffold materials. This could be due to the manufacturing process of the scaffolds which involved a particle leaching technique which creates randomly distributed pores which may have trapped the cells during seeding and therefore not recorded a difference of cell number and the two types of polymers.

1.4.6 Polycaprolactone scaffolds

1.4.6.1 Polycaprolactone scaffold manufacture

As with PLGA various solvents and coagulation baths were tested to determine which combination produced the most geometrically sound scaffolds. It was concluded that the best results were obtained by dissolving the PCL in acetic acid (Sarasam and Madihally 2005) in order to yield a concentration of 30% w/v. The dissolved polymer was then extruded in a bath of IMS to precipitate out the PCL. These parameters were concluded after a lot of iterative work as can be seen in section 1.3.6.

The first test involving polycaprolactone (PCL) was performed by dissolving the polymer (M_n 80,000) in chloroform and extruding it into isopropyl alcohol (Nelson et al. 2003). The initial results were promising as strands were created and this showed that this technique had potential. After numerous attempts where changes were made to the polymer average molecular number weight, concentration and with changes to the pressure and plotting speed it was concluded that this combination of solvents would not yield a satisfactory scaffold (Figure 52). The solvent was then changed to acetone (Williamson and Coombes 2004)

however scaffolds manufactured with this solvent were not created correctly as the geometry of the strands was distorted. It was also discovered that the polymers precipitated out after several hours and created a white cloud in the stock solution. This was unsatisfactory as during extrusion, the precipitate would affect the plotting parameters and would alter the concentration of the plotting solution.

After numerous attempts the most successful results were obtained with acetic acid (Sarasam and Madihally 2005) and IMS. As can be seen from figure 58, structurally the scaffold displayed no collapse of the any layers and there was clear fusion of layers (Figure 59) which was reinforced by the SEM images. Figure 59c shows that the surface is rough which might be an advantage for cell adhesion which was mentioned in the literature regarding polycaprolactone scaffolds (Ciapetti et al. 2003). Alternative manufacturing methods for polycaprolactone scaffolds have been reported in the literature, these included electrospinning (Khil et al. 2005, Ma et al. 2005, Thomas et al. 2006), particle leaching (Hou et al. 2003), selective laser sintering (Tan et al. 2005a, Williams et al. 2005) and fused deposition modelling (Ramanath et al. 2008, Shor et al. 2007, Zein et al. 2002) however electrospinning and particle leaching yields random scaffold geometries and pore size cannot be controlled in contrast selective laser sintering and fused deposition modelling created well defined scaffold geometries with user defined scaffold parameters (Hutmacher 2001).

1.4.6.2 Mechanical testing of manufactured polycaprolactone scaffolds

As can be seen from the results section 1.3.6.2, the double stranded (DSNO) with a Young's modulus of 3.2 ± 0.22 MPa and the single stranded with no offset (SSNO) with a Young's modulus of 2.0 ± 0.12 MPa had the highest Young's modulus in their respective groups (Moroni et al. 2006, Zein et al. 2002). This was expected as both the scaffolds with 'no offset' created 'columns' throughout the scaffold which bore the load and therefore rendered the scaffold mechanically stronger in the longitudinal direction which in turn increased the Young's modulus. It was also observed that the double stranded scaffolds with offset and with the 45º rotation of the layer (DSO45) had the lowest Young's modulus in that group however the opposite was true for the single stranded scaffold with offset and a 45º

rotation of the layer (SSO45) where it had the second highest Young's modulus value. This result is due to the scaffold being double or single stranded. In the double stranded scaffolds (DSO45) because there are two layers extruded on top of each other this effectively creates a taller strand and therefore a taller layer, this then implies that there are less changes in layer direction, i.e. from 0º to 45º to 90º etc… which meant that when the scaffold was compressed in a vertical direction, naturally the scaffold will also rotate and because there were less changes in layer direction, this weakens the scaffold which lowers the Young's modulus (Moroni et al. 2006). However in the single stranded scaffold (SSO45), these changes in layer direction occur at every layer rendering the scaffold more resistant to rotations of the layers and therefore when compressed the Young's modulus remained higher.

It was also observed that the double stranded with offset (DSO) had the second highest Young's modulus however the single stranded offset (SSO) had the lowest in its group. This can be explained as in the double stranded scaffold with offset (DSO) the double layer strengthens the scaffold however in the single stranded with offset (SSO) the single layer in weak when compressed which in turn reduces the Young's modulus.

The Young's modulus obtained from the mechanical testing of the various scaffolds gave in some cases similar results to what exists in the literature. In work performed by Shao *et al*, particle leaching was used to obtain a porous polycaprolactone scaffold which yielded a scaffold with a Young's modulus of 0.81 MPa (Shao et al. 2006a). These scaffolds involved dissolving the polymer in a solvent and adding the particles to be leached out and were intended for the regeneration of cartilage. In work published by Thomas et al, the electrospinning technique was used to generate scaffolds with a Young's modulus of between 6.12 MPa and 11.93 MPa (Thomas et al. 2006). In work published by Zein *et al* and Hutmacher *et al*, fused deposition modelling was used to create scaffolds which involved heated polycaprolactone and extruding it layer by layer into a 3D scaffold. The mechanical properties of the single strand no offset scaffold (SSNO) was reported to be 69.2 ± 3.6 MPa and when a rotational layer was introduced, the Young's modulus was reduced to 47.1 ± 1.9 MPa (Zein et al. 2002). In work presented by Shor *et al*, fused deposition was also used and single stranded scaffolds manufactured with Young's modulus of 30 MPa and it was also reported that the addition of hydroxyapatite to the PCL significantly increased the Young's

modulus to 76 MPa (Shor et al. 2007). In the published work by Thomas *et al* and Shao *et al*, the PCL was dissolved in a solvent in order to manufacture 3D scaffolds which mechanically alter the properties of the PCL therefore reducing the Young's modulus of the scaffolds. This result was observed in the work presented in this thesis. In comparison work by Zein *et al*, Hutmacher *et al* and Shor *et al*, the PCL was heated and extruded in a molten state which did not alter the mechanical properties. This was also observed and results can be seen in chapter 2. It has also been reported that the Young's modulus of trabecular bone from human mandibles ranged from 3.5 to 125 MPa (Misch et al. 1999) therefore from the mechanical characterization, it can be concluded that the PCL scaffolds have the potential to be applied in tissue engineering of bone and cartilage.

1.4.6.3 In vitro assessment of polycaprolactone scaffolds and marrow stromal cells

As can be observed from section 1.3.6.3., Von Kossa staining was clearly seen to be present on the section of the scaffold. This demonstrates that MSCs are capable of forming calcium deposits under static conditions and in osteogenic differentiation media. The section stained with DAPI also demonstrates that cells were present at the end of the experiment. Similar results showing good biocompatibility of PCL in combination with human cells have been observed by other groups (Marra et al. 1999, Mondrinos et al. 2006). Osteoblastic differentiation of MSCs seeded on a PCL scaffolds was observed after 15 days (Endres et al. 2003). In another group electrospun PCL scaffolds seeded with MSCs mineralized and extra cellular matrix was observed after 4 weeks (Shin et al. 2004). In work presented by Darling and Sun, it was reported that PCL scaffolds manufactured by precision extrusion deposition supported the proliferation of cultured rat cardiomyoblasts, however no detailed analysis of cellular metabolism and proliferation were not provided (Darling and Sun 2004). Hutmacher *et al* used primary human fibroblasts and human osteoprogenitor cells to demonstrate the biocompatibility of PCL scaffolds however the capacity of these scaffolds to induce bone formation was not addressed (Hutmacher et al. 2001b). Marra *et al* concluded from their two-dimensional studies that PCL is superior to poly(lactide co glycolide) (PLGA) for bone cell

growth (Marra et al. 1999). It can be conclude from the data that PCL scaffolds demonstrated good biocompatibility for hard tissue formation when seeded with MSC.

1.4.6.4 In vivo assessment of polycaprolactone scaffold

As can be observed from section 1.3.6.4., the scaffolds implanted into the calvarial defect showed deposits of mineralized residues, as shown by the Von Kossa stain which further confirmed that the 3D environment was conducive to osteogenesis which has also been observed in other studies (Schantz et al. 2003). The scaffolds provided a suitable environment for the MSC to differentiate into osteoblasts in the absence of differentiation medium as in the *in vitro* experiment. A similar enhanced osteoblast differentiation was observed in polymer scaffolds (Ishaug et al. 1997). Previous reports showing that PCL scaffolds fabricated using various manufacturing processes displayed good biocompatibility *in vivo.* Williams *et al*, used selective laser sintering (SLS) to manufacture PCL scaffolds that were seeded with human fibroblasts genetically modified to express bone morphogenic protein-7 (BMP-7) and implanted into subcutaneous pockets of immunocompromised mice. These scaffolds supported the development of new bone over a period of 4 weeks as demonstrated by μCT detection of mineralized tissue (Williams et al. 2005). Experiments involving PCL scaffolds have been reported in the literature where models of human phalanges and small joints were seeded with bovine periosteum cells and implanted in nude mice (Landis et al. 2005). In the 15 month long study performed by Landis *et al*, bone formation was observed and no toxic effect of the PCL scaffold was reported. *In vivo* repair of osteochondral defects have also been reported in the literature (Shao et al. 2006b, Swieszkowski et al. 2007) with positive results. Shao et al demonstrated that a hybrid PCL scaffold/cell construct could promote functional and structural repair of a critical size osteochondral defect in the first 3 months. It can be conclude from the current work, that the PCL scaffold demonstrated promising matrix for bone regeneration.

1.5 Summary

A scaffold manufacturing technique using the Bioplotter™ was investigated and successfully applied in this research to produce novel 3D scaffolds with fully interconnected channel networks and highly controllable geometry. Several different materials including chitosan, alginate, poly(lactide-co-glycolide) (PLGA) and polycaprolactone (PCL) were effectively manufactured into scaffolds by a computer controlled extrusion and deposition method. Scaffolds were made of layers of aligned microfilaments within a geometrical 3D structure. Analysis of the mechanical properties of the PCL scaffolds contributed to a better understanding of the nature of the different designs. The mechanical properties were found to generally depend on the layer pattern which was in agreement with theoretical concepts on structural properties. The efficacy of scaffold manufacturing technique has been proven by scaffold design and fabrication and the results of the *in vitro* and *in vivo* studies demonstrate good biocompatibility.

Chapter 2.

Finite element method and analysis

2.1 Introduction

Mechanical strain is an important consideration when trying to induce cell differentiation and it would be very useful to control and measure strain in scaffolds. This would enable the optimum scaffold geometry and material to be determined. Several techniques exist to measure strain, the most common is the strain gauge which relies on a small metal foil pattern which is attached securely to the surface of the material to be measured, when deformation occurs, the resistance of the metal foil changes and hence strains can be measured. This technique has been used on numerous occasions to determine the strains generated during, bone remodelling (Szivek and Magee 1989), loading of the temporomandibular joint (Throckmorton and Dechow 1994), in vivo axial strain of a human femur (Aamodt et al. 1997) and tibia (Funk and Crandall 2006). However due to the size of the strain gauge which is approximately 10mm x 10mm, it is not a suitable method for measuring strains generated in scaffolds.

Another method used for measuring strain is the laser speckle interferometry. This technique relies on the interferometric properties of coherent light (laser) to measure the direction and extent of deformations occurring in an object when a force is applied to it and has been used to measure strain in mandibular joints, long bones and the skull (Horta et al. 2003, Kragt et al. 1982, Roman et al. 1999, Sanghavi et al. 2004, Zaslansky et al. 2005). This technique is highly sensitive and is able to measure small deformations (Verrue et al. 2001). Unfortunately due to the inherent nature of the technique, strains generated inside the scaffold could not be measured as the laser beam could not reach the scaffold strands situated at the centre.

However, finite element method (FEM), which has been successfully applied to the mechanical study of stresses and strains in engineering, renders it possible to transpose the technique to a biomechanical situation. An important advantage of this technique is the ability to determine the strains and stresses that occur inside a scaffold during loading and simulate various loading situations once an adequate finite element model is created. FEM has been used to determine the mechanical properties of library of various scaffolds (micro-structures) that can be combined according to the mechanical function required (Wettergreen

et al. 2005). Young's modulus of porous calcium phosphate scaffolds (Lacroix et al. 2006) and an extruded hot melt polycaprolactone scaffold (Fang et al. 2005) were reported. Finite element analysis has also been reported to determine the stresses and strains in an *in vivo* cyclically compressed poly (lactide-co-lactide) scaffold (Duty et al. 2007).

2.1.1 Basic concept and background of the finite element method

Finite element analysis (FEA) is a computer based numerical technique while finite element method (FEM) is considered as the methodology by which the analysis is converted into a set of simultaneous equations.

The finite element method of analysis is a very powerful and modern computational tool as it is non-destructive analytical method that yields very useful insights into structures. The method has been used globally during the past 50 years to solve very complex engineering problems, particularly in the structural engineering (Sarkani et al. 2000, Thevendran et al. 1999, Yang et al. 2000), automotive (Alaylioglu and Ali 1978, Rao and Muthuveerappan 1993) and aircraft industry (Giglio 1999). It has now gained wide acceptance in many other disciplines such as thermal analysis (Jaafar et al. 2007), fluid mechanics (del Coz Diaz et al. 2007), electromagnetic (Garcia-Castillo et al. 2005), biomechanical analyses (Huiskes and Chao 1983, Kolston and Ashmore 1996, Korioth and Versluis 1997a) and physical anthropology (Ryan and Rietbergen 2005). The basic idea of the finite element method is to solve a complex problem by simplifying it. Because the actual problem is simplified and assumptions are made, only an approximate solution is created however this can be refined by using more computation effort.

Although the name finite element method has only recently been utilised, the concept has been used for several centuries. Ancient mathematicians found the circumference of a circle by approximating it as a polygon (Figure 64). By considering the polygon $S^{(u)}$ one can obtain an upper bound and by considering $S^{(l)}$ one can obtain the lower bound of the circle circumference S. As the number of sides of the polygon increase, the approximate value converges to the true value. These characteristics hold true in general finite element method.

An approach similar to finite element method which involves the use of continuous functions defined over triangular regions was first suggested by Courant in 1943 in applied literature of mathematics (Courant 1943). The finite element method that is known today, was presented by Turner *et al* in 1956 in which the application of simple finite elements for the analysis of aircraft structure was suggested (Turner et al. 1956). This work was widely considered as one of the key contributions in the development of finite element method. With the invention of the computer, a rapid way of performing the numerous calculations involved in the finite element analysis (FEA) was developed, making the method practically viable.

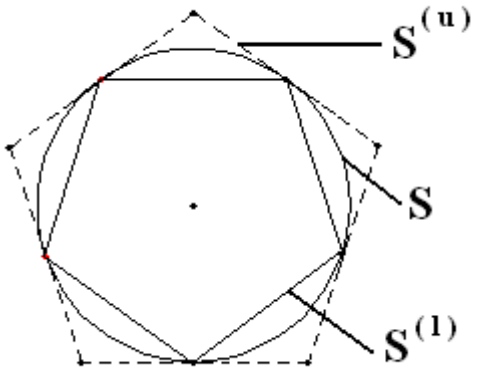

Figure 64: Lower and upper bounds to circumference of a circle

With the continuous development and increased processing power of computers, the application of the finite element method also progressed at a rapid rate. The finite element method started being presented as a solution to stress analysis problems (Przemieniecki 1968) and even to any general field problem (Zienkiewicz and Cheung 1967).

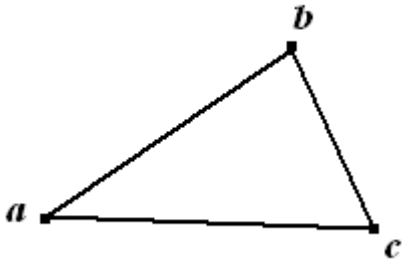

Figure 65: Triangular element with three nodes

2.1.2 Finite element method

The fundamental idea behind the finite element method is to divide the body, structure or region that requires analysing into a vast number of finite elements. These elements may be one, two or three dimensional. A widely used two dimensional element is the triangle (Figure 65). When a two-dimensional (2D) structure is divided into hundreds or even thousands of these non-overlapping triangles it can be observed that all planar geometries can be divided into finite elements. The particular element has three nodes (*a, b, c*) placed at the vertices of the triangle (Figure 65).

For illustration, figure 66a shows an irregular shaped plate which will be divided and represented with the use of finite elements (figure 66b).

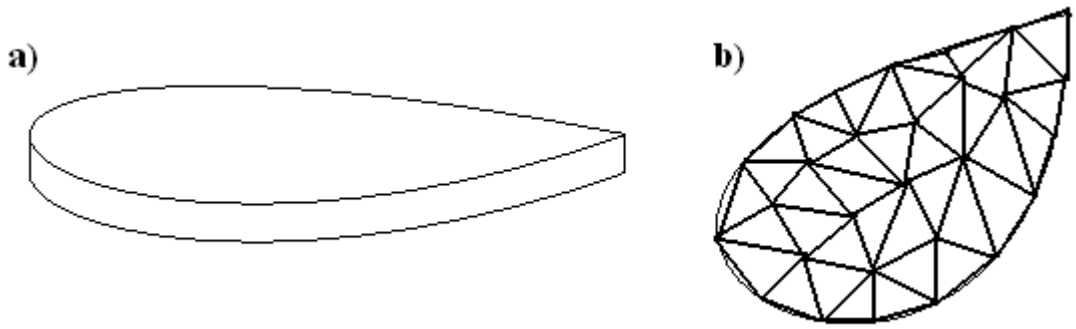

Figure 66: a) Irregular shaped plate, b) Irregular shaped plate discretized into many triangular elements

If the stress distribution for the above plate was required, the field variable of interest is the stress however because there are an infinite number of points in the plate there also are an infinite number of stresses to be measured. This problem can therefore be said to have an infinite number of degrees of freedom. Instead of requiring that the stress be determined at every point in the plate which is an unreasonable option, let the stress be determined at a finite number of points. The points used are the interconnected joints of the triangular elements known as nodes or nodal points. The nodes lie on the element boundary where adjacent elements are connected. It should also be noted that the curved boundaries are approximated by the several triangular elements (Figure 66b). The finite element method will only provide the stresses of the plate at the nodal points. Knowledge of the stresses at the nodal point (nodal stresses) will permit one to determine the general stresses within the region.

In order to obtain a solution of a more general problem by the finite element method where different field variables such as displacement, temperature, velocity or pressure are involved, the process involved always follows a step by step method. The procedure can be divided in six steps:

- Discretization of the model, i.e. replacing an infinite dimensional linear problem with a finite dimensional version
- Selection of a proper interpolation model
- Derivation of element stiffness matrix and load vectors
- Assembly of an element equation to obtain the overall equilibrium
- Solution of the unknown nodal variables
- Computation of the element strains and stresses

These will be discussed in the following section.

2.1.2.1 Discretization

The discretization of the body into finite elements is the first step in the finite element method. This is equivalent to replacing the body's infinite degrees of freedom to a system

having a finite number of degrees of freedom. The shapes, sizes, number and configuration of the elements have to be selected carefully so that the original body is simulated as closely as possible.

2.1.2.1.1 Basic element shapes

For any given model, a certain amount of judgement needs to be used when selecting the appropriate elements for discretization. The choice of the type of element is dictated by the geometry of the model and the number of special coordinates required to describe the system i.e. whether the model is in one-, two- or three-dimensions, with some of the most commonly used elements shown in figure 67, 68 and 69.

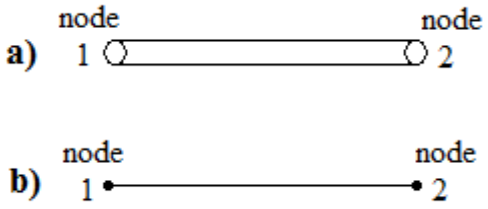

Figure 67: a) One-dimensional element, b) schematic representation of a)

When the geometry of the model, material properties or other parameters such as stress, displacement, pressure or temperature can be modelled in terms of only one spatial coordinate, the one-dimensional element can be used (Figure 67). Although the element has a cross-sectional area, it is represented schematically as a line segment (Figure 67b).

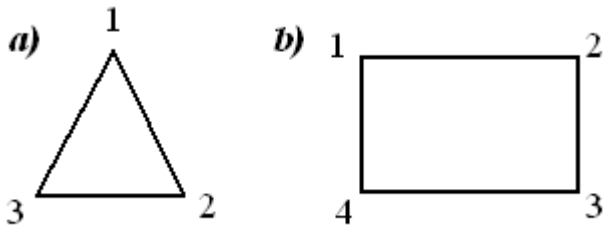

Figure 68: Two-dimensional finite elements, a) triangular element,

b) quadrilateral (rectangular) element

In certain models, the cross-sectional area of the element vary along the length and when the configuration and other parameters (i.e. stress, displacement, pressure and temperature) of the model can be described in two independent spatial coordinates, a two-dimensional element is required (Figure 68). The basic element useful for two dimensional analysis is the triangular element (Figure 68a), although the quadrilateral element (or its special forms, i.e. rectangle (Figure 68b), and parallelogram) can be obtained by combining two or four triangular elements, in some cases the use of the quadrilateral (in particular rectangular) elements proves to be advantageous when modelling rectangular models. If the geometry, material properties and other parameters of the model can be described in three independent spatial coordinates, the three-dimensional elements can be used. The basic three-dimensional element, analogous to the triangular elements in the two-dimensional case is the tetrahedron element (Figure 69a), whereas in some cases, the rectangular prism provides an advantageous solution (Figure 70) when modelling short rectangular beams.

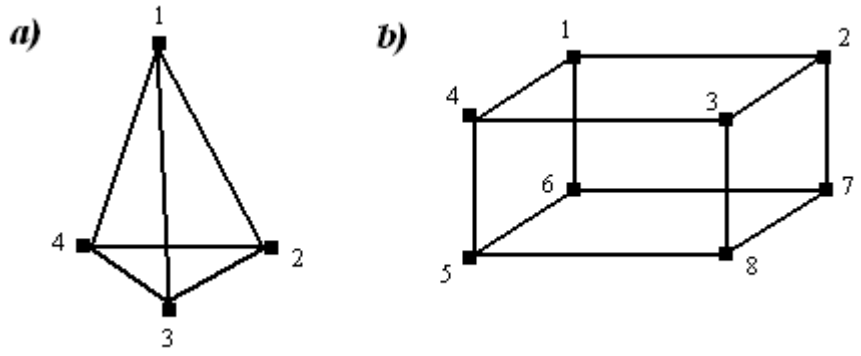

Figure 69: Three-dimensional finite elements, a) tetrahedron, b) rectangular prism

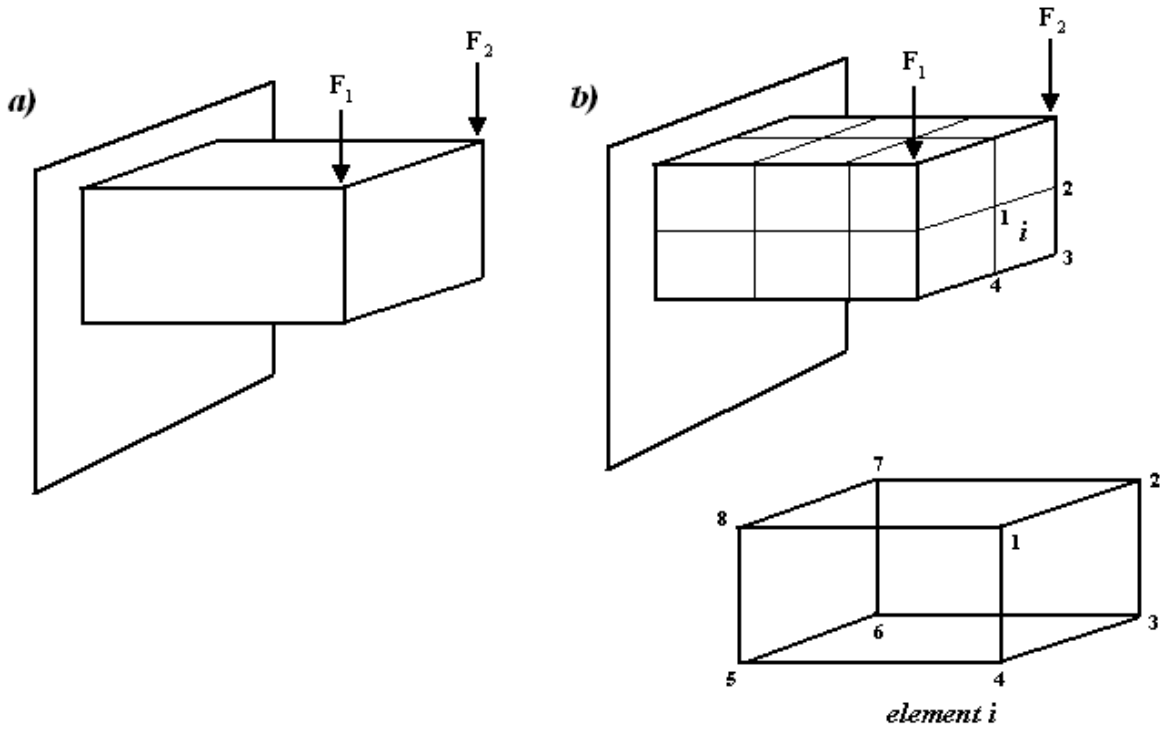

Figure 70: Three-dimensional solid elements for idealization of short beam, a) original beam, b) idealization using three-dimensional rectangular prism elements

2.1.2.1.2 Size of elements

The size of elements needs to be selected carefully as it will have a direct influence on the convergence of the solution. If the size of the element is small, the final solution would be expected to be more accurate, however the smaller elements are this will have a direct impact on the length of time required to solve the problem (Clough 1969).

2.1.2.1.3 Location of nodes

If the model has no abrupt changes in geometry and material properties, the model can be divided into equal sub-divisions and hence the spacing of the nodes can be uniform (Figure 71a). If discontinuities are present, nodes need to be introduced at these discontinuities (Figure 71b).

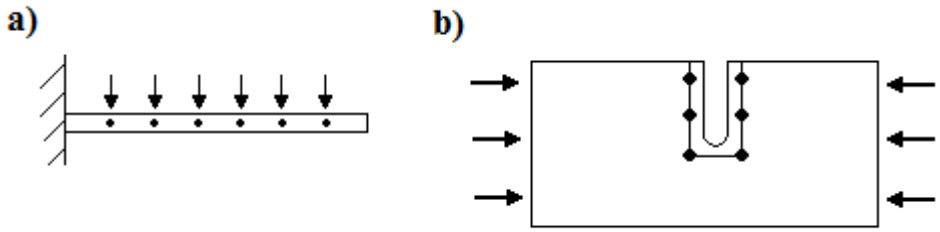

Figure 71: Location of nodes, a) uniform spacing, b) discontinuity in geometry

2.1.2.1.4 Number of elements

The number of elements chosen for idealization is related to the accuracy required and the size of elements involved. An increased number of elements generally yield more accurate results however for any given problem there will be a certain number of elements beyond which the accuracy cannot be considerably improved, a graphical representation of this can be seen in the following graph (Figure 72).

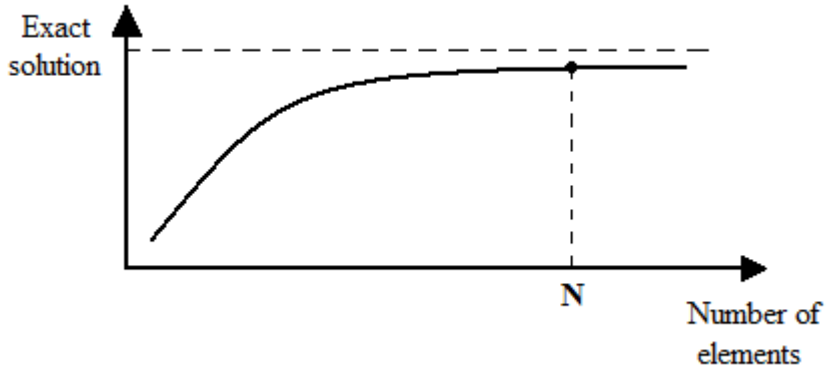

Figure 72: Effect of varying the number of elements on solution with no considerable improvement beyond N

2.1.2.2 Interpolation model selection

The idea of the finite element method is to obtain an approximation to a complicated problem by dividing the region of interest into finite elements and approximating the solution over each sub-region by a simple function. The nodal points of the elements offer strategic points for writing mathematical functions to describe the shape of the distribution of the unknown quantity over the domain of the elements, therefore an important and necessary step is the choice of a simple function for the solution in each element. The functions used to represent the behaviour within the elements are known as interpolation functions or approximating functions. A number of mathematical functions such as polynomials and trigonometric series can be used for this purpose, especially polynomials due to the simplicity of simplification and the ease of performing differentiation and integration. The accuracy of the result can be improved by increasing the order of the polynomial (Figure 73) therefore theoretically a polynomial of infinite order corresponds to the exact solution but in practice, polynomials of finite order are used. Although trigonometric functions possess some of the polynomial properties, they are seldom used in finite element analysis as these functions are difficult to manipulate mathematically in complex models (Krahula and Polhemus 1968). The polynomial interpolation function can be expressed in general terms as:

$$u = \Phi_1 u_1 + \Phi_2 u_2 + \Phi_3 u_3 + \ldots + \Phi_m u_m$$

Where u denotes the unknown and where $u_1, u_2, u_3, \ldots, u_m$, denote the values of the unknowns at the nodal points and $\Phi_1, \Phi_2, \Phi_3, \ldots, \Phi_m$ are the interpolation functions.

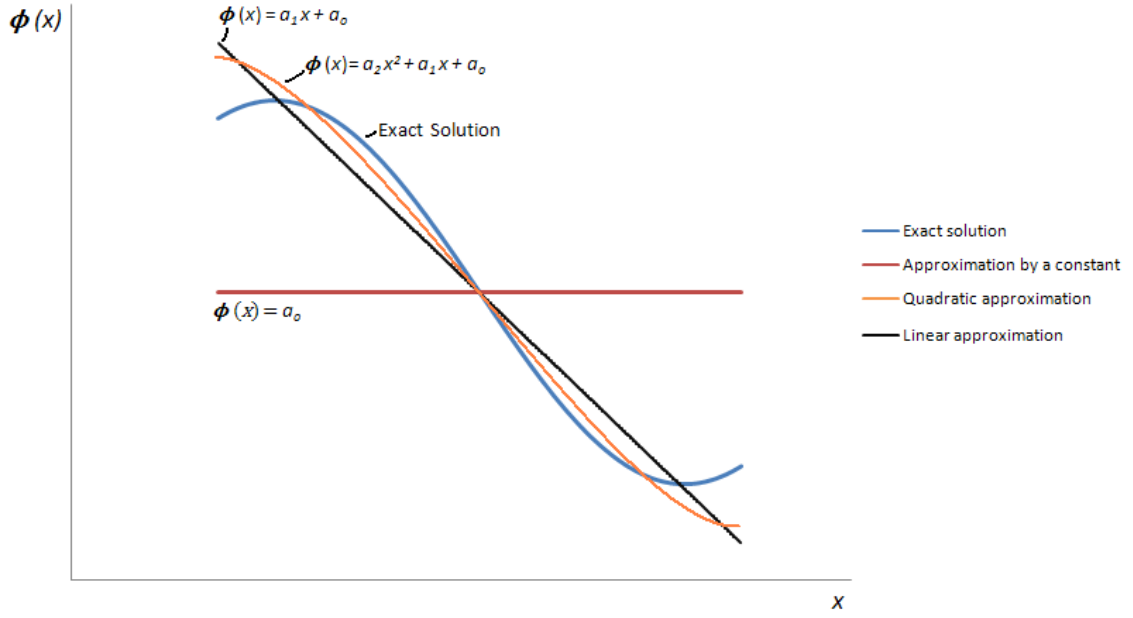

Figure 73: Polynomial approximations

For example in the case of a planar deformation problem where there are only two displacements at each node, the line element (Figure 67) with two end nodes will have u_1 and u_2 as degrees of freedom or unknowns, for the triangular element (Figure 68a), there will be six degrees of freedom or unknowns, u_1, u_2, $u_3, \ldots, u_6$. A degree of freedom can be defined as an independent displacement (unknown displacement) that can occur at any point.

2.1.2.3 Derivation of element stiffness matrix and load vectors

By applying known laws and principles, equations can be obtained that govern the behaviour of the element. The equations are obtained in general terms and therefore can be used for all elements in the discretized model. A number of possibilities exist for the derivation of element equations, with the three most common being the direct approach, the energy approach and the weighted residual approach.

2.1.2.3.1 The direct approach

In this method, direct physical reasoning is used to determine the element properties, i.e. the characteristic matrices and vectors, in terms of the relevant variables. Although this method is limited to simple types of elements, it demonstrates the physical interpretation of the finite element method. The following example will illustrate this method.

A stepped bar (Figure 74) with various different steps which are assumed to have different lengths *(l)*, areas of cross section *(A)* and Young's modulii *(E)* will be considered. It can be deduced that the way to discretize this system is by considering each step as an element; the system will therefore consist of three elements and four nodes (Figure 74b).

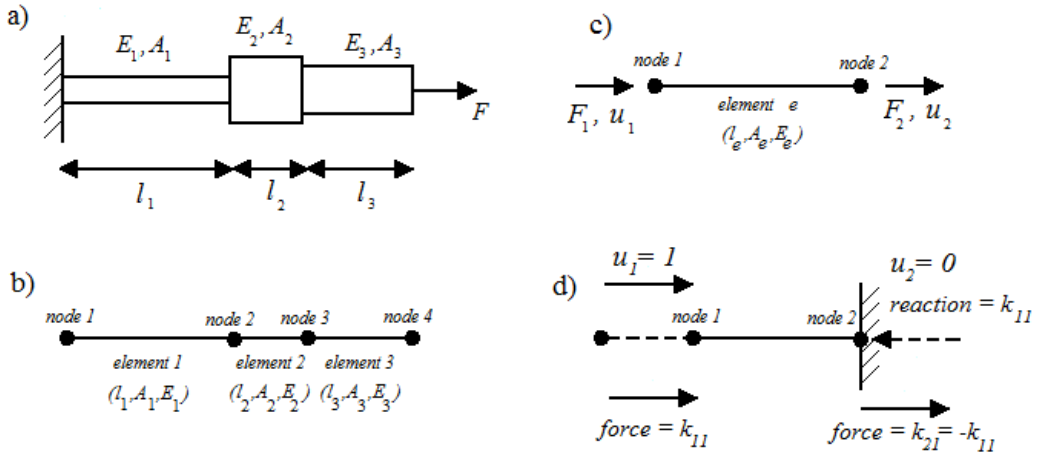

Figure 74: Stepped bar under axial load, a) Physical system, b) Finite element discretization, c) One element of the system, d) finding k_{11} and k_{21}

The element equations are required in this case to determine the force-displacement equations of the steps. In order to derive these equations, the element is isolated (Figure 74c) into a typical element *e*, where a force *(F)* and a displacement *(u)* is defined at each end of the two nodes in the positive direction of the *x*-axis. The unknown variable in this example is the displacement *(u)*. The element equations can be expressed in matrix form as

$$[k] \times \vec{u} = \vec{F}$$

or

$$\begin{bmatrix} k_{11} & k_{12} \\ k_{21} & k_{22} \end{bmatrix} \times \begin{Bmatrix} u_1 \\ u_2 \end{Bmatrix} = \begin{Bmatrix} F_1 \\ F_2 \end{Bmatrix}$$

where $[k]$ is called the stiffness or characteristic matrix, $\vec{u}$ is the vector of nodal displacements and $\vec{F}$ is the vector of nodal forces of the element. The element stiffness matrix can be derived from the basic definition of the stiffness coefficient and no assumed interpolation polynomials are required. In structural mechanics, the stiffness influence coefficient k_{ij} is defined as the force required at node *i*, in the direction of u_i, to create a unit displacement at node *j* ($u_j = 1$) while other nodes are restrained (Martin 1966). This definition can be used to generate the matrix $[k]$. When a unit displacement is applied at node 1 and node 2 is restrained (Figure 74d), a force k_{11} is induced. As

$$Stress = \frac{Force}{Cross\ sectional\ Area}\ rearraged\ gives:$$

$$Force = Stress \times Cross\ sectional\ Area$$

But:

$$Young's\ modulus\ (E) = \frac{Stress}{Strain}\ rearranged\ gives:$$

$$Stress = E\ \times Strain, and\ Strain = \frac{Change\ in\ length\ (\Delta l)}{Original\ Length\ (l)}$$

Therefore

$$Force = \left(\frac{Change\ in\ length\ (\Delta l)}{Original\ length\ (l)}\right) \times Young's\ modulus\ (E) \times Cross\ sectional\ area\ (A)$$

So if change in length = 1

$$Force = \frac{1}{l} \times A \times E = \frac{A\,E}{l}$$

So for figure 74d, the induced force k_{11} is equal to $\frac{A_e E_e}{l_e}$ at node 1 and the reaction force k_{21} at node 2 is equal to $-\frac{A_e\,E_e}{l_e}$. Similarly values of k_{22} and k_{12} can be obtained by giving a unit displacement to node 2 and restraining node 1 which will result in $\frac{A_e E_e}{l_e}$ and $-\frac{A_e E_e}{l_e}$ respectively. Thus the stiffness matrix of the element is given by:

$$[k] = \begin{bmatrix} k_{11} & k_{12} \\ k_{21} & k_{22} \end{bmatrix} = \begin{bmatrix} (A_e E_e / l_e) & -(A_e E_e / l_e) \\ -(A_e E_e / l_e) & (A_e E_e / l_e) \end{bmatrix} = \frac{A_e E_e}{l_e} \begin{bmatrix} 1 & -1 \\ -1 & 1 \end{bmatrix}$$

2.1.2.3.2 The minimum potential energy approach

The principle of minimum total potential energy may be stated as follows: out of all the possible displacement fields that satisfy the geometric boundary conditions, the one that also satisfies the equations of static equilibrium results in the minimum total potential energy of the structure or body (Love 1944), which was then rigorously proved by Sokolnikoff (Sokolnikoff 1956). The total potential energy (Π) is defined to be the sum of the two different types of potential energy, i.e. the internal strain energy or the internal potential energy (U_i) and the external potential energy (U_e) generated by the external forces acting on the system or:

$$\Pi = U_i + U_e$$

However for conservative force systems, the loss in external potential energy during loading is equal to the work done (W_e) on the system by the external forces so $W_e = -U_e$, so the previous equation becomes:

$$\Pi = U_i - W_e$$

When the principles of minimum potential energy is applied, it is required that Π be at a minimum for stable equilibrium. In order to minimize Π, the first variation or derivative of the total potential energy is required to equate to zero, so:

$$\delta\Pi = \delta U_i - \delta W_e = 0$$

or

$$\delta U_i = \delta W_e$$

2.1.2.3.3 The weighted residual approach

The weighted residual method is a powerful technique that can be used to obtain approximate solutions to linear and nonlinear equations. A number of weighted residual methods can be employed but four particular functions are most often used (Argyris 1960, Crandall 1956, Desai and Abel 1972, Finlayson 1972). The four most popular weighted residual methods are referred to as:

- Point collocation method
- Subdomain collocation method
- Least squares method
- Galerkin method

Before describing the four methods, a general structure around which the various methods are developed will be presented.

2.1.2.3.3.1 General concepts

A single governing equation with only one independent variable will be used to illustrate the general concept. Let the governing equation be represented by:

$$f[T(x)] = 0 \quad in\ D$$

where T represents the function sought that is a function of *x* only. *D* represents the domain of the region governed by the previous equation. In addition, the boundary conditions can be symbolically specified in the form:

$$f_1[T(x)] = 0 \quad on\ V_1$$

and

$$f_2[T(x)] = 0 \quad on\ V_2$$

where V_1 and V_2 include only the parts of the domain D that are on the boundary (Figure 75).

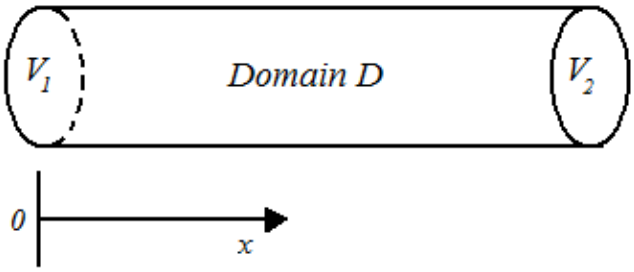

Figure 75: Schematic representation of a one-dimensional problem domain *D* with two boundaries V_1 and V_2

An approximation of the solution to the equations can be obtained by an approximate function *T'* where

$$T' = T'(x;\, a_1, a_2, \cdots, a_n) = \sum_{i=1}^{n} a_i N_i(x)$$

which has one or more constant unknown parameters a_1, a_2, … , a_n and which satisfies the boundary conditions at V_1 and V_2. The prime ($'$) denotes an approximate solution and not a derivative. The functions N_i (x) are referred to as the trial functions. If the approximate solution T' is substituted back into $f[T(x)] = 0$, it will not necessarily satisfy the equation exactly, that is some residual error $R(x, a_1, a_2, \cdots, a_n)$ will result. This can therefore by written:

$$f[T'(x, a_1, a_2, \cdots, a_n)] = R(x, a_1, a_2, \cdots, a_n)$$

where the notation indicates the residual *R* is a function of *x* and the parameters $a_1, a_2, \cdots, a_n$. The exact solution is obtained when the residual *R* is zero for all the points in the domain *D*.

The weighted residual approach requires that the parameters $a_1, a_2, \cdots, a_n$ be determined by satisfying:

$$\int_D w_i(x)\, R(x; a_1, a_2, \cdots, a_n) dx = 0 \quad where\ i = 1, 2, \cdots, n \qquad (Equation\ 1)$$

where the functions $w_i(x)$ are the *n* arbitrary weighting functions (Stasa 1985).

2.1.2.3.3.2 Point collocation method

In the point collocation method, the residual *R* is set to zero at *n* points in the domain *D*, the weighting function $w_i(x)$ are denoted as $\delta(x - x_i)$ and defined such that

$$\int_a^b \delta(x - x_i) dx = 1 \quad for\ x = x_i$$

$$\int_a^b \delta(x - x_i) dx = 0 \quad for\ x \neq x_i$$

The collocation points, the x_i's, are selected arbitrarily to cover the domain *D* uniformly. The δ indicates the Dirac delta function and is not the variational operator (Rao 1989). Substitution of $\delta(x - x_i)$ for $w_i(x)$ in Eq 1 gives:

$$\int_D \delta(x - x_i)\, R(x;\, a_1, a_2, \cdots, a_n) dx = 0 \;\; where\; i = 1, 2, \cdots, n$$

This procedure yields *n* simultaneous algebraic equations in *n* unknowns which are the constant parameters $a_1, a_2, \cdots, a_n$. Once these are determined the approximate solution is given by equation

$$T' = T'(x;\, a_1, a_2, \cdots, a_n) = \sum_{i=1}^{n} a_i N_i(x)$$

and the problem is approximately solved.

2.1.2.3.3.3 Subdomain collocation method

In the Subdomain collocation method, the weighting functions are chosen to be unity over a portion of the domain and zero elsewhere. Therefore mathematically the weighting function w_i (x), can be expressed

$$w_1(x) = \begin{cases} 1 & for\ x\ in\ D_1 \\ 0 & for\ x\ not\ in\ D_1 \end{cases}$$

$$w_2(x) = \begin{cases} 1 & for\ x\ in\ D_2 \\ 0 & for\ x\ not\ in\ D_2 \end{cases}$$

$$\vdots$$

$$w_n(x) = \begin{cases} 1 & for\ x\ in\ D_n \\ 0 & for\ x\ not\ in\ D_n \end{cases}$$

where D_1 is a portion of the domain not included in D_2, D_3, … , D_n, this can be represented graphically for n = 3 (Figure 76).

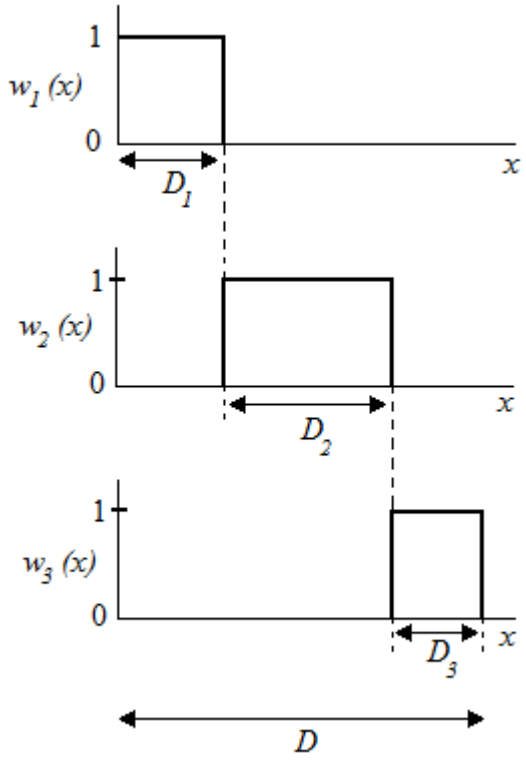

Figure 76: Subdomains and weighting functions for the subdomain collocation weighted residual method

2.1.2.3.3.4 Least squares method

In this method, the integral I of the weighted square of the residual over the domain is required to be a minimum, that is

$$I = \int_D [R(x;\ a_1, a_2, \cdots, a_n)]^2\ dx = minimum$$

The problem is reduced to the determination of the parameters $a_1, a_2, \cdots, a_n$ such that the values of the integral *I* is minimized. Therefore the partial derivative of *I* must be obtained with respect to a_1 and set to zero, then with respect to a_2 and set to zero and so forth. This can be mathematically written as:

$$\frac{\partial I}{\partial a_1} = \frac{\partial}{\partial a_1} \int_D [R(x;\, a_1, a_2, \cdots, a_n)]^2 \, dx = 0$$

$$\frac{\partial I}{\partial a_2} = \frac{\partial}{\partial a_2} \int_D [R(x;\, a_1, a_2, \cdots, a_n)]^2 \, dx = 0$$

$$\vdots$$

$$\frac{\partial I}{\partial a_n} = \frac{\partial}{\partial a_n} \int_D [R(x;\, a_1, a_2, \cdots, a_n)]^2 \, dx = 0$$

where *D* includes the entire domain. As the limits on the integral are not a function of the unknowns $a_1, a_2, \cdots, a_n$, the order of the integration and the differentiation may be interchanged. Carrying out the differentiation and dividing by the constant factor 2 and not including the arguments on *R* for now, gives

$$\int_D R \frac{\partial R}{\partial a_1} \, dx = 0$$

$$\int_D R \frac{\partial R}{\partial a_2} \, dx = 0$$

$$\vdots$$

$$\int_D R \frac{\partial R}{\partial a_n} \, dx = 0$$

So in order to determine the weighting functions, it is necessary to compare the above equation with equation 1 which yields:

$$w_1(x) = \frac{\partial R}{\partial a_1}$$

$$w_2(x) = \frac{\partial R}{\partial a_2}$$

$$\vdots$$

$$w_n(x) = \frac{\partial R}{\partial a_n}$$

That can be summarized as:

$$w_i(x) = \frac{\partial R}{\partial a_i} \quad for\ i = 1, 2, \ldots, n$$

Therefore the least-squares weighted-residual method requires the solutions of the *n* equations given by equation 1 for the *n* unknowns parameters $a_1, a_2, \cdots, a_n$ where the w_i (x)'s are obtained from equation

$$w_i(x) = \frac{\partial R}{\partial a_i} \quad for\ i = 1, 2, \ldots, n$$

2.1.2.3.3.5 Galerkin method

In the Galerkin weighted-residual method, the trial functions $N_i(x)$ are used as the weighting functions or:

$$w_i(x) = N_i(x)$$

So for the Galerkin method, equation 1 becomes:

$$\int_D N_i(x)\, R(x; a_1, a_2, \cdots, a_n) dx = 0 \quad for\ i = 1, 2, \ldots, n$$

Because only one trial function being present for each unknown parameter, the above equation gives *n* equations that when solved, yield the values of the unknown parameters $a_1, a_2, \cdots, a_n$. The values obtained for the unknown parameters $a_1, a_2, \cdots, a_n$ depend on the trial function initially selected. This weighted-residual method is the most commonly used for finite element applications (Desai and Kundu 2001).

2.1.2.4 Assembly of an element equation to obtain the overall equilibrium

2.1.2.4.1 Assembly of element equation

Once the element matrices and the element vectors are found, the next step is to construct the overall or system equations. The process used for constructing the system equations from the element characteristics is the same regardless of the type of problem and the number and type of elements.

The method of assembling the element matrices and vectors is based on the need of compatibility at the element nodes. This means that at the nodes where the elements are connected, the values of the unknown nodal degrees of freedom are the same for all the elements joined at that node. The nodal variables are usually generalized displacements

which can be rotations, curvatures or other spatial derivatives of translations. When the generalized displacements are matched at the common node, the nodal stiffnesses and nodal loads of each of the shared elements are added to yield the net stiffness and net load at that node which will lead to equations describing the behaviour of an element, which are commonly expressed as

$$\{F\} = [k] \times \{u\}$$

where $\{F\}$ is the vector of element nodal forces, $[k]$ is the global stiffness matrix which is constructed from the stiffness matrices of each element, and $\{u\}$ is the vector of nodal displacements (Korioth and Versluis 1997b). It is the nodal displacements which are solved given a set of nodal forces, constraints and global stiffness matrix.

2.1.2.4.2 Boundary conditions

As indicated above, after assembling the global stiffness matrix $[k]$ and the vector of element nodal forces, the overall system equations of the entire domain can be expressed as:

$$\{F\} = [k] \times \{u\}$$

however these equations cannot be solved as the loaded body is free to undergo unlimited rigid body motion unless some boundary conditions are imposed to support the body in space and hence in equilibrium under the loads.

A boundary condition expresses a prescribed value of displacement on a part of the boundary of the structure and establishes how the body is supported in space. After the introduction of these boundary conditions, the structure is capable of withstanding applied forces. Without boundary conditions the structure is free to undergo an unlimited rigid body motions and hence an infinite number of possible solutions exist.

Three types of boundary conditions exist which are described as, displacements, gradients of unknowns or both. They are also called first or Dirichlet boundary conditions (displacements), second or Neumann boundary conditions and third or mixed boundary conditions (gradients).

For instance, if a column is supported such that the axial displacement at the base is specified, this represents the first condition; if the base is fixed such that the gradient is specified, it is the second condition; if the base is completely fixed this constitutes the mixed condition.

2.1.2.5 Solution of the unknown nodal variables

The finite element analysis of any problem results in a system of matrix equations and after the incorporation of the boundary conditions in the assembled system of equations, the final matrix equations are obtained. The methods available for solving the final matrix equations can be divided into two types: direct and iterative. The direct methods will yield the exact solution in the absence of round-off and other errors. The errors arising from round-off and truncation may lead to poor and maybe useless results. The basic method used for direct solutions is the Gaussian elimination but even with this method, there are several varieties depending on the computer programme used to calculate and hence yield the results (Rao 1989).

Iterative methods are those which start with an initial approximation and by applying a suitable algorithm, lead to a better approximation. When the process converges, it can be expected that the approximate solution obtained will be improved. The main advantages of the iterative methods are the simplicity and uniformity of the calculations to be performed, that make them suitable for use on computers and their minimal insensitivity to the cumulative augmentation of round-off errors (Rao 1989).

2.1.2.6 Computation of the element stains and stresses

For the displacement formulation, nodal displacements are the primary unknowns as they must be computed first and then the secondary quantities (strains, stresses, moments, shear forces etc.) can be obtained by using the known relations between displacement and the desired secondary unknown.

2.1.3 Concepts in elasticity

Stress is defined as force per unit area and strain as elongation per unit length. A linear elastic material behaves in such a way that when loaded and subsequently unloaded, the stress-strain relationship is linear (Figure 77). The elastic limit of a material is reached when permanent deformation occurs.

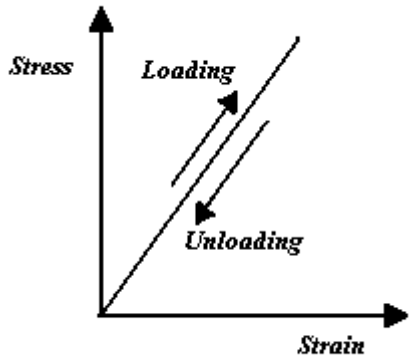

Figure 77: Stress-strain curve for a linear elastic material

2.1.3.1 Stress

Consider a loaded body in static equilibrium with external forces F_1, F_2, etc, which are transmitted through the body in a complex manner. An infinitesimally small volume element positioned at a point in a global in a global *x y z*-coordinate (Figure 78). There are six faces to the cube and on each face there is a normal and two shear stresses that act. The two subscripts are identical for the normal stresses whereas they are different for the shear stresses which will eliminate any ambiguity as the symbols for normal and shear stresses are identical. The

classification used follows the subsequent convention. The first subscript is associated with the outward normal to the plane over which the stress acts, and the second subscript is associated with the direction of the stress. Positive faces are defined to have outward normals in the same direction as the coordinate axes and the negative faces have the outward normals in the opposite direction to the coordinate axes. In figure 78a the three visible faces are positive and the three hidden faces are negative.

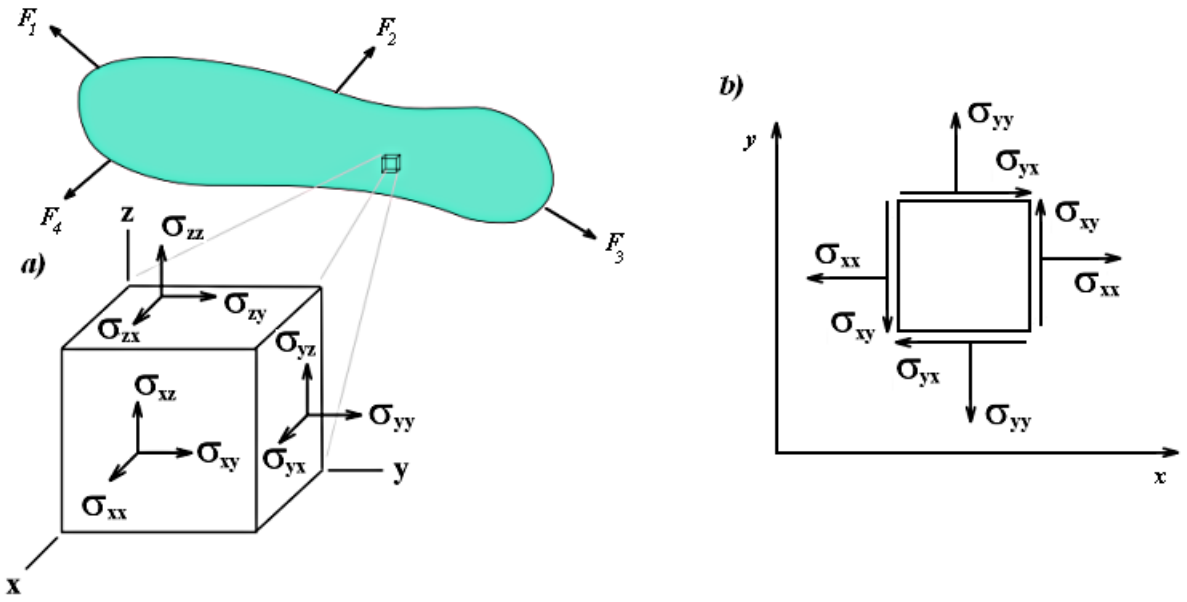

Figure 78: a) External forces acting on a body and infinitesimal volume element with normal and shear stresses in three-dimensions, b) in two-dimensions

With the concept of positive and negative faces clarified, the convention adopted for normal and shear stresses are considered positive if directed in the positive coordinate direction on a positive face and are also considered positive if directed in the negative coordinate direction on a negative face. Otherwise, the stresses are considered to be negative which ensures that positive normal stresses are tensile whereas negative normal stresses are compressive (Stasa 1985).

2.1.3.2 Strain

Strain in a body generally varies from one point to another under load. An illustration of strain can be observed in figure 79 where a square element whose sides are of unit length is subjected (Figure 79a) to some external load which results in the element deforming such that the sides of the element are no longer perpendicular (Figure 79b). The normal strains ε_{xx} and ε_{yy} are defined in figure 79b as:

$$\varepsilon_{xx} = x'_A - x_A \quad and \quad \varepsilon_{yy} = y'_B - y_B$$

based on the fact that the sides of the square element are of unity length before deformation. The normal and shear strains are all shown as positive, therefore the shear strain ε_{xy} is positive when the angle *BOA* is smaller than π/2. Strain is dimensionless but it is usually reported in units of millimetre/millimetre (mm/mm) or as microstrain (με) which is 10^{-6} strain.

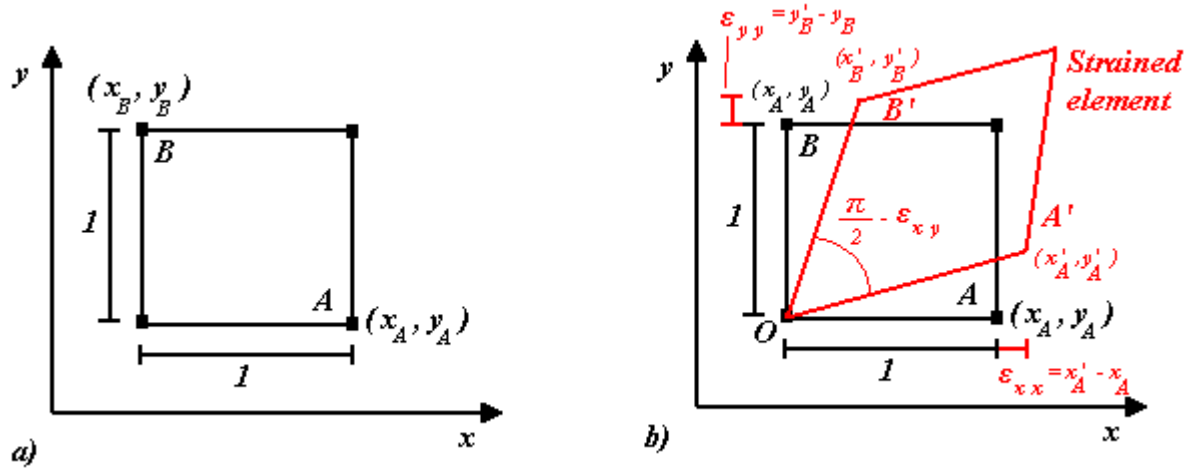

Figure 79: Definition of normal and shear strains, a) unstrained element with sides of unit length, b) distorted element

2.1.3.3 Strain – displacement relations

In stress analysis, the Lagrangian point of view is usually adopted in that a point in the body is followed as it moves due to deformation induced by the loading. An arbitrary point undergoes displacements in the *x*, *y* and *z* directions, which are denoted as *u*, *v* and *w*. The strains and displacements are not independent but are related for small deformations in two-dimensional problems as:

$$\epsilon_{xx} = \frac{\partial u}{\partial x} \qquad \epsilon_{yy} = \frac{\partial v}{\partial y} \qquad \epsilon_{xy} = \frac{\partial v}{\partial x} + \frac{\partial u}{\partial y}$$

and in three-dimensional problems as:

$$\epsilon_{xx} = \frac{\partial u}{\partial x} \qquad \epsilon_{yy} = \frac{\partial v}{\partial y} \qquad \epsilon_{zz} = \frac{\partial w}{\partial z}$$

$$\epsilon_{xy} = \frac{\partial v}{\partial x} + \frac{\partial u}{\partial y} \qquad \epsilon_{yz} = \frac{\partial w}{\partial y} + \frac{\partial v}{\partial z} \qquad \epsilon_{zx} = \frac{\partial u}{\partial z} + \frac{\partial w}{\partial x}$$

The two equations for 2D and 3D problems are known as the strain-displacement relation but it should be noted that these equations hold only for small deformation and will not work for stress analysis involving large deformations.

2.1.3.4 Hooke's law

For Hooke's law to be appropriately used, the deformations must not result in strains that would cause the material to exceed the proportional limit and that the material remains within the elastic limits. In its most simple form, Hooke's law states that the normal stress (σ) is proportional to the normal strain (ε) in a uniaxial state of stress or:

$$\sigma = E\ \varepsilon$$

where

$$Stress\ (\sigma) = \frac{Force}{Area} = \frac{F}{A} \quad and \quad Strain\ (\varepsilon) = \frac{Change\ in\ length}{Original\ length} = \frac{\Delta L}{L}$$

where *E* is known as Young's modulus, the elastic modulus or the modulus of elasticity which is a measure of stiffness of a material i.e. how much a material deforms under axial load (Figure 80). Since strain is dimensionless, the Young's modulus has units the same as stress which are Newtons per square metre (N/m^2).

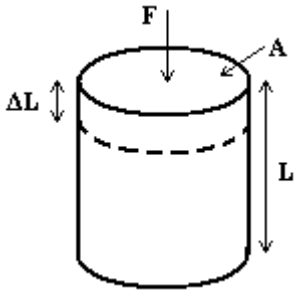

Figure 80: Representation of dimensions required for obtaining Young's modulus (*E*)

2.1.3.5 Poisson's ratio

Poisson's ratio (ν) is a measure of the ability of a material to resist change of volume and change of shape and is defined as the lateral strain divided by the axial strain (Figure 81) which is represented by the formula:

$$\nu_{xy} = -\frac{\varepsilon_x}{\varepsilon_y}$$

Where:

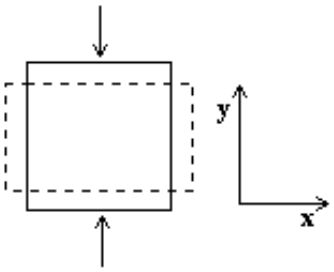

Figure 81: Illustration of Poisson's ratio, solid square represents object before axial strain and dashed object after strain

2.2 Method

Before an analysis can take place, the scaffolds were first drawn using a CAD programme that represented the real manufactured structures. The scaffolds were then transferred to the FEA program and the material properties were assigned. The boundary conditions were then put in place and the analysis carried out which yielded information regarding the surface strain distribution throughout the scaffolds.

2.2.1 Model creation

Creation of a realistic model requires the geometry of the structure to be inputted into a computer program. Several techniques exist to accomplish this and they include an automated and a manual method. One automated approach involves converting laser scans of the desired object into a wire frame model that is then converted into an FE model. This method generates a high-resolution representation of the outer surface of the object but cannot give information on the internal geometry. Computer tomography (CT) scan voxels (3D pixels) can be transformed into an FE model with high resolution but also requires some complex issues in finding the appropriate threshold algorithms to define the boundaries through the structure accurately (Fajardo et al. 2002).

Manual methods include obtaining images (e.g., MRI, CT and photos) and manually digitizing them into a computer aided design (CAD) model or alternatively creating a structure using CAD software that can then be converted into an FE model. This latter technique was used for generating a CAD model from the manufactured PCL scaffolds. On creating the PCL scaffold (as mentioned in earlier chapter), images were taken using an Olympus microscope at 20 times magnification that would provide information regarding the scaffold dimensions, strand diameters, distance between strands and between layers. These images were then observed using a histomorphometric program (BioQuant) that permitted the average layer thickness, strand distance and strand thickness to be obtained and hence used to create an accurate computer representation of a real manufactured scaffold (Figure 82).

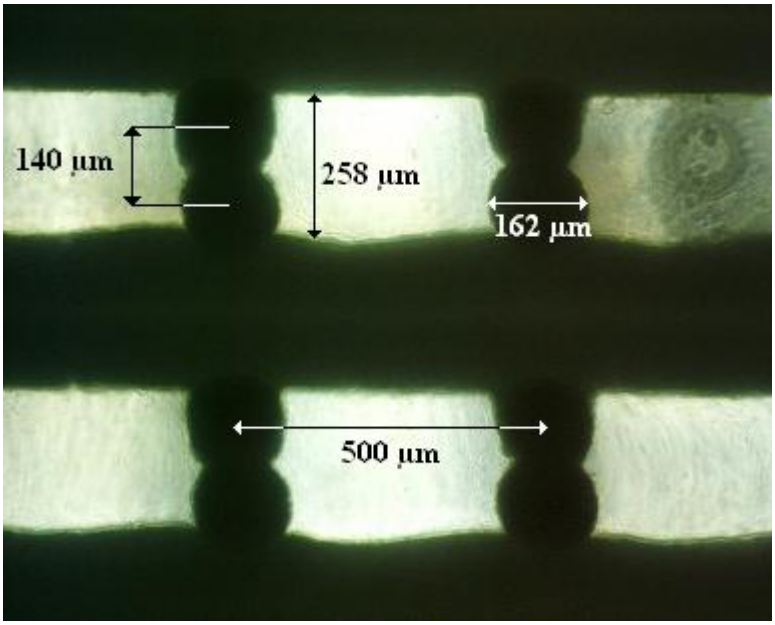

Figure 82: Dimensions measured and used to create CAD model

2.2.2 Generated Computer Aided Design models

CAD models were created for the FEA analysis. The dimensions of the computer generated scaffolds were obtained from the histomorphometric measurements made on the plotted scaffolds. Solid Works 2003 was the CAD program used to generate the computer models of the scaffolds. The general method for creating the virtual scaffold models was started by drawing a single strand (Figure 83a) with arbitrary length which was then copied to form the first layer (Figure 83b). The second layer which was perpendicular the first layer was initiated by drawing a strand (Figure 83c) which was then copied to generate the second layer (Figure 83d). These two layers were then joined so forming a single object which was then copied and stacked to give height to the scaffold of 5.062 mm (Figure 83e). The scaffold was then cut to a form a cube 5 x 5 mm (Figure 83f).

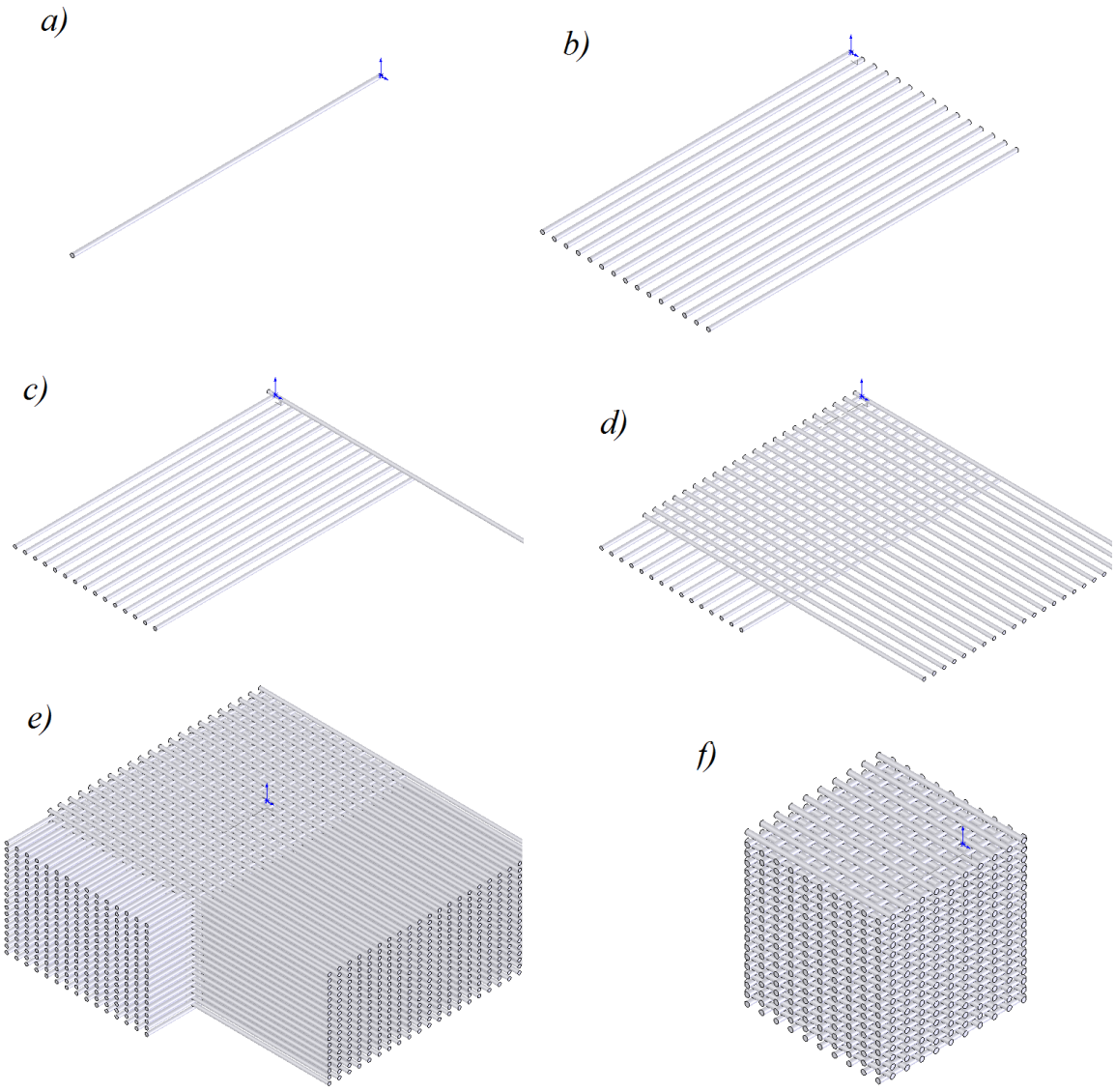

Figure 83: Steps involved in creating a virtual scaffold using a CAD program

Eight different scaffolds with different layer orientation and strands per layer were created which represented the manufactured scaffolds that could be created using the Bioplotter™ (Figure 84 and 85), these included:

- Single strand no offset (SSNO) (Figure 84a)
- Single strand with offset (SSO) (Figure 84b)
- Single strand no offset with 45° rotation (SSNO45) (Figure 84c)
- Single strand with offset and 45° rotation (SSO45) (Figure 84d)
- Double strand no offset (DSNO) (Figure 85a)
- Double strand with offset (DSO) (Figure 85b)
- Double strand no offset with 45° rotation (DSNO45) (Figure 85c)
- Double strand with offset and 45° rotation (DSO45) (Figure 85d)

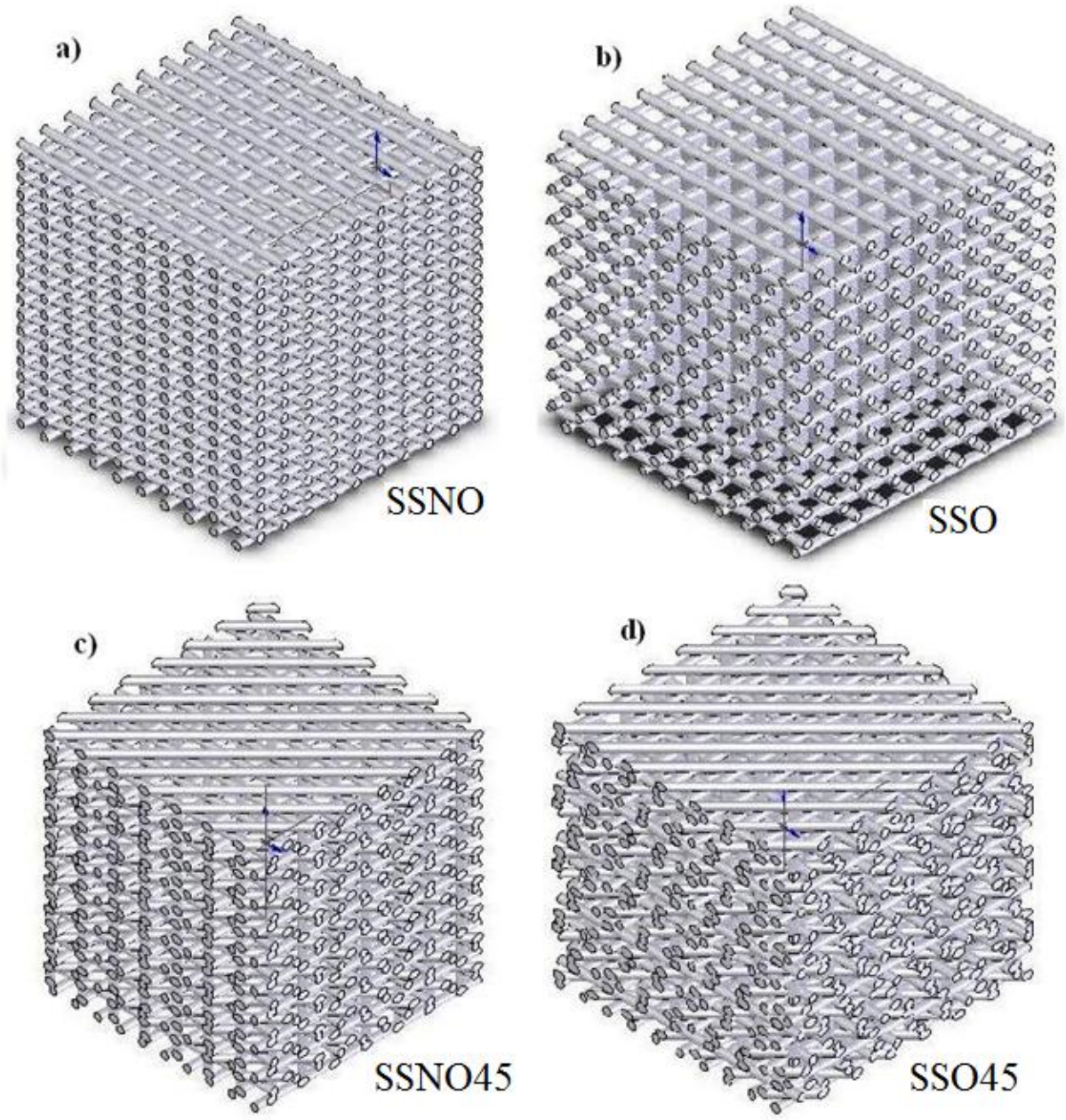

Figure 84: CAD models of single stranded scaffolds, a) no offset, b) with offset, c) no offset with 45° rotation, d) with offset and 45° rotation

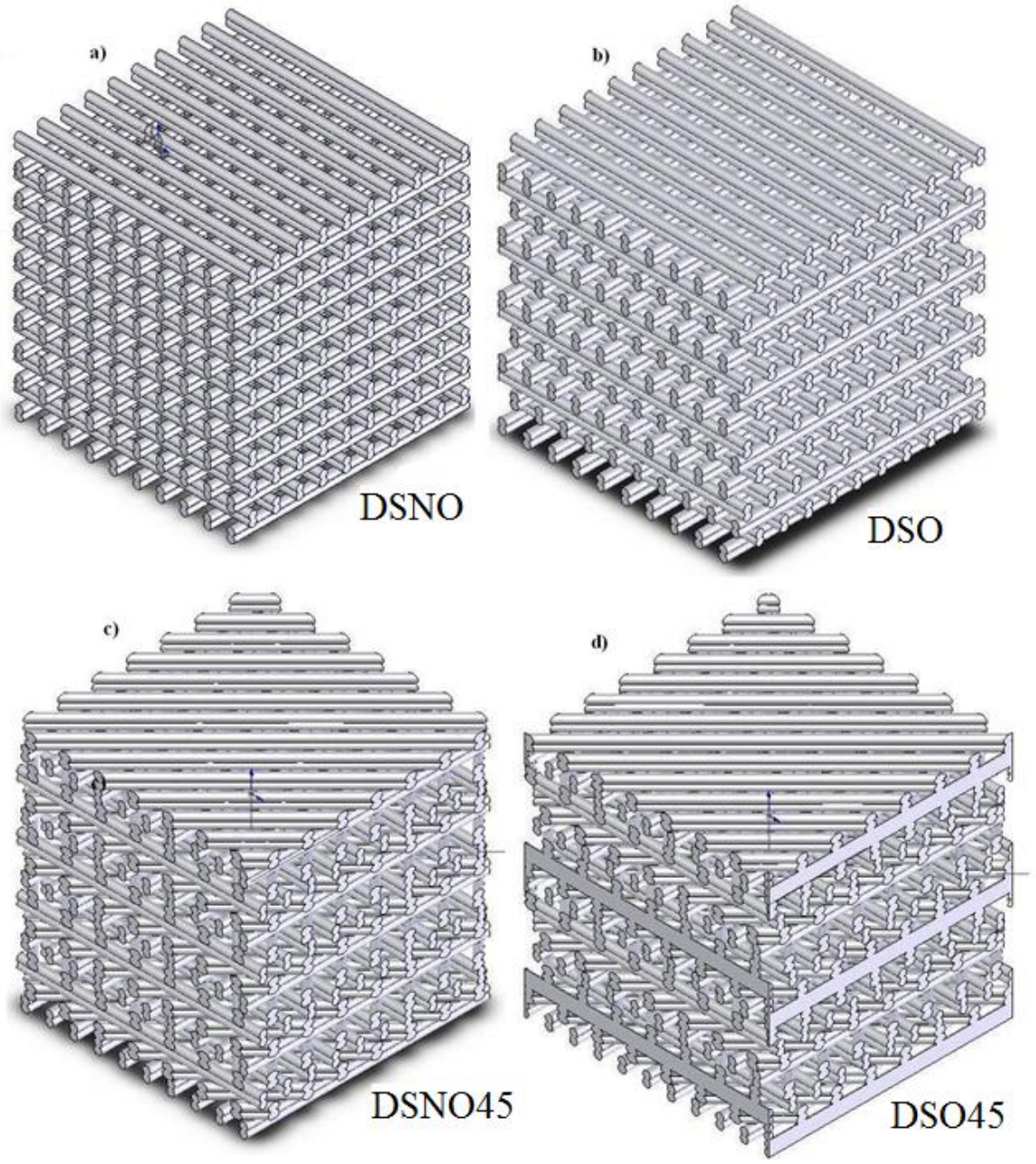

Figure 85: CAD models of Double Stranded scaffolds, a) No offset, b) with offset, c) No offset with 45° rotation, d) With offset and 45° rotation

2.2.3 Assessing the Young's modulus of Polycaprolactone

Before the CAD models were transferred to the FEA program, material properties of the polycaprolactone were required so that the results generated by the analysis were realistic. The first method used to obtain the Young's modulus of polycaprolactone of molecular number 10000, 42000 and 80000, was to melt pellets of the material in a test tube and allow it cool and hence solidify. The test tube was then broken, leaving a solid cylinder of PCL. The cylinder was then cut using a low speed circular saw (Buehler, Isomet) to smaller cylinders that were 10 mm high. The samples were then tested in compression using a mechanical tester (Zwick-Roel, UK) with a 10kN load cell (GTM, Germany) at a compression rate of 1mm/min. A graph of the compressive stress against strain was then plotted and the Young's modulus obtained by calculating the gradient of the linear portion of the graph (Figure 90).

The mechanical properties of polycaprolactone were determined by creating three different cylinders with three different molecular numbers and obtaining the Young's modulus by compressive testing. From the graph of stress against strain, it can be observed that the gradient of PCL M_n 10,000 is steeper which indicates a greater young's modulus however the graph also shows that the ultimate compressive strength is lower which indicates a brittle substance as the graph rapidly decreases as the strain is increased. The other two molecular numbers of polycaprolactone (M_n 42,500 and M_n 80,000) have a slightly flatter gradient and the ultimate compressive strength is not reached (Figure 90). Values of the Young's modulus obtained this way were correct (Table 10) but did not represent the Young's modulus of the polycaprolactone that was precipitated out while making the scaffolds. Therefore another measurement needed to be collected that more closely matched the mechanical properties of the extruded polycaprolactone. Strands of 30% w/v polycaprolactone with M_n 42,500 were extruded and processed the same way as one would a scaffold. Strands were kept wet and were fastened securely into a mechanical testing rig by using adhesive tape and were marked to determine whether slippage of the stand occurred and then the length of the strand was recorded. The strand was then subjected to a tensile strain with the force and displacement recorded. A graph was then plotted (Figure 91) and the Young's modulus calculated (Table 12). From these graphs, it can be seen that the linear part of all three graphs coincide and the resulting Young's modulus are similar. These properties

were lower than the initial test because when the strand is dissolved, extruded and precipitated, the mechanical properties of the structure are weakened.

The second method involved PCL (M_n 42,000) that was dissolved in glacial acetic acid. This was then extruded into a bath of IMS (Sigma, UK). The resultant strands were cut and the lengths and diameters measured using Verniers callipers. The strands were tested in tension using a mechanical tester (Dartec, UK) with a 10N load cell. A smaller load cell was used as this provided more accurate measurements due to its increased sensitivity. A graph was then plotted of tensile stress against strain and the gradient calculated of the linear part to yield the Young's modulus.

2.2.4 Finite element analysis assessment of scaffold geometries

The finite element programme used was ABAQUS version 6.5. The CAD models were saved in standard ACIS text (SAT) format which is a format that can be imported into the ABAQUS program. When the scaffold part is imported it has to be given material properties such as the Young's modulus and the Poisson's ratio. The Young's modulus of the PCL was obtained from a previous experiment which is described in paragraph 2.3. The Poisson's ratio selected for the PCL was 0.3 as cited in the literature (Fang et al. 2005).

The model was then assigned three boundary conditions; the first represented a flat surface at the bottom of the scaffold which prevented any displacement in the direction of the applied force (Figure 86a). The second boundary condition was set as a displacement which corresponded to the desired global strain at the top of the scaffold therefore to obtain 3000με, the required displacement was 0.0152 mm which acted as the applied force (Figure 87). The third was a fixed anchor point which prevented lateral movement of the virtual scaffold (Figure 86b). The models were then meshed (Figure 88) with a global seed value of 0.11, which represents the size of the meshing elements and with all the required steps completed, the analysis was launched.

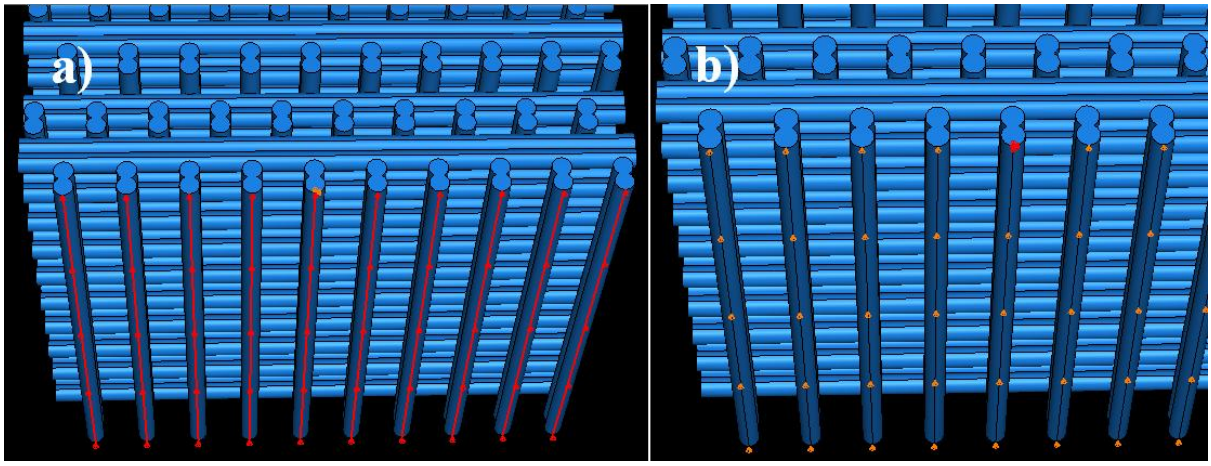

Figure 86: Boundary conditions on the bottom surface of scaffold, a) Stops the scaffold moving in the direction of compression, b) Fixed point (highlighted in red)

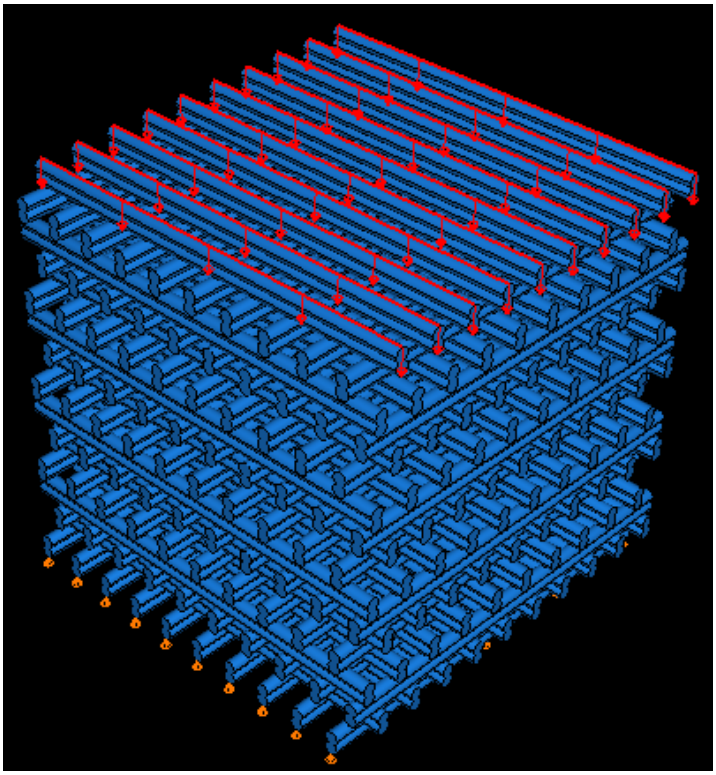

Figure 87: Boundary condition representing the top displacement of scaffold

In order for the strain distribution throughout the scaffold to be determined, a programme was written in Python programming language (to achieve this, help rendered by Dr A. Phillips is kindly acknowledged).

Once the analysis was completed, the data was represented graphically with different colours representing different strains (Figure 89).

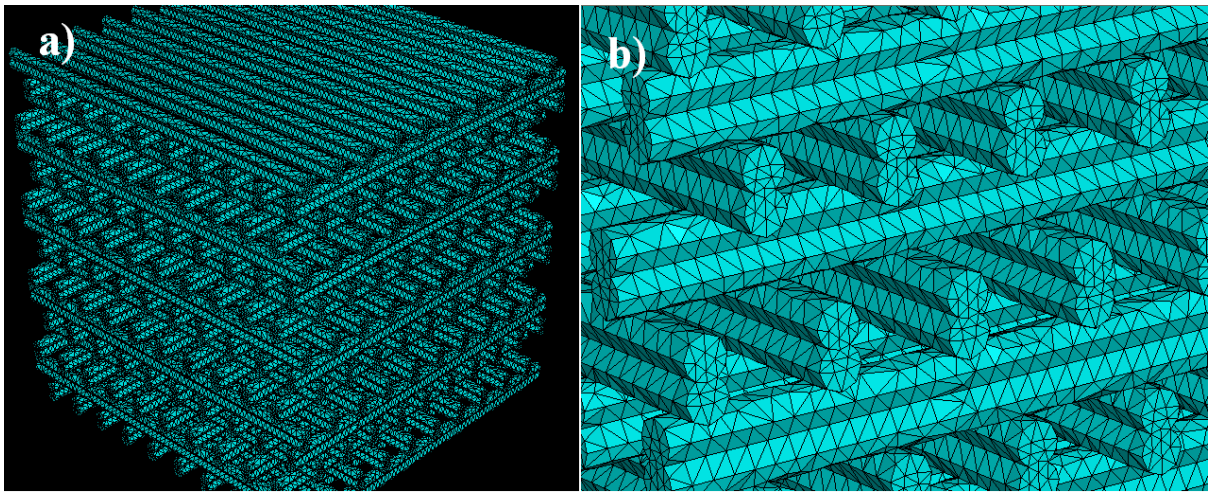

Figure 88: Meshing of FEA model, a) Meshed scaffold, b) close-up of tetrahedral meshing

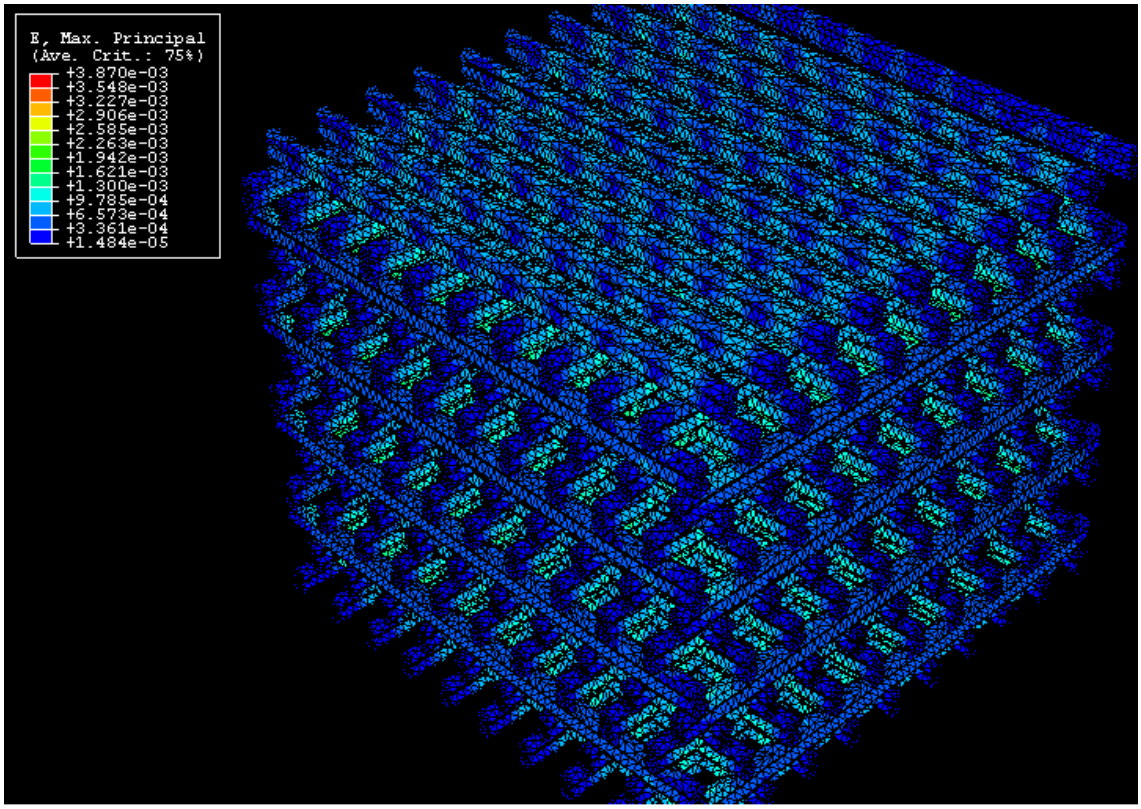

Figure 89: FEA analysis of scaffold where various colours represent different strains

2.3 Results

2.3.1 Young's modulus of polycaprolactone

Briefly, the mechanical properties of polycaprolactone were determined by creating three different cylinders with three different molecular numbers and obtaining the Young's modulus using compressive testing. From the graph of stress against strain (Figure 90), it can be observed that the gradient of PCL M_n 10,000 is steeper which indicates a greater Young's modulus however the graph also shows that the ultimate compressive strength is lower which indicates a brittle substance as the graph rapidly decreases as the strain is increased. The other two molecular numbers of polycaprolactone (M_n 42,500 and M_n 80,000) have a slightly more horizontal gradient and the ultimate compressive strength is not reached. Values of the Young's modulus obtained this way were correct (Hutmacher et al. 2001b, Mondrinos et al. 2006, Wang et al. 2004) but did not represent the Young's modulus of the polycaprolactone that was precipitated out while making the scaffolds. Therefore another measurement needed to be collected that more closely matched the mechanical properties of the extruded polycaprolactone. Strands of 30% w/v polycaprolactone with M_n 42,500 were extruded and processed the same way as one would a scaffold. Strands were kept wet and were fastened into a mechanical testing rig with the length of the strand recorded. The strand was then subjected to a tensile strain with the force and displacement recorded. A graph was then plotted and the Young's modulus calculated. From figure 91, it can be seen that the linear part of all three graphs coincide and the resulting Young's modulus are similar. These properties were lower than the initial test because when the strand is dissolved, extruded and precipitated, the mechanical properties of the structure are weakened (Shao et al. 2006a).

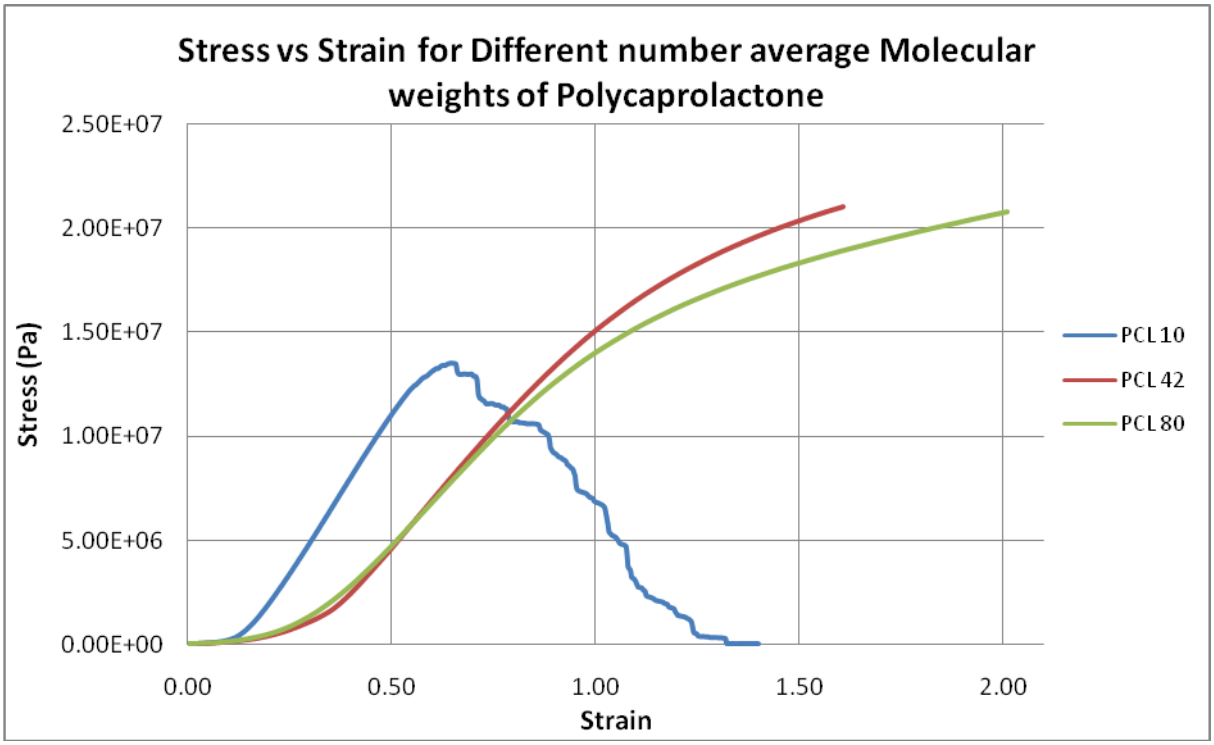

Figure 90: Stress versus Strain graph of three different number average molecular weights of melted and solidified polycaprolactone

From figure 90, the Young's Modulus of the individual number average molecular weights of polycaprolactone was calculated by determining the gradient of the linear part of the plot, this can be seen in table 10.

	Young's Modulus (MPa)
PCL M_n 10,000	306
PCL M_n 42,000	226
PCL M_n 80,000	206

Table 11: Young's Modulus of three different number average molecular weights of PCL

Three PCL strands (M_n 42,000) were tested in tension and the lengths and diameters recorded (Table 11) to enable calculations of the Young's modulus by determining the gradient of the linear part of the graphs.

	Length (mm)	Diameter (mm)	Area (mm^2)
Strand 1	25.00	0.145	0.017
Strand 2	19.67	0.145	0.017
Strand 3	18.13	0.145	0.017

Table 12: Dimensions of polycaprolactone strands

The results of the tensile experiment yielded a stress against strain graph (Figure 91) from which the Young's modulus of the polycaprolactone strand could be calculated.

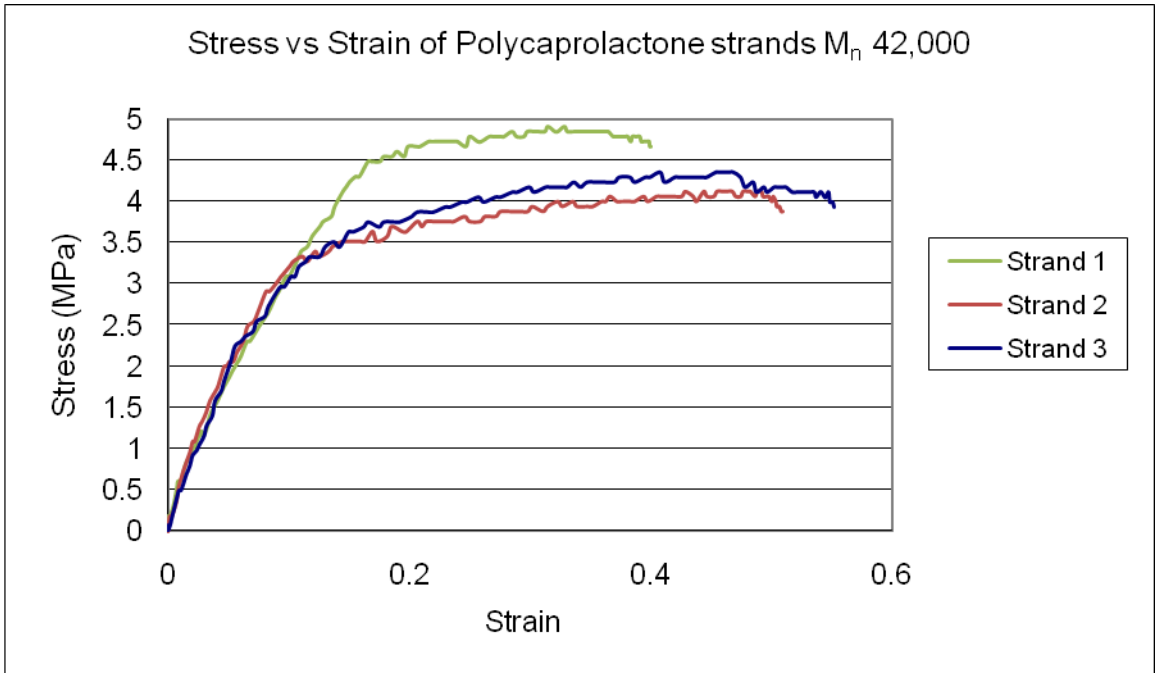

Figure 91: Stress versus Strain curve of PCL strands

	Young's Modulus (MPa)
Strand 1	36.57
Strand 2	52.39
Strand 3	49.18
Average	46.05

Table 13: Young's modulus of extruded strands of PCL M_n 42,000

2.3.2 Young's modulus of scaffold through FEA analysis

The Young's modulus of the scaffold was determined by firstly inputting the Young's modulus of the material which was obtained as described previously in section 2.2.3., the

finite element analysis was firstly performed by using the material properties of the polycaprolactone that was melted and solidified and then the extruded polycaprolactone properties were used. The reaction force at the bottom boundary condition was obtained, this then represented the actual force being exerted on the top surface and hence the Young's Modulus was obtained by using the equation:

$$Young's\ Modulus\ (E) = \frac{Stress}{Strain} = \frac{Force/Area}{Change\ in\ length/Original\ length}$$

For the melted and solidified PCL (Table 10 and Figure 90) and the extruded and precipitated PCL (Table 12 and Figure 91) the Young's modulus was calculated by knowing the height (L), area (A) and displacement (ΔL) which were 5.062 mm, 25 mm^2 and 0.0152 mm respectively. The reaction forces given in table 13 were obtained by subjecting the FEA model to a global strain of 3000 με.

Scaffold geometry	Reaction force (N)	Young's modulus of scaffold (MPa)
DSNO	1.750	23.31
DSO	1.264	16.84
DSNO45	1.489	19.84
DSO45	1.480	19.72
SSNO	1.655	22.05
SSO	0.470	6.26
SSNO45	0.824	10.98
SSO45	1.032	13.77

Table 14: Young's Modulus of various scaffold geometries using the material properties of the melted and solidified PCL

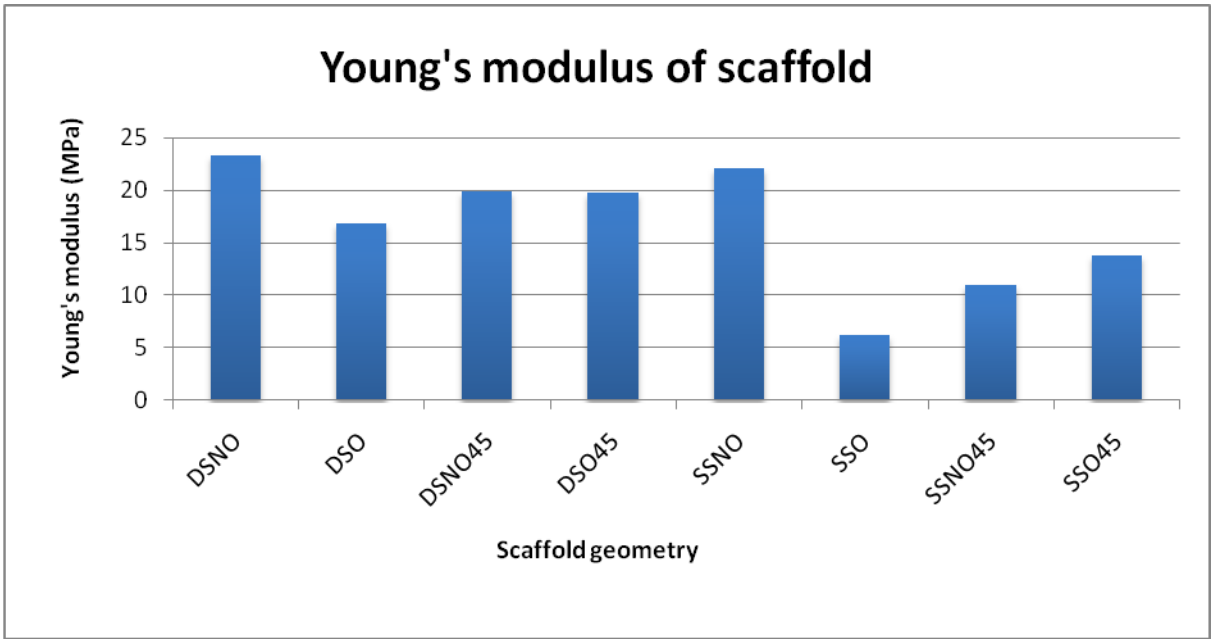

Figure 92: Representation of Young's Modulus of different scaffold geometries using material properties of the melted/solidified PCL

Scaffold geometry	Young's modulus of scaffold (MPa)
DSNO	3.1
DSO	2.2
DSNO45	2.6
DSO45	2.6
SSNO	2.9
SSO	0.8
SSNO45	1.5
SSO45	2.1

Table 15: Young's Modulus of various scaffold geometries using the material properties of the extruded PCL

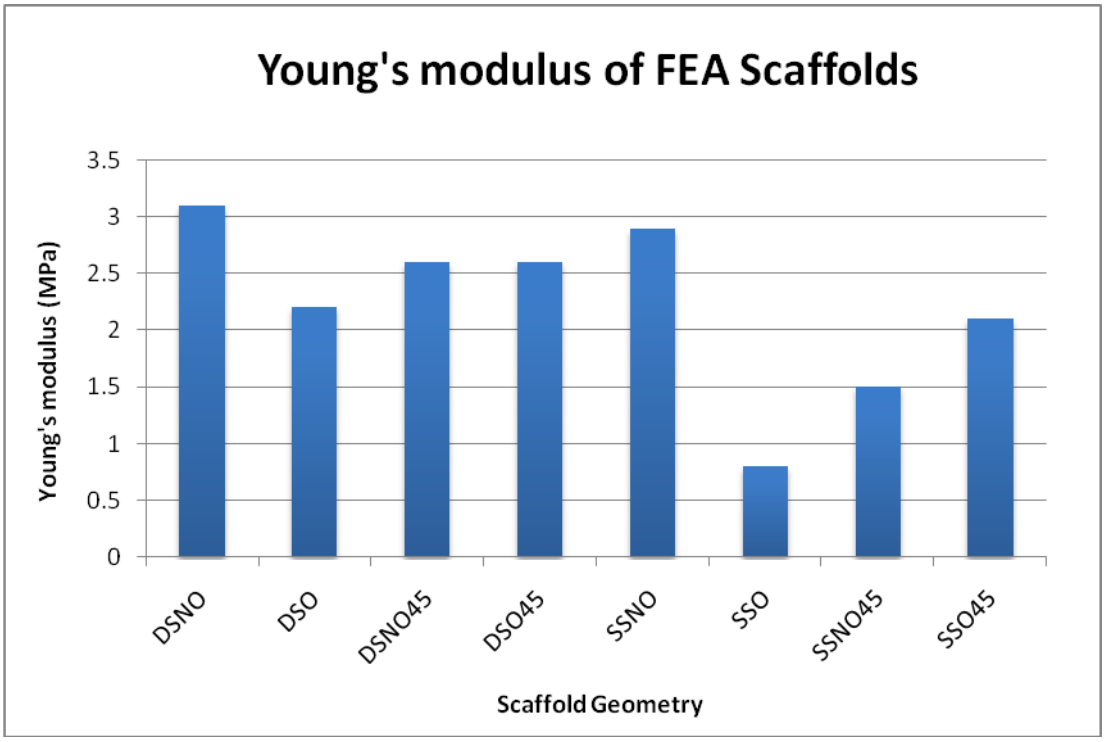

Figure 93: Young's modulus of scaffolds using the properties of the extruded PCL

From the results obtained from the two different material properties of PCL, it can be observed that the Young's modulii obtained with the melted and then solidified PCL properties are approximately 7 times higher. An interesting observation is that the trend of the scaffolds Young's modulii with the two different initial PCL properties remains similar. In figure 92 and 93, the DSNO scaffold geometry has the highest and the SSO scaffold geometry has the smallest Young's modulus.

2.3.3 Surface strain distribution throughout scaffolds

In order to assess the surface strain distribution i.e. the surface strain distributed throughout the entire scaffolds, at a physiologically relevant surface strains of 3000 µstrain (Burr et al. 1996, Mann et al. 2006, Milgrom et al. 2000), the percentage of the surface of the

scaffold strained between 2000 and 4000 µstrain was determined. The finite element analysis was performed using the Young's Modulus obtained from the extruded PCL (M_n 42,000) as described in paragraph 2.3. Two global strains of 3000 and 5000 µstrain were chosen to compress the scaffold, as these strains are generated in the Zetos™ bioreactor during mechanical stimulating (Mann et al. 2006) (See chapter 3 for more detail).

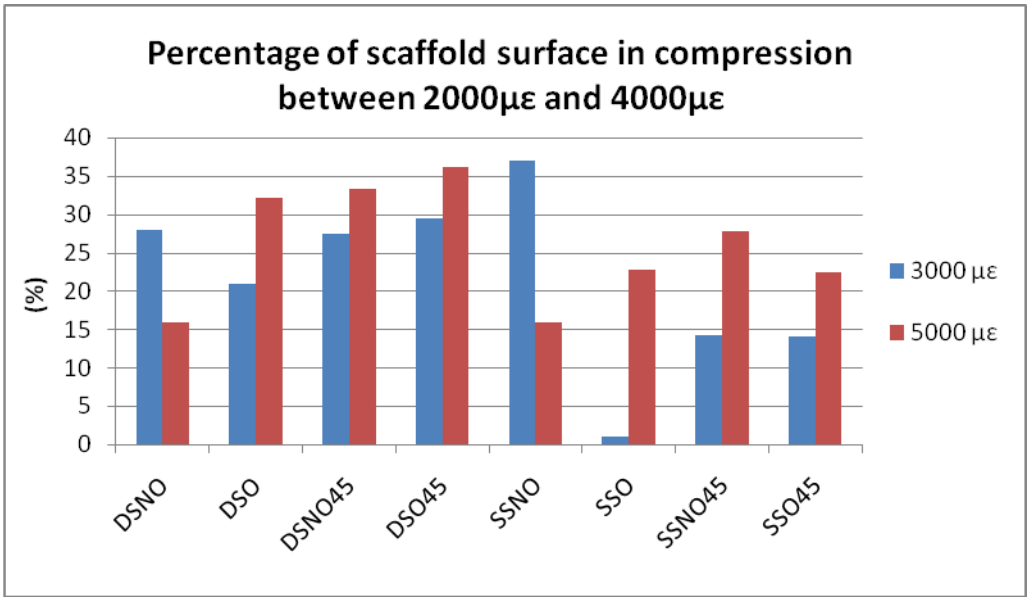

Figure 94: Surface of scaffold strained in compression between 2000 µε and 4000 µε with induced global strain of 3000 µε and 5000 µε

The two different global strains were analysed and from figure 94, it can be observed that in most cases, an increased global strain yielded an increased compressive surface strain. The two scaffold geometries where this is not true are the double strand no offset (DSNO) and the single strand no offset (SSNO) which can be explained due to the scaffold geometry. These two geometries form 'columns' due to the stacking of the layers as there is no offset or rotation of the layers and hence the majority of the compressive surface strain between 2000µε and 4000 µε are located at these supporting 'columns'. When the global strain was increased from 3000 µε to 5000 µε, the percentage of surface strain was reduced as the

physiological window of 2000με - 4000με was exceeded and therefore reducing the percentage surface strain.

In figure 95, where the surface strain in tension is shown, it can be seen that an increased global strain considerably augmented the surface strained in tension. However the dominant surface strain in the scaffolds is compressive.

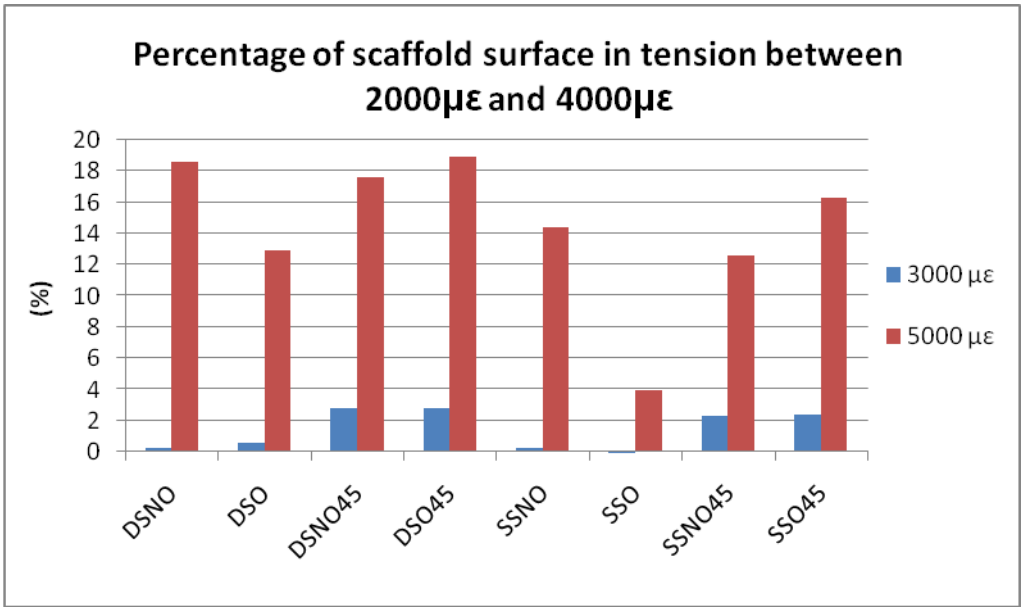

Figure 95: Surface of scaffold strained in tension between 2000με and 4000με with an induced global strain of 3000με and 5000με

The total strains generated throughout the scaffolds were then investigated (Figure 96), which represents the sum of the compressive and tensile strains. This then demonstrates the percentage of the surface strained throughout the scaffolds.

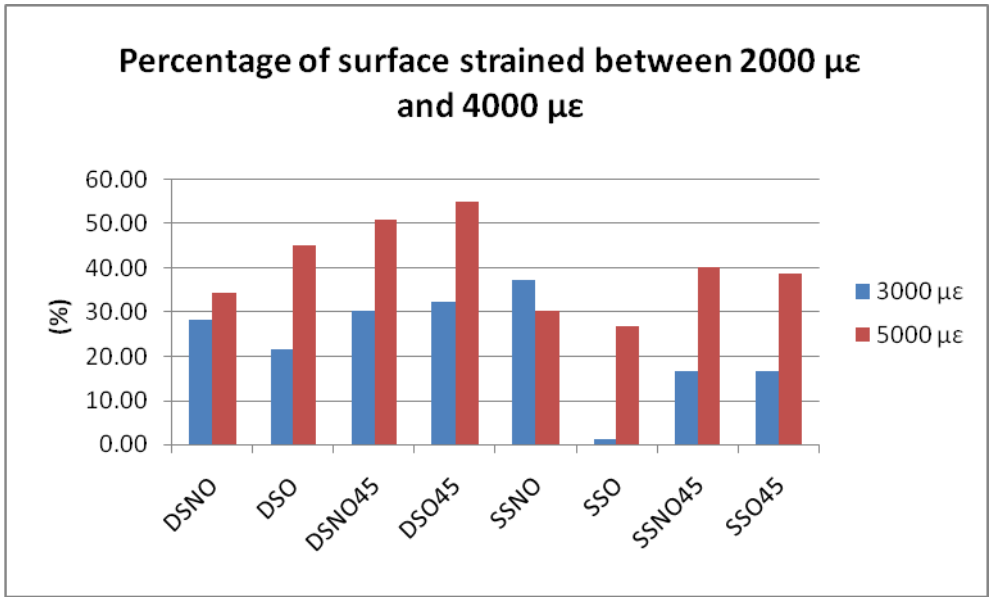

Figure 96: Total surface strain distributed throughout scaffolds

2.4 Discussion

The computer aided design models (CAD) were created by using the histomorphometric measurements performed on a polycaprolactone scaffold where various dimensions and lengths that would be required to create an accurate CAD model were measured. The main values required were the strand diameter, the height between strands and the distance between strands. The values were measured on six different locations on the scaffold so that an average value could be used that would more appropriately represent the dimensions of the required measurements and also to minimise the measuring errors that might have been introduced during the histomorphometric measurements. These errors occurred because the distances were measured by hand as the software BioQuant did not have the option to measure distances between two points using a pre-programmed straight line but the line had to be generated by hand which induced an error. Histomorphometry has not been reported in the literature for measuring scaffold geometry but is commonly used to determine distances between cells and areas of bone (Eriksen et al. 1989, Nafe and Schlote 2004, Revell 1983). Other groups that have done related work have used micro-computer tomography (CT) to generate exact CAD models of the generated scaffolds which then underwent FEA (Duty et al. 2007, Lacroix et al. 2006, Lin et al. 2004, Su et al. 2006).

After all the scaffold geometries were created, the files had to be converted to the standard ACIS text (SAT) format so that they could be opened by FEA program ABAQUS. Once all the models were converted and transferred, the Young's modulus and the Poisson's ratio had to be assigned. The value chosen for Poisson's ratio of polycaprolactone was 0.3 as this value was used in the literature (Fang et al. 2005, Sun et al. 2004).

After assigning the material properties, the models were given boundary conditions and meshed. The accuracy of the meshing caused several problems and had to be chosen carefully. It was discovered that a very fine mesh (global seeding value 0.07) could not be accomplished as the desktop computer (Pentium 4, 2.80GHz, 512 Mb RAM) ran out of memory and took a long time to process. This low seeding density was initially chosen as another group that performed analyses with the same ABAQUS program used a similar value of 0.075 (Wettergreen et al. 2005) however there was no report of any problems with their

computers which was probably due to using more powerful computers. Slightly lowered seeding density were then used (global seed value 0.09) which generated a mesh but when the analysis was initiated the computer ran out of memory and the analysis was halted. A global seed value of 0.11 was then discovered by iteration to be the lowest that did not crash the FEA software and did not affect the accuracy of the results. Hart *et al*, suggested that the precision of a particular FE model through a convergence test in which the model is repeatedly calculated with increasingly finer meshes until the magnitude of the chosen test area reaches a plateau, converging towards a precise solution of that model (Hart 1990). In the past, assessing precision was an important step due to limitations on computer power required researchers to determine an appropriate degree of mesh refinement that was reasonably precise and minimized computational demand however this has become less of an issue with more powerful computers (Richmond et al. 2005). Cook and Avrashi stated that no matter how finely a structure was meshed and how precisely the calculations were performed, the computed answer may still be wrong (Cook and Avrashi 1992) and that independent experimental support was critical to any FEA attempting to model a mechanical problem in a realistic manner by direct measurement of strain. However this view of FEA may be slightly dated and reports of the accuracy of FEA have been widely reported (Autuori et al. 2006, Burgers et al. 2008, Diego et al. 2006, Duty et al. 2007). FEA has been used in many biological applications in which individual skeletal elements or joints, such as the proximal femur (Beaupré et al. 1990) or skull (Strait et al. 2005) are modelled to better understand how the bones involved behave in response to applied loads. Beaupré *et al*, tested their theory of bone remodelling by comparing real bone structure with the results obtained of an FEA model that was repeatedly loaded and altered following the rules of the theory. In this way, Beaupré *et al* were able to assess the utility of the remodelling theory and demonstrate that similar stress related phenomena might be responsible for bone morphogenesis as well as functional adaptation in response to altered mechanical loads (Beaupré et al. 1990). Preuschoft and Witzel used FE modelling to test hypotheses about the evolutionary rules that govern skull morphology by applying muscle loads to a block with only minimal skull form i.e. orbits, dental arcade and location of muscle and compared the resulting stress distribution against a real skull form (Preuschoft and Witzel 2005). Li *et al*, used FE modelling to simulate the pressures involved in the intervertebral and lumbar disks to calculate the stress

and strain distribution and the deformation of the spine (Li and Wang 2006). These cases demonstrate that FE modelling has reached a level of sophistication and accessibility that renders it a powerful and useful tool to aid in measuring strain distribution and mechanical properties of scaffolds.

The Young's modulus of the scaffolds obtained from the FE analyses where the mechanical properties used were that of the melted and solidified PCL were much higher than the actual Young's modulii of the manufactured and mechanically tested scaffolds (see chapter 1). However Wang *et al* who used PCL to create scaffolds by liquefying the polymer to just above its melting point reported a Young's modulus approximately 10 times greater (Wang et al. 2004) than that obtained in the finite element analyses in this chapter. This could be due to the fact that the geometry of the tested scaffolds were different, in Wang *et al*'s work, the strand distance was 0.41 mm as opposed to 0.6 mm, the layer thickness was 0.254 mm whereas in this work it was 0.14 mm and the strand thicknesses were the same (0.25 mm). This then means that the effective distance between strands is 0.16 mm (0.41 - 0.25 = 0.16) which would considerably increase the overall mechanical properties of the scaffold. In work produced by Charles-Harris *et al*, polylactic acid (PLA) scaffolds were manufactured by salt leaching and scanned using a Synchrotron X-ray microtomography which yielded a 3D image which was then analysed using FEA. The Young's modulii ranged between 0.05 and 0.2 MPa , these lower values of Young's modulus were caused by the large pores that were present in the scaffolds due to the use of salt particles between 300 and 600 μm (Charles-Harris et al. 2007). In FE analyses performed by Lacroix et al, calcium phosphate bone cement was compressed and yielded a Young's modulus of 41 MPa however due to the nature of the scaffold, the random pore orientation and various thicknesses of the internal walls, it was reported that parts of the scaffold underwent much higher strains than others and were not uniformly distributed (Lacroix et al. 2006) which was not the case in the extruded scaffolds.

The FEA analyses performed with the Young's modulus obtained from the extruded strands (section 2.3), yielded values of Young's modulus similar to the manufactured PCL ones (Chapter 1). This would indicate that the extrusion process that the polycaprolactone underwent altered its mechanical properties and reduced its Young's modulus. The changes

to the mechanical properties could be due to the polymer chain reduction and maybe the introduction of bubbles during the extrusion process which would reduce the strength of the polymer. These reduced mechanical properties were also observed in the literature where the polymer was dissolved in a solvent in order to be manufactured into a scaffold (Charles-Harris et al. 2007, Shao et al. 2006b).

Another factor which affected the difference between the Young's modulus of the manufactured and the computer generated scaffolds was that the scaffolds created in the CAD program had no defects and were theoretical ideal representations of the manufactured scaffolds. It can be observed from the SEM images (see chapter 1) and figure 59, that the strands are not perfect cylinders as was represented in the CAD models and that the strands experience a slight amount of sagging, this phenomenon can also be observed in other work done by Wang *et al* and Moroni *et al* (Moroni et al. 2006, Wang et al. 2004).

From the results obtained from section 3.3 regarding surface strain distribution throughout the scaffold, the two global strain values chosen were 3000 and 5000 με, as these were the global strains that the scaffold was subjected to in the Zetos™ bioreactor system. If the displacement of the piston which generates the compression in the bioreactor could be altered, the global strain could be increased which would then generate more surface strain between 2000 and 4000 με throughout the scaffold which would then affect more of the cells that were seeded on the scaffold. This increased surface strain would in principle push more of the MSCs down the osteoblastic lineage and hence create more bone mineral. In work produced by Duty *et al*, it was reported that the average strains generated in their scaffold was 2000με however the proportion of the scaffold surface strained was not mentioned (Duty et al. 2007). In the work reported by Lacroix *et al* who created porous calcium phosphate scaffolds, it was observed that 90% of the strain distributed throughout the scaffold was lower than 2200με (Lacroix et al. 2006) which is at low end of the effective strain experienced in trabecular bone. However the work performed in this chapter suggests a greater effective strain distribution throughout the scaffold with approximately 40% of the scaffold surface being strained between 2000με and 4000με.

2.5 Summary

FE analysis has been shown to be a reliable tool to precisely characterize the strain distribution and the mechanical properties of the 3D scaffolds. Furthermore the use of histomorphometry has made it possible to create a mathematical model that can then be analysed using a finite element analysis package and determine the strain profile of the scaffold when loaded and its mechanical properties. From the finite element analyses performed on the CAD scaffold models; these were represented by the values of the Young's modulus obtained by mechanically stimulating the manufactured PCL scaffolds which provides validation of the FE model of the scaffolds. By obtaining similar results for the Young's modulus, it can be concluded that the strains distributed throughout the scaffolds are also similar as the ratio of the stress and the strain are comparable. This then enables the creation of scaffolds with specific surface strain characteristics to be created by first modelling them using FEA by varying the scaffold architecture. This prevents using materials that will not meet the desired surface strain requirements. Finite element analysis can be used to determine various scaffold geometries and establish which scaffold geometry is best suited for the desired application.

Chapter 3.

Zetos ™ bioreactor and manufactured scaffolds

3.1 Introduction

In the 19th century, Julius Wolff suggested that mechanical stress was responsible for determining the architecture of bone but more importantly suggested that mechanical stress and the form of bone are related by a mathematical law called Wolff's law of transformation (Wolff 1892). Although it is accepted that certain aspects of Wolff's law are not entirely correct i.e. that bone remodelling occurs by a set of mathematical laws, (Bertram and Swartz 1991, Lovejoy et al. 2003, Pearson and Lieberman 2004), the idea that mechanical stress affects bone architecture is well documented in the literature and widely accepted, (Carter 1987, Frost 1992, Lanyon et al. 1982, Mosley 2000). Increased loading of the skeleton has been shown to increase bone mass (Bassey and Ramsdale 1994, Jones et al. 1977, Woo et al. 1981) and retard bone loss in postmenopausal women (Brockie 2006, Krolner et al. 1983, Simkin et al. 1987). Conversely a reduction of bone formation (Morey and Baylink 1978, Wronski and Morey 1983) and mineral content (Cann and Adachi 1983, Rambaut and Johnston 1979, Vico et al. 1987) are associated with the un-loading of the skeleton in spaceflight. However during spaceflight, bone loss occurs in a non-uniform manner with the distal leg bones experiencing the greatest bone loss (Collet et al. 1997, Vogel and Whittle 1976). This has been hypothesized to occur due to the lack of normal high frequency heel strike activity under microgravity conditions (Goodship et al. 1998).

Some interpretations of Wolff's law have suggested that changes in bone structure are brought about by a feedback system that occurs between the local mechanical signals and the bone cells which results in changes of bone arrangement. The best accepted theory is the 'mechanostat' hypothesis proposed by Frost (Frost 1983, Frost 1987, Frost 1990). Frost's mechanostat theory is unique in its distinction between modelling and remodelling processes with thresholds for activating lamellar or woven bone formation. Frost describes a window of mechanical usage that should be considered as physiological or normal. When local mechanical load in bone exceed the upper boundary of the physiological window, bone will undergo modelling and adapt its structure to reduce the local strains. If the mechanical loads on the bone are very large, the local strains will be pushed into pathological overload which causes woven bone formation on the bone surface and conversely if the local strains are low, bone will be resorbed until the strains in the bone are increased (Frost 1987).

3.1.1 Mechanotransduction

The mechanostat and the mechanisms that make it work are not completely understood however there is a requirement for some sort of cellular mechanotransduction (Turner and Pavalko 1998), which is the conversion of a biophysical force into a cellular response. In bone, the mechanotransduction can be divided into four distinctive phases:

- Mechanocoupling
- Biochemical coupling
- Transmission of signal
- The implementer cell response

3.1.1.1 Mechanocoupling

Mechanocoupling is the transduction of a mechanical load applied to the bone into a local mechanical signal that is detected by a sensor cell. In bone, the mechanical loads that are associated with normal everyday use cause a deformation in the bone known as strain. One micro-strain (με) is equivalent to one micrometer (μm) of deformation per meter. The levels of these strains are different depending on the activity and can range between 400 and 3000 με (Burr et al. 1996, Milgrom et al. 2000). The typical use of long bones combines compressive forces and bending (Bertram and Biewener 1988, Rubin and Lanyon 1982) which creates large differences of strain on the bone surface. The peak magnitudes generated in bone have been associated with the degree of bone adaptation (Rubin and Lanyon 1985), but there are other factors that contribute to the adaptive response. During mechanical loading of bone, the bone tissue deforms and creates a pressure difference in the bone's canalicular system which engenders movement of extracellular fluid transporting nutrients to the osteocytes and creates fluid shear stresses on the osteocytes cell membrane (Burger and Klein-Nulend 1999, Weinbaum et al. 1994). The shear stresses cause cell deformation and is followed by metabolic activity via integrins and the cytoskeleton (Ajubi et al. 1996). The osteocytes and the bone lining cells act as the sensors for the local bone strain as they are appropriately situated in the bone for this function (Aarden et al. 1994, Burger and Klein-

Nulend 1999, Turner and Forwood 1995). Osteocytes and the bone lining cells are stretched the same amount as the bone tissue when it is loaded with the mechanical stimulus on the osteocytes being biaxial as when the bone is compressed in the longitudinal direction, it expands slightly in the perpendicular direction (Duncan and Turner 1995). In addition, the strains caused by loading generate extracellular fluid flow across the osteocytes. It is unclear which type of stimulus, mechanical stretch or fluid flow has a greater effect on the bone cells. It is probable that the latter respond to more than one component of their mechanical environment. This is supported by the ability of mechanical strain and fluid flow to promote bone cell activity (Ajubi et al. 1996, Burger et al. 1995, Davies et al. 2006, Mann et al. 2006, Reich et al. 1990b, Weinbaum et al. 1994). Because *in vivo* loading is always accompanied by fluid flow, bone cells might respond to changes in their strain environment by a combined assessment of both fluid flow and physical deformation.

3.1.1.2 Biochemical coupling

Biochemical coupling is the transduction of a mechanical signal sensed by the cell into a biochemical signal which would alter gene expression. The bone cells possess glycoprotein integrins that are rigidly adhered, on one side to the bone matrix and on the other to the cell cytoskeleton. If there is a disruption in the tension of the extracellularly exposed integrins, a signal would be transmitted to the osteocyte nucleus (Duncan and Turner 1995). Stretch-activated channels such as the potassium channel or the guanine nucleotide binding proteins (G-proteins) located on the cell membrane may be activated by fluid flow. These pathways are thought to work together or independently depending on the type of mechanical signal received (Turner and Pavalko 1998).

3.1.1.3 Transmission of signal

There are two possible pathways by which a biochemical signal in the sensor cell is transmitted to the implementer cell to increase osteogenic activity after a mechanical stimulus. First, active osteoblasts located on the bone surface are able to detect mechanical

strain and also act as the implementer cell that increases bone formation. This situation is supported by Harter and Burger who observed an increase in the production of expression of matrix proteins when osteoblasts-like cells were exposed to a cyclic mechanical stretch (Harter et al. 1995). However, active osteoblasts make up only 5% of the bone surface in adult humans with bone lining cells making up 94% of the bone surface and osteoclasts making up the remaining 1% (Parfitt 1983). Therefore stimulation of active osteoblasts alone is not sufficient to generate substantial increases in bone mass. Osteocytes and bone lining cells make up in excess of 95% of all cells of the osteoblastic lineage that are attached to the bone (Frost 1960, Parfitt 1983), in addition the osteocytes have the ability to communicate with other bone cells by using an extensive network of cellular processes connected through functional gap junctions (Noble and Reeve 2000, Stains and Civitelli 2005, Taylor et al. 2007) and are responsive to mechanical stimulus *in vivo* (Dodds et al. 1993, Pead et al. 1988, Skerry et al. 1989). Therefore it is assumed that these cells act as sensors to mechanical stimuli but since osteocytes and bone lining cells are nonproliferative and are unable to actively form or resorb bone, they must signal to the implementer cells (osteoblasts or osteoclasts) before any change in bone structure can be initiated. The most likely intermediaries for the transmission of the biochemical signal between the sensor cells and the implementer cells are the prostaglandins (Klein-Nulend et al. 1995, Klein-Nulend et al. 1997) and nitric oxide (NO) (Johnson et al. 1996, Pitsillides et al. 1995), with both being produced when mechanical stimuli was applied to cells *in vitro*. Blocking the production of prostaglandin *in vivo* with selective inhibitors eliminates mechanically induced bone formation (Forwood 1996) and inhibitors of nitric oxide synthases also suppress mechanically induced bone formation in rats (Fox et al. 1996, Turner et al. 1996).

3.1.1.4 Implementer cell response

The response of bone formation to mechanical loads involves the proliferation and nonproliferation of the implementer cells or in the case of bone formation, osteoprogenitor cells. Within forty eight hours after mechanical loading an early bone formation response is induced and osteoblasts are recruited from the bone lining cells or the non-dividing

preosteoblasts (Turner and Pavalko 1998). Proliferating osteoprogenitor cells are stimulated by mechanical loading and differentiate into osteoblasts 72 to 96 hours after mechanical stimulus (Turner et al. 1998).

3.1.1.5 Mesenchymal stem cells

Mesenchymal stem cells (MSC) were first described in bone marrow where they were also termed 'marrow stromal cells' (Friedenstein et al. 1974). However it is now known that similar but heterogeneous populations of progenitor cells are also present in many other tissues. Mesenchymal stem cells can be isolated from periosteum (De Bari et al. 2006, Nakahara et al. 1991), muscle (Sampath et al. 1984), synovium (De Bari et al. 2001), synovial fluid (Jones et al. 2004), liver and blood (Campagnoli et al. 2001), umbilical cord blood (Erices et al. 2000), and fat (Lee et al. 2004b). The source of the mesenchymal stem cells has an influence on phenotype and functional properties which was reported in the study carried out by De Bari et al where human mesenchymal stem cells from periosteum have a greater capacity to create bone *in vitro* than do human mesenchymal stem cells from the synovial membranes (De Bari et al. 2006).

Many adult tissues contain population of stem cells that have the capacity for renewal after trauma, disease or aging. The adult bone marrow contains mesenchymal stem cells that are thought to be multipotent cells. MSCs can replicate as undifferentiated cells and have the potential to differentiate to lineages of mesenchymal tissue which includes bone, cartilage, fat, tendon, muscle and marrow stromal cells (Dennis and Charbord 2002). The potential use of MSCs to treat genetic disorders and for tissue engineering for reconstruction of bone tissue has fuelled attempts to isolate and purify MSC populations but this has been difficult.

Work done by Horwitz *et al* for the International Society of Cellular Therapy made a statement to define theses progenitor cells and termed them 'multipotent mesenchymal stromal cells' and more recently by Dominici *et al* who also proposed a minimum criteria to define human MSC. These cells should firstly be plastic adherent in up to five days when maintained in standard culture conditions and have a fibroblast-like morphology, secondly

must bear some stromal markers (CD73, CD90 and CD105) and be negative for haematopoietic marker (CD14 or CD11b, CD34 and CD45) and thirdly the cells must be able to differentiate to osteoblasts, adipocytes and chondroblasts under standard in vitro conditions (Dominici et al. 2006, Horwitz et al. 2005).

Commitment of MSCs to tissue-specific cell types is orchestrated by morphogens (molecules that play a role in the development of organs), developmental signalling pathways and transcriptional regulators that act as 'master switches' (Figure 97) the main one being Wnt, Runx2 and Osterix. The Wnt/β-catenin pathways provides initial developmental cues that indirectly enable the initial cascade of gene expression for skeletal development, bone formation and osteoblast differentiation (Church and Francis-West 2002, Logan and Nusse 2004). Wnts play an extensive role in skeletogenisis from embryonic skeletal patterning, through fetal skeletal development and remodelling of the adult skeleton which was demonstrated by multiple skeletal defects in mice with mutations in Wnts (Kato et al. 2002).

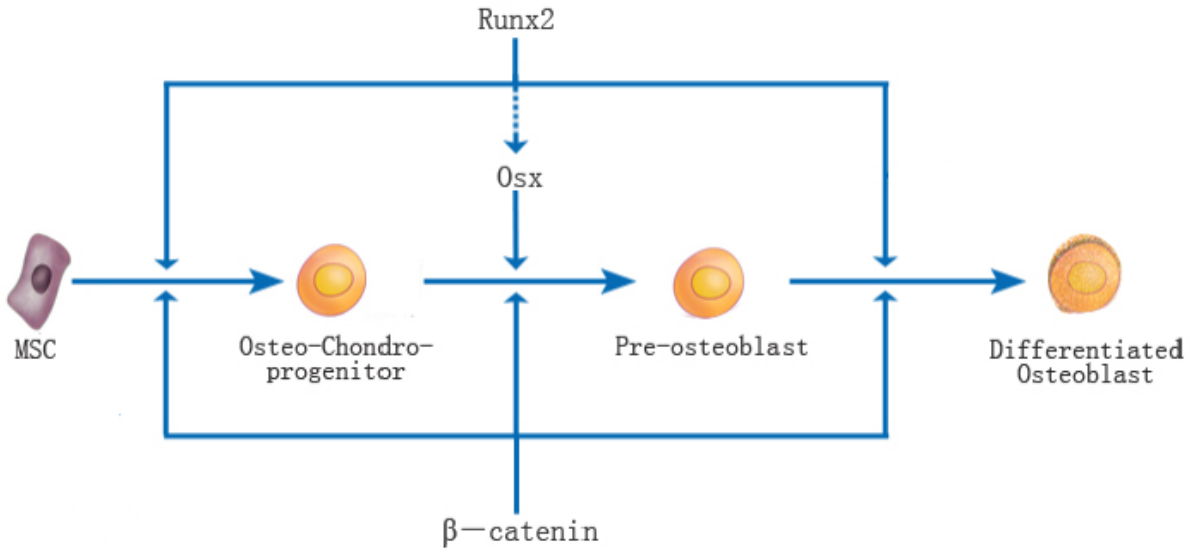

Figure 97: Regulation of osteoblast differentiation by transcription factors

Runx2 transcription factor which is also known as CBFA1 (Core Binding Factor 1) is a central regulator of bone formation and is essential for osteoblast differentiation, this differentiation program also requires other genes such as osterix, which encodes a transcription factor genetically 'downstream' of Runx2 (Karsenty and Wagner 2002). The targeted disruption of Runx2 results in a complete lack of bone formation by osteoblasts which indicates that Runx2 is essential for endochondral and bone formation (Komori et al. 1997).

Osterix (Osx) is a bone morphogenic protein 2 (BMP2) inducing gene which contains a deoxyribonucleic acid (DNA) binding domain. In Osx-null mutant mice, no endochondral or bone formation occurs (Nakashima et al. 2002). The mesenchymal cells in Osx-null mutant mice do not deposit bone matrix and cells in the periosteum and the condensed mesenchyme of membranous skeletal elements cannot differentiate into osteoblasts, although these cells express normal levels of Runx2. Osx-null osteoblast precursors in the periosteum of the membranous bones express chondrocyte markers (Sox9 and Col2a1) which suggests that Runx2 expressing preosteoblasts are still bipotential cells and Osx acts downstream of Runx2 to induce osteoblastic differentiation in the osteochondroprogenitor cells (Nakashima et al. 2002).

Committed preosteoblasts are recognised close to the bone surface by their proximity to surface osteoblasts and by histochemical detection of alkaline phosphatase enzyme activity which is one of the earliest markers of the osteoblast phenotype whereas osteocalcin is a late marker that is upregulated only in post-proliferative mature osteoblasts (Aubin 2001).

3.1.2 Mechanical stimulation of bone cells

Due to the complexity of the *in vivo* environment, *in vitro* representations are heavily relied on to study the phenomena of cellular response to mechanical stimulation. Such work has generally involved cell culture systems with controlled delivery of a substrate strain, fluid shear or a mechanical input. Laboratory apparatuses created for that purpose span a range of

complexity and precision with varied levels of mechanical input signal with magnitudes ranging from 200 με to 100,000 με.

Early efforts in the field of *in vitro* mechanostimulus were of a non-quantative nature. Pioneering work was performed by Glücksmann in 1939, who used numerous interesting biological loading models. One of these involved endosteal cell cultures from embryonic chick tibiae which were grown on substrates of explanted intercostal muscle to which pairs of neighbouring ribs were left attached (Glucksmann 1939). Over a period of days the endosteal cell cultures were compressed as the ribs were drawn together due to degeneration of the muscle tissue. Presently multiple *in vitro* techniques have been used to simulate *in vivo* strain on cultured cells including hypotonic swelling (Chen et al. 2005, Duncan and Hruska 1994), longitudinal mechanical stretch (Harell et al. 1977, Jones et al. 1991), biaxial mechanical stretch (Brighton et al. 1991, Buckley et al. 1988, Hasegawa et al. 1985), substrate bending (Bottlang et al. 1997, Pitsillides et al. 1995), fluid shear (Reich et al. 1990a, Reich and Frangos 1991), hydrostatic pressure (van Kampen et al. 1985, Veldhuijzen et al. 1979) and compressive loading (Davies et al. 2006, el Haj et al. 1990). These different methods of *in vitro* strain application produce different types of cellular deformation (Figure 98). Variation in cell deformation engendered by these methods of applying strain makes it questionable whether cells respond differently to dissimilar types of strain.

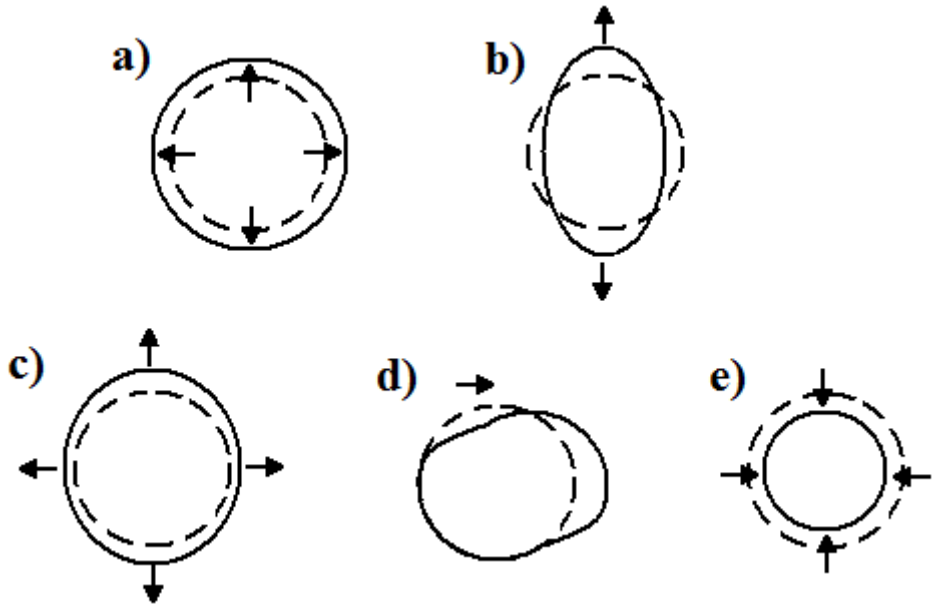

Figure 98: Schematic representation of cellular deformation in vitro under different types of loading. a) Hypotonic swelling, b) Uniaxial stretch, c) Biaxial stretch, d) Fluid shear, e) Hydrostatic pressure

Considering that bone cells are probably loaded *in vivo* by mechanical stretch and fluid shear, hypotonic swelling and biaxial stretch are probably the least physiologically relevant *in vitro* models as hypotonic swelling does not occur in bone under physiological conditions and biaxial stretch does not accurately represent the effects that occur in mineralised bone (Duncan and Turner 1995). Hydrostatic pressure rarely occurs in mineralized bone but can be observed in certain very specific cases i.e. during endochondral ossification of long bones where cartilage increases in size and is replaced by bone (Carter and Wong 1988, Ochoa et al. 1991).

3.1.2.1 Mechanical stretching systems

Stretching systems that utilize a controlled uniaxial deformation of substrate have many advantages and have been widely used (Figure 99). These types of systems trace their roots

back to the 1980s by work performed by Somjen et al who developed a static loading system (Somjen et al. 1980) but developments have been made in control of parameters and the accuracy of applied strain. Leung showed the potential for an oscillating load by using a motorized plunger-linkage system adapted to stretching rectangular elastin substrates seeded with aortic smooth muscle cells (Leung et al. 1977). However the heterogeneity of the strain distribution was due to the effects of the end grips and the different physical properties and geometric irregularities of the natural elastin.

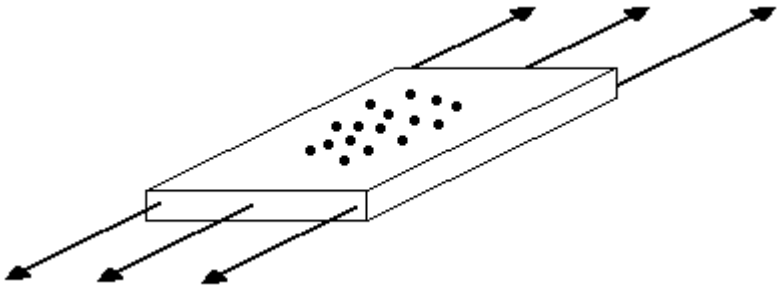

Figure 99: Uniaxial substrate tension (stretch)

Improvements were made by Ives et al by simplifying the motor system to a spring-loaded pulley/cable arrangement and by replacing the natural substrate with a more homogeneous and geometrically regular polyetherurethane urea substrate (Ives et al. 1986). Individual rectangular wells sealed into a common polycarbonate base sheet have been described with the mechanical strain being generated by the base sheet tensioned cyclically (Murray and Rushton 1990), but no method was presented to measure the strain distribution on the culture surface. Another device employing rectangular wells was described four years later where individually cast silicone rubber dishes were gripped by brackets and driven by a DC (direct current) motor. Strain distribution for both the axial and transverse (Poisson effect) components were measured by optical measurements of grid ruling which led to the input strain fields being well quantified (Neidlinger-Wilke et al. 1994). There have been some specialized developments of the longitudinal stretch system where microscopic and electrophysiological measurements can be undertaken on the substrates (Jones et al. 1991).

3.1.2.2 Biaxial mechanical stretch

Biaxial stretch of a substrate can be achieved by pulling a membrane segment in two perpendicular directions (Figure 100). This system is not vulnerable to frictional problems (discussed further in later examples), but is demanding in terms of hardware implementation and only provides biaxial strain at sites located away from the grips (Norton et al. 1995).

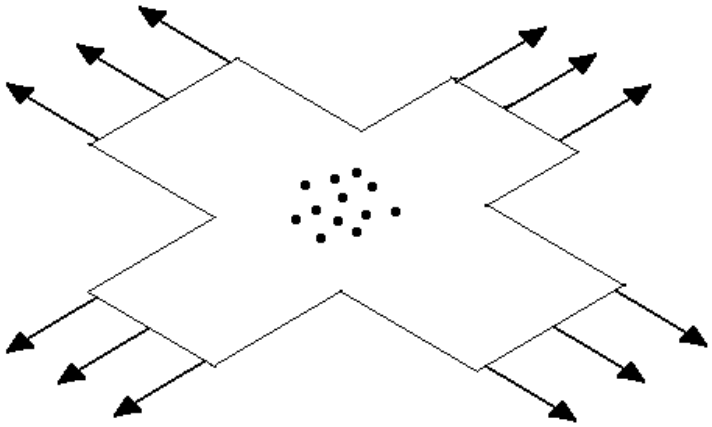

Figure 100: Biaxial substrate strain

Another system of achieving biaxial strain was by a vertically pulsating circular ring with low friction outer rim which served to stretch a portion of a cell culture membrane (Figure 101) (Hung and Williams 1994).

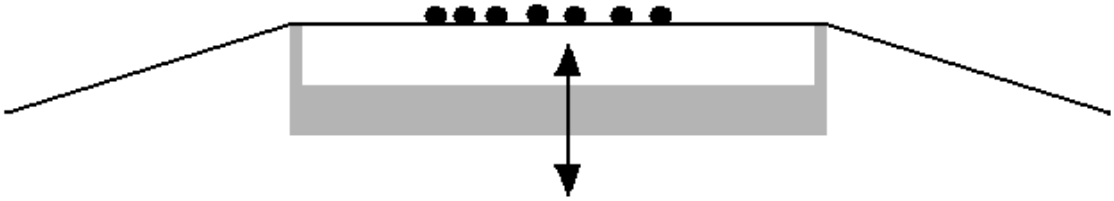

Figure 101: Biaxial circumferential strain by frictionless ring

3.1.2.3 Substrate bending

Substrate bending (Figure 102) provides an alternative method for the generation of uniaxial longitudinal strains to a culture surface. A four point bending systems have been developed to deliver a low strain level which coincides with the strains experienced in bone *in vivo*, typically several hundred to approximately 3000 με (Bottlang et al. 1997). Cast silicone rectangular dishes were bent using a four point bending set up by means of an electromagnetic actuator and homogeneity of strain was demonstrated optically using holographic interferometry as the strain levels were low (Bottlang et al. 1997). Other four point bending systems have been devised using plastic strips onto which osteoblasts-like cells and osteocytes were seeded (Pitsillides et al. 1995). Another four point bending system created by Jones *et al* used rectangular culture plates made of polycarbonate or glass suspended within a silicone rubber culture well which enabled the study of either compressive or tensile strains depending on the sides of the substrate being loaded (Jones et al. 1991). In this study, it was reported that strains of over 10,000 με de-differentiated the osteoblasts and changed the cell morphology to become fibroblasts-like.

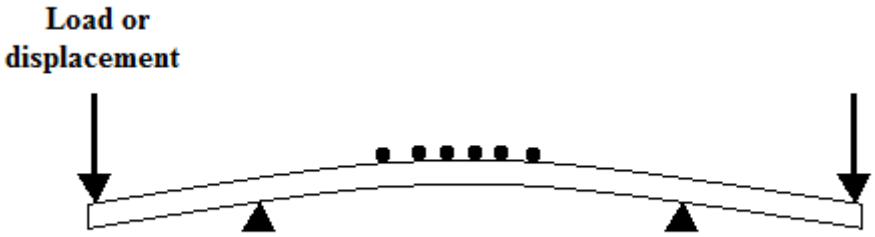

Figure 102: Longitudinal substrate bending

3.1.2.4 Fluid shear systems

Another approach to cell culture mechanostimulus reported in the literature has been by applying fluid shear as a wide range of cellular phenomena have been reported to be

influenced by fluid shear including cellular response and mechanoreception (Davies 1995, Klein-Nulend et al. 1997). Two main types of apparatus configurations have been reported including the cone-and-plate system (Figure 103a) and the parallel flow chamber (Figure 103b). The cone-and-plate system generates fluid shear by rotation of a cone around its central axis which is orientated perpendicularly to a flat plate (Hermann et al. 1997, Mohtai et al. 1996, van Grondelle et al. 1984). The other fluid shear system, the parallel plate flow chamber, relies on a pressure differential created between two openings at either end of a rectangular chamber which generates a laminar flow across the culture surface. This system holds many practical benefits including the homogeneity of the shear stimulus, simplicity of the equipment, ease of changing of the cell medium, simplicity of access to the culture and small volumetric requirement (Brown 2000).

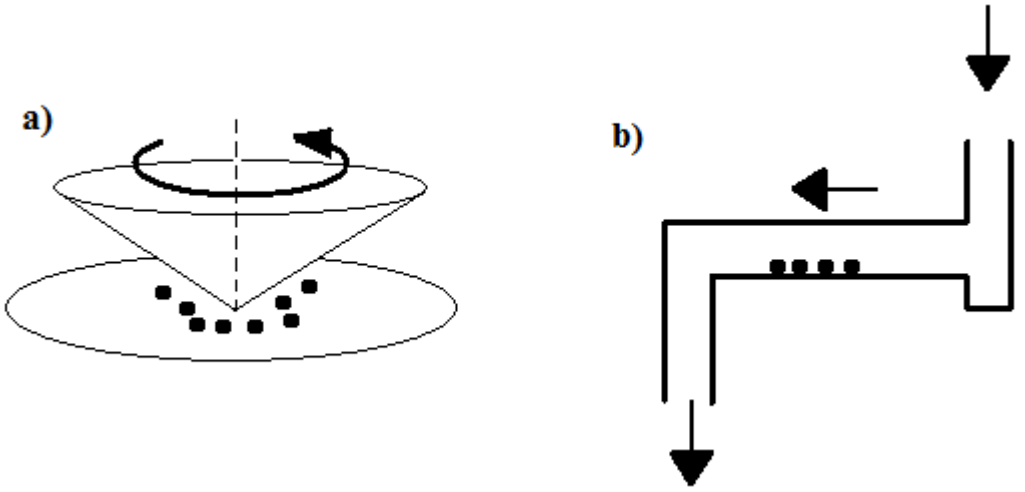

Figure 103: a) Cone and plate chamber, b) Parallel plate flow chamber

3.1.2.5 Hydrostatic pressure

Hydrostatic pressurization (Figure 104), has been a very frequently used method for compression of cells, tissue and explanted cultures (Bagi and Burger 1989, Bourret and Rodan 1976, Klein-Nulend et al. 1986, Lippiello et al. 1985, Wu et al. 2007). Both negative and positive pressures has also been described (Yousefian et al. 1995). Hydrostatic compression holds numerous attractive points including simplicity of the equipment,

homogeneity of the stimulus, simplicity of configuration multiple loading replicates and ease of delivering and generating either static or short dynamic loading inputs. Because there is no direct contact from piston there is no concern of cellular compaction and there is no dependency on the state of adhesion of the cell culture and the substrate. In order to create the hydrostatic pressure, the incubator gas pressures required are high which in turn produces increased levels of oxygen and carbon dioxide in the cell medium, which then requires a compensatory treatment step involving changing the ratio of CO_2 and oxygen (Ozawa et al. 1990).

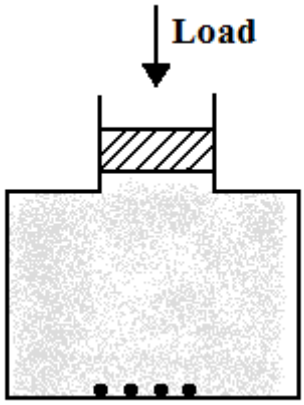

Figure 104: Hydrostatic pressure

3.1.2.6 Compressive loading

This loading technique has been attractive for cartilage and bone stimulation due to its similarity to *in vivo* loading. Pneumatically controlled systems in which small cartilage explanted discs were loaded in an unconfined uniaxial compression have been reported (Torzilli et al. 1997). Earlier variations have been described where constant or low-cycle intermittent loads were manually applied to cartilage explants by means of dead weights (Burton-Wurster et al. 1993), or a motorized micrometer and a sensitive load cell were used to deliver a precise and controlled load over three orders of magnitude (0.001-1.0 MPa) in multi-hour experiments (Guilak et al. 1994).

Axial compression for bone has also been developed. A pneumatically driven culture system for the axial compression of 10 mm core biopsies of cancellous bone have been developed by el Haj et al, but in addition to the axial compression the system provided controlled delivery of nutrient fluid by means of portals in the compression piston (el Haj et al. 1990). Other pneumatically driven axial systems that are able to stimulate up to 24 rat mandibular condyles explants specimens have been reported (Copray et al. 1985). Similar multi-specimen unconfined compression systems were reported using a ring to control axial displacement of the specimens, however there was no attempt made to quantify strain delivered to the individual specimens but only estimates made of strains ranging between 50 and 80% (Cheng et al. 1996). Another system was developed by Tanaka with particular interest in bone strain (Tanaka 1999). This system used a piezoelectric actuator which was driven by a power amplifier as to achieve axial piston displacements. It was capable of importing waveforms which could govern the frequency and the generated strains. An *in vivo* technique for mechanically loading cells seeded on a polymer scaffold has been reported by Duty *et al* in which cylindrical scaffolds seeded with rat MSCs were implanted subcutaneously in a specially designed chamber which delivered a 30 minute load three times a week for two weeks. The chamber assembly was then left for a further 4 weeks to maximise the mineral deposition in response to the loading (Duty et al. 2007).

3.1.2.6.1 Zetos bioreactor and mechanical loading system

A more recent mechanical compression system was developed in 2003 and called the Zetos™ system (Figure 105). The Zetos™ is a highly accurate mechanical loading and measurement system with a combined diffusion culture/loading chamber which acts as a bioreactor. It was specifically designed to study trabecular bone under controlled culture and loading conditions for long periods of time. The loading system has been designed to function in two main modes. The first is to apply a specific compressive strain to the sample and the second is to deliver a specific force to the specimen and record the resulting deformation. The Zetos™ can load precisely cut bone cores at frequencies between 0.1 Hz to

50 Hz with amplitudes over 7000με. The system allows accurate measurement of numerous mechanical properties including Young's Modulus (Jones et al. 2003).

The loading system consists of a frame of six hardened steel bolts with stainless steel end caps encased in an aluminium housing. A screw mechanism raises and lowers the load sensor; a piezoelectric actuator unit, including strain gauge with the load sensor (Figure 105a). The screw mechanism can also be used to deliver a small static preload to the sample which brings the interfacing surfaces of the machine and the machine/bone interfaces into contact (Jones et al. 2003). The piezoelectric actuator (Figure 105b) is controlled by a high voltage amplifier whose input is connected to a microcontroller circuit and is capable of applying forces of 4500 N, with a maximum expansion of typically 60 μm. Combined with a WINDOWS based user interface program, one is able to apply a quantifiable force or deformation of the bone core in the culture/loading chamber (Figure 105c). The microcontroller and associated electronic system and sensors work independently of the computer's operating system and are capable of recording both the piezoelectric expansion from the strain gauge, and the force from the load cell. The current configuration of the loading system is to test bone cores 5mm in height and 10mm in diameter which are housed in the culture/loading chambers.

Previously discussed bone testing and loading systems used to evaluate and test living tissue rely on hydraulics or a variety of levers, cams and screws which are unable to provide tightly controlled real-time measurements of force and deformation under dynamic loading conditions. A precise and quantifiable loading system is necessary to apply well defined mechanical loads that mimic *in vivo*, loads to samples that can vary in their material and structural properties. This is why the Zetos™ was used to mechanically stimulate the polycaprolactone scaffolds seeded initially with MG63, an osteoblast-like cell line and then with marrow stromal cells.

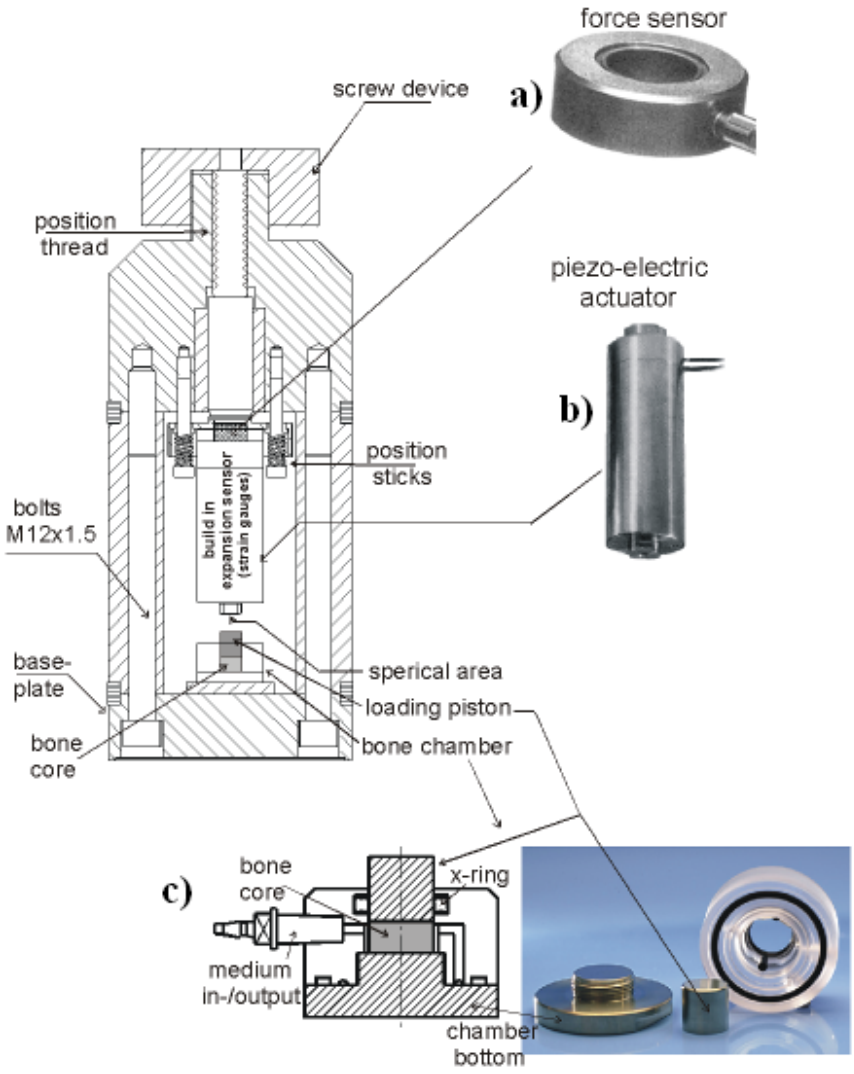

Figure 105: Zetos™ bioreactor system, a) force sensor, b) piezoelectric actuator, c) culture/loading chamber. (Image adapted from Jones et al. 2003)

Previous work done using the Zetos™ bioreactor has generated encouraging data. Explanted ovine, bovine and human cancellous bone cores were cultured in the Zetos™ culture/loading chambers to compare the macro and micro-architecture of the three bone types so that a source of experimental material could be selected (Davies et al. 2006). In another study, the Zetos™ bioreactor was used to maintain osteocyte viability and investigate the effects of mechanical loading on osteocyte apoptosis in human trabecular bone (Mann et al. 2006).

3.2 Method

3.2.1 Polycaprolactone scaffold preparation

Before cells could be seeded on the polycaprolactone (PCL) scaffolds (see paragraph 1.3.6), the latter had to undergo several steps before they were ready. After the scaffolds had been manufactured, they were washed thrice in sterile distilled water and stored in a freezer at -20 ºC so that they could be used when required. Before the experiment could start, the scaffolds were removed from -20ºC and thawed by immersing in sterile distilled water for 40 minutes at room temperature. The scaffolds were then cored our using a 5 mm diameter biopsy punch and placed in 100% industrial methylated spirit (IMS) for 15 minutes to sterilise the scaffold. The scaffolds were then removed and washed three times in sterile distilled water in a tissue culture hood which removed any remaining IMS and maintained the scaffolds in a sterile environment. The scaffolds then underwent different steps depending on the type of experiment.

3.2.2 PCL scaffolds seeded with MG63 in Zetos™ bioreactor

All manipulations were carried out under sterile conditions. The Zetos™ bioreactor system (Figure 106) was originally designed to maintain *ex vivo* bone cores with the application of a controlled cyclic mechanical loading pattern (Davies et al. 2006, Jones et al. 2003). Instead of bone cores, the PCL scaffolds were placed in the chambers and were maintained by the constant perfusion of nutrients and oxygen. The Zetos™ bioreactor consists of a set of diffusion chambers in which the scaffolds are placed. These chambers are connected via tubing (Tygon, France) to a reservoir of media that supplies the scaffold by the use of a perfusion pump with a flow rate of 7 ml/hour. The scaffolds within the chambers were mechanically stimulated on a daily basis for the duration of the experiment, using loads that engendered a peak strain of 5000 με at a frequency of 1 Hz in a wave pattern corresponding to physiological jumping exercise based on studies in bovine bone (Mann et al. 2006) (Figure 107).

The chambers contain a loading piston at the top (Figure 108a) which transmits the load to the scaffold however there is no recoil mechanism for the piston, as the intended specimen is bone and due to its inherent mechanical properties, naturally recoil the piston. Due to this and the nature of the scaffolds, rubber rings (Figure 108c) were manufactured that would fit around the scaffold and also fit in the chambers. This would enable the piston to recoil by the help of the rubber rings and hence permit the scaffolds to be loaded cyclically.

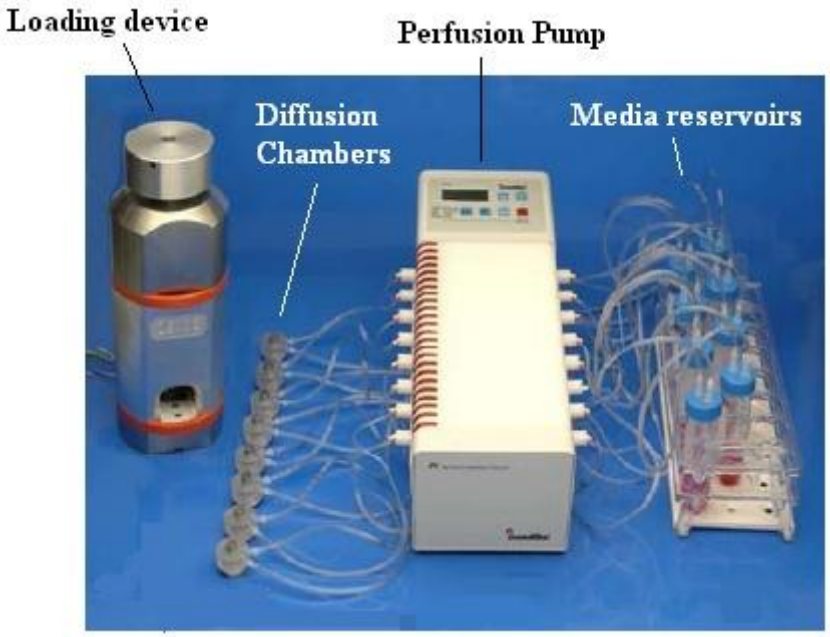

Figure 106: Zetos™ bioreactor system with chambers, perfusion pump and reservoir of media

Scaffolds first were treated as previously mentioned in paragraph 3.2.1, then 10 scaffolds were immersed in 0.2% w/v gelatin for 30 minutes the gelatin was previously filter sterilised (see chapter 1) to increase cell adhesion. MG63s were selected as this cell line proliferates rapidly which was useful as 6 million cells were required for the experiment. Ultimately the experiment was repeated with MSCs however the MG63 cell line provided valuable information in determining whether cells on PCL scaffolds in the Zetos™ chambers were capable of survival.

Figure 107: Physiological mechanical stimulation

During the preparations of the scaffolds, the MG63 cell line was being prepared for seeding onto the scaffolds. This was accomplished by first removing the media from the T75 flask (Corning) followed by three washes with PBS. One millilitre of trypsin, an enzyme that is used to detach the cells from the flask, was added to the flask to wash the cells and removed after 5 seconds. Another millilitre of trypsin was added to the flask for 5 minutes, the flask was tapped occasionally to encourage the cells to detach. The trypsin was then neutralised by adding 9ml of growth media to the flask. Ten micro-litres (µl) were removed from the cell suspension and deposited on the haemocytometer to determine cell number. The scaffolds were placed in two large cell culture Petri dishes (Corning, 150 mm x 25 mm) and growth media added to the cell suspension to obtain a cell concentration of 4.2 million cells/ml. The scaffolds (10 treated with gelatin and 10 un-treated) were seeded with 250,000 cells in 60µl. The scaffolds were flipped every 30 minutes for 4 hours so that cells were evenly distributed throughout the scaffold, then 45ml of growth media was added to each Petri dish until the scaffolds were submerged and they were left over night. The scaffolds were then transferred to non tissue culture plastic 48 well plate and 500µl of growth media was added to each scaffold and the plate was then left for 3 days. Two coated and 2 non-coated scaffolds were removed which would be used to represent the start of the experiment (T_0) and cut in half, with one half flash frozen in super cooled hexane (-80°C) bath and the other dipped in OCT embedding matrix (Raymond A Lamb) before flash freezing to be used for cryostat sectioning. Four coated and four non coated scaffolds were placed in a 50 ml universal tube with 5 ml of Zetos™ growth media, the rest of the scaffolds were placed in the Zetos™ chambers and connected to the reservoirs filled with 10ml of Zetos™ bioreactor

culture media. The Zetos™ growth media consisted of 13.38g of powdered DMEM (Gibco, UK), 2.38g of HEPES (final concentration 10 mM/l), 1.08g of β-glycerol 2- phosphate disodium salt hydrate (BGP) (final concentration 5 mM/l), 1.6ml of 7.5% sodium hydrogen carbonate (final concentration 0.14 mM/l) and finally adding 1000ml of ultra pure water. The mixture was stirred using a magnetic stirrer and the pH was measured using a pH meter (Thermo Orion, model 410) and adjusted to 7.25 - 7.3 by adding dropwise 1M sodium hydroxide (NaOH) solution. The media was then filtered through a Nalgene bottle top filter (75 mm diameter membrane, 0.2 μm pore size) and separated into 450ml amounts. The media was then supplemented with 10% Foetal calf serum (FCS) (Autogen Bioclear), penicillin (final concentration 50IU/ml) streptomycin (final concentration 50μg/ml) and 5ml of l-glutamine were added to the growth media.

At days 3 and 7 (T_3, T_7), two gelatin treated and two non-treated scaffolds were removed and frozen as previously described. The media that the scaffolds were bathed in was divided in two, one part was frozen for storage and the other had its pH measured (Thermo Orion, model 410).

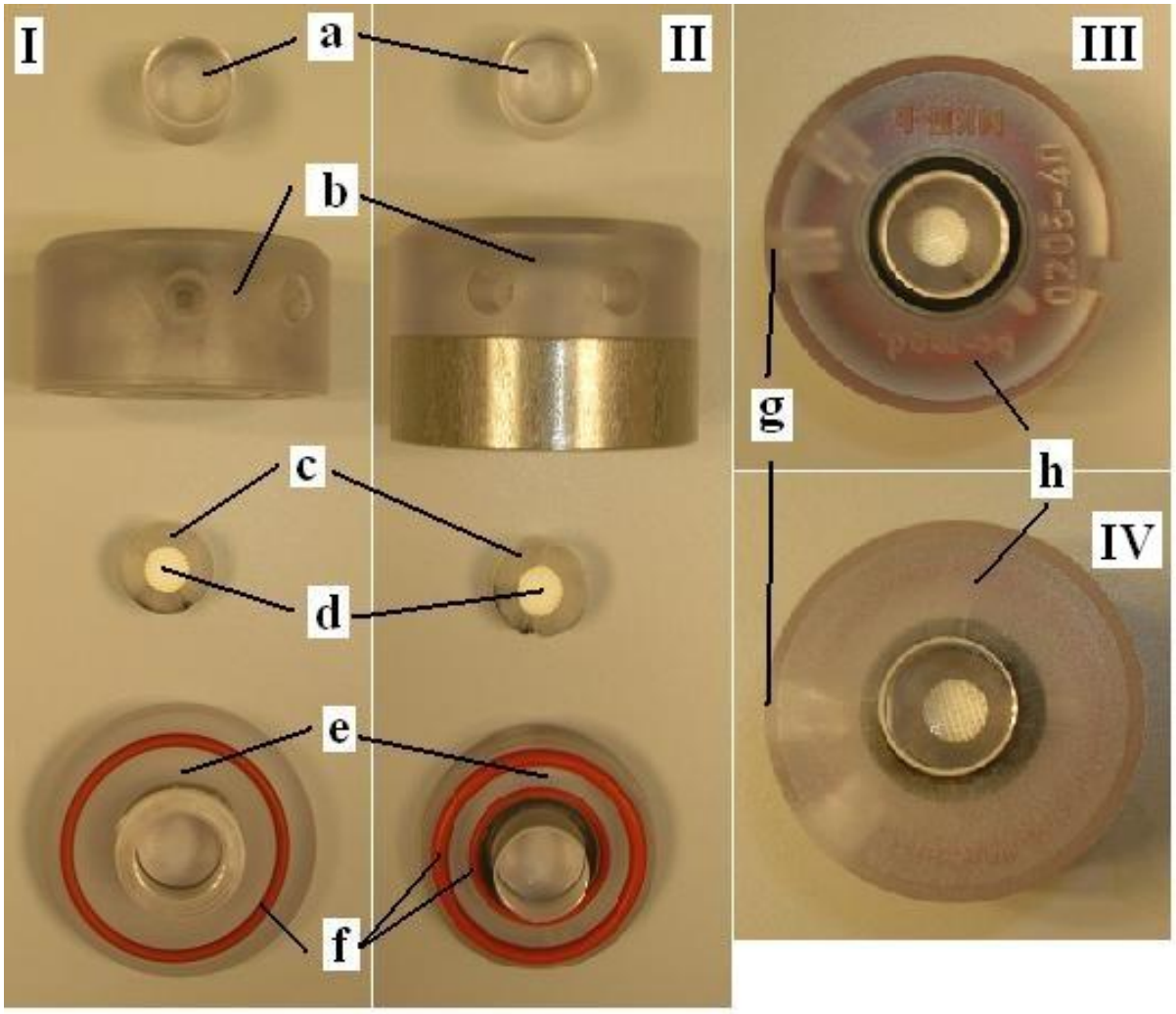

Figure 108: First (I and IV) and Second (II and III) types of Zetos culture/loading chambers, a) tip piston through which load is transmitted, b) main body of chamber where scaffold is housed, c) rubber support with grooves to allow improved flow of media, d) scaffold seeded with MSC, e) bottom of chamber which screws into the main body, f) rubber washers to prevent leaks, g) inlet/outlet for media, h) assembled chambers.

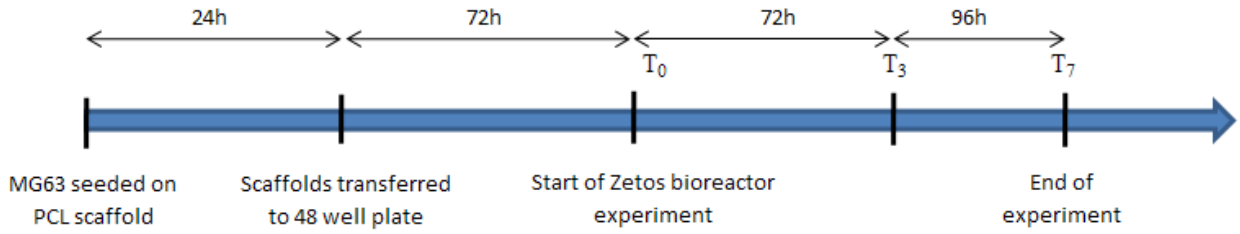

Figure 109: Timeline flow chart of MG63 Zetos bioreactor experiment

3.2.3 PCL scaffold seeded with MSCs and mechanically loaded in Zetos™ bioreactor

All manipulations were carried out under sterile conditions. The methodology for this experiment resembles the previous experiment with a few differences. The cell concentration was the same as the previous experiment (4.2 million cells/ml) but once the cells were seeded on the scaffolds (250,000 cells per scaffold) (Figure 110) they were turned upside down every half hour for four hours to obtain an even cell distribution and to increase the number of cells attaching to the scaffold. If the scaffolds were not turned upside down, gravity would have taken effect and the cells would have ended up at the bottom of the scaffold with little cells attached to the scaffold.

Drops of media were added in between the scaffolds to increase humidity in the Petri dish as this would minimise the amount of evaporation from the media on the scaffolds (Figure 110). After four hours growth media was added to the Petri dish and the scaffolds were left overnight before being transferred to a 48 well plate. The scaffolds were left in those conditions for 7 days with media changes every two days. In this experiment, the effect of scaffold geometry on osteogenesis was also investigated so 2 different geometries were used. The first was ‘double strand with offset’ (DSO) and the second ‘double strand with offset and 45º rotation’ (DSO45) (see chapter 1). All the scaffolds were coated with 0.2% w/v gelatin but 4 DSO and 4 DSO45 were not seeded with cells and were used as a control. MSCs were also plated out in 8 wells of four different sets of 24 well plates, with two plates kept in an incubator where one plate seeded with MSCs was fed with growth media and the other plate with MSC was fed with osteogenic differentiation media.

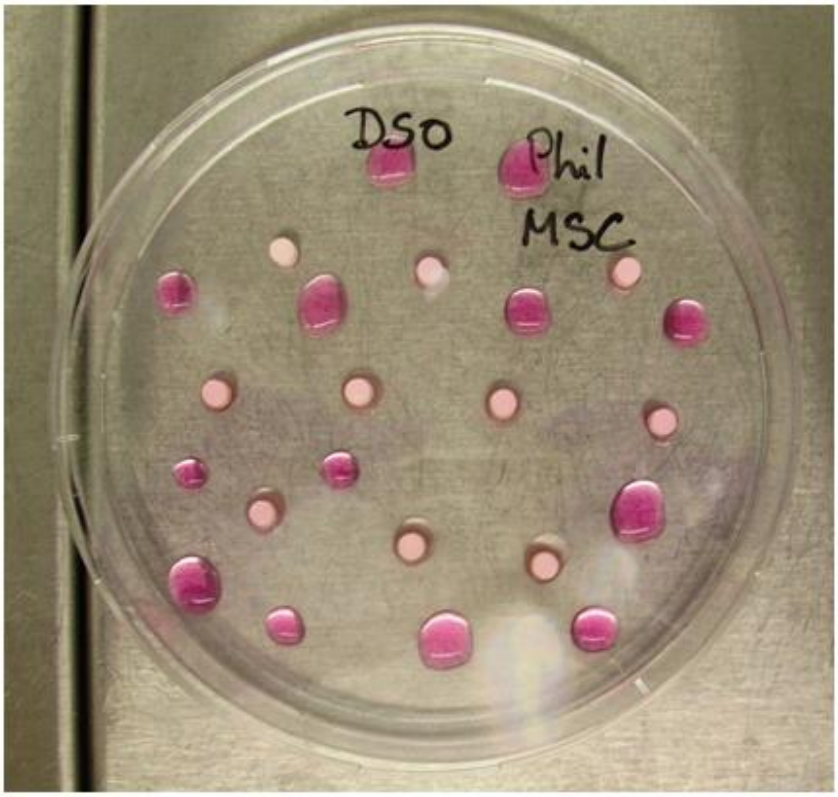

Figure 110: Initial static seeding of scaffolds

The other two plates were taped up to mimic the closed environmental conditions that the cells were experiencing in the Zetos™ chambers and kept in the walk-in Zetos™ environmental chamber which contained the plates, the peristaltic pump, the media and the Zetos loading device which were maintained at 37°C. The two plates with 8 of the wells fed Zetos™ osteogenic differentiation media and the remaining 8 wells were fed Zetos™ culture media. This experiment had four groups which included the loaded group, the flow group, the static group and the no cell group with three scaffolds per group. The loaded group was mechanically loaded daily with a preset wave pattern corresponding to physiological jumping exercise for 5 minutes daily using forces that engendered peak strains of 5,000 με at a frequency of 1 Hz (Figure 107). The flow group were in Zetos™ chambers but were not mechanically stimulated and only experienced fluid flow that was generated by the pump that provided media for the cells seeded on the scaffold. The static group which did not involve mechanical stimulated or fluid flow were in separate tightly sealed universals with 5ml of

Zetos™ osteogenic differentiation media and the no cell group were not seeded with cells and were kept in the same static conditions. The media was changed every 2 days and replaced with fresh media. The pH of the used media was recorded (Thermo Orion, model 410) to provide important information regarding the efficacy of the buffer which would influence the environment in which the cells were present.

Zetos™ osteogenic differentiation media comprised of 2.16g of β glycerol-2-phosphate (BGP) (final concentration 10mM/l) was added prior to adjusting the pH to 7.25 – 7.3 followed by 2.5ml of ascorbic acid (final concentration 50μM/l) and 50μl of dexamethasone (final concentration 0.1μM/l.

3.2.4 Analysis of scaffolds

On completion of the experiment, the scaffolds were removed from the chambers and the media retained to measure pH levels in order to determine whether the pH was within physiological range. The scaffolds were then cut in half longitudinally using a disposable scalpel (Swann-Morton) , half was flash frozen in a super cooled hexane bath (-80ºC) for quantifying the amount of calcium present by the o-cresolphthalein method (see below), and the other half dipped in OCT embedding matrix (Raymond A Lamb) for cryostat sectioning before being flash frozen. The samples placed in bijous and labelled then were refrigerated and stored in minus eighty (-80ºC).

The embedded samples were mounted on a bronze chuck and cryostat sectioned with sections 10μm thick. The sections were cut and stuck onto tape to facilitate the removal of the section from the cryostat blade and to maximise the integrity and quality of the section. The sections were then fixed with 4 % w/v paraformaldehyde (Sigma, UK) dissolved in PBS and then stained with DAPI which binds with cellular DNA and with Von Kossa which binds with calcium ions and produces a black deposit that can be viewed using a microscope. The stained sections were then viewed and images captured with a DXM1200 camera mounted on the microscope (Nikon, Eclipse E800) using a 10x/0.30 ∞/1.2 magnification lens. Four different areas of the sections were viewed and digitally saved. Fluorescence was used so that

the PI could be seen and a bright field image was also taken so that Von Kossa staining could be observed. The digitally saved images were then processed using ImageJ (Collins 2007) so that a cell count and a mineralised area could be measured.

The other half of the scaffold was treated using the o-cresolphthalein complexone method which determines the quantity of calcium resent in a given sample. This technique has been used in numerous other papers with positive outcomes (Lorentz 1982, Wible, Jr. and Hynes 2004). The technique and method that was used for the analysis was taken from the American Clinical Chemistry database (Toffaletti and Kirvan 1980).

Briefly two solutions were required, 2-Amino-2-methyl-1-propanol (AMP) buffer and the colour reagent. The AMP buffer was created by adding 15.12ml of AMP to 60ml of distilled water. This was then adjusted to 10.7 with a 6N hydrochloric acid (HCl) solution. The mixture was then poured into a volumetric flask and distilled water was added until the 100ml mark was reached. The mixture was then stored and refrigerated in a sealed covered bottle to limit the exposure to air and to sunlight. Under these conditions, the mixture is stable for three weeks. The second mixture was prepared by adding 6ml of concentrated HCl to 10 ml of distilled water in a 100ml volumetric flask. To the diluted HCl solution 10mg of o-cresolphthalein (Sigma, UK) and 100mg of 8-hydroxyguinole (Sigma, UK) were added. Distilled water was then added until the 100ml mark was reached. The mixture was then transferred to a sealed covered glass bottle and stored at room temperature. The solution is stable for one month.

The scaffolds were individually placed in a 1ml Eppendorf with 500µl of 1N HCl in an orbital shaker over night to dissolve the calcium. With this method, a calibration curve needed to be created so various known quantities of calcium were generated. This was achieved by using a calcium source, in this case calcium phosphate ($CaHPO_4$) and weighing out 250mg and dissolving it in 10ml of 1N HCl. This concentration was suggested by Toffaletti as higher ones would yield inaccurate results as this was beyond the range of the assay. When the calcium had completely dissolved, the solution was then divided in two and 5ml of 1N HCl was added to one of the solutions which halved the calcium concentration. This was repeated until the final calcium concentration reached 1.06mg/dl.

To perform the analysis, 250µl of colour reagent and 250µl of AMP buffer were mixed together in a 1ml Eppendorf tube. 12.5µl of calcium solution was removed from the scaffold solution and from the prepared calcium solutions and placed in a 1ml Eppendorf tube and mixed vigorously. The solution turned purple if calcium was present. A 96 well plate (Costar) was then used and 4 x 100µl of each calcium solutions were added and read using a Cytofluor multi well plate reader (Series 4000). The frequency set for the plate reader was 540nm and the filter set at 750nm.

3.2.4.1 Statistical analysis

All statistical analysis was performed using quantative data analysis with SPSS release 16 for Windows. Data was checked for normal distribution by applying the homogeneity of variance (Levene) test. In cases where the randomly selected data were shown to have normal (Gaussian) distribution, i.e. where 95% of the data fell within plus or minus 1.96 standard deviations from the mean, parametric statistical tests such as two-tailed Analysis of Variance (ANOVA) and the post-hoc Tukey-Kramer test were performed directly to determine statistical significance between the groups. When the p value of the ANOVA test was $p<0.05$, the use of the Tukey-Kramer post-hoc test allowed comparison of more than two means at once without introducing the type I error associated with multiple t-tests (Fielding and Gilbert 2000, Zar 1984). Results are expressed as means ± S.E. $p < 0.05$ was considered to be statistical significance. In some cases, the homogeneity of variance was not met and therefore a non-parametric Mann-Whitney t-test was performed with a confidence interval of 95%.

3.2.5 Combining finite element analysis measurements with manufactured scaffold properties

The aim of this study was to determine whether the surface strain generated during cyclic mechanical stimulation of the scaffolds and the measured surface strain using the finite element models would coincide. Two different scaffold geometries were also tested with the DSO45 scaffold generating 10% more surface strain compared to the DSO scaffold under the

same mechanical stimulus and additionally the Young's modulus of the mechanically tested DSO scaffolds were on average 2.6 times greater than the DSO45 scaffolds. These two scaffold geometries were chosen as the only difference between them is the rotation of the layers. It can be seen from the results in chapter 2 that greater surface strain differences exist between different scaffold geometries however that would involve introducing another variable which would make the comparison of scaffolds difficult.

It is noted that the cellular organization is different from that in living bone to that of the cell-seeded scaffolds due to the absence of embedded osteocytes and functional canalicular networks (Kenny and Raisz 2002, Noble and Reeve 2000). However understanding the effects of mechanical loading on scaffolds and determining whether scaffold design is capable of altering MSC differentiation is important as repair sites are usually load bearing (Shao et al. 2006a).

3.3 Results

3.3.1 Polycaprolactone scaffold and MG63 cells in Zetos™ bioreactor

Briefly, media was changed and the pH measured every 2 days (T_2 and T_4) however there was no media change at day six as the experiment would be terminating at day seven. Two coated and two non-coated scaffolds were removed at the start of the experiment (T_0) and at day three (T_3) with the remaining scaffolds removed at the end of the experiment at day 7 (T_0). Before changing the media the pH was adjusted to between 7.25 – 7.3 with 1M NaOH. Due to the removal of the scaffolds from the Zetos™ chambers, the table below (Table 15) has some missing values as at the time points the scaffolds were removed and images were taken to determine cell survival (Figure 112, 113, 114).

	Treatment	Scaffold Number	pH (T_2)	pH (T_4)	pH (T_7)
Static	Not Coated with Gelatin	1	7.29	x	x
		2	7.27	x	x
		3	7.27	7.04	6.93
		4	7.27	7.12	6.86
	Coated with Gelatin	5	7.29	x	x
		6	7.29	x	x
		7	7.29	7.10	6.93
		8	7.29	7.07	6.91
Zetos	Not Coated with Gelatin	9	7.49	x	x
		10	7.46	x	x
		11	7.48	7.46	7.44
		12	7.47	7.45	7.44
	Coated with Gelatin	13	7.53	x	x
		14	7.48	x	x
		15	7.50	7.48	7.44
		16	7.55	7.51	7.45

Table 16: pH measurement of media of MG63 in Static and in Zetos™ chambers

It can be observed from the table above, that in the static condition, the pH becomes more acidic over time which could be due to the increased number of cells present on the scaffold producing more lactic acid due to anaerobic growth and also due to the smaller volume of media administered to avoid issues of oxygen reaching the cells seeded on the scaffold, improving the oxygen gradient. In the Zetos™ chambers, the pH was more alkaline than the static condition but a decrease in pH over time can also be observed (Figure 111).

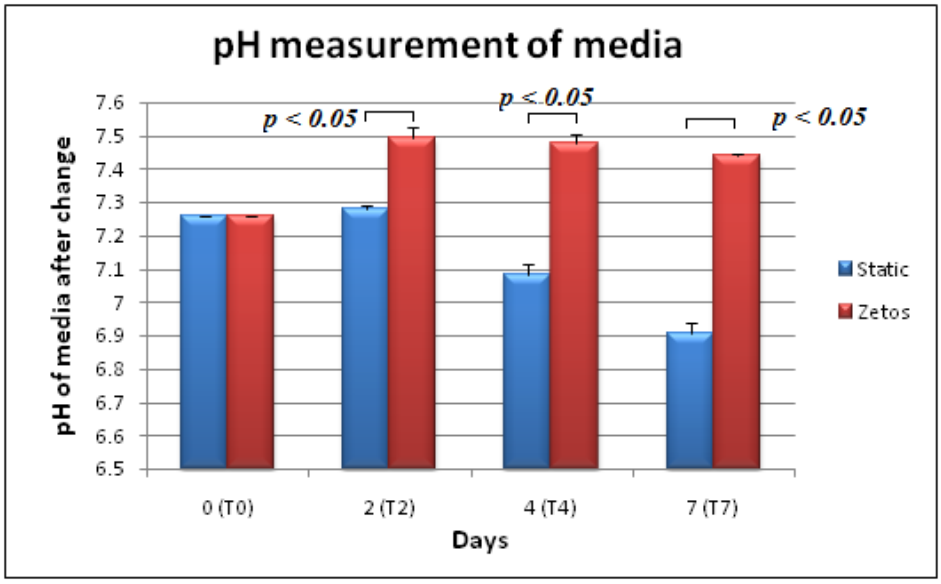

Figure 111: Recorded pH of media during seven day static and Zetos™ chamber experiment

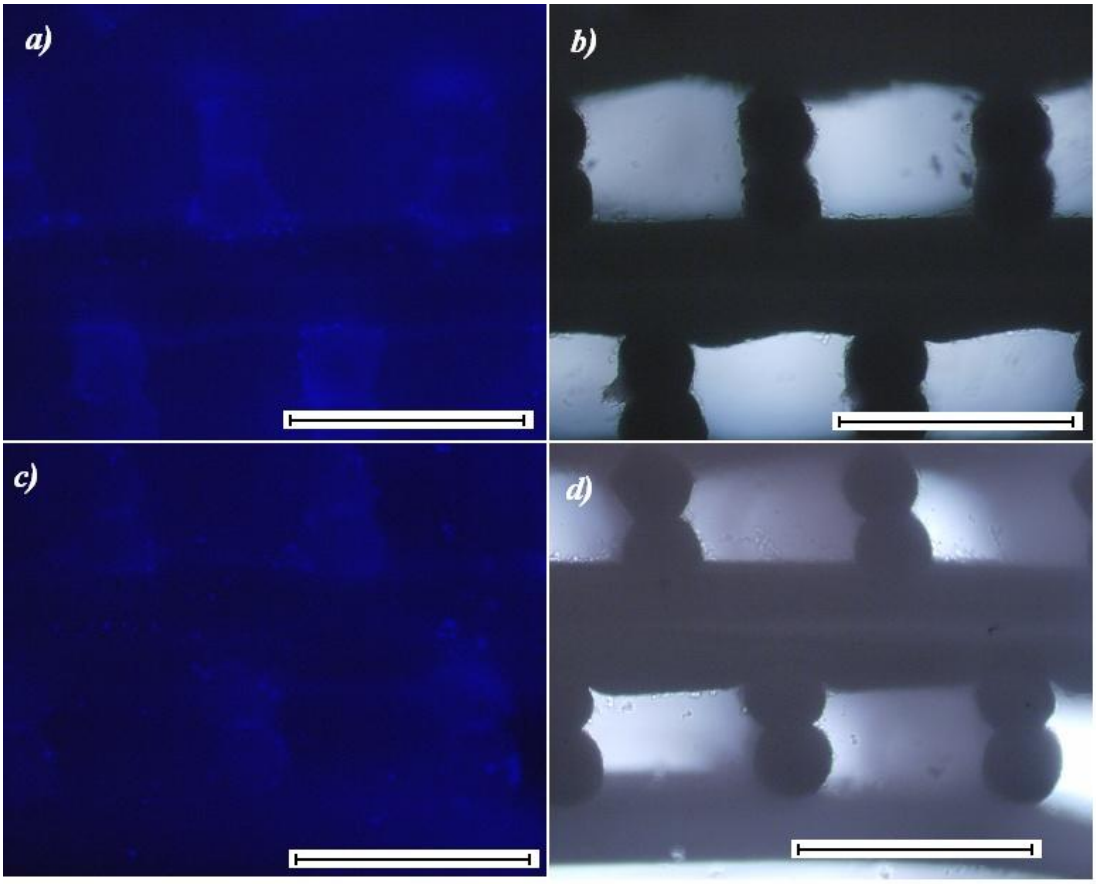

Figure 112: Images of PCL seeded with MG63 cell line at T_0, a) DAPI stain coated with 0.2% gelatin, b) bright field coated with 0.2% gelatin, c) DAPI stained and d) bright field non-coated PCL scaffolds (scale bar = 600 μm)

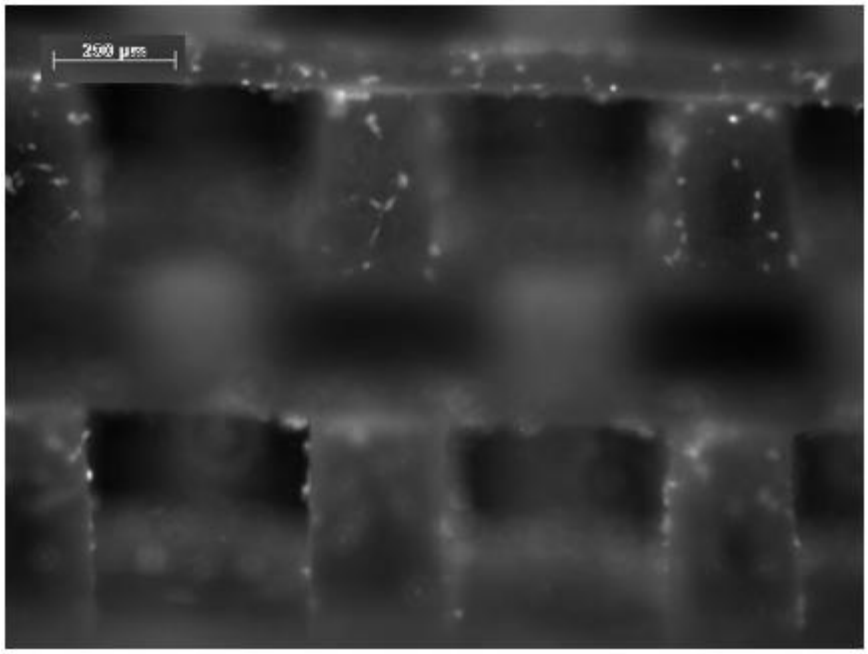

Figure 113: DSO scaffold seeded with MG63 at day 3 (T_3) stained with DAPI

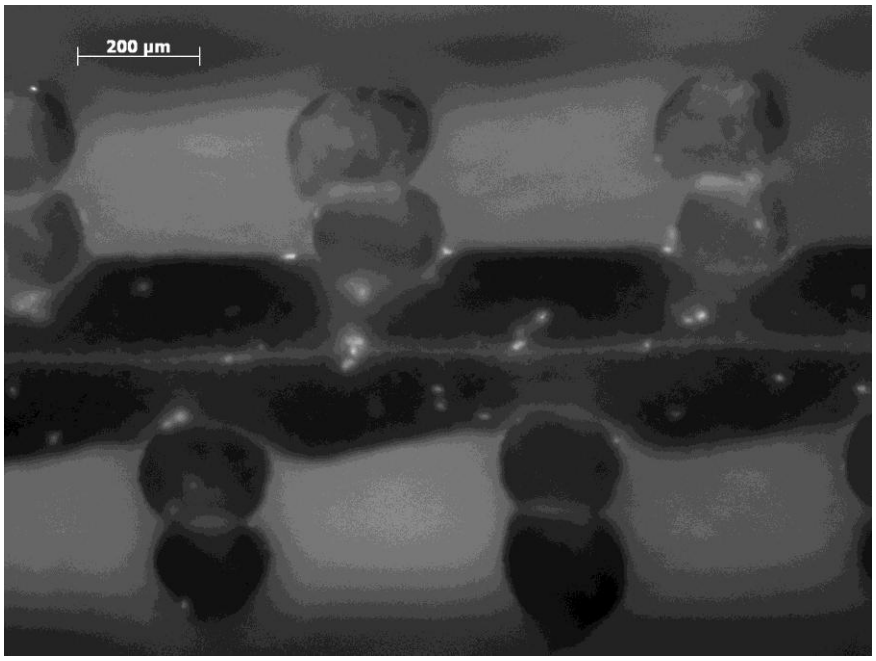

Figure 114: DSO45 scaffold seeded with MG63 at day 7 (T_7) stained with DAPI

3.3.2 Polycaprolactone scaffold and marrow stromal cells loaded in Zetos™bioreactor

Briefly, the scaffolds were seeded statically with MSCs and placed into the Zetos system for 14 days. This experiment was repeated three times with the marrow stromal cells (MSCs) obtained from different patients for each individual experiment (Table 16). The quantity of calcium in half of the scaffold was then measured using the o-cresolphthalein complexone method, which first required a calibration curve so that the optical densities obtained from the scaffolds could be used to determine the amount of calcium present.

	Age	Sex
Run 1	70	M
Run 2	69	F
Run 3	74	F

Table 17: Age and sex of patients from which MSC were obtained

3.3.2.1 First Zetos™ bioreactor results

During the course of this initial experiment, the pH was measured after each media change to determine whether the pH of the osteogenic differentiation media stays within the neutral range and that there are no unexpected and unwanted changes that might affect the cells. From figures 115 and 116, it can be observed that the pH remains within the neutral range and therefore would not be expected to endanger the MSC cells.

The next results involved quantifying the amount of calcium produced using the o-cresolphthalein method which is described in paragraph 2.4.

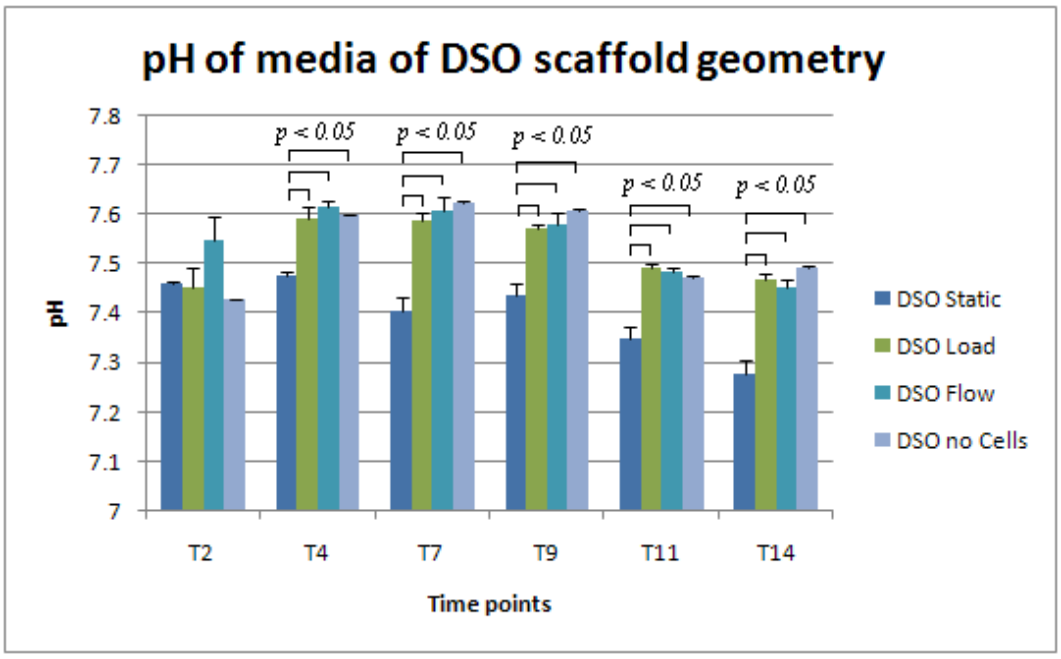

Figure 115: pH of media during the course of the experiment with DSO scaffold geometry

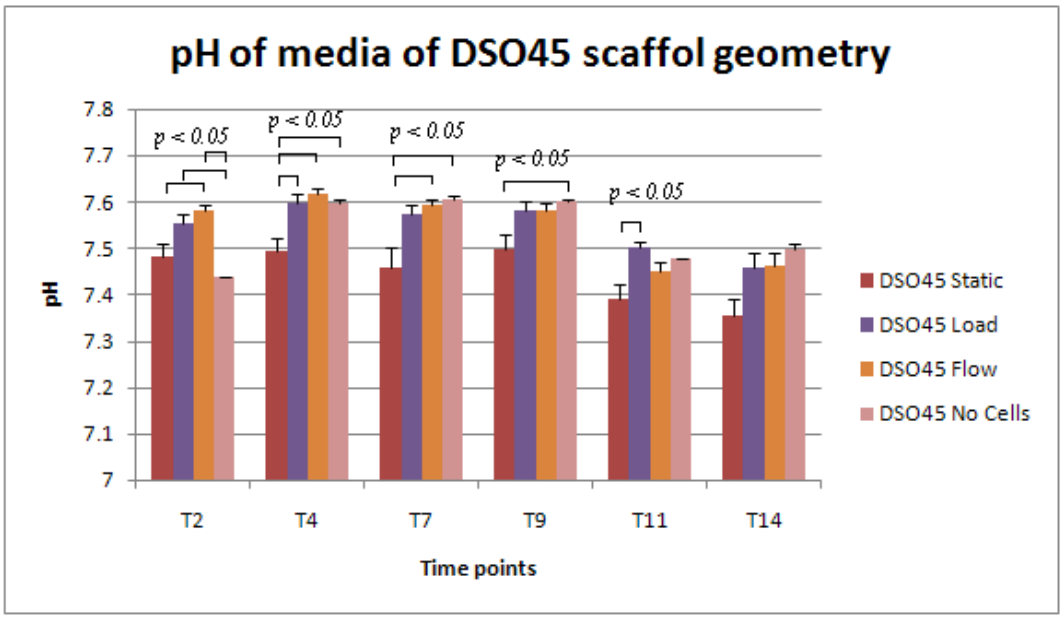

Figure 116: pH of media during the course of the experiment with DSO45 scaffold geometry

Concentration (mg/dl)	Optical density				Average
12.5	0.267	0.273	0.278	0.277	0.274
6.25	0.15	0.15	0.152	0.156	0.152
3.125	0.077	0.078	0.081	0.077	0.078
1.5625	0.047	0.047	0.046	0.037	0.044

Table 18: Calcium concentration and respective optical density

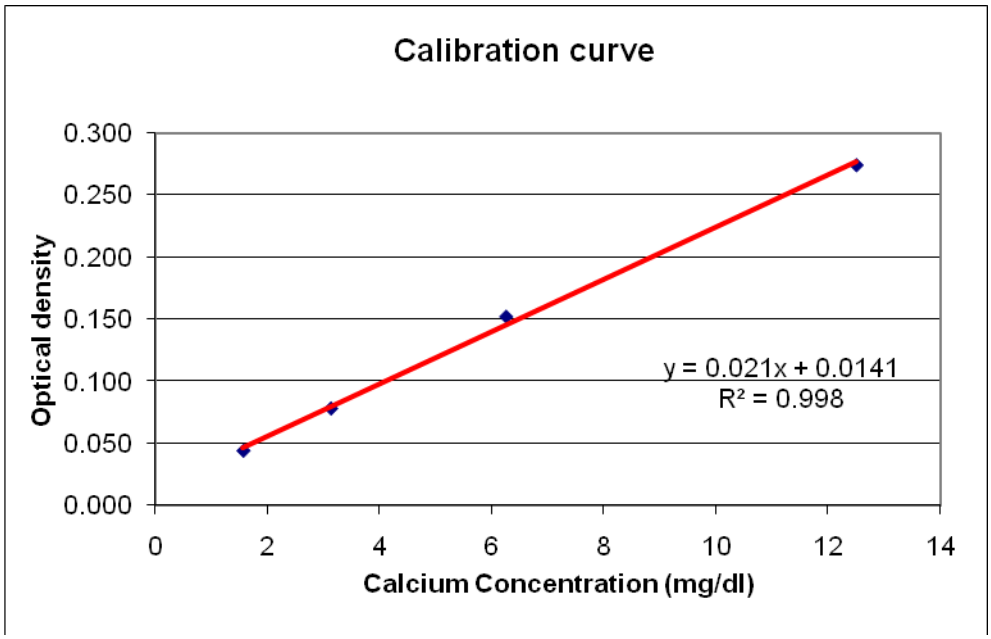

Figure 117: Calibration curve for o-cresolphthalein complexone method

From the calibration curve, a formula was then derived ($y = 0.021x + 0.0141$) to represent a correlation between calcium concentration and optical density. The optical densities from the calcium solutions obtained from the scaffolds were then inputted into the

formula and which yielded the calcium concentration present in the scaffold solution for both the scaffold geometries and treatments (Figure 118 and 119). Before obtaining the concentration the first step of the calculation was to normalise the weight of calcium present in each scaffold by dividing it by the weight of the scaffold which was measured after freeze drying and before starting the o-cresolphthalein complexone method. The normalization process was required as when the scaffolds were cut in half prior to flash freezing, the halves were not exact as this was performed by hand and this would have skewed the results of the calcium concentration as larger scaffold 'halves' would have a larger calcium concentration.

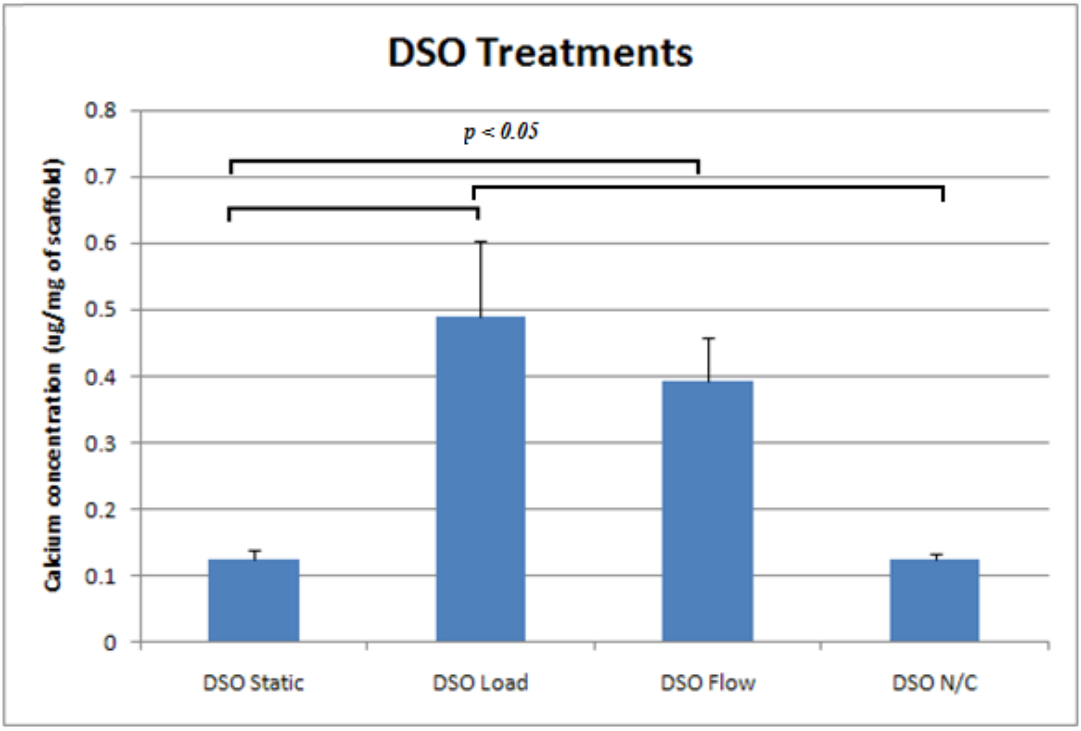

Figure 118: DSO scaffolds with different treatments versus average weight of calcium per mg of scaffold

The two different scaffold geometries tested were the double stranded offset (DSO) (Figure 118) and the double stranded offset with 45° rotation (DSO45) (Figure 119). Each scaffold with different geometry was seeded with MSCs and underwent different treatments, i.e. static, load and flow and a control where no cells were present. It can be observed from

figure 118 that there was statistical difference between the static treatment and both the mechanically loaded and flow treatment and between the mechanically loaded and the no cell group, however no statistical significance was present between the other treatments. From the results of the DSO45 scaffold geometry (Figure 119), it can be seen that statistical significance was observed between the mechanically loaded and both the static and the no cell control treatment furthermore statistical significance was also visible between the static and the flow treatment.

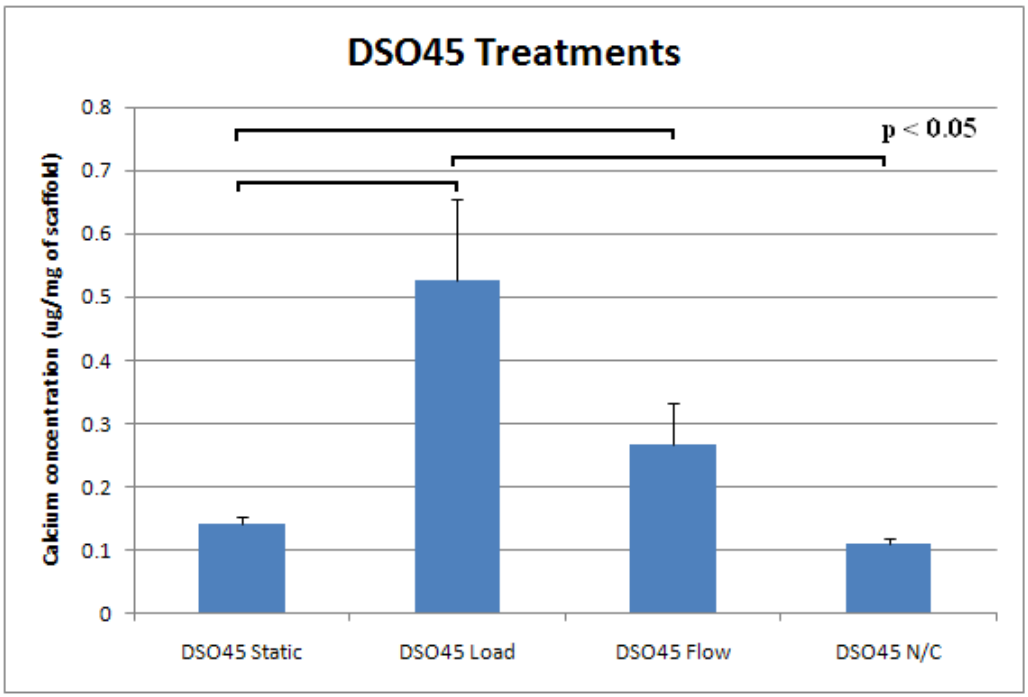

Figure 119: DSO45 scaffolds with different treatments versus average weight of calcium per mg of scaffold

Briefly, transversal cryostat sections of 7µm were obtained from the other half of the scaffolds and the sections were first fixed using 4% w/v paraformaldehyde dissolved in PBS and allowed to dry at room temperature, then stained with Von Kossa which stains mineral in the section and propidium iodide (PI) which stains cellular DNA and finally the section was covered with a glass cover slip. The stained sections were then captured digitally using a camera (DXM1200) mounted on an Eclipse E800 microscope (Nikon) and by using an

imaging program (ImageJ), areas of Von Kossa and number of cells per section were measured. The area of Von Kossa stained mineral was measured to compare with the results obtained from the o-cresolphthalein complexone method for the DSO scaffold geometry (Figure 120). The cell count was also performed to investigate the number of cells present at the end of the experiment (Figure 121). Von Kossa staining can be observed in figure 124 in the areas I and II which represents two successive sections. This demonstrates that some components of the mechanical stimulus generated by the Zetos™ mechanical stimulator are capable of inducing osteoblastic differentiation of MSC.

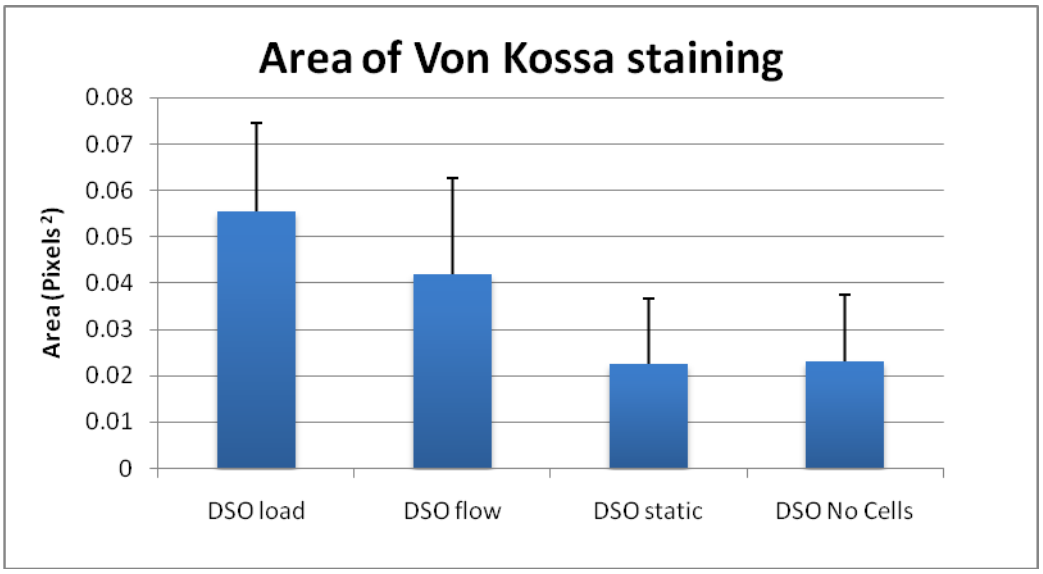

Figure 120: Area of mineral stained by Von Kossa measured using Image J (No significant difference between groups)

From figure 120, it can be seen that the area of Von Kossa staining was the largest in the DSO loaded group and followed by the DSO flow group however no statistical significance was observed between the groups. This result however demonstrates that more Von Kossa stained mineral was observed in the DSO loaded group which was also shown in the o-cresolphthalein results (Figure 118). A similar result can be observed with the DSO45 scaffolds, with the largest Von Kossa staining seen in the mechanically loaded scaffold (Figure 121) which coincides with the results obtained from the o-cresolphthalein method.

The PI stained cell count for the DSO scaffold (Figure 122) and the DSO45 scaffold yielded similar results with no statistical significance observed between the treatments. However there was a trend observed in both the different scaffold geometries where the static treatment had the highest cell count average (Figure 122 – 123) and large error bar. The mechanically compressed scaffold had the second highest cell count average in both cases and the scaffold with no cells had the lowest in both scaffold geometries (Figure 122 – 123).

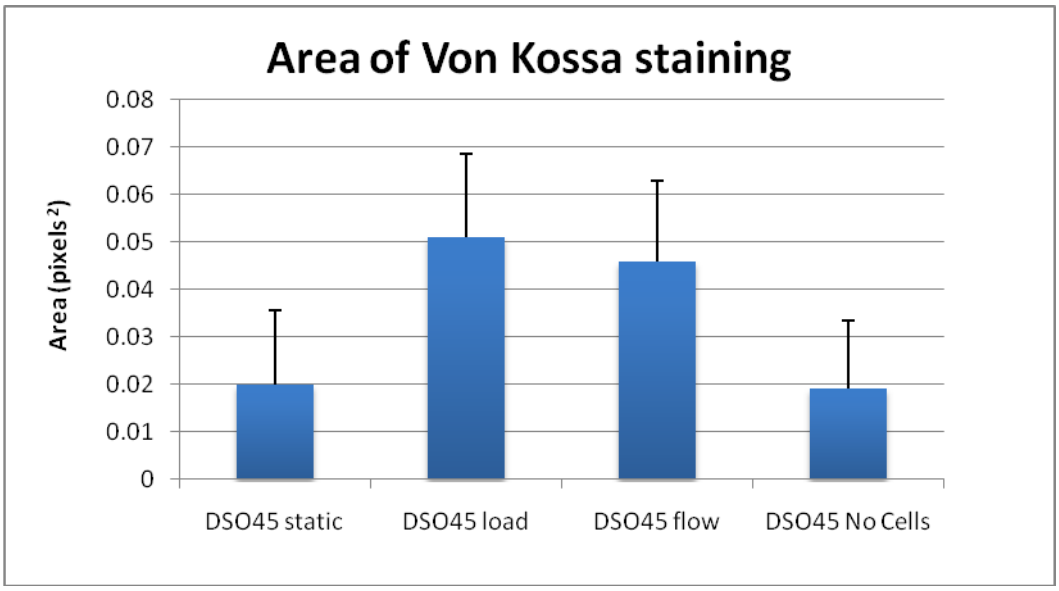

Figure 121: Area of mineral stained by Von Kossa measured using Image J (No significant difference between groups)

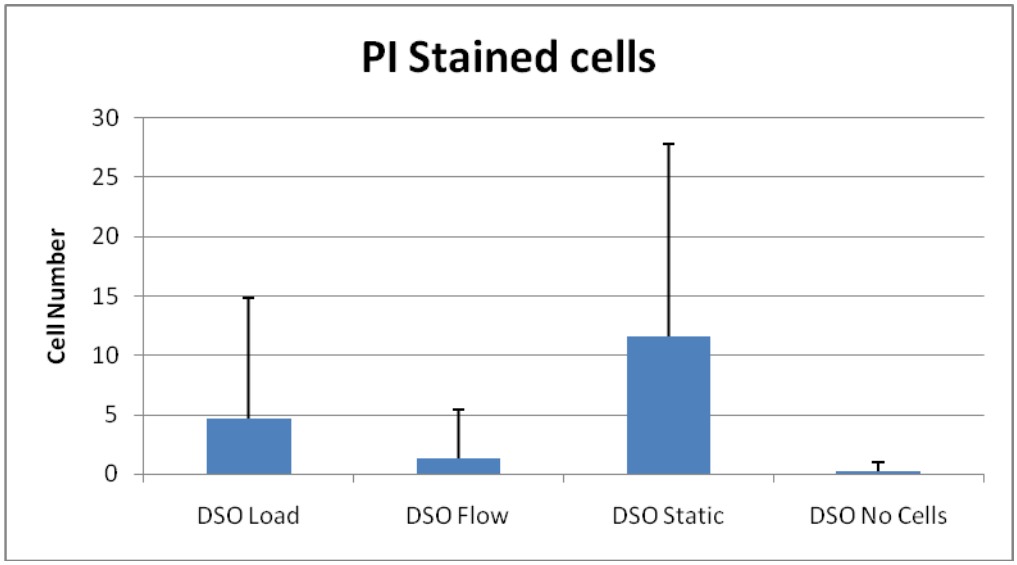

Figure 122: PI stained cells counted with Image J

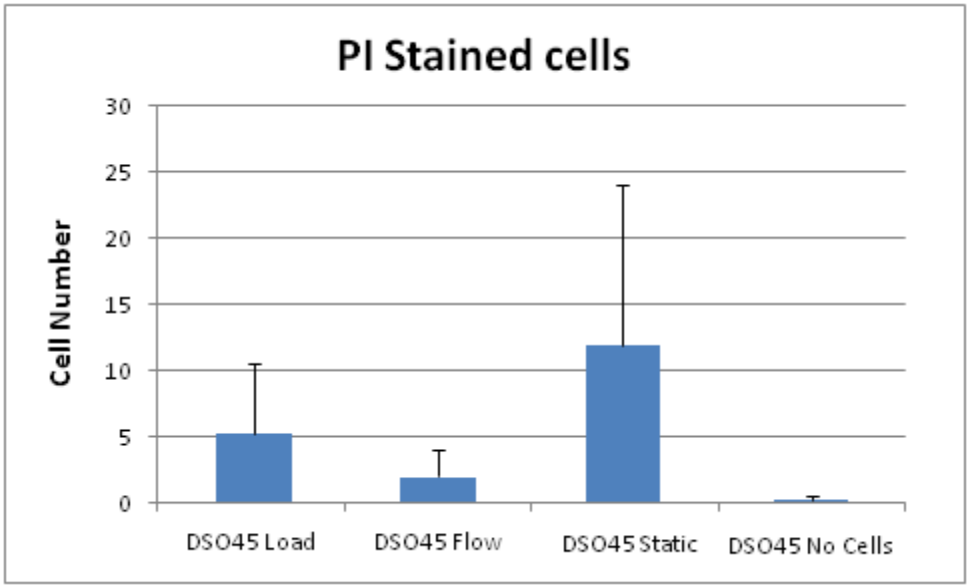

Figure 123: PI stained cells counted using Image J

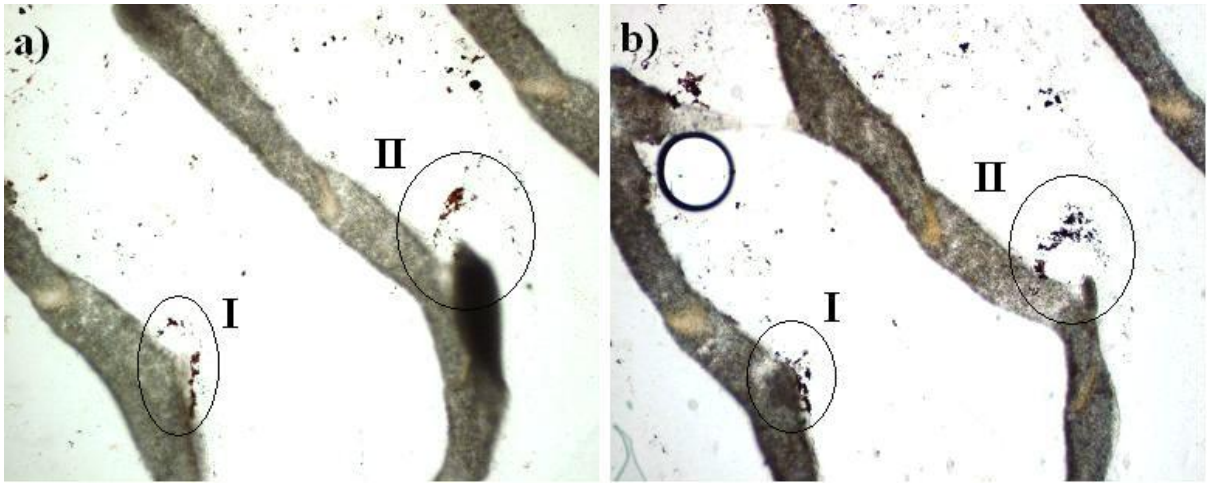

Figure 124: Von Kossa staining of DSO45 Loaded of the same area of two consecutive sections, a) 1550 µm b) 1560 µm from top of scaffold

3.3.2.2 Second Zetos™ bioreactor results

During the course of the second experiment, the pH of the changed media was recorded and the values illustrated in figures 125 and 126.

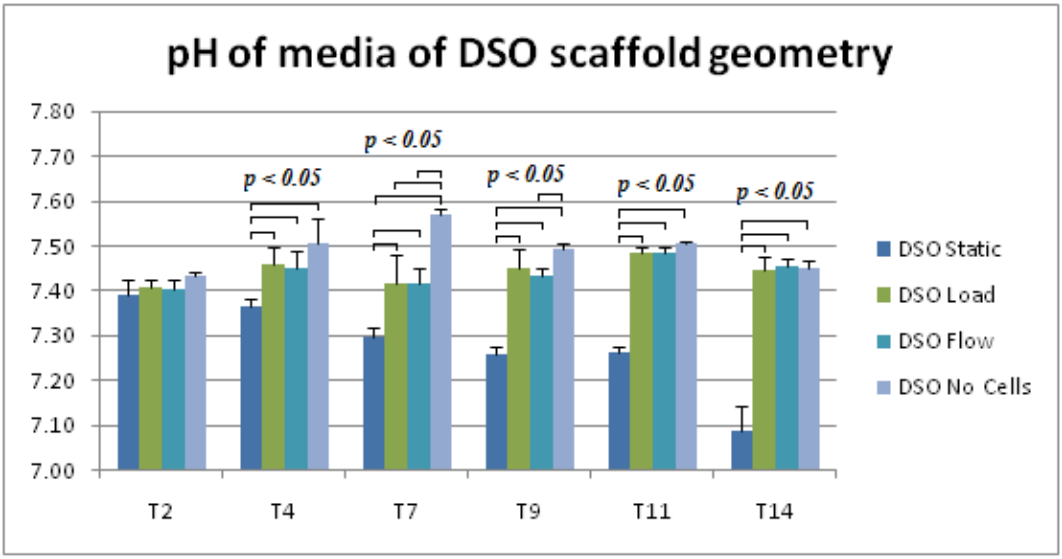

Figure 125: pH of media during the course of the second MSC in Zetos system experiment with DSO scaffold geometry

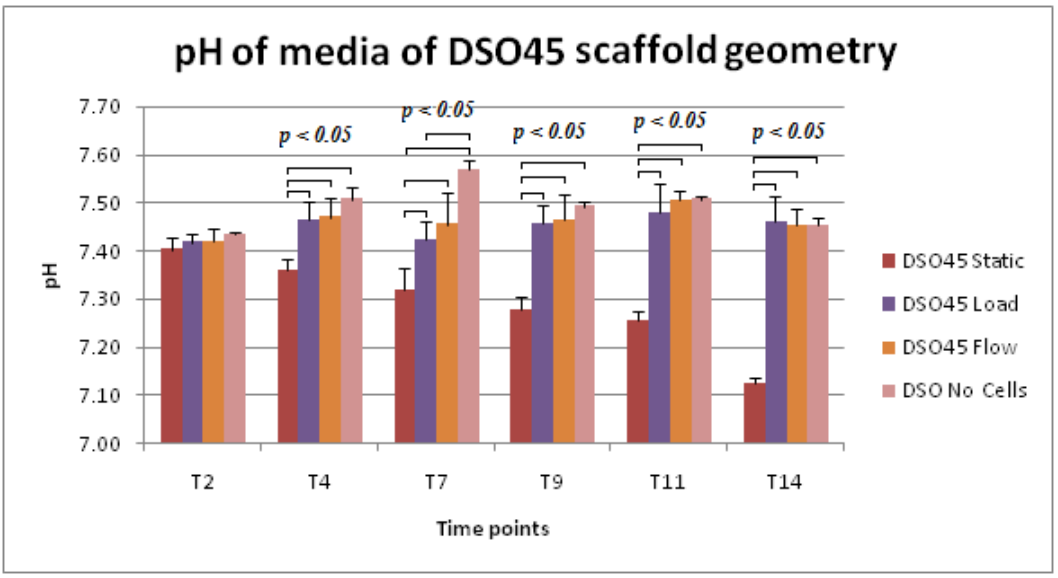

Figure 126: pH of media during the course of the second MSC in Zetos system experiment with DSO45 scaffold geometry

As previously mentioned in paragraph 3.2.1., a calibration curve was plotted (Figure 127) which would permit the quantity of calcium present in the scaffold to be determined. Briefly, calcium phosphate was dissolved in 3N HCl to an initial concentration of 25mg/dl, followed by a serial dilution where the final calcium ion concentration was 0.78125mg/dl.

At the start of this experiment, the number of scaffolds per treatment was four however during the two week course of the experiment; three Zetos™ chambers broke which reduced the number of scaffolds per treatment to three.

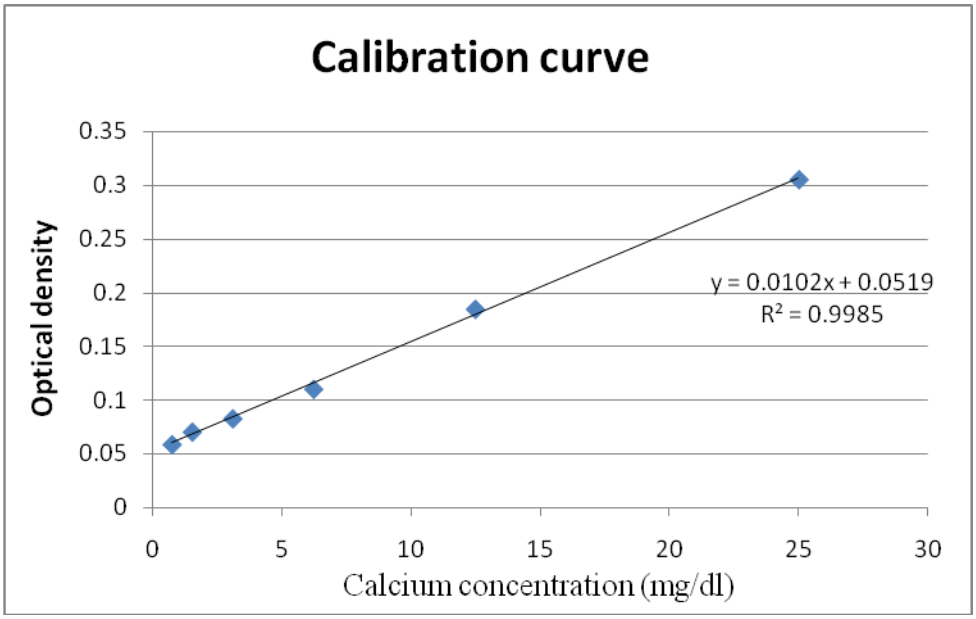

Figure 127: Calibration curve for second Zetos bioreactor experiment

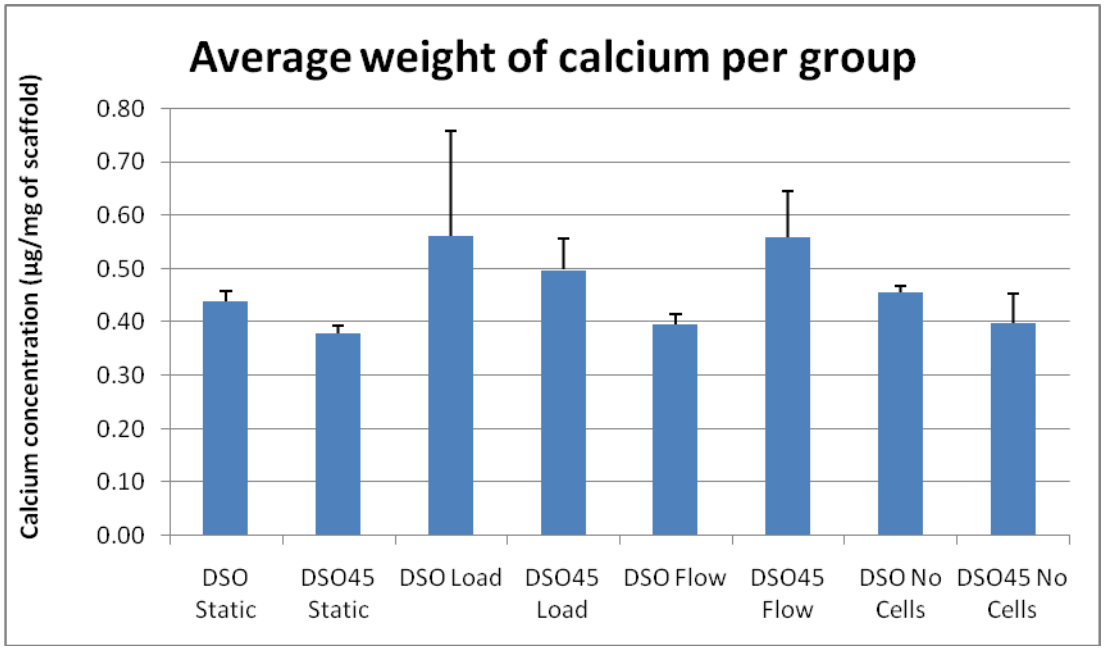

Figure 128: Calcium concentration per weight of scaffold for all the treatments (no statistical significance between different scaffold geometries of the same treatment group)

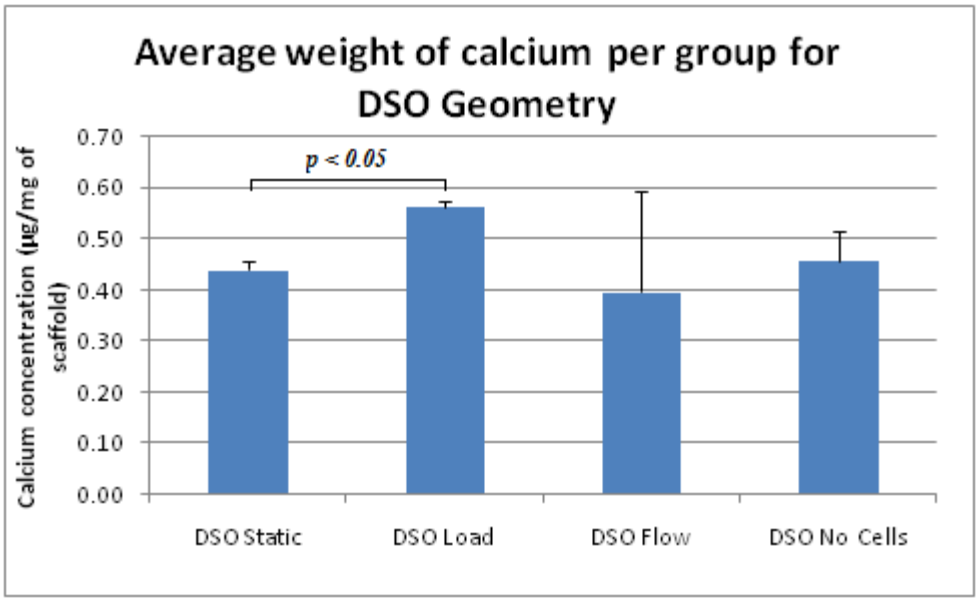

Figure 129: Calcium concentration for DSO scaffold geometry

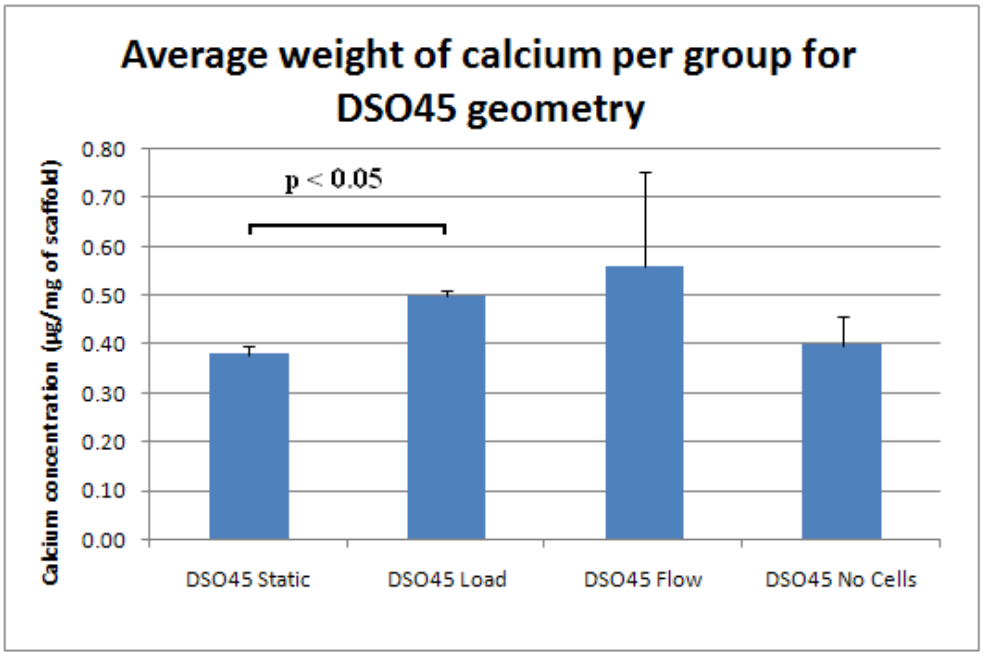

Figure 130: Average calcium weight for DSO45 scaffold geometry

From the second run of the Zetos™ bioreactor it can be seen that in the DSO scaffold geometry group (Figure 129), statistical significance was observed between the DSO static and mechanically loaded group however no statistical difference was obtained between the other different treatments. This trend of the largest amount of calcium produced in the mechanically loaded group, was also observed in the initial Zetos™ run. The other treatments yielded similar values which were unexpected as results from fluid flow and static conditions were similar to the control group which had no MSC. This would imply that no calcium was produced in the fluid flow group, the static group as no cells were present in the final group and therefore no calcium could be produced.

The other scaffold geometry DSO45 (Figure 130), statistical significance was observed between mechanically loaded and static scaffolds treatments which were also observed in the first Zetos™ run, however the treatment which generated the highest quantity of calcium was the fluid flow treatment where the seeded scaffolds were in individual Zetos chambers with the absence of mechanical compression of the scaffold.

Image J was used to determine the area of stained mineral and the number of PI positive cells. The area of Von Kossa present on the four sections at a distance 150μm from the top of the scaffold can be observed in figure 131 for the DSO scaffolds and figure 132 for the DSO45 scaffolds with no statistical significance observed. The number of cells present on the same four sections can be observed in figure 133 for the DSO scaffolds and figure 134 for the DSO45 scaffolds. In the cells stained with PI statistical significance was observed between the DSO load group and both the DSO flow and DSO no cells group (Figure 133). However in the DSO45 scaffold geometry, statistical significance was only observed between the DSO45 group and the remaining three groups (Figure 134). Representative images used to measure the mineral stained with Von Kossa and PI can be seen in figure 135 and 136 respectively.

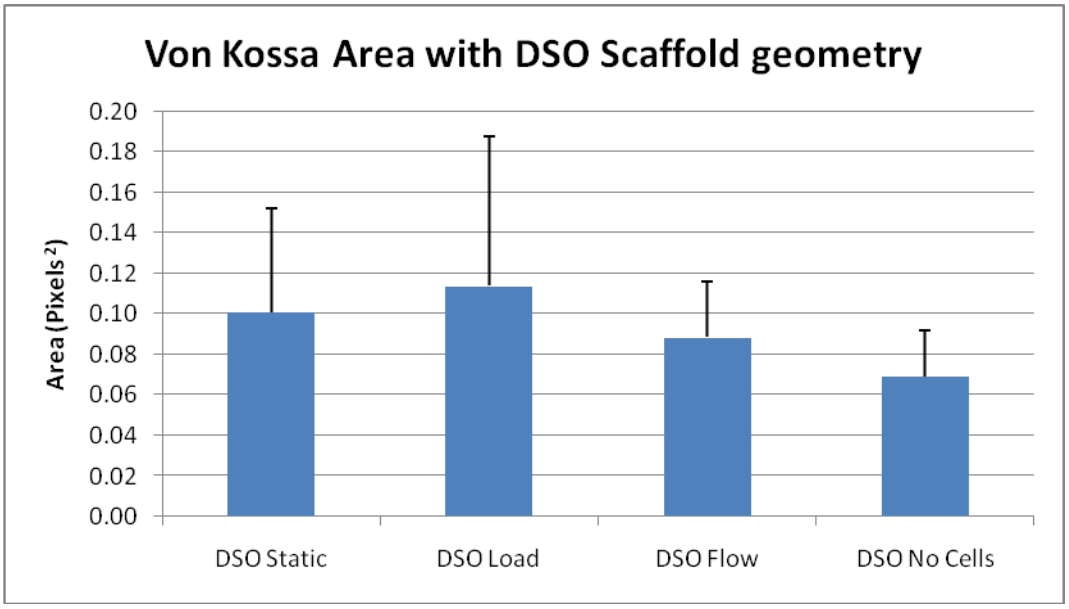

Figure 131: Area of mineral stained on sections of DSO scaffolds using Von Kossa measured using Image J (No statistical significance)

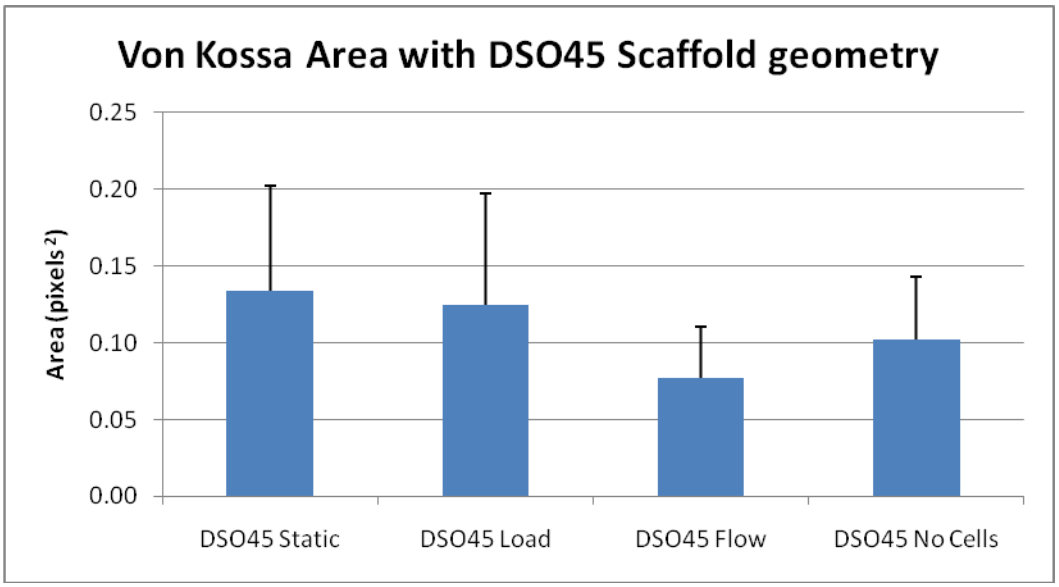

Figure 132: Area of mineral stained on sections of DSO45 scaffolds using Von Kossa measured using Image J (No statistical significance)

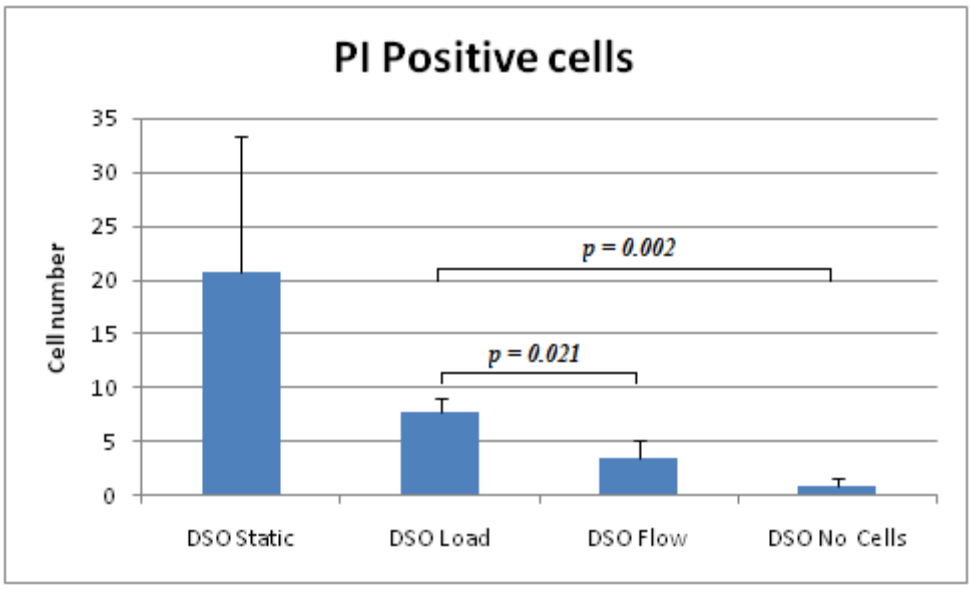

Figure 133: Cells positively stained for PI which indicates average number of cells present at distances 150µm – 153µm from the top of the scaffolds in the DSO scaffolds

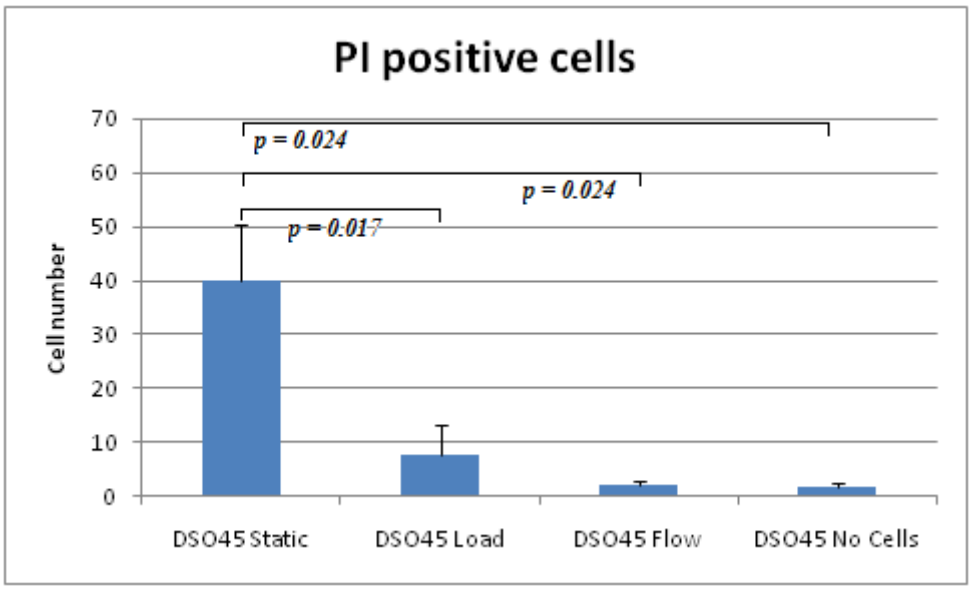

Figure 134: Cells positively stained for PI which indicates average number of cells present at distances 150µm – 153µm from the top of the scaffolds in the DSO45 scaffolds

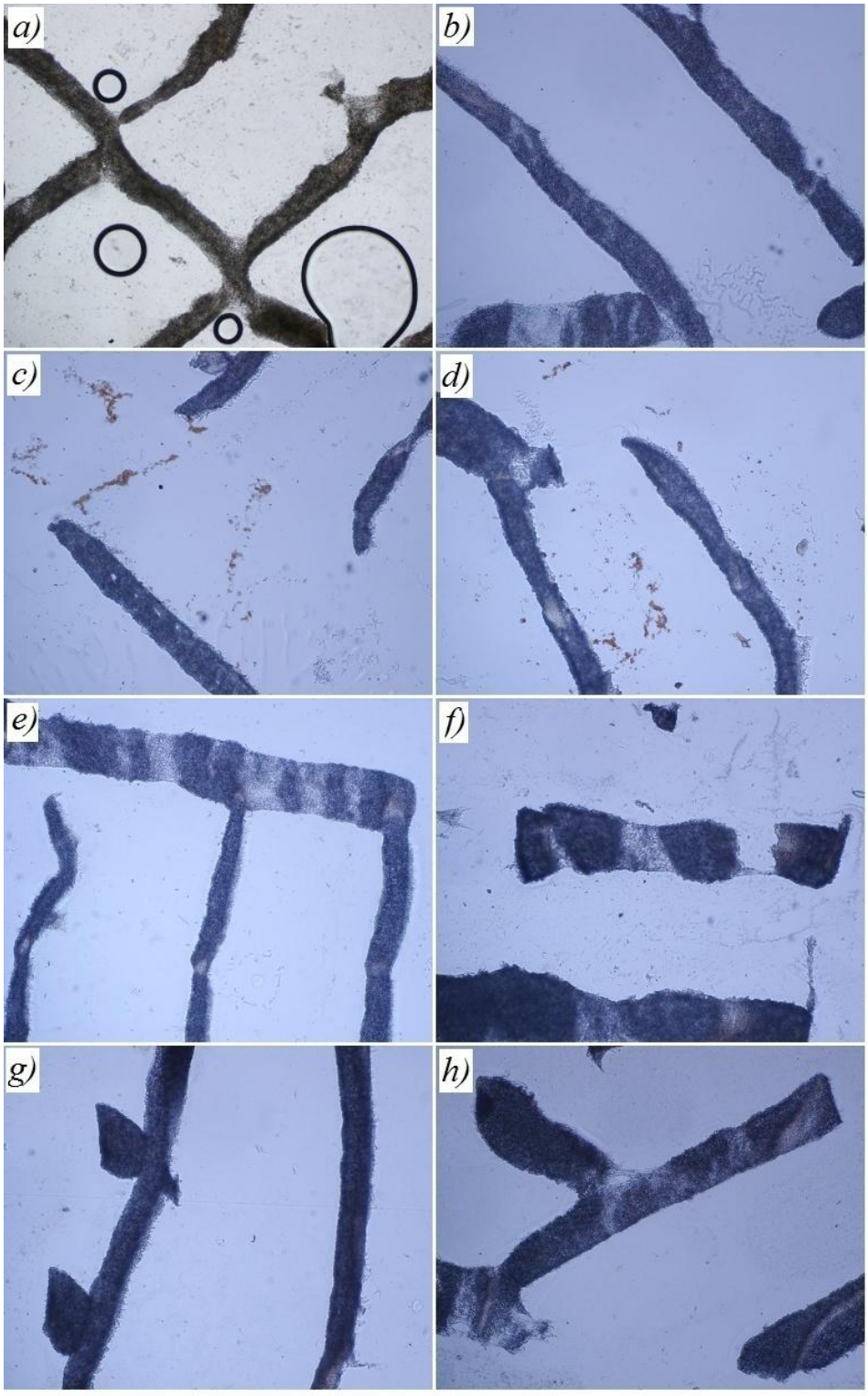

Figure 135: Representative bright field images, a) DSO Static, b) DSO45 Static, c) DSO Load, d) DSO45 Load, e) DSO Flow, f) DSO45 Flow, g) DSO No Cells, h) DSO45 No Cells

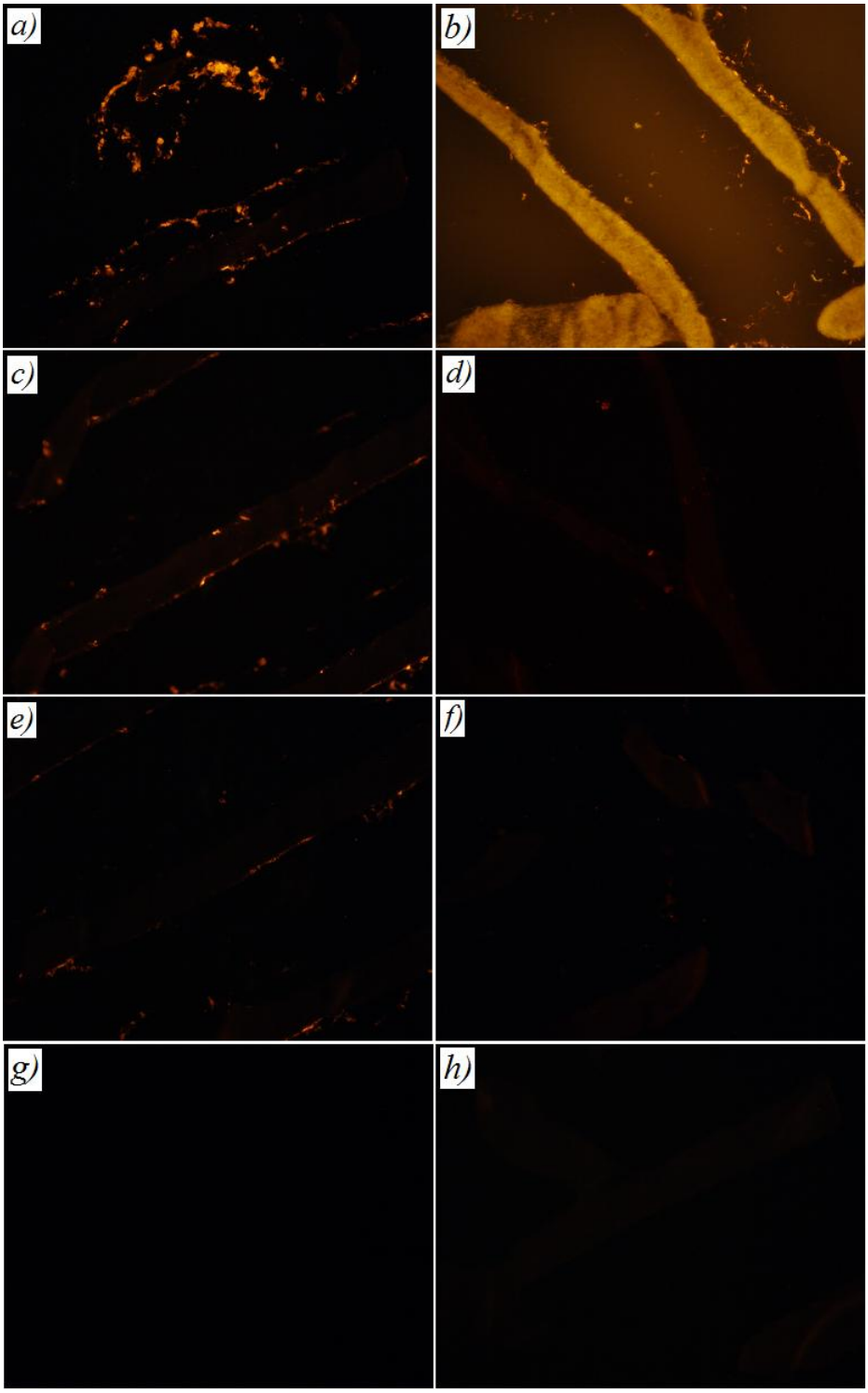

Figure 136: Representative PI fluorescent images, a) DSO Static, b) DSO45 Static, c) DSO Load, d) DSO45 Load, e) DSO Flow, f) DSO45 Flow, g) DSO No Cells, h) DSO45 No Cells

3.3.2.3 Third Zetos™ bioreactor results

For the third repeat of the experiment and due to the failed chambers from the previous run, new chambers were used which were all identical which would render the experiment more uniform and eliminate any factor which might have affected the outcome. For this experiment, an increased numbers of scaffolds per treatment (n=4) were used and therefore not enough wells were available in a 96 well plate to accommodate a calibration curve and solutions that were required to be measured. Therefore each treatment was allocated a separate calibration curve which was analysed together with the treatment; this created a separate calibration curve for each treatment group (Figure 137 – 140).

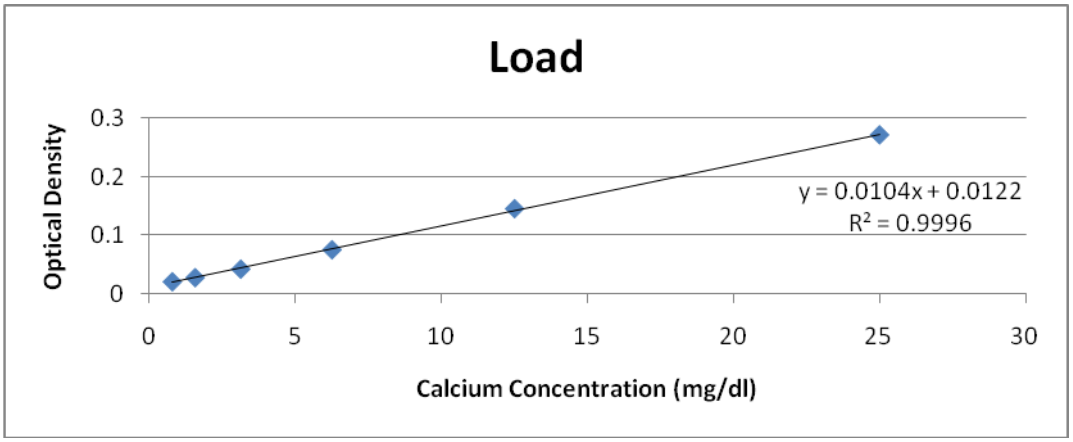

Figure 137: Calibration curve for mechanically loaded scaffolds in Zetos bioreactor

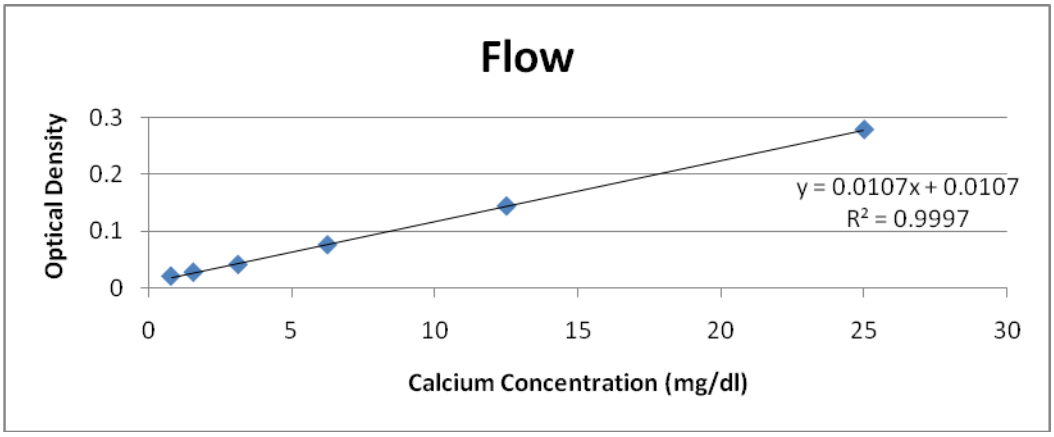

Figure 138: Calibration curve for flow scaffolds in Zetos bioreactor

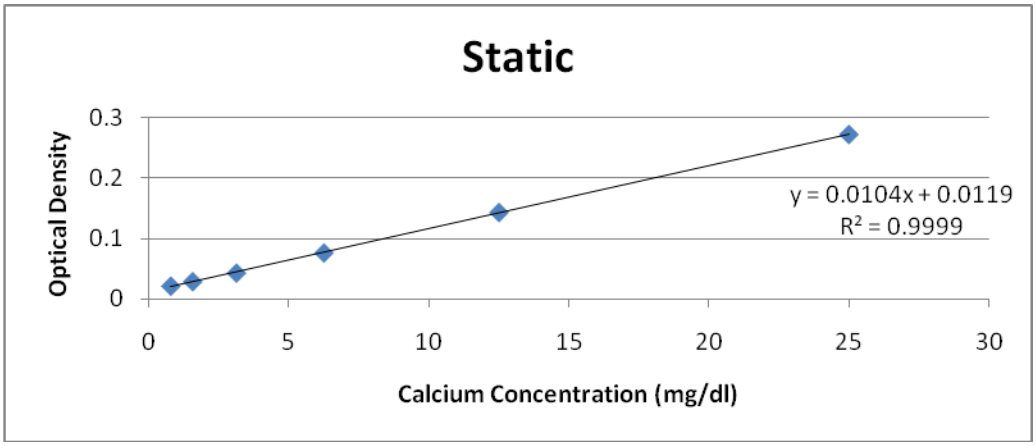

Figure 139: Calibration curve for static scaffolds in Zetos bioreactor

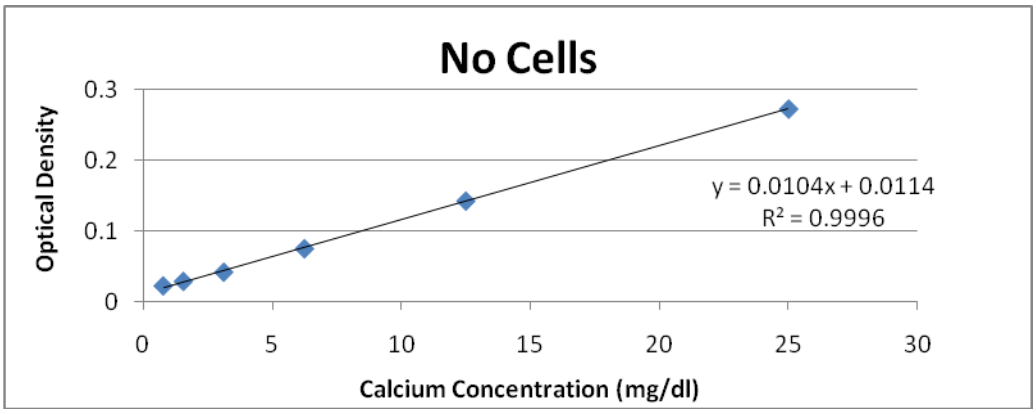

Figure 140: Calibration curve for no cells scaffolds in Zetos bioreactor

In can be seen from figure 141 that statistical significance was observed between the mechanically compressed (DSO loaded) group and both the DSO static and the DSO no cell group. In the DSO45 scaffold geometry group, statistical significance was only observed between the DSO45 flow group and the DSO45 no cell group (Figure 142).

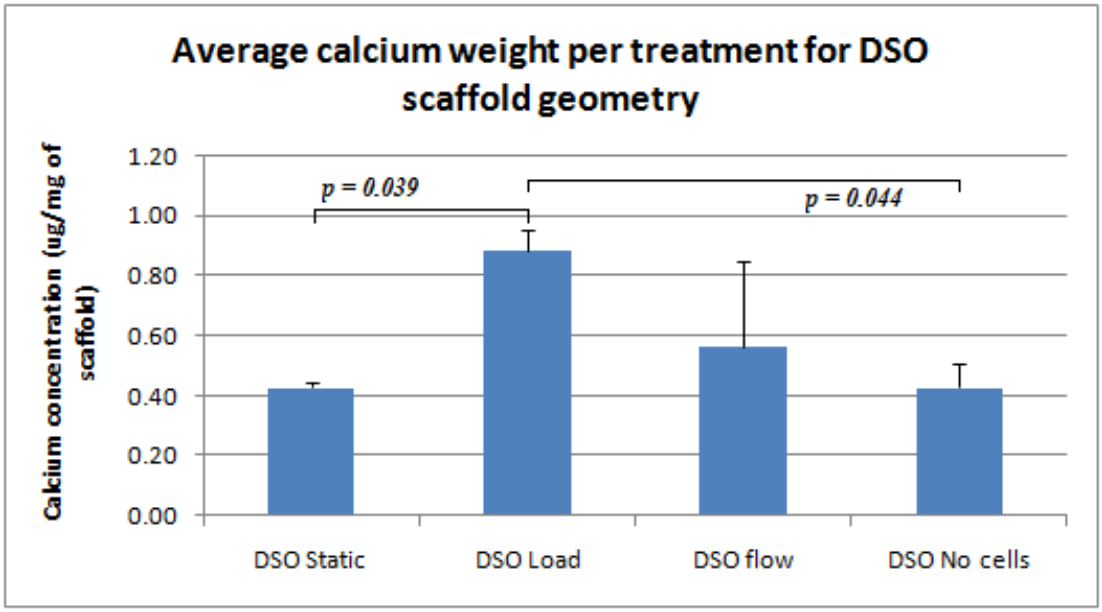

Figure 141: Calcium weight for different treatments obtained with the DSO scaffold geometry

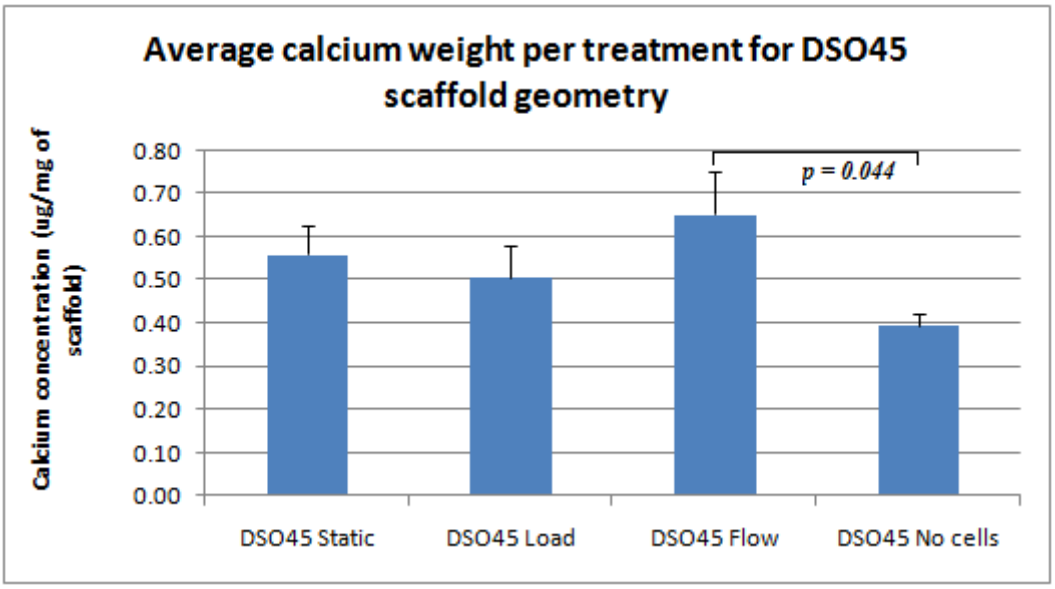

Figure 142: Calcium weight for different treatments obtained with the DSO45 scaffold geometry.

Briefly, cryostat sections of 7µm were cut of all the scaffolds with different treatments and sections at a distance 150µm – 153µm were stained using the Von Kossa technique and PI. The sections were then observed using an upright microscope (Nikon, Eclipse E800) and the images recorded digitally so that they can be processed using an imaging program (Image J).

The area of Von Kossa stained mineral for the DSO scaffolds (Figure 142) and the DSO45 scaffold (Figure 143) were measured. The PI positive cells were also counted using the program and cell numbers for the DSO scaffolds (Figure 144) and the DSO45 (Figure 145) scaffolds were recorded.

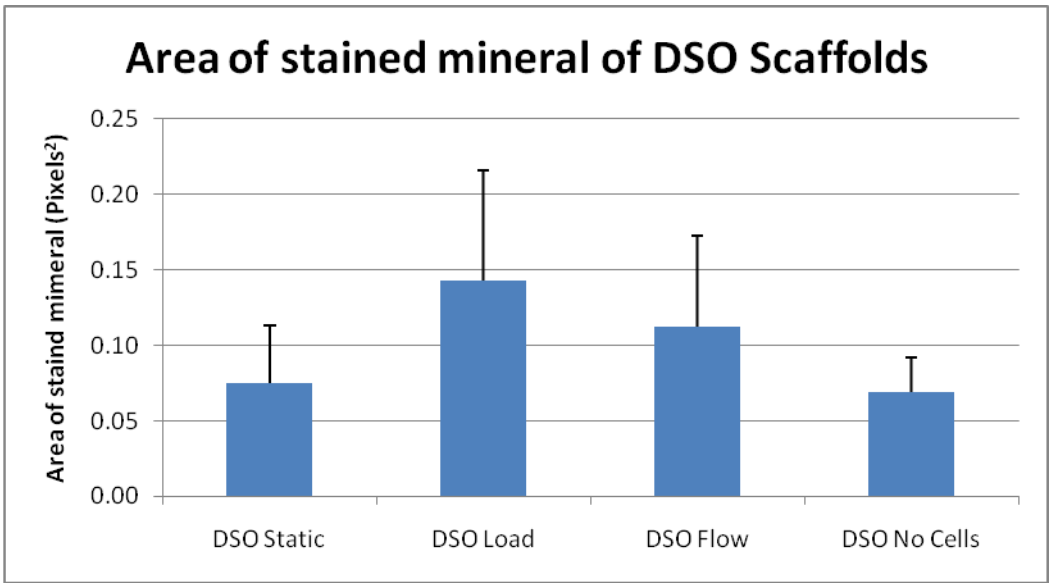

Figure 143: Area of stained mineral observed on sections stained by the Von Kossa technique measured using Image J (No statistical significance)

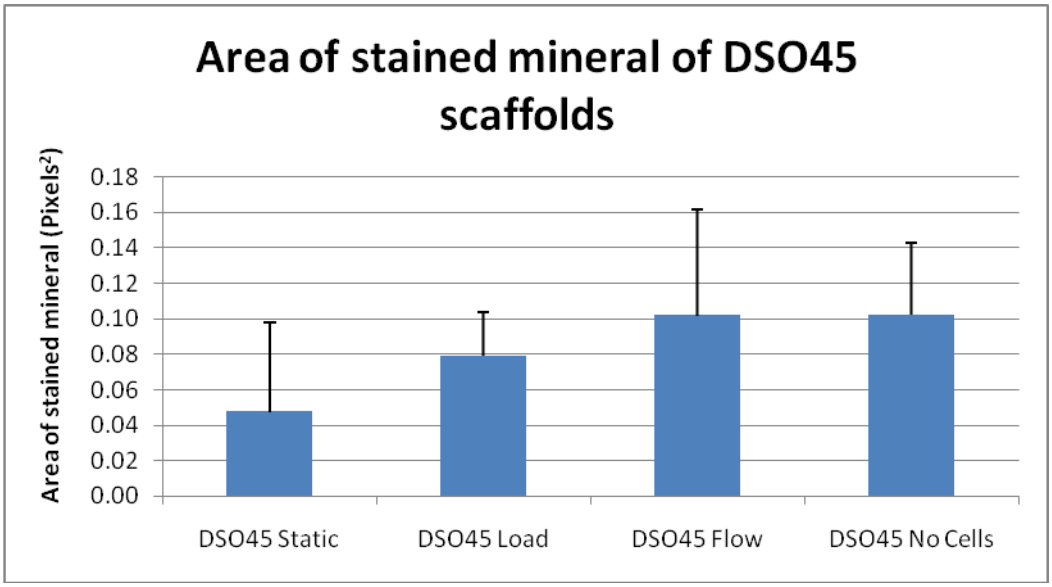

Figure 144: Area of stained mineral observed on sections stained using the Von Kossa technique measured using Image J (No statistical significance)

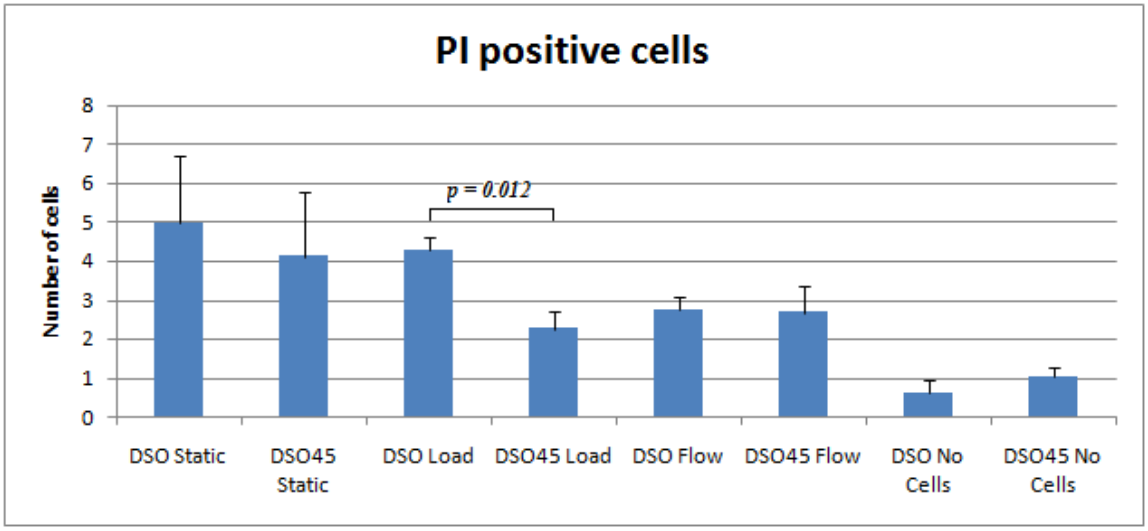

Figure 145: Average number of PI stained cells, comparison of different scaffold geometries subjected to the same treatments

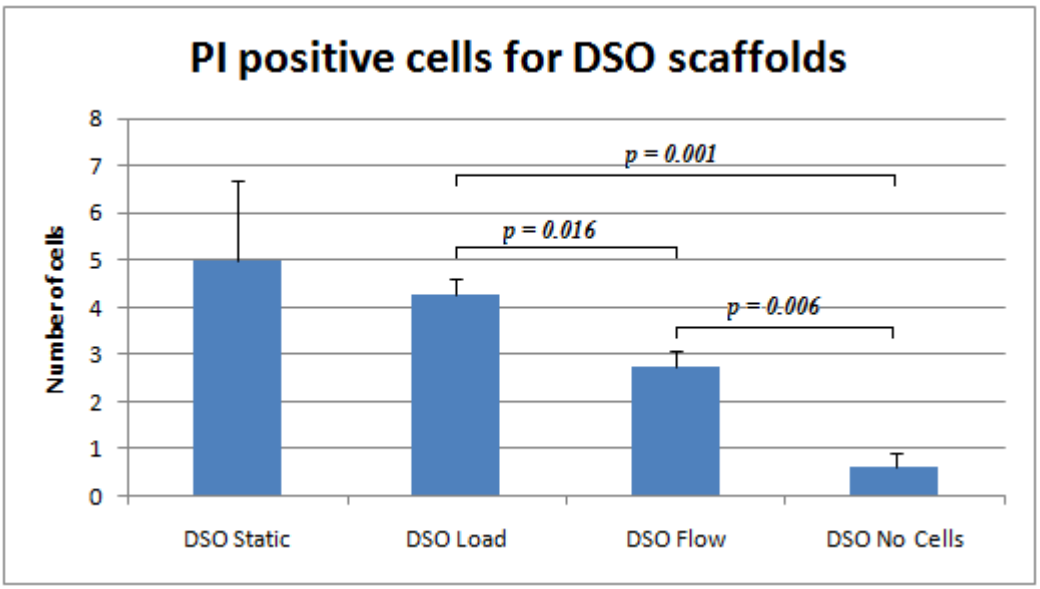

Figure 146: Average number of cells measured on sections 150µm – 153µm from the top of the scaffolds

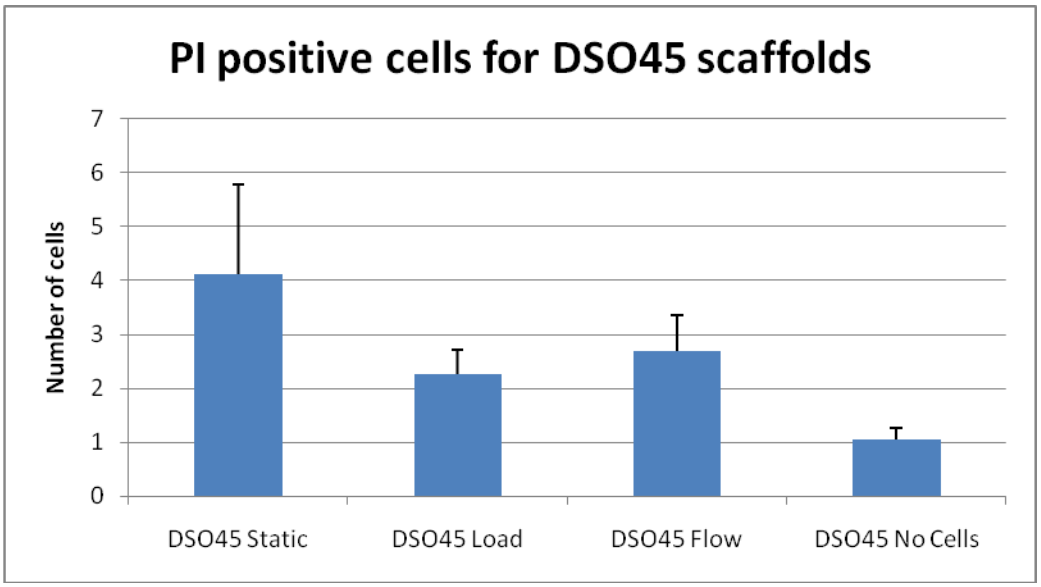

Figure 147: Average number of cells measured on sections 150µm - 153µm from the top of the scaffolds

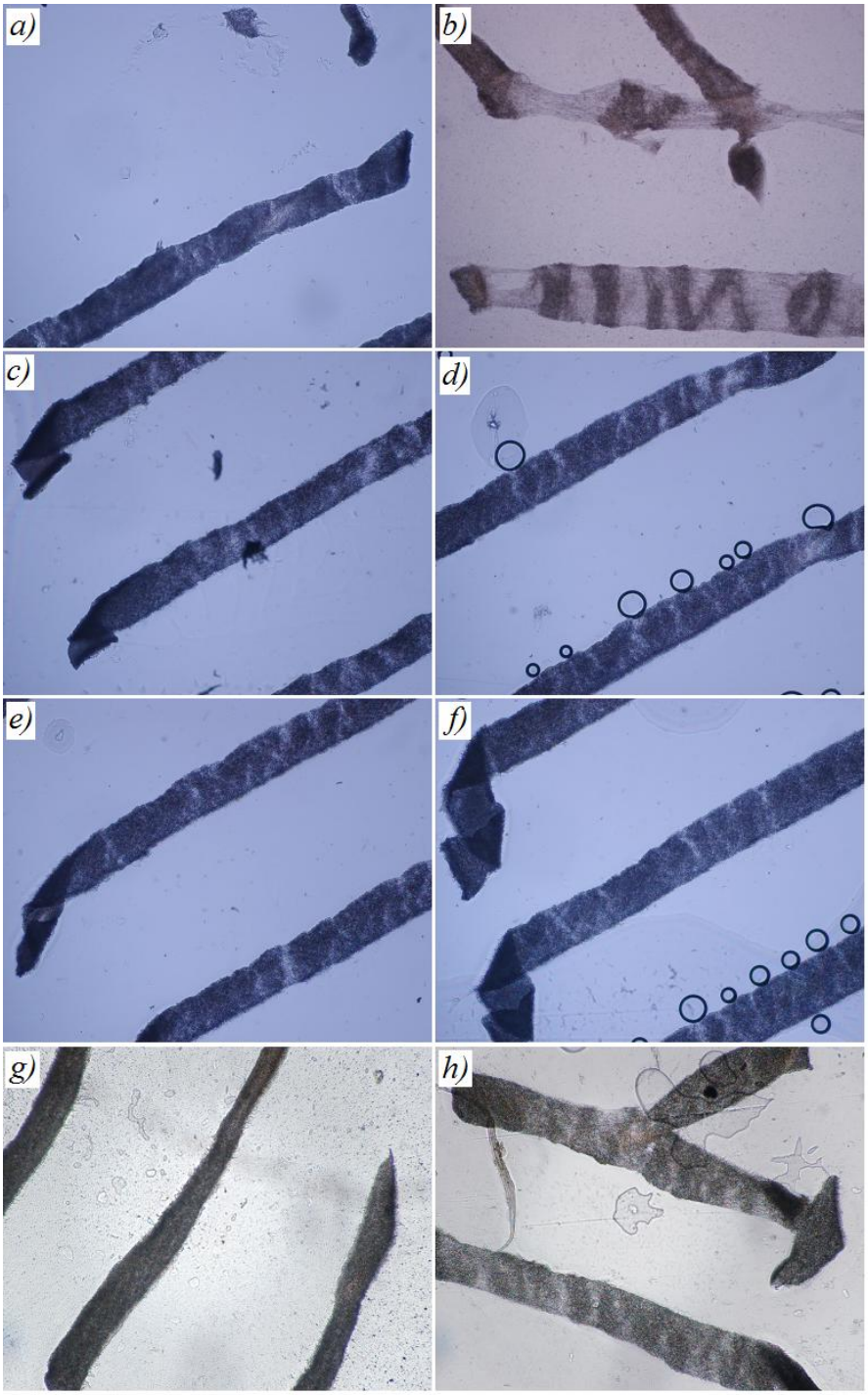

Figure 148: Representative bright field images, a) DSO Static, b) DSO45 Static, c) DSO Load, d) DSO45 Load, e) DSO Flow, f) DSO45 Flow, g) DSO No Cells, h) DSO45 No Cells

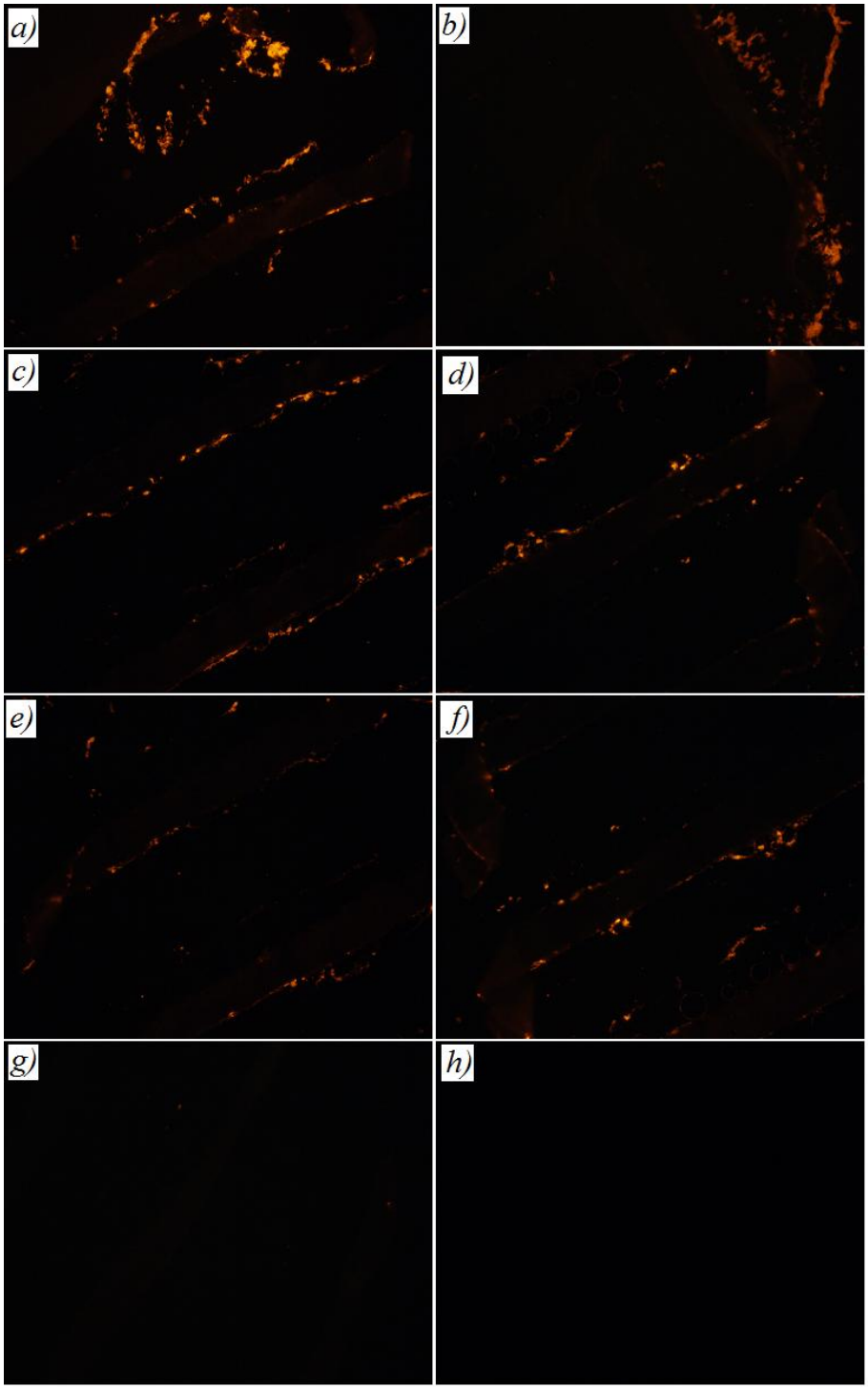

Figure 149: Representative PI fluorescent images, a) DSO Static, b) DSO45 Static, c) DSO Load, d) DSO45 Load, e) DSO Flow, f) DSO45 Flow, g) DSO No Cells, h) DSO45 No Cells

Image J was used to determine the area of stained mineral and the number of PI positive cells. The area of Von Kossa present on the four sections at a distance 150μm from the top of the scaffold can be observed in figure 148 for the DSO scaffolds and figure 149 for the DSO45 scaffolds with no statistical significance observed in both cases. For the PI stained cells the only case where statistical significance was observed between the two scaffold geometries was in the case of DSO load and DSO45 load (Figure 145). The number of cells present on the sections can be observed in figure 146 for the DSO scaffolds and figure 147 for the DSO45 scaffolds. For the DSO scaffold group, statistical significance of the PI stained cells was observed between the DSO load group and both the DSO flow and DSO no cells group (Figure 146). However in the DSO45 scaffold geometry, no statistical significance was observed between any of the groups (Figure 147). Representative images used to measure the mineral stained with Von Kossa and PI can be seen in figure 149.

3.3.3 Combining FEA determined surface strain distribution and mechanically stimulated scaffolds in the Zetos™ bioreactor system

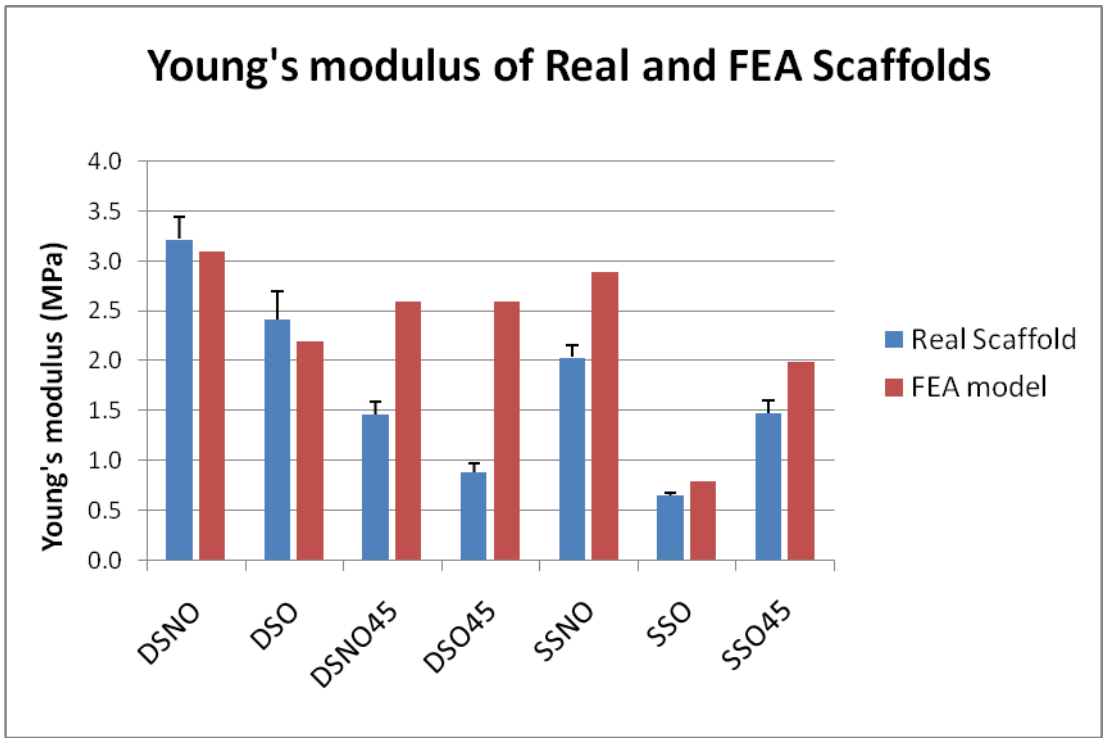

Figure 150: Comparison of Young's modulus of FEA and manufactured PCL scaffolds

From figure 150 it can be seen that the Young's modulii obtained from the mechanical testing and the FE analyses are in most cases fairly similar however for the DSNO45 and the DSO45 scaffolds the FEA determined Young's modulus are greatly different to the Young's modulus obtained by mechanical testing.

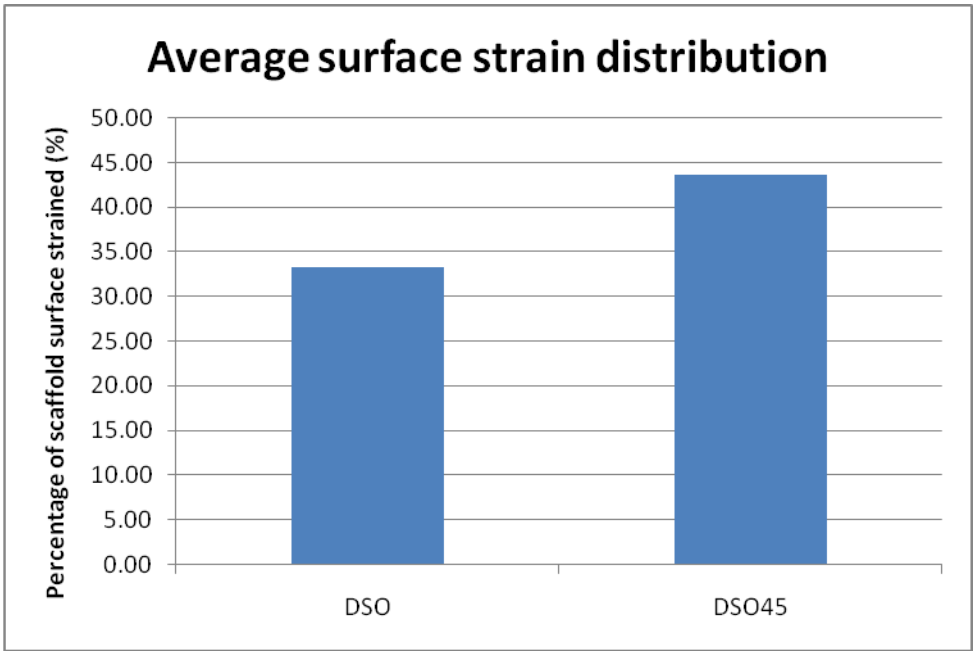

Figure 151: Average surface strain distribution throughout different scaffold geometries

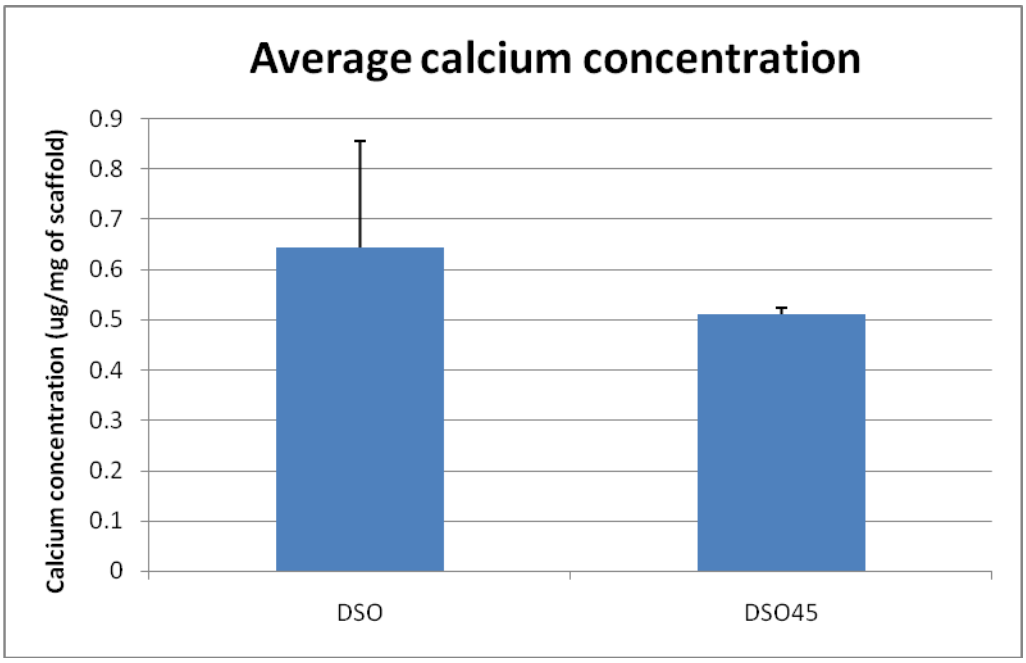

Figure 152: Average calcium concentration for DSO and DSO45 scaffold geometries

3.4 Discussion

3.4.1 Polycaprolactone scaffold and MG63 cells in Zetos™ bioreactor

The aim of the first experiment was to determine whether cells could survive on test scaffolds in the Zetos™ chambers for a week. After the *in vitro* experiment where the PCL scaffolds were seeded with MG63 cells (see chapter 1) yielded a positive outcome, an experiment was undertaken which demonstrated that similar cell survival could occur in the Zetos™ system.

The reason for choosing the MG63 cell line was due to their ability to proliferate more rapidly than the marrow stromal cells and therefore obtaining the numbers of cells required for the experiment (6 million cells required) speedily (approx 2 weeks). The MG63 cell line (Sakai et al. 2006), despite being a cancerous cell line has been reported to exhibit some osteoblastic traits characteristic to bone forming cells (Bachle and Kohal 2004) and has been widely used as a model for osteoblast research and toxicology studies (Hsu et al. 2007, Takagishi et al. 2006). The MG63 cell line was therefore chosen for the initial experiment to test their ability of survival on the PCL scaffold.

During the course of the experiment, the pH was monitored to observe changes during the experiment. This was important as the polycaprolactone scaffold might have been breaking down and hence altering the pH of the media which would have had an effect on cell survival. The media used was the same as that used in similar experiments involving the Zetos™ bioreactor and bone cores (Mann et al. 2006) and needed to be investigated.

As can be observed from paragraph 3.1, the pH of the media under static conditions with cells was more acidic compared to the control scaffold with no cells and the Zetos™ media in the ‘flow’ and ‘load’ group with cells. Statistical significance was observed between the ‘static’ group with cells and the remaining three groups at the same time points during the course of the experiment at all the time points. It was also observed that that the control group with no cells was the least acidic at the time points which would indicate that the decrease in pH was due to cellular activity (Waldman et al. 2004). The pH of the media with the scaffold under static conditions was also due to the fact that the volume used was half (5ml) of that in

the media used in the Zetos™ system for each chambers (10ml) and that the acidity decreased more rapidly in the smaller volume. As the media was circulating through the Zetos™ system it was being refreshed and oxygenated, which could have reduced the anaerobic metabolism of the cells which in turn would have reduced the lactic acid production of the cells (Mekhail et al. 2004). This could explaining the significant difference between the pH of the 'static' group with cells and the pH of the media circulating in the Zetos™ system. The pH could have also been affected by the chambers which might have allowed a small quantity of air into the system which would have altered the pH. Overall the pH did not deviated greatly from the initial pH of 7.25 – 7.3 except for the static conditions and therefore was decided that HEPES would be a suitable buffer to use in media mixture for the future experiments involving the Zetos™ bioreactor (Mann et al. 2006). Although HEPES has been reported to be an effective buffer and has been demonstrated to inhibit acidic culture media with various cell types including osteoblasts (Kaysinger and Ramp 1998, Ramp et al. 1994), bone marrow stromal cells (Kohn et al. 2002) and chondrocytes (Waldman et al. 2004), adverse effects can arise from its use (Altura et al. 1980) including the production of free radicals (Simpson et al. 1988) and cytotoxic effects after exposure to light (Zigler et al. 1985). In contrast the HCO_3^- ions which are present in the sodium bicarbonate ($NaHCO_3$) added to the Zetos™ growth media, are effective buffers under acidic conditions and also have the additional advantage of being able to neutralize acid by removing the CO_2 (Waldman et al. 2004). However because HCO_3^- is a base, the presence of a non-bicarbonate buffer, i.e. HEPES, was also required to reduce the alkalization that occurs when sodium bicarbonate was added to the media (Levraut et al. 2001), thus the combined effect of HEPES and HCO_3^- should provide better maintenance of pH during the Zetos™ experiment (Mann et al. 2006).

The effectiveness of the Zetos™ media was further supported by the images taken of the scaffolds under fluorescence which illuminated the cells present after they were stained with DAPI. It can be seen that at T_0 in both geometries cells are visible (Figure 112) and that during the course of the experiment at time points T_3 and T_7 (Figures 113 and 114) cells were also present on the scaffold which demonstrates that cells were able to attach to the scaffold and they are were capable of being maintained in Zetos™ system by using the Zetos™ media

mixture described by Mann *et al*. It was visually observed that the number of cells at the end of the experiment was less than at the start however DAPI stained cells were still observed at the end of the experiment indicating viable cells.

3.4.2 Polycaprolactone scaffold and MSC in Zetos™ bioreactor

The aim of this experiment was to determine whether mechanical stimulation of primary human stromal cells seeded on PCL scaffolds maintained in the Zetos™ bioreactor system in osteogenic differentiation media are able to undergo osteogenesis and bone formation.

Briefly, the scaffolds were divided into four groups, 'loaded' where the scaffolds were mechanically loaded and experienced media flow, 'flow' where the scaffolds were in the Zetos™ chambers but only experienced the media flow, 'static' were the scaffolds were not in the Zetos™ system but in universals with no flow or mechanical loading and finally 'no cells' which were scaffolds that were used as controls not seeded with cells. After 14 days, the scaffolds were removed and the amount of calcium produced measured as this would indicate which treatment created more calcium which would be synonymous with bone production. The pH of the media was recorded at every media change to determine whether the pH reached a toxic level for the cells.

From the results of the first pH experiment it can be seen that statistical significance was observed between the 'static' group and the rest of the groups. This interestingly was also observed in the Zetos™ bioreactor and MG63 experiment described above. The pH also tended to gradually decrease over time, this may have been due to the proliferation of cells which in turn lowered the pH by anaerobic metabolism of the cells creating lactic acid (Funes et al. 2007, Reyes et al. 2006) however could alternatively be due to the increased metabolic cellular activity. For the calcium quantification, the scaffolds with the two different geometries that were seeded with MSC and that were mechanically loaded created statistically more calcium than the 'no cells' group and the 'static' group, with statistical significance also observed between the 'flow' group and the 'static' group in both scaffold geometries. It was also noticed that between the two mechanically compressively loaded

scaffold geometries (DSO and DSO45) there was a trend towards more calcium production in the DSO45 scaffold although this was not statistically significant. The sections obtained of the scaffolds that were stained with Von Kossa further backed the presence of calcium in the scaffold. The images of the consecutive sections (Figure 124) demonstrated that the Von Kossa stains occurred at the same place on the scaffold and that the stained areas are not a chance occurrence. Statistical significance was observed between DSO load and both the DSO static and No cell groups with a similar result obtained with the DSO45 scaffold geometry. Similar observations were made by Duty *et al*, where histological examination of loaded scaffolds, showed a larger area of positive Von Kossa staining compared to the scaffold with no cells (Duty et al. 2007). In this chapter the quantification of the area stained with the Von Kossa technique was performed using an imaging program (Image J) which yielded results that reinforced what was observed with the calcium quantification technique. In the work performed by Duty *et al*, a different method was used to quantify the amount of bone formation on the scaffold using micro-CT (Duty et al. 2007) which was more accurate as the entire scaffold was scanned and not just analysed sections. From the results obtained from the Image J analyses to determine the positively stained PI cells, it was observed that the cell number was greatest in the statically treated scaffold (Figure 123). Certain problems occurred during the cell counting as the program sometimes was unable to distinguish between the scaffold and the cells which in certain cases lead to a very high or low cell count. These unusual cases were then reviewed and manually counted. It can also been observed that a cell count was measured in scaffolds that were not seeded with cells which indicates that the programme occasionally falsely counted cells. Previous studies have reported that PCL scaffolds seeded with cells were able to promote cell attachment and maintain cells viability (Hutmacher et al. 2001a, Mondrinos et al. 2006, Wang et al. 2004).

For the second repeat, pH was also recorded and it was observed that statistical significance was observed between the static group and the other groups in both the experiments where the two different scaffold geometries were tested, which was also seen in the first repeat, this may have been due to the proliferation of cells which in turn lowered the pH by anaerobic metabolism of the cells creating lactic acid (Funes et al. 2007, Reyes et al. 2006, Waldman et al. 2004). Statistical significance was observed in the calcium

concentration in the DSO scaffold geometry treatments between the mechanically compressed (DSO load) and the ‘static’ group. The static treatment yielded similar calcium concentrations as the scaffold seeded with no cells which would signify that no calcium was created. In the fluid flow treatment, the error bar was large which shows that one of the scaffolds seeded with MSCs under these conditions produced calcium but with the number of scaffolds in this treatment being only three, no statistical significance was obtained.

In the DSO45 scaffold group, the mechanically compressed ‘load’ group seeded with MSC yielded more calcium and was statistically significant compared to the static treatment (Duty et al. 2007). No statistical significance was observed between the other treatments in the group however the ‘flow’ group produced more calcium which was unexpected as this did not correspond to the results obtained from the first run.

The area of Von Kossa stains reflected the general trend that was observed in the first run with the loaded DSO scaffolds with this treatment expressing the highest level of Von Kossa however no statistical significance was observed between the treatments. The DSO45 loaded and the static had similar levels of Von Kossa staining which would indicate that the zone that was sectioned had no mineral present as the o-cresolphthalein method demonstrated the presence of calcium. The reason for a reading being detected the no cells treatment during the imaging process was due to some background noise that in some cases was detected by Image J (Figure 131 – 132). For the PI stained MSC the largest value was observed in the static group however no statistical significance was observed with this group and the other groups. Statistical significance was observed between the ‘load’ group and both the ‘flow and ‘no cell’ groups for the DSO scaffold geometry. For the DSO45 scaffold geometry statistical significance was observed between the static group and the three other groups.

For the third repeat of the Zetos™ and MSC experiment, the DSO scaffold group had statistical significance between the mechanically loaded and both the static and the no cell treatments. For the DSO45 scaffold group, statistical significance was observed between the fluid flow group and the ‘no cell’ group. Observations were also witnessed between DSO load and DSO45 load (Figure 145) which may have been due to the different mechanical

properties and strain distributions or different fluid flow characteristics or a combination of both mechanical and fluid flow.

To the author's knowledge, this unique technique of using the Zetos™ bioreactor to mechanically stimulate cells seeded on scaffolds has not been reported in previous studies. This technique also demonstrated proof of principle and potential for bone regeneration with a few modifications. A few reasons were determined which might have had an effect on the results leading to reduced statistical power. Firstly during the first and second run involving the Zetos™ bioreactor, some of the chambers broke by releasing the media, which reduced the number of chambers thus affecting the outcome. Furthermore because some had failed it could be possible that some of the other chambers were faulty and were maybe not mechanically compressing the scaffolds uniformly. Secondly the rubber rings used to support the scaffold in the loading chambers had grooves cut out to facilitate the diffusion of media throughout the scaffold however on placing the ring with the scaffold into the loading chamber and pumping media through the system, in at least 2 cases air was trapped and hindered the diffusion of the media to some areas of the scaffold which would have deprived the cells of vital nutrients. Thirdly as previously mentioned, the Zetos™ chambers were designed for bone which is considerably stiffer than the scaffolds and the rubber rings. The results obtained tended to demonstrate that mechanically stimulated scaffolds seeded with MSCs created more calcium deposit.

It has been of interest to many people for a number of years as to the effects of fluid flow (Klein-Nulend et al. 1997, Reich et al. 1990a) and mechanical strain (Duncan and Turner 1995, Harter et al. 1995) and their results on osteoblasts. During mechanical compression of the PCL scaffolds the deformations of the construct caused volume changes in the interconnecting pores which in turn resulted in temporary pressure gradients, which produced different fluid velocities within the scaffold (Steck et al. 2003). The magnitude and complexity of the fluid flow during and without compressing in the two scaffold geometries were probably dissimilar therefore it is difficult to determine whether the fluid flow generated by the compression of the scaffold had more of an effect than the surface strain. The mechanical compression may have had a secondary effect by further mixing the media which could have supplied the cells with additional fresh media and removed waste products

(Darling and Athanasiou 2003). Steady fluid flow as used in the Zetos bioreactor system, has been used in previous studies in perfusion bioreactors with scaffolds (Cartmell et al. 2003, Kitagawa et al. 2006) and has been shown to stimulate mineral deposition on scaffolds with increased deposition observed with increased flow induced shear stress (Bancroft et al. 2002, Sikavitsas et al. 2003). Oscillatory fluid flow has also been shown to increase bone formation by osteoblasts on a 3D scaffold (Vance et al. 2005) however it has also been reported that osteoblasts were more mechano-responsive in a 2D culture experiment to pulsatile fluid flow than to steady and oscillatory flow (Jacobs et al. 1998). Therefore it remains unclear which flow is optimal for stimulating osteoblasts on 3D scaffolds. Previous studies have reported that mechanically stimulated osteoblasts adapt to their mechanical environment (Jaasma et al. 2007, Robling et al. 2002) and stimulates bone formation

The detected presence of the calcium while using the o-cresolphthalein method and the positively stained areas of Von Kossa demonstrated the potential of this novel technique. Other studies have reported using x-ray refraction to determine bone formation which was proven to be highly accurate with small structures, non invasive and able to distinguish between bone and other less dense materials (Hashimoto et al. 2006, Kelly et al. 2008, Wagner et al. 2006). In some cases, the analysed scaffolds showed low levels of calcium mineral relative to the other scaffolds in the same group, this might have been due to the efficiency at which the cells were initially seeded on the scaffold. Turning the scaffolds upside down every half an hour for four hours might not have increased the static seeding technique. The problem of successfully seeding scaffolds has been mentioned in the literature (Duty et al. 2007). Another factor that was observed in the literature was the loading cycle and the duration. In Duty *et al*, the seeded *in vivo* scaffolds were mechanically stimulated for 30 min, three times a week for two weeks and then the scaffolds were left implanted for another 4 weeks to allow for mineralization to occur that was induced by the loading stimulus. The waveform applied was a sinusoidal one at a frequency of 1Hz (Duty et al. 2007) however a jumping waveform delivered daily has also been shown to yield positive results (Mann et al. 2006) with other groups also delivering a daily load to trabecular bone *in vivo* (Guldberg et al. 1997, Jones et al. 2003, Moalli et al. 2000, Robling et al. 2000).

The MSC used for the experiments came from three different patients which could explain the differences between the experiments and the varied results for the same treatments as has been reported in the literature (Bernardo et al. 2007, Temenoff et al. 2004).

From the results obtained it can be observed that in most cases the FEA determined Young's modulus and the mechanically determined Young's modulii coincide, however for the DSNO45 and the DSO45 the two modulii are different. This demonstrates that the FE method can be a powerful tool in predicting mechanical properties however it does not mean that mechanical testing should be completely replaced by FE modelling as proven by the two cases that do not follow the FE analyses (Li and Wang 2006). In theses FEA analyses, tetrahedral elements were chosen as they were the default setting on the ABAQUS software however they have a tendency to be overly stiff which might have affected the results obtained comparing the Young's modulii of the manufactured and the computer models especially in the cases of the DSNO45 and DSO45 scaffold geometry (Figure 150). An alternative method could have been to design the meshing of the strands with a different element i.e. hexahedral. As the beam span was short compared to the overall scaffold design the use of tetrahedral elements appropriate however more accurate results would have been obtained by using an alternative meshing design.

3.5 Summary

It can be observed from the results of the calcium content of the scaffolds that in the first run, the mechanically loaded scaffold seeded with MSC in both the DSO and the DSO45 scaffold group generated the most calcium mineral. The fluid flow treatment produced the second highest calcium concentration in both the scaffold groups. The results obtained from the first run of the experiment are the results that were expected as from the literature mechanical loading and fluid flow can affect MSC and potentially turn them into osteoblasts. In the first run, the results suggest that mechanical loading of the scaffold seeded with MSC had a greater effect and differentiated the MSC into osteoblasts with greater success.

The second run had much less statistical significance between treatments however in the DSO scaffold group the mechanically loaded produced more calcium compared to the other treatments with statistical significance. The DSO45 scaffolds seeded with MSCs only had statistical significance between the mechanically loaded and the static group. The results obtained from the second run would indicate that mechanical loading of the scaffold affects the MSC which are seeded on them but without statistical significance in the DSO group it is impossible to be certain.

The results obtained from the third repeat would suggest that in the DSO scaffold seeded with MSC, the mechanically loaded treatment produced the greatest amount of calcium followed by the fluid flow treatment. These results follow the same trend as the results obtained in the first run. In the DSO45 scaffold geometry seeded with MSC, no statistical significance was observed between the DSO45 Flow and No Cells treatments.

From all the results obtained from the three Zetos™ runs, it can be concluded that mechanical loading has an effect on the MSCs seeded on the PCL scaffolds even though patient variability may have affected the results in some cases, overall the mechanically loaded scaffolds seeded with MSCs produced more calcium mineral. This is encouraging and demonstrates that mechanically stimulated polycaprolactone scaffolds seeded with MSCs could be used to regenerate bone once the process has been further investigated.

Chapter 4.

Conclusions and future work

Scaffolds were created using natural and synthetic materials. Out of the natural materials, none of the scaffolds would have been suitable as load bearing scaffolds however many other natural materials exist which could be used to manufacture scaffolds and this could be investigated in the future. Out of the synthetic materials, scaffolds manufactured using PCL were by far mostly used in the experiments involving scaffolds and MSCs due to the biocompatibility, availability of the polymer and the mechanical properties of the scaffolds. It was demonstrated that cells seeded on the scaffold were capable of survival *in vitro* and *in vivo* for numerous weeks. The PCL scaffolds also required a gelatin coating which introduced additional complexity which could be investigated to further understand the effect of the coating on cellular adhesion.

PLGA has been widely used in medical applications and several papers have been published reporting the benefits of this polymer. It would be interesting to further investigate PLGA as a scaffold material and perform similar experiments as with the PCL scaffolds. Particularly interesting would be to mechanically test the PLGA scaffolds as the literature suggests that PLGA has a higher Young's modulus than PCL therefore making it capable of bearing greater loads (Cao et al. 2006) and determine the osteogenic potential of MSC cultured on PLGA scaffolds which has been reported to be successful (Chastain et al. 2006).

The finite element analysis experiment demonstrated that the values of the Young's modulus obtained by mechanically loading the manufactured scaffolds were similar as those that were obtained from the finite element analysis. Due to these similarities in Young's modulii between the mechanically loaded and finite element analyses it can be assumed that the predicted strains distributed throughout the scaffold by the finite element analyses would correspond to the strain distribution that would occur in the mechanically stimulated manufactured scaffolds. An interesting future experiment would be to determine other scaffold geometries which would distribute strain even more throughout the scaffold compared to the geometries that were tested. The mechanical properties of different materials i.e. PLGA, would be interesting to include in the finite element analysis to determine the strain distribution of different materials and different geometries.

From the Zetos™ bioreactor experiment with the mechanically compressed PCL scaffolds seeded with MSC, it was observed that the calcium mineral deposited was greater than in the scaffolds with no form of mechanical stimulation. The MSC seeded on the scaffolds which were only mechanically stimulated by fluid flow also produced more calcium deposit than those MSCs that had no mechanical stimulation. These results were encouraging and demonstrated that mechanical loading of scaffolds seeded with MSCs had the potential to push the MSCs down the osteoblastic lineage and generate calcium deposits. Interesting experiments would be to involve manufacturing scaffolds with different types of such as PLGA and seeding them with MSCs and stimulating them mechanically in the Zetos™ bioreactor.

Reference List

Aamodt, A., Lund-Larsen, J., Eine, J., Andersen, E., Benum, P., and Husby, O. S., In vivo measurements show tensile axial strain in the proximal lateral aspect of the human femur. *J. Orthop. Res* 1997, 15:927-931.

Aarden, E. M., Burger, E. H., and Nijweide, P. J., Function of osteocytes in bone. *J. Cell Biochem.* 1994, 55:287-299.

Ajubi, N. E., Klein-Nulend, J., Nijweide, P. J., Vrijheid-Lammers, T., Alblas, M. J., and Burger, E. H., Pulsating fluid flow increases prostaglandin production by cultured chicken osteocytes--a cytoskeleton-dependent process. *Biochem. Biophys. Res Commun.* 1996, 225:62-68.

Alaylioglu, H. and Ali, R., Analysis of an automotive structure using hybrid stress finite elements. *Computers & Structures* 1978, 8:237-242.

Altura, B. M., Carella, A., and Altura, B. T., Adverse effects of Tris. HEPES and MOPS buffers on contractile responses of arterial and venous smooth muscle induced by prostaglandins. *Prostaglandins Med.* 1980, 5:123-130.

Anal, A. K., Stevens, W. F., and Remunan-Lopez, C., Ionotropic cross-linked chitosan microspheres for controlled release of ampicillin. *Int. J. Pharm.* 2006, 312:166-173.

Ang, T. H., Sultana, F. S. A., Hutmacher, D. W., Wong, Y. S., Fuh, J. Y. H., Mo, X. M., Loh, H. T., Burdet, E., and Teoh, S. H., Fabrication of 3D chitosan-hydroxyapatite scaffolds using a robotic dispensing system. *Materials Science & Engineering C-Biomimetic and Supramolecular Systems* 2002, 20:35-42.

Argyris, J. H., Energy theorems and structural analysis. 1960,

Aubin, J. E., Regulation of osteoblast formation and function. *Rev. Endocr. Metab Disord.* 2001, 2:81-94.

Autuori, B., Bruyere-Garnier, K., Morestin, F., Brunet, M., and Verriest, J. P., Finite element modeling of the head skeleton with a new local quantitative assessment approach. *IEEE Trans. Biomed. Eng* 2006, 53:1225-1232.

Bachle, M. and Kohal, R. J., A systematic review of the influence of different titanium surfaces on proliferation, differentiation and protein synthesis of osteoblast-like MG63 cells. *Clin. Oral Implants. Res* 2004, 15:683-692.

Bagi, C. and Burger, E. H., Mechanical stimulation by intermittent compression stimulates sulfate incorporation and matrix mineralization in fetal mouse long-bone rudiments under serum-free conditions. *Calcif. Tissue Int.* 1989, 45:342-347.

Bancroft, G. N., Sikavitsas, V. I., van den, Dolder J., Sheffield, T. L., Ambrose, C. G., Jansen, J. A., and Mikos, A. G., Fluid flow increases mineralized matrix deposition in 3D perfusion culture of marrow stromal osteoblasts in a dose-dependent manner. *Proc. Natl. Acad. Sci. U. S. A* 2002, 99:12600-12605.

Bassey, E. J. and Ramsdale, S. J., Increase in femoral bone density in young women following high-impact exercise. *Osteoporos. Int.* 1994, 4:72-75.

Beaupré, G. S., Orr, T. E., and Carter, D. R., An approach for time-dependent bone modeling and remodeling-application: a preliminary remodeling simulation. *J. Orthop. Res.* 1990, 8:662-670.

Bernardo, M. E., Zaffaroni, N., Novara, F., Cometa, A. M., Avanzini, M. A., Moretta, A., Montagna, D., Maccario, R., Villa, R., Daidone, M. G., Zuffardi, O., and Locatelli, F., Human bone marrow derived mesenchymal stem cells do not undergo transformation after long-term in vitro culture and do not exhibit telomere maintenance mechanisms. *Cancer Res.* 2007, 67:9142-9149.

Bertoni, F., Barbani, N., Giusti, P., and Ciardelli, G., Transglutaminase reactivity with gelatine: perspective applications in tissue engineering. *Biotechnol. Lett.* 2006, 28:697-702.

Bertram, J. E. and Biewener, A. A., Bone curvature: sacrificing strength for load predictability? *J. Theor. Biol.* 1988, 131:75-92.

Bertram, J. E. and Swartz, S. M., The 'law of bone transformation': a case of crying Wolff? *Biol. Rev. Camb. Philos. Soc* 1991, 66:245-273.

Bigi, A., Cojazzi, G., Panzavolta, S., Roveri, N., and Rubini, K., Stabilization of gelatin films by crosslinking with genipin. *Biomaterials* 2002, 23:4827-4832.

Bigi, A., Cojazzi, G., Panzavolta, S., Rubini, K., and Roveri, N., Mechanical and thermal properties of gelatin films at different degrees of glutaraldehyde crosslinking. *Biomaterials* 2001a, 22:763-768.

Bigi, A., Cojazzi, G., Panzavolta, S., Rubini, K., and Roveri, N., Mechanical and thermal properties of gelatin films at different degrees of glutaraldehyde crosslinking. *Biomaterials* 2001b, 22:763-768.

Bigi, A., Panzavolta, S., and Rubini, K., Relationship between triple-helix content and mechanical properties of gelatin films. *Biomaterials* 2004, 25:5675-5680.

Blanco-Prieto, M. J., Besseghir, K., Zerbe, O., Andris, D., Orsolini, P., Heimgartner, F., Merkle, H. P., and Gander, B., In vitro and in vivo evaluation of a somatostatin analogue released from PLGA microspheres. *J. Control Release* 2000, 67:19-28.

Bolgen, N., Vargel, I., Korkusuz, P., Menceloglu, Y. Z., and Piskin, E., In vivo performance of antibiotic embedded electrospun PCL membranes for prevention of abdominal adhesions. *J. Biomed. Mater. Res. B Appl. Biomater.* 2006,

Bottlang, M., Simnacher, M., Schmitt, H., Brand, R. A., and Claes, L., A cell strain system for small homogeneous strain applications. *Biomed. Tech. (Berl)* 1997, 42:305-309.

Boudriot, U., Dersch, R., Greiner, A., and Wendorff, J. H., Electrospinning approaches toward scaffold engineering-a brief overview. *Artif. Organs* 2006, 30:785-792.

Bourret, L. A. and Rodan, G. A., The role of calcium in the inhibition of cAMP accumulation in epiphyseal cartilage cells exposed to physiological pressure. *J. Cell Physiol* 1976, 88:353-361.

Brighton, C. T., Strafford, B., Gross, S. B., Leatherwood, D. F., Williams, J. L., and Pollack, S. R., The proliferative and synthetic response of isolated calvarial bone cells of rats to cyclic biaxial mechanical strain. *J. Bone Joint Surg. Am* 1991, 73:320-331.

Brockie, J., Exercise for women in the early postmenopausal years. *J. Br. Menopause. Soc* 2006, 12:126-127.

Brown, T. D., Techniques for mechanical stimulation of cells in vitro: a review. *J. Biomech.* 2000, 33:3-14.

Buckley, M. J., Banes, A. J., Levin, L. G., Sumpio, B. E., Sato, M., Jordan, R., Gilbert, J., Link, G. W., and Tran Son, Tay R., Osteoblasts increase their rate of division and align in response to cyclic, mechanical tension in vitro. *Bone Miner.* 1988, 4:225-236.

Burger, E. H. and Klein-Nulend, J., Mechanotransduction in bone--role of the lacuno-canalicular network. *FASEB J.* 1999, 13 Suppl:S101-S112.

Burger, E. H., Klein-Nulend, J., van der, Plas A., and Nijweide, P. J., Function of osteocytes in bone--their role in mechanotransduction. *J. Nutr.* 1995, 125:2020S-2023S.

Burgers, T. A., Mason, J., Niebur, G., and Ploeg, H. L., Compressive properties of trabecular bone in the distal femur. *J. Biomech.* 2008, 41:1077-1085.

Burr, D. B., Milgrom, C., Fyhrie, D., Forwood, M., Nyska, M., Finestone, A., Hoshaw, S., Saiag, E., and Simkin, A., In vivo measurement of human tibial strains during vigorous activity. *Bone* 1996, 18:405-410.

Burton-Wurster, N., Vernier-Singer, M., Farquhar, T., and Lust, G., Effect of compressive loading and unloading on the synthesis of total protein, proteoglycan, and fibronectin by canine cartilage explants. *J. Orthop. Res* 1993, 11:717-729.

Campagnoli, C., Roberts, I. A., Kumar, S., Bennett, P. R., Bellantuono, I., and Fisk, N. M., Identification of mesenchymal stem/progenitor cells in human first-trimester fetal blood, liver, and bone marrow. *Blood* 2001, 98:2396-2402.

Cann, C. E. and Adachi, R. R., Bone resorption and mineral excretion in rats during spaceflight. *Am J. Physiol* 1983, 244:R327-R331.

Cao, Y., Croll, T. I., Oconnor, A. J., Stevens, G. W., and Cooper-White, J. J., Systematic selection of solvents for the fabrication of 3D combined macro- and microporous polymeric scaffolds for soft tissue engineering. *J. Biomater. Sci. Polym. Ed* 2006, 17:369-402.

Carter, D. R., Mechanical loading history and skeletal biology. *J. Biomech.* 1987, 20:1095-1109.

Carter, D. R. and Wong, M., Mechanical stresses and endochondral ossification in the chondroepiphysis. *J. Orthop. Res.* 1988, 6:148-154.

Cartmell, S. H., Porter, B. D., Garcia, A. J., and Guldberg, R. E., Effects of medium perfusion rate on cell-seeded three-dimensional bone constructs in vitro. *Tissue Eng* 2003, 9:1197-1203.

Charles-Harris, M., del, Valle S., Hentges, E., Bleuet, P., Lacroix, D., and Planell, J. A., Mechanical and structural characterisation of completely degradable polylactic acid/calcium phosphate glass scaffolds. *Biomaterials* 2007, 28:4429-4438.

Chastain, S. R., Kundu, A. K., Dhar, S., Calvert, J. W., and Putnam, A. J., Adhesion of mesenchymal stem cells to polymer scaffolds occurs via distinct ECM ligands and controls their osteogenic differentiation. *J. Biomed. Mater. Res. A* 2006, 78:73-85.

Chau, D. Y., Collighan, R. J., Verderio, E. A., Addy, V. L., and Griffin, M., The cellular response to transglutaminase-cross-linked collagen. *Biomaterials* 2005, 26:6518-6529.

Chen, G., Sato, T., Ushida, T., Ochiai, N., and Tateishi, T., Tissue engineering of cartilage using a hybrid scaffold of synthetic polymer and collagen. *Tissue Eng* 2004, 10:323-330.

Chen, X., Macica, C. M., Ng, K. W., and Broadus, A. E., Stretch-induced PTH-related protein gene expression in osteoblasts. *J. Bone Miner. Res.* 2005, 20:1454-1461.

Cheng, G. C., Libby, P., Grodzinsky, A. J., and Lee, R. T., Induction of DNA synthesis by a single transient mechanical stimulus of human vascular smooth muscle cells. Role of fibroblast growth factor-2. *Circulation* 1996, 93:99-105.

Chiono, V., Pulieri, E., Vozzi, G., Ciardelli, G., Ahluwalia, A., and Giusti, P., Genipin-crosslinked chitosan/gelatin blends for biomedical applications. *J. Mater. Sci. Mater. Med.* 2007,

Chong, E. J., Phan, T. T., Lim, I. J., Zhang, Y. Z., Bay, B. H., Ramakrishna, S., and Lim, C. T., Evaluation of electrospun PCL/gelatin nanofibrous scaffold for wound healing and layered dermal reconstitution. *Acta Biomater.* 2007, 3:321-330.

Chu, T. M., Hollister, S. J., Halloran, J. W., Feinberg, S. E., and Orton, D. G., Manufacturing and characterization of 3-d hydroxyapatite bone tissue engineering scaffolds. *Ann. N. Y. Acad. Sci.* 2002, 961:114-117.

Church, V. L. and Francis-West, P., Wnt signalling during limb development. *Int. J. Dev. Biol.* 2002, 46:927-936.

Ciapetti, G., Ambrosio, L., Savarino, L., Granchi, D., Cenni, E., Baldini, N., Pagani, S., Guizzardi, S., Causa, F., and Giunti, A., Osteoblast growth and function in porous poly epsilon -caprolactone matrices for bone repair: a preliminary study. *Biomaterials* 2003, 24:3815-3824.

Clough, R. W, Comparison of three dimesional finite elements. *Proceedings of the symposium on application of finite element methods in civil engineering* 1969, 1-26.

Collet, P., Uebelhart, D., Vico, L., Moro, L., Hartmann, D., Roth, M., and Alexandre, C., Effects of 1- and 6-month spaceflight on bone mass and biochemistry in two humans. *Bone* 1997, 20:547-551.

Collins, T. J., ImageJ for microscopy. *Biotechniques* 2007, 43:25-30.

Cook, R. D. and Avrashi, J., Error estimation and adaptive meshing for vibration problems. *Computers & Structures* 1992, 44:619-626.

Cooke, M. N., Fisher, J. P., Dean, D., Rimnac, C., and Mikos, A. G., Use of stereolithography to manufacture critical-sized 3D biodegradable scaffolds for bone ingrowth. *J. Biomed. Mater. Res. B Appl. Biomater.* 2003, 64B:65-69.

Copray, J. C., Jansen, H. W., and Duterloo, H. S., An in-vitro system for studying the effect of variable compressive forces on the mandibular condylar cartilage of the rat. *Arch. Oral Biol.* 1985, 30:305-311.

Courant, R, Variation methods for the solution of problems of equilibrium and vibrations. *Bull Am Math Soc* 1943, 49:1-23.

Crandall, S. H., Engineering analysis. 1956,

Darling, A. L. and Sun, W., 3D microtomographic characterization of precision extruded poly-epsilon-caprolactone scaffolds. *J. Biomed. Mater. Res. B Appl. Biomater.* 2004, 70:311-317.

Darling, E. M. and Athanasiou, K. A., Articular cartilage bioreactors and bioprocesses. *Tissue Eng* 2003, 9:9-26.

Davies, C. M., Jones, D. B., Stoddart, M. J., Koller, K., Smith, E., Archer, C. W., and Richards, R. G., Mechanically loaded ex vivo bone culture system 'Zetos': systems and culture preparation. *Eur. Cell Mater.* 2006, 11:57-75.

Davies, P. F., Flow-mediated endothelial mechanotransduction. *Physiol Rev.* 1995, 75:519-560.

De Bari, C., Dell'Accio, F., Tylzanowski, P., and Luyten, F. P., Multipotent mesenchymal stem cells from adult human synovial membrane. *Arthritis Rheum.* 2001, 44:1928-1942.

De Bari, C., Dell'Accio, F., Vanlauwe, J., Eyckmans, J., Khan, I. M., Archer, C. W., Jones, E. A., McGonagle, D., Mitsiadis, T. A., Pitzalis, C., and Luyten, F. P., Mesenchymal multipotency of adult human periosteal cells demonstrated by single-cell lineage analysis. *Arthritis Rheum.* 2006, 54:1209-1221.

del Coz Diaz, J. J., Garcia Nieto, P. J., Vilan Vilan, J. A., Martin Rodriguez, A., Prado Tamargo, J. R., and Lozano Martinez-Luengas, A., Non-linear analysis and warping of tubular pipe conveyors by the finite element method. *Mathematical and Computer Modelling* 2007, 46:95-108.

Dennis, J. E. and Charbord, P., Origin and differentiation of human and murine stroma. *Stem Cells* 2002, 20:205-214.

Dennis, J. E., Haynesworth, S. E., Young, R. G., and Caplan, A. I., Osteogenesis in marrow-derived mesenchymal cell porous ceramic composites transplanted subcutaneously: effect of fibronectin and laminin on cell retention and rate of osteogenic expression. *Cell Transplant.* 1992, 1:23-32.

Desai, C. S and Abel, J. F., Introduction to finite element analysis. 1972,

Desai, C. S and Kundu, T., Introductory finite element method. 2001,

Di Martino, A., Sittinger, M., and Risbud, M. V., Chitosan: a versatile biopolymer for orthopaedic tissue-engineering. *Biomaterials* 2005, 26:5983-5990.

Diego, R. B., Estelles, J. M., Sanz, J. A., Garcia-Aznar, J. M., and Sanchez, M. S., Polymer scaffolds with interconnected spherical pores and controlled architecture for tissue engineering: Fabrication, mechanical properties, and finite element modeling. *J. Biomed. Mater. Res. B Appl. Biomater.* 2006,

Digenis, G. A., Gold, T. B., and Shah, V. P., Cross-linking of gelatin capsules and its relevance to their in vitro-in vivo performance. *J. Pharm. Sci.* 1994, 83:915-921.

Dodds, R. A., Ali, N., Pead, M. J., and Lanyon, L. E., Early loading-related changes in the activity of glucose 6-phosphate dehydrogenase and alkaline phosphatase in osteocytes and periosteal osteoblasts in rat fibulae in vivo. *J. Bone Miner. Res* 1993, 8:261-267.

Doillon, C. J., Whyne, C. F., Brandwein, S., and Silver, F. H., Collagen-based wound dressings: control of the pore structure and morphology. *J. Biomed. Mater. Res.* 1986, 20:1219-1228.

Dominici, M., Le, Blanc K., Mueller, I., Slaper-Cortenbach, I., Marini, F., Krause, D., Deans, R., Keating, A., Prockop, Dj, and Horwitz, E., Minimal criteria for defining multipotent mesenchymal stromal cells. The International Society for Cellular Therapy position statement. *Cytotherapy.* 2006, 8:315-317.

Doshi, J. and Reneker, D. H., Electrospinning process and applications of electrospun fibers. *Journal of Electrostatics* 1995, 35:151-160.

Duncan, R. L. and Hruska, K. A., Chronic, intermittent loading alters mechanosensitive channel characteristics in osteoblast-like cells. *Am J. Physiol* 1994, 267:F909-F916.

Duncan, R. L. and Turner, C. H., Mechanotransduction and the functional response of bone to mechanical strain. *Calcif. Tissue Int.* 1995, 57:344-358.

Dung, T. H., Lee, S. R., Han, S. D., Kim, S. J., Ju, Y. M., Kim, M. S., and Yoo, H., Chitosan-TPP nanoparticle as a release system of antisense oligonucleotide in the oral environment. *J. Nanosci. Nanotechnol.* 2007, 7:3695-3699.

Durkut, S., Elcin, Y. M., and Elcin, A. E., Biodegradation of chitosan-tripolyphosphate beads: in vitro and in vivo studies. *Artif. Cells Blood Substit. Immobil. Biotechnol.* 2006, 34:263-276.

Duty, A. O., Oest, M. E., and Guldberg, R. E., Cyclic mechanical compression increases mineralization of cell-seeded polymer scaffolds in vivo. *J. Biomech. Eng* 2007, 129:531-

Dyer, A. M., Hinchcliffe, M., Watts, P., Castile, J., Jabbal-Gill, I., Nankervis, R., Smith, A., and Illum, L., Nasal delivery of insulin using novel chitosan based formulations: a comparative study in two animal models between simple chitosan formulations and chitosan nanoparticles. *Pharm. Res.* 2002, 19:998-1008.

el Haj, A. J., Minter, S. L., Rawlinson, S. C., Suswillo, R., and Lanyon, L. E., Cellular responses to mechanical loading in vitro. *J. Bone Miner. Res.* 1990, 5:923-932.

Endres, M., Hutmacher, D. W., Salgado, A. J., Kaps, C., Ringe, J., Reis, R. L., Sittinger, M., Brandwood, A., and Schantz, J. T., Osteogenic induction of human bone marrow-derived mesenchymal progenitor cells in novel synthetic polymer-hydrogel matrices. *Tissue Eng* 2003, 9:689-702.

Erices, A., Conget, P., and Minguell, J. J., Mesenchymal progenitor cells in human umbilical cord blood. *Br. J. Haematol.* 2000, 109:235-242.

Eriksen, E. F., Steiniche, T., Mosekilde, L., and Melsen, F., Histomorphometric analysis of bone in metabolic bone disease. *Endocrinol. Metab Clin. North Am.* 1989, 18:919-954.

Fajardo, R. J., Ryan, T. M., and Kappelman, J., Assessing the accuracy of high-resolution X-ray computed tomography of primate trabecular bone by comparisons with histological sections. *Am J. Phys. Anthropol.* 2002, 118:1-10.

Fang, Z., Starly, B., and Sun, W., Computer-aided characterization for effective mechanical properties of porous tissue scaffolds. *Computer-Aided Design* 2005, 37:65-72.

Fielding, J. and Gilbert, N., Understanding social statistics. 2000,

Finlayson, B. A., The method of weighted residuals and variational principles. 1972,

Formhals, A., US Patent 1,975,504. 1934,

Forwood, M. R., Inducible cyclo-oxygenase (COX-2) mediates the induction of bone formation by mechanical loading in vivo. *J. Bone Miner. Res* 1996, 11:1688-1693.

Fox, S. W., Chambers, T. J., and Chow, J. W., Nitric oxide is an early mediator of the increase in bone formation by mechanical stimulation. *Am J. Physiol* 1996, 270:E955-E960.

Friedenstein, A. J., Deriglasova, U. F., Kulagina, N. N., Panasuk, A. F., Rudakowa, S. F., Luria, E. A., and Ruadkow, I. A., Precursors for fibroblasts in different populations of hematopoietic cells as detected by the in vitro colony assay method. *Exp. Hematol.* 1974, 2:83-92.

Frost, H. M., Measurement of osteocytes per unit volume and volume components of osteocytes and canaliculae in man. *Henry. Ford. Hosp. Med. Bull* 1960, 8:208-211.

Frost, H. M., Skeletal structural adaptations to mechanical usage (SATMU): 1. Redefining Wolff's law: the bone modeling problem. *Anat. Rec.* 1990, 226:403-413.

Frost, H. M., Bone "mass" and the "mechanostat": a proposal. *Anat. Rec.* 1987, 219:1-9.

Frost, H. M., A determinant of bone architecture. The minimum effective strain. *Clin. Orthop. Relat Res* 1983, 286-292.

Frost, H. M., Perspectives: bone's mechanical usage windows. *Bone Miner.* 1992, 19:257-271.

Fuchsbauer, H. L., Gerber, U., Engelmann, J., Seeger, T., Sinks, C., and Hecht, T., Influence of gelatin matrices cross-linked with transglutaminase on the properties of an enclosed bioactive material using beta-galactosidase as model system. *Biomaterials* 1996, 17:1481-1488.

Funes, J. M., Quintero, M., Henderson, S., Martinez, D., Qureshi, U., Westwood, C., Clements, M. O., Bourboulia, D., Pedley, R. B., Moncada, S., and Boshoff, C., Transformation of human mesenchymal stem cells increases their dependency on oxidative phosphorylation for energy production. *Proc. Natl. Acad. Sci. U. S. A* 2007, 104:6223-6228.

Funk, J. R. and Crandall, J. R., Calculation of tibial loading using strain gauges. *Biomed. Sci. Instrum.* 2006, 42:160-165.

Garcia-Castillo, Luis E., Gomez-Revuelto, Ignacio, Saez de Adana, Francisco, and Salazar-Palma, Magdalena, A finite element method for the analysis of radiation and scattering of electromagnetic waves on complex environments. *Computer Methods in Applied Mechanics and Engineering* 2005, 194:637-655.

Giglio, M., FEM submodelling fatigue analysis of a complex helicopter component. *International Journal of Fatigue* 1999, 21:445-455.

Gilon, D., Cape, E. G., Handschumacher, M. D., Song, J. K., Solheim, J., VanAuker, M., King, M. E., and Levine, R. A., Effect of three-dimensional valve shape on the hemodynamics of aortic stenosis: three-dimensional echocardiographic stereolithography and patient studies. *J. Am. Coll. Cardiol.* 2002, 40:1479-1486.

Glucksmann, A., Studies on bone mechanics in vitro II. The role of tension and pressure in chondrogenesis. *Anatomical Record* 1939, 73:39-55.

Godbee, J., Scott, E., Pattamunuch, P., Chen, S., and Mathiowitz, E., Role of solvent/non-solvent ratio on microsphere formation using the solvent removal method. *J. Microencapsul.* 2004, 21:151-160.

Goodridge, R. D., Dalgarno, K. W., and Wood, D. J., Indirect selective laser sintering of an apatite-mullite glass-ceramic for potential use in bone replacement applications. *Proc. Inst. Mech. Eng [H.]* 2006, 220:57-68.

Goodship, A. E., Cunningham, J. L., Oganov, V., Darling, J., Miles, A. W., and Owen, G. W., Bone loss during long term space flight is prevented by the application of a short term impulsive mechanical stimulus. *Acta Astronaut.* 1998, 43:65-75.

Guilak, F., Meyer, B. C., Ratcliffe, A., and Mow, V. C., The effects of matrix compression on proteoglycan metabolism in articular cartilage explants. *Osteoarthritis. Cartilage.* 1994, 2:91-101.

Guldberg, R. E., Caldwell, N. J., Guo, X. E., Goulet, R. W., Hollister, S. J., and Goldstein, S. A., Mechanical stimulation of tissue repair in the hydraulic bone chamber. *J. Bone Miner. Res.* 1997, 12:1295-1302.

Gupta, A., Dixit, A., Sales, K. M., Winslet, M. C., and Seifalian, A. M., Tissue engineering of small intestine--current status. *Biomacromolecules.* 2006, 7:2701-2709.

Harell, A., Dekel, S., and Binderman, I., Biochemical effect of mechanical stress on cultured bone cells. *Calcif. Tissue Res* 1977, 22 Suppl:202-207.

Hart, R. T., A theoretical study of the influence of bone maturation rate on surface remodeling predictions: idealized models. *J. Biomech.* 1990, 23:241-257.

Harter, L. V., Hruska, K. A., and Duncan, R. L., Human osteoblast-like cells respond to mechanical strain with increased bone matrix protein production independent of hormonal regulation. *Endocrinology* 1995, 136:528-535.

Hasegawa, S., Sato, S., Saito, S., Suzuki, Y., and Brunette, D. M., Mechanical stretching increases the number of cultured bone cells synthesizing DNA and alters their pattern of protein synthesis. *Calcif. Tissue Int.* 1985, 37:431-436.

Hashimoto, E., Maksimenko, A., Sugiyama, H., Hyodo, K., Shimao, D., Nishino, Y., Ishikawa, T., and Ando, M., First application of X-ray refraction-based computed tomography to a biomedical object. *Zoolog. Sci.* 2006, 23:809-813.

Hermann, C., Zeiher, A. M., and Dimmeler, S., Shear stress inhibits H2O2-induced apoptosis of human endothelial cells by modulation of the glutathione redox cycle and nitric oxide synthase. *Arterioscler. Thromb. Vasc. Biol.* 1997, 17:3588-3592.

Hong, L., Peptan, I., Clark, P., and Mao, J. J., Ex vivo adipose tissue engineering by human marrow stromal cell seeded gelatin sponge. *Ann. Biomed. Eng* 2005, 33:511-517.

Horta, J., Brostow, W., Martinez, G., and Castano, V. M., Characterization of bones by speckle interferometry. *J. Med. Eng Technol.* 2003, 27:49-53.

Horwitz, E. M., Le, Blanc K., Dominici, M., Mueller, I., Slaper-Cortenbach, I., Marini, F. C., Deans, R. J., Krause, D. S., and Keating, A., Clarification of the nomenclature for MSC: The International Society for Cellular Therapy position statement. *Cytotherapy.* 2005, 7:393-395.

Hou, Q., Grijpma, D. W., and Feijen, J., Preparation of interconnected highly porous polymeric structures by a replication and freeze-drying process. *J. Biomed. Mater. Res. B Appl. Biomater.* 2003, 67:732-740.

Hsu, S. S., Huang, C. J., Cheng, H. H., Chou, C. T., Lee, H. Y., Wang, J. L., Chen, I. S., Liu, S. I., Lu, Y. C., Chang, H. T., Huang, J. K., Chen, J. S., and Jan, C. R., Anandamide-induced Ca2+ elevation leading to p38 MAPK phosphorylation and subsequent cell death via apoptosis in human osteosarcoma cells. *Toxicology* 2007, 231:21-29.

Huiskes, R. and Chao, E. Y., A survey of finite element analysis in orthopedic biomechanics: the first decade. *J. Biomech.* 1983, 16:385-409.

Hung, C. T. and Williams, J. L., A method for inducing equi-biaxial and uniform strains in elastomeric membranes used as cell substrates. *J. Biomech.* 1994, 27:227-232.

Hutmacher, D. W., Scaffold design and fabrication technologies for engineering tissues--state of the art and future perspectives. *J. Biomater. Sci. Polym. Ed* 2001, 12:107-124.

Hutmacher, D. W., Goh, J. C., and Teoh, S. H., An introduction to biodegradable materials for tissue engineering applications. *Ann. Acad. Med. Singapore* 2001a, 30:183-191.

Hutmacher, D. W., Schantz, T., Zein, I., Ng, K. W., Teoh, S. H., and Tan, K. C., Mechanical properties and cell cultural response of polycaprolactone scaffolds designed and fabricated via fused deposition modeling. *J. Biomed. Mater. Res.* 2001b, 55:203-216.

Ishaug, S. L., Crane, G. M., Miller, M. J., Yasko, A. W., Yaszemski, M. J., and Mikos, A. G., Bone formation by three-dimensional stromal osteoblast culture in biodegradable polymer scaffolds. *J. Biomed. Mater. Res.* 1997, 36:17-28.

Ito, A., Mase, A., Takizawa, Y., Shinkai, M., Honda, H., Hata, K., Ueda, M., and Kobayashi, T., Transglutaminase-mediated gelatin matrices incorporating cell adhesion factors as a biomaterial for tissue engineering. *J. Biosci. Bioeng.* 2003, 95:196-199.

Ives, C. L., Eskin, S. G., and McIntire, L. V., Mechanical effects on endothelial cell morphology: in vitro assessment. *In Vitro Cell Dev. Biol.* 1986, 22:500-507.

Jaafar, M. S., Bayagoob, K. H., Noorzaei, J., and Thanoon, Waleed A. M., Development of finite element computer code for thermal analysis of roller compacted concrete dams. *Advances in Engineering Software* 2007, 38:886-895.

Jaasma, M. J., Jackson, W. M., Tang, R. Y., and Keaveny, T. M., Adaptation of cellular mechanical behavior to mechanical loading for osteoblastic cells. *J. Biomech.* 2007, 40:1938-1945.

Jacobs, C. R., Yellowley, C. E., Davis, B. R., Zhou, Z., Cimbala, J. M., and Donahue, H. J., Differential effect of steady versus oscillating flow on bone cells. *J. Biomech.* 1998, 31:969-976.

Jang, J. H., Rives, C. B., and Shea, L. D., Plasmid delivery in vivo from porous tissue-engineering scaffolds: transgene expression and cellular transfection. *Mol. Ther.* 2005, 12:475-483.

Johnson, D. L., McAllister, T. N., and Frangos, J. A., Fluid flow stimulates rapid and continuous release of nitric oxide in osteoblasts. *Am J. Physiol* 1996, 271:E205-E208.

Jones, D. B., Broeckmann, E., Pohl, T., and Smith, E. L., Development of a mechanical testing and loading system for trabecular bone studies for long term culture. *Eur. Cell Mater.* 2003, 5:48-59.

Jones, D. B., Nolte, H., Scholubbers, J. G., Turner, E., and Veltel, D., Biochemical signal transduction of mechanical strain in osteoblast-like cells. *Biomaterials* 1991, 12:101-110.

Jones, E. A., English, A., Henshaw, K., Kinsey, S. E., Markham, A. F., Emery, P., and McGonagle, D., Enumeration and phenotypic characterization of synovial fluid multipotential mesenchymal progenitor cells in inflammatory and degenerative arthritis. *Arthritis Rheum.* 2004, 50:817-827.

Jones, H. H., Priest, J. D., Hayes, W. C., Tichenor, C. C., and Nagel, D. A., Humeral hypertrophy in response to exercise. *J. Bone Joint Surg. Am* 1977, 59:204-208.

Kang, H. G., Kim, S. Y., and Lee, Y. M., Novel porous gelatin scaffolds by overrun/particle leaching process for tissue engineering applications. *J. Biomed. Mater. Res. B Appl. Biomater.* 2006, 79:388-397.

Kang, H. W., Tabata, Y., and Ikada, Y., Fabrication of porous gelatin scaffolds for tissue engineering. *Biomaterials* 1999, 20:1339-1344.

Karsenty, G. and Wagner, E. F., Reaching a genetic and molecular understanding of skeletal development. *Dev. Cell* 2002, 2:389-406.

Kato, M., Patel, M. S., Levasseur, R., Lobov, I., Chang, B. H., Glass, D. A., Hartmann, C., Li, L., Hwang, T. H., Brayton, C. F., Lang, R. A., Karsenty, G., and Chan, L., Cbfa1-independent decrease in osteoblast proliferation, osteopenia, and persistent embryonic eye vascularization in mice deficient in Lrp5, a Wnt coreceptor. *J. Cell Biol.* 2002, 157:303-314.

Kaysinger, K. K. and Ramp, W. K., Extracellular pH modulates the activity of cultured human osteoblasts. *J. Cell Biochem.* 1998, 68:83-89.

Kelly, M. E., Beavis, R. C., Fiorella, D., Schultke, E., Allen, L. A., Juurlink, B. H., Zhong, Z., and Chapman, L. D., Analyzer-based imaging of spinal fusion in an animal model. *Phys. Med. Biol.* 2008, 53:2607-2616.

Kenny, A. M. and Raisz, L. G., Mechanisms of bone remodeling: implications for clinical practice. *J. Reprod. Med.* 2002, 47:63-70.

Khalil, S., Nam, J., and Sun, W., Multi-nozzle deposition for construction of 3D biopolymer tissue scaffolds. *Rapid Prototyping Journal* 2005b, 11:9-17.

Khalil, S., Nam, J., and Sun, W., Multi-nozzle deposition for construction of 3D biopolymer tissue scaffolds. *Rapid Prototyping Journal* 2005a, 11:9-17.

Khil, M. S., Bhattarai, S. R., Kim, H. Y., Kim, S. Z., and Lee, K. H., Novel fabricated matrix via electrospinning for tissue engineering. *J. Biomed. Mater. Res. B Appl. Biomater.* 2005, 72:117-124.

Khor, E., Methods for the treatment of collagenous tissues for bioprostheses. *Biomaterials* 1997, 18:95-105.

Kim, S. S., Ahn, K. M., Park, M. S., Lee, J. H., Choi, C. Y., and Kim, B. S., A poly(lactide-co-glycolide)/hydroxyapatite composite scaffold with enhanced osteoconductivity. *J. Biomed. Mater. Res. A* 2006a, 80A:206-215.

Kim, S. S., Utsunomiya, H., Koski, J. A., Wu, B. M., Cima, M. J., Sohn, J., Mukai, K., Griffith, L. G., and Vacanti, J. P., Survival and function of hepatocytes on a novel three-dimensional synthetic biodegradable polymer scaffold with an intrinsic network of channels. *Ann. Surg.* 1998, 228:8-13.

Kim, T. K., Yoon, J. J., Lee, D. S., and Park, T. G., Gas foamed open porous biodegradable polymeric microspheres. *Biomaterials* 2006b, 27:152-159.

Kitagawa, T., Yamaoka, T., Iwase, R., and Murakami, A., Three-dimensional cell seeding and growth in radial-flow perfusion bioreactor for in vitro tissue reconstruction. *Biotechnol. Bioeng.* 2006, 93:947-954.

Klein-Nulend, J., Burger, E. H., Semeins, C. M., Raisz, L. G., and Pilbeam, C. C., Pulsating fluid flow stimulates prostaglandin release and inducible prostaglandin G/H synthase mRNA expression in primary mouse bone cells. *J. Bone Miner. Res* 1997, 12:45-51.

Klein-Nulend, J., van der, Plas A., Semeins, C. M., Ajubi, N. E., Frangos, J. A., Nijweide, P. J., and Burger, E. H., Sensitivity of osteocytes to biomechanical stress in vitro. *FASEB J.* 1995, 9:441-445.

Klein-Nulend, J., Veldhuijzen, J. P., and Burger, E. H., Increased calcification of growth plate cartilage as a result of compressive force in vitro. *Arthritis Rheum.* 1986, 29:1002-1009.

Kobayashi, K., Nomoto, Y., Suzuki, T., Tada, Y., Miyake, M., Hazama, A., Kanemaru, S., Nakamura, T., and Omori, K., Effect of fibroblasts on tracheal epithelial regeneration in vitro. *Tissue Eng* 2006a, 12:2619-2628.

Kobayashi, M., Nakajima, T., Mori, A., Tanaka, D., Fujino, T., and Chiyokura, H., Three-dimensional computer graphics for surgical procedure learning: Web three-dimensional application for cleft lip repair. *Cleft Palate Craniofac. J.* 2006b, 43:266-271.

Kohn, D. H., Sarmadi, M., Helman, J. I., and Krebsbach, P. H., Effects of pH on human bone marrow stromal cells in vitro: implications for tissue engineering of bone. *J. Biomed. Mater. Res.* 2002, 60:292-299.

Kolston, P. J. and Ashmore, J. F., Finite element micromechanical modeling of the cochlea in three dimensions. *J. Acoust. Soc. Am.* 1996, 99:455-467.

Komori, T., Yagi, H., Nomura, S., Yamaguchi, A., Sasaki, K., Deguchi, K., Shimizu, Y., Bronson, R. T., Gao, Y. H., Inada, M., Sato, M., Okamoto, R., Kitamura, Y., Yoshiki, S., and Kishimoto, T., Targeted disruption of Cbfa1 results in a complete lack of bone formation owing to maturational arrest of osteoblasts. *Cell* 1997, 89:755-764.

Kong, H. J., Smith, M. K., and Mooney, D. J., Designing alginate hydrogels to maintain viability of immobilized cells. *Biomaterials* 2003, 24:4023-4029.

Korioth, T. W. and Versluis, A., Modeling the mechanical behavior of the jaws and their related structures by finite element (FE) analysis. *Crit Rev. Oral Biol. Med.* 1997a, 8:90-104.

Korioth, T. W. and Versluis, A., Modeling the mechanical behavior of the jaws and their related structures by finite element (FE) analysis. *Crit Rev. Oral Biol. Med.* 1997b, 8:90-104.

Kragt, G., Duterloo, H. S., and ten Bosch, J. J., The initial reaction of a macerated human skull caused by orthodontic cervical traction determined by laser metrology. *Am J. Orthod.* 1982, 81:49-56.

Krahula, J. and Polhemus, J., Use of Fourier series in Finite Element Method. *AIAA Journal* 1968, 6:726-728.

Krolner, B., Toft, B., Pors, Nielsen S., and Tondevold, E., Physical exercise as prophylaxis against involutional vertebral bone loss: a controlled trial. *Clin. Sci. (Lond)* 1983, 64:541-546.

Kulkarni, R. K., Pani, K. C., Neuman, C., and Leonard, F., Polylactic acid for surgical implants. *Arch. Surg.* 1966, 93:839-843.

Kuznetsov, S. A., Krebsbach, P. H., Satomura, K., Kerr, J., Riminucci, M., Benayahu, D., and Robey, P. G., Single-colony derived strains of human marrow stromal fibroblasts form bone after transplantation in vivo. *J. Bone Miner. Res* 1997, 12:1335-1347.

Lacroix, D., Chateau, A., Ginebra, M., and Planell, J. A., Micro-finite element models of bone tissue-engineering scaffolds. *Biomaterials* 2006, 27:5326-5334.

Landis, W. J., Jacquet, R., Hillyer, J., Lowder, E., Yanke, A., Siperko, L., Asamura, S., Kusuhara, H., Enjo, M., Chubinskaya, S., Potter, K., and Isogai, N., Design and assessment of a tissue-engineered model of human phalanges and a small joint. *Orthod. Craniofac. Res.* 2005, 8:303-312.

Langer, R. and Vacanti, J. P., Tissue engineering. *Science* 1993, 260:920-926.

Lanyon, L. E., Goodship, A. E., Pye, C. J., and MacFie, J. H., Mechanically adaptive bone remodelling. *J. Biomech.* 1982, 15:141-154.

Lavik, E. and Langer, R., Tissue engineering: current state and perspectives. *Appl. Microbiol. Biotechnol.* 2004, 65:1-8.

Leclerc, E., Corlu, A., Griscom, L., Baudoin, R., and Legallais, C., Guidance of liver and kidney organotypic cultures inside rectangular silicone microchannels. *Biomaterials* 2006, 27:4109-4119.

Lee, J. E., Kim, S. E., Kwon, I. C., Ahn, H. J., Cho, H., Lee, S. H., Kim, H. J., Seong, S. C., and Lee, M. C., Effects of a chitosan scaffold containing TGF-beta1 encapsulated chitosan microspheres on in vitro chondrocyte culture. *Artif. Organs* 2004a, 28:829-839.

Lee, K. Y. and Mooney, D. J., Hydrogels for tissue engineering. *Chem. Rev.* 2001, 101:1869-1879.

Lee, R. H., Kim, B., Choi, I., Kim, H., Choi, H. S., Suh, K., Bae, Y. C., and Jung, J. S., Characterization and expression analysis of mesenchymal stem cells from human bone marrow and adipose tissue. *Cell Physiol Biochem.* 2004b, 14:311-324.

Lee, S. B., Kim, Y. H., Chong, M. S., Hong, S. H., and Lee, Y. M., Study of gelatin-containing artificial skin V: fabrication of gelatin scaffolds using a salt-leaching method. *Biomaterials* 2005, 26:1961-1968.

Leong, K. F., Cheah, C. M., and Chua, C. K., Solid freeform fabrication of three-dimensional scaffolds for engineering replacement tissues and organs. *Biomaterials* 2003, 24:2363-2378.

Leung, D. Y., Glagov, S., and Mathews, M. B., A new in vitro system for studying cell response to mechanical stimulation. Different effects of cyclic stretching and agitation on smooth muscle cell biosynthesis. *Exp. Cell Res.* 1977, 109:285-298.

Levraut, J., Giunti, C., Ciebiera, J. P., de, Sousa G., Ramhani, R., Payan, P., and Grimaud, D., Initial effect of sodium bicarbonate on intracellular pH depends on the extracellular nonbicarbonate buffering capacity. *Crit Care Med.* 2001, 29:1033-1039.

Li, H. and Wang, Z., Intervertebral disc biomechanical analysis using the finite element modeling based on medical images. *Comput. Med. Imaging Graph.* 2006, 30:363-370.

Li, M., Mondrinos, M. J., Chen, X., Gandhi, M. R., Ko, F. K., and Lelkes, P. I., Co-electrospun poly(lactide-co-glycolide), gelatin, and elastin blends for tissue engineering scaffolds. *J. Biomed. Mater. Res. A* 2006, 79:963-973.

Li, W. J., Tuli, R., Okafor, C., Derfoul, A., Danielson, K. G., Hall, D. J., and Tuan, R. S., A three-dimensional nanofibrous scaffold for cartilage tissue engineering using human mesenchymal stem cells. *Biomaterials* 2005, 26:599-609.

Li, Z. and Zhang, M., Chitosan-alginate as scaffolding material for cartilage tissue engineering. *J. Biomed. Mater. Res. A* 2005, 75:485-493.

Lin, C. Y., Kikuchi, N., and Hollister, S. J., A novel method for biomaterial scaffold internal architecture design to match bone elastic properties with desired porosity. *J. Biomech.* 2004, 37:623-636.

Lippiello, L., Kaye, C., Neumata, T., and Mankin, H. J., In vitro metabolic response of articular cartilage segments to low levels of hydrostatic pressure. *Connect. Tissue Res.* 1985, 13:99-107.

Liu, H., Mao, J., Yao, K., Yang, G., Cui, L., and Cao, Y., A study on a chitosan-gelatin-hyaluronic acid scaffold as artificial skin in vitro and its tissue engineering applications. *J. Biomater. Sci. Polym. Ed* 2004, 15:25-40.

Logan, C. Y. and Nusse, R., The Wnt signaling pathway in development and disease. *Annu. Rev. Cell Dev. Biol.* 2004, 20:781-810.

Lorentz, K., Improved determination of serum calcium with 2-cresolphthalein complexone. *Clin. Chim. Acta* 1982, 126:327-334.

Love, A. E. H., A treatise on the matematical theory of elasticity. 1944,

Lovejoy, C. O., McCollum, M. A., Reno, P. L., and Rosenman, B. A., Developmental biology and human evolution. *Annu. Rev. Anthropol.* 2003, 32:85-109.

Lu, H. H., El-Amin, S. F., Scott, K. D., and Laurencin, C. T., Three-dimensional, bioactive, biodegradable, polymer-bioactive glass composite scaffolds with improved mechanical properties support collagen synthesis and mineralization of human osteoblast-like cells in vitro. *J. Biomed. Mater. Res. A* 2003, 64:465-474.

Lu, L., Peter, S. J., Lyman, M. D., Lai, H. L., Leite, S. M., Tamada, J. A., Uyama, S., Vacanti, J. P., Langer, R., and Mikos, A. G., In vitro and in vivo degradation of porous poly(DL-lactic-co-glycolic acid) foams. *Biomaterials* 2000, 21:1837-1845.

Luu, Y. K., Kim, K., Hsiao, B. S., Chu, B., and Hadjiargyrou, M., Development of a nanostructured DNA delivery scaffold via electrospinning of PLGA and PLA-PEG block copolymers. *J. Control Release* 2003, 89:341-353.

Ma, Z., He, W., Yong, T., and Ramakrishna, S., Grafting of gelatin on electrospun poly(caprolactone) nanofibers to improve endothelial cell spreading and proliferation and to control cell Orientation. *Tissue Eng* 2005, 11:1149-1158.

Madihally, S. V. and Matthew, H. W., Porous chitosan scaffolds for tissue engineering. *Biomaterials* 1999, 20:1133-1142.

Malda, J., Woodfield, T. B., van, der, V, Wilson, C., Martens, D. E., Tramper, J., van Blitterswijk, C. A., and Riesle, J., The effect of PEGT/PBT scaffold architecture on the composition of tissue engineered cartilage. *Biomaterials* 2005, 26:63-72.

Mann, V., Huber, C., Kogianni, G., Jones, D., and Noble, B., The influence of mechanical stimulation on osteocyte apoptosis and bone viability in human trabecular bone. *J. Musculoskelet. Neuronal. Interact.* 2006, 6:408-417.

Marra, K. G., Szem, J. W., Kumta, P. N., DiMilla, P. A., and Weiss, L. E., In vitro analysis of biodegradable polymer blend/hydroxyapatite composites for bone tissue engineering. *J. Biomed. Mater. Res.* 1999, 47:324-335.

Martin, H. C., Introduction to matrix methods of structural analysis. 1966,

Mathieu, L. M., Mueller, T. L., Bourban, P. E., Pioletti, D. P., Muller, R., and Manson, J. A., Architecture and properties of anisotropic polymer composite scaffolds for bone tissue engineering. *Biomaterials* 2006, 27:905-916.

McDermott, M. K., Chen, T., Williams, C. M., Markley, K. M., and Payne, G. F., Mechanical properties of biomimetic tissue adhesive based on the microbial transglutaminase-catalyzed crosslinking of gelatin. *Biomacromolecules.* 2004, 5:1270-1279.

Mei, X., Etzler, F. M., and Wang, Z., Use of texture analysis to study hydrophilic solvent effects on the mechanical properties of hard gelatin capsules. *Int. J. Pharm.* 2006, 324:128-135.

Mekhail, K., Khacho, M., Gunaratnam, L., and Lee, S., Oxygen sensing by H+: implications for HIF and hypoxic cell memory. *Cell Cycle* 2004, 3:1027-1029.

Mendelson, K. and Schoen, F. J., Heart Valve Tissue Engineering: Concepts, Approaches, Progress, and Challenges. *Ann. Biomed. Eng* 2006, 34:1799-1819.

Middleton, J. C. and Tipton, A. J., Synthetic biodegradable polymers as orthopedic devices. *Biomaterials* 2000, 21:2335-2346.

Milgrom, C., Finestone, A., Levi, Y., Simkin, A., Ekenman, I., Mendelson, S., Millgram, M., Nyska, M., Benjuya, N., and Burr, D., Do high impact exercises produce higher tibial strains than running? *Br. J. Sports Med.* 2000, 34:195-199.

Misch, C. E., Qu, Z., and Bidez, M. W., Mechanical properties of trabecular bone in the human mandible: implications for dental implant treatment planning and surgical placement. *J. Oral Maxillofac. Surg.* 1999, 57:700-706.

Miyazaki, S., Ishii, K., and Nadai, T., The use of chitin and chitosan as drug carriers. *Chem. Pharm. Bull (Tokyo)* 1981, 29:3067-3069.

Moalli, M. R., Caldwell, N. J., Patil, P. V., and Goldstein, S. A., An in vivo model for investigations of mechanical signal transduction in trabecular bone. *J. Bone Miner. Res.* 2000, 15:1346-1353.

Mohamed, M. H., Bogdanovich, A. E., Dickinson, L. C., Singletary, J. N., and Lienhart, R. B., A new generation of 3D woven fabric preforms and composites. *Sampe Journal* 2001, 37:8-17.

Mohtai, M., Gupta, M. K., Donlon, B., Ellison, B., Cooke, J., Gibbons, G., Schurman, D. J., and Smith, R. L., Expression of interleukin-6 in osteoarthritic chondrocytes and effects of fluid-induced shear on this expression in normal human chondrocytes in vitro. *J. Orthop. Res.* 1996, 14:67-73.

Mondrinos, M. J., Dembzynski, R., Lu, L., Byrapogu, V. K., Wootton, D. M., Lelkes, P. I., and Zhou, J., Porogen-based solid freeform fabrication of polycaprolactone-calcium phosphate scaffolds for tissue engineering. *Biomaterials* 2006, 27:4399-4408.

Montjovent, M. O., Mathieu, L., Hinz, B., Applegate, L. L., Bourban, P. E., Zambelli, P. Y., Manson, J. A., and Pioletti, D. P., Biocompatibility of bioresorbable poly(L-lactic acid) composite scaffolds obtained by supercritical gas foaming with human fetal bone cells. *Tissue Eng* 2005, 11:1640-1649.

Mooney, D. J., Baldwin, D. F., Suh, N. P., Vacanti, J. P., and Langer, R., Novel approach to fabricate porous sponges of poly(D,L-lactic-co-glycolic acid) without the use of organic solvents. *Biomaterials* 1996, 17:1417-1422.

Morey, E. R. and Baylink, D. J., Inhibition of bone formation during space flight. *Science* 1978, 201:1138-1141.

Moroni, L., de, Wijn, Jr., and van Blitterswijk, C. A., Three-dimensional fiber-deposited PEOT/PBT copolymer scaffolds for tissue engineering: influence of porosity, molecular network mesh size, and swelling in aqueous media on dynamic mechanical properties. *J. Biomed. Mater. Res. A* 2005, 75:957-965.

Moroni, L., Poort, G., Van, Keulen F., de, Wijn, Jr., and van Blitterswijk, C. A., Dynamic mechanical properties of 3D fiber-deposited PEOT/PBT scaffolds: an experimental and numerical analysis. *J. Biomed. Mater. Res. A* 2006, 78:605-614.

Mosley, J. R., Osteoporosis and bone functional adaptation: mechanobiological regulation of bone architecture in growing and adult bone, a review. *J. Rehabil. Res. Dev.* 2000, 37:189-199.

Moutos, F. T., Freed, L. E., and Guilak, F., A biomimetic three-dimensional woven composite scaffold for functional tissue engineering of cartilage. *Nat. Mater.* 2007, 6:162-167.

Murray, D. W. and Rushton, N., The effect of strain on bone cell prostaglandin E2 release: a new experimental method. *Calcif. Tissue Int.* 1990, 47:35-39.

Nafe, R. and Schlote, W., Histomorphometry of brain tumours. *Neuropathol. Appl. Neurobiol.* 2004, 30:315-328.

Nakahara, H., Dennis, J. E., Bruder, S. P., Haynesworth, S. E., Lennon, D. P., and Caplan, A. I., In vitro differentiation of bone and hypertrophic cartilage from periosteal-derived cells. *Exp. Cell Res* 1991, 195:492-503.

Nakashima, K., Zhou, X., Kunkel, G., Zhang, Z., Deng, J. M., Behringer, R. R., and de, Crombrugghe B., The novel zinc finger-containing transcription factor osterix is required for osteoblast differentiation and bone formation. *Cell* 2002, 108:17-29.

Neidlinger-Wilke, C., Wilke, H. J., and Claes, L., Cyclic stretching of human osteoblasts affects proliferation and metabolism: a new experimental method and its application. *J. Orthop. Res.* 1994, 12:70-78.

Nelson, K. D., Romero, A., Waggoner, P., Crow, B., Borneman, A., and Smith, G. M., Technique paper for wet-spinning poly(L-lactic acid) and poly(DL-lactide-co-glycolide) monofilament fibers. *Tissue Eng* 2003, 9:1323-1330.

Nettles, D. L., Elder, S. H., and Gilbert, J. A., Potential use of chitosan as a cell scaffold material for cartilage tissue engineering. *Tissue Eng* 2002, 8:1009-1016.

Ng, K. W., Khor, H. L., and Hutmacher, D. W., In vitro characterization of natural and synthetic dermal matrices cultured with human dermal fibroblasts. *Biomaterials* 2004a, 25:2807-2818.

Ng, K. W., Khor, H. L., and Hutmacher, D. W., In vitro characterization of natural and synthetic dermal matrices cultured with human dermal fibroblasts. *Biomaterials* 2004b, 25:2807-2818.

Noble, B. S. and Reeve, J., Osteocyte function, osteocyte death and bone fracture resistance. *Mol. Cell Endocrinol.* 2000, 159:7-13.

Norton, L. A., Andersen, K. L., renholt-Bindslev, D., Andersen, L., and Melsen, B., A methodical study of shape changes in human oral cells perturbed by a simulated orthodontic strain in vitro. *Arch. Oral Biol.* 1995, 40:863-872.

Notin, L., Viton, C., Lucas, J. M., and Domard, A., Pseudo-dry-spinning of chitosan. *Acta Biomater.* 2006, 2:297-311.

Ochoa, J. A., Sanders, A. P., Heck, D. A., and Hillberry, B. M., Stiffening of the femoral head due to inter-trabecular fluid and intraosseous pressure. *J. Biomech. Eng* 1991, 113:259-262.

Olde Damink, L. H. H., Dijkstra, P. J., Vanluyn, M. J. A., Vanwachem, P. B., Nieuwenhuis, P., and Feijen, J., Glutaraldehyde As A Cross-Linking Agent for Collagen-Based Biomaterials. *Journal of Materials Science-Materials in Medicine* 1995, 6:460-472.

Oliveira, J. M., Rodrigues, M. T., Silva, S. S., Malafaya, P. B., Gomes, M. E., Viegas, C. A., Dias, I. R., Azevedo, J. T., Mano, J. F., and Reis, R. L., Novel hydroxyapatite/chitosan bilayered scaffold for osteochondral tissue-engineering applications: Scaffold design and its performance when seeded with goat bone marrow stromal cells. *Biomaterials* 2006, 27:6123-6137.

Otani, Y., Tabata, Y., and Ikada, Y., Hemostatic capability of rapidly curable glues from gelatin, poly(L-glutamic acid), and carbodiimide. *Biomaterials* 1998, 19:2091-2098.

Ozawa, H., Imamura, K., Abe, E., Takahashi, N., Hiraide, T., Shibasaki, Y., Fukuhara, T., and Suda, T., Effect of a continuously applied compressive pressure on mouse osteoblast-like cells (MC3T3-E1) in vitro. *J. Cell Physiol* 1990, 142:177-185.

Pankajakshan, D., Krishnan, V. K., and Krishnan, L. K., Vascular tissue generation in response to signaling molecules integrated with a novel poly(epsilon-caprolactone)-fibrin hybrid scaffold. *J. Tissue Eng Regen. Med.* 2007, 1:389-397.

Parfitt, A. M., Recent developments in bone physiology. *Henry. Ford. Hosp. Med. J.* 1983, 31:209-210.

Park, A., Wu, B., and Griffith, L. G., Integration of surface modification and 3D fabrication techniques to prepare patterned poly(L-lactide) substrates allowing regionally selective cell adhesion. *J. Biomater. Sci. Polym. Ed* 1998, 9:89-110.

Park, H. and Kim, D., Swelling and mechanical properties of glycol chitosan/poly(vinyl alcohol) IPN-type superporous hydrogels. *J. Biomed. Mater. Res. A* 2006, 78:662-667.

Pead, M. J., Suswillo, R., Skerry, T. M., Vedi, S., and Lanyon, L. E., Increased 3H-uridine levels in osteocytes following a single short period of dynamic bone loading in vivo. *Calcif. Tissue Int.* 1988, 43:92-96.

Pearson, O. M. and Lieberman, D. E., The aging of Wolff's "law": Ontogeny and responses to mechanical loading in cortical bone. *Am J. Phys. Anthropol.* 2004, Suppl 39:63-99.

Pitsillides, A. A., Rawlinson, S. C., Suswillo, R. F., Bourrin, S., Zaman, G., and Lanyon, L. E., Mechanical strain-induced NO production by bone cells: a possible role in adaptive bone (re)modeling? *FASEB J.* 1995, 9:1614-1622.

Preuschoft, H. and Witzel, U., Functional shape of the skull in vertebrates: which forces determine skull morphology in lower primates and ancestral synapsids? *Anat. Rec. A Discov. Mol. Cell Evol. Biol.* 2005, 283:402-413.

Przemieniecki, J. S., Theory of matrix structural analysis. 1968,

Rago, R., Mitchen, J., and Wilding, G., DNA fluorometric assay in 96-well tissue culture plates using Hoechst 33258 after cell lysis by freezing in distilled water. *Anal. Biochem.* 1990, 191:31-34.

Ramanath, H. S., Chua, C. K., Leong, K. F., and Shah, K. D., Melt flow behaviour of poly-epsilon-caprolactone in fused deposition modelling. *J. Mater. Sci. Mater. Med.* 2008, 19:2541-2550.

Rambaut, P. C. and Johnston, R. S., Prolonged weightlessness and calcium loss in man. *Acta Astronaut.* 1979, 6:1113-1122.

Ramp, W. K., Lenz, L. G., and Kaysinger, K. K., Medium pH modulates matrix, mineral, and energy metabolism in cultured chick bones and osteoblast-like cells. *Bone Miner.* 1994, 24:59-73.

Rao, Ch and Muthuveerappan, G., Finite element modelling and stress analysis of helical gear teeth. *Computers & Structures* 1993, 49:1095-1106.

Rao, S. S., The finite element method in engineering. 1989, 2nd:

Reich, K. M. and Frangos, J. A., Effect of flow on prostaglandin E2 and inositol trisphosphate levels in osteoblasts. *Am J. Physiol* 1991, 261:C428-C432.

Reich, K. M., Gay, C. V., and Frangos, J. A., Fluid shear stress as a mediator of osteoblast cyclic adenosine monophosphate production. *J. Cell Physiol* 1990a, 143:100-104.

Reich, K. M., Gay, C. V., and Frangos, J. A., Fluid Shear-Stress As A Mediator of Osteoblast Cyclic Adenosine-Monophosphate Production. *Journal of Cellular Physiology* 1990b, 143:100-104.

Revell, P. A., Histomorphometry of bone. *J. Clin. Pathol.* 1983, 36:1323-1331.

Reyes, J. M., Fermanian, S., Yang, F., Zhou, S. Y., Herretes, S., Murphy, D. B., Elisseeff, J. H., and Chuck, R. S., Metabolic changes in mesenchymal stem cells in osteogenic medium measured by autofluorescence spectroscopy. *Stem Cells* 2006, 24:1213-1217.

Richmond, B. G., Wright, B. W., Grosse, I., Dechow, P. C., Ross, C. F., Spencer, M. A., and Strait, D. S., Finite element analysis in functional morphology. *Anat. Rec. A Discov. Mol. Cell Evol. Biol.* 2005, 283:259-274.

Robinson, B. P., Hollinger, J. O., Szachowicz, E. H., and Brekke, J., Calvarial bone repair with porous D,L-polylactide. *Otolaryngol. Head Neck Surg.* 1995, 112:707-713.

Robling, A. G., Burr, D. B., and Turner, C. H., Partitioning a daily mechanical stimulus into discrete loading bouts improves the osteogenic response to loading. *J. Bone Miner. Res.* 2000, 15:1596-1602.

Robling, A. G., Hinant, F. M., Burr, D. B., and Turner, C. H., Shorter, more frequent mechanical loading sessions enhance bone mass. *Med. Sci. Sports Exerc.* 2002, 34:196-202.

Rodriguez, L. V., Alfonso, Z., Zhang, R., Leung, J., Wu, B., and Ignarro, L. J., Clonogenic multipotent stem cells in human adipose tissue differentiate into functional smooth muscle cells. *Proc. Natl. Acad. Sci. U. S. A* 2006, 103:12167-12172.

Rohanizadeh, R., Swain, M. V., and Mason, R. S., Gelatin sponges (Gelfoam) as a scaffold for osteoblasts. *J. Mater. Sci. Mater. Med.* 2008, 19:1173-1182.

Roman, J. F., Fernandez, P., Moreno, V., Abeleira, M., Gallas, M., and Suarez, D., The mechanical behaviour of human mandibles studied by electronic speckle pattern interferometry. *Eur. J. Orthod.* 1999, 21:413-421.

Rubin, C. T. and Lanyon, L. E., Limb Mechanics As A Function of Speed and Gait - A Study of Functional Strains in the Radius and Tibia of Horse and Dog. *Journal of Experimental Biology* 1982, 101:187-211.

Rubin, C. T. and Lanyon, L. E., Regulation of bone mass by mechanical strain magnitude. *Calcif. Tissue Int.* 1985, 37:411-417.

Ryan, T. M. and Rietbergen, B., Mechanical significance of femoral head trabecular bone structure in Loris and Galago evaluated using micromechanical finite element models. *Am. J. Phys. Anthropol.* 2005, 126:82-96.

Sakai, S., Yamada, Y., Yamaguchi, T., and Kawakami, K., Prospective use of electrospun ultra-fine silicate fibers for bone tissue engineering. *Biotechnol. J.* 2006, 1:958-962.

Sampath, T. K., Nathanson, M. A., and Reddi, A. H., In vitro transformation of mesenchymal cells derived from embryonic muscle into cartilage in response to extracellular matrix components of bone. *Proc. Natl. Acad. Sci. U. S. A* 1984, 81:3419-3423.

Sanghavi, P., Bose, D., Kerrigan, J., Madeley, N. J., and Crandall, J., Non-contact strain measurement of biological tissue. *Biomed. Sci. Instrum.* 2004, 40:51-56.

Sarasam, A. and Madihally, S. V., Characterization of chitosan-polycaprolactone blends for tissue engineering applications. *Biomaterials* 2005, 26:5500-5508.

Sarkani, Shahram, Tritchkov, Vesselin, and Michaelov, George, An efficient approach for computing residual stresses in welded joints. *Finite Elements in Analysis and Design* 2000, 35:247-268.

Schantz, J. T., Teoh, S. H., Lim, T. C., Endres, M., Lam, C. X., and Hutmacher, D. W., Repair of calvarial defects with customized tissue-engineered bone grafts I. Evaluation of osteogenesis in a three-dimensional culture system. *Tissue Eng* 2003, 9 Suppl 1:S113-S126.

Schirmer, K., Ganassin, R. C., Brubacher, J. L., and Bols, N. C., A DNA fluorometric asay for measuring fish cell proliferation in microplates with different well sizes. *Journal of Tissue Culture Methods* 2004, 16:133-142.

Shao, X., Goh, J. C., Hutmacher, D. W., Lee, E. H., and Zigang, G., Repair of large articular osteochondral defects using hybrid scaffolds and bone marrow-derived mesenchymal stem cells in a rabbit model. *Tissue Eng* 2006a, 12:1539-1551.

Shao, X. X., Hutmacher, D. W., Ho, S. T., Goh, J. C., and Lee, E. H., Evaluation of a hybrid scaffold/cell construct in repair of high-load-bearing osteochondral defects in rabbits. *Biomaterials* 2006b, 27:1071-1080.

Shen, H., Hu, X., Yang, F., Bei, J., and Wang, S., Combining oxygen plasma treatment with anchorage of cationized gelatin for enhancing cell affinity of poly(lactide-co-glycolide). *Biomaterials* 2007, 28:4219-4230.

Shi, D. H., Cai, D. Z., Zhou, C. R., Rong, L. M., Wang, K., and Xu, Y. C., Development and potential of a biomimetic chitosan/type II collagen scaffold for cartilage tissue engineering. *Chin Med. J. (Engl.)* 2005, 118:1436-1443.

Shin, M., Yoshimoto, H., and Vacanti, J. P., In vivo bone tissue engineering using mesenchymal stem cells on a novel electrospun nanofibrous scaffold. *Tissue Eng* 2004, 10:33-41.

Shor, L., Guceri, S., Wen, X., Gandhi, M., and Sun, W., Fabrication of three-dimensional polycaprolactone/hydroxyapatite tissue scaffolds and osteoblast-scaffold interactions in vitro. *Biomaterials* 2007, 28:5291-5297.

Shu, X. Z. and Zhu, K. J., Controlled drug release properties of ionically cross-linked chitosan beads: the influence of anion structure. *Int. J. Pharm.* 2002, 233:217-225.

Sikavitsas, V. I., Bancroft, G. N., Holtorf, H. L., Jansen, J. A., and Mikos, A. G., Mineralized matrix deposition by marrow stromal osteoblasts in 3D perfusion culture increases with increasing fluid shear forces. *Proc. Natl. Acad. Sci. U. S. A* 2003, 100:14683-14688.

Simkin, A., Ayalon, J., and Leichter, I., Increased trabecular bone density due to bone-loading exercises in postmenopausal osteoporotic women. *Calcif. Tissue Int.* 1987, 40:59-63.

Simmons, C. A., Alsberg, E., Hsiong, S., Kim, W. J., and Mooney, D. J., Dual growth factor delivery and controlled scaffold degradation enhance in vivo bone formation by transplanted bone marrow stromal cells. *Bone* 2004, 35:562-569.

Simpson, J. A., Cheeseman, K. H., Smith, S. E., and Dean, R. T., Free-radical generation by copper ions and hydrogen peroxide. Stimulation by Hepes buffer. *Biochem. J.* 1988, 254:519-523.

Skerry, T. M., Bitensky, L., Chayen, J., and Lanyon, L. E., Early strain-related changes in enzyme activity in osteocytes following bone loading in vivo. *J. Bone Miner. Res* 1989, 4:783-788.

Sokolnikoff, I. S., Mathematical theory of elasticity. 1956, 2nd ed:

Somjen, D., Binderman, I., Berger, E., and Harell, A., Bone remodelling induced by physical stress is prostaglandin E2 mediated. *Biochim. Biophys. Acta* 1980, 627:91-100.

Stains, J. P. and Civitelli, R., Gap junctions in skeletal development and function. *Biochim. Biophys. Acta* 2005, 1719:69-81.

Stasa, F. L., Applied finite element analyis for engineers. 1985,

Steck, R., Niederer, P., and Knothe Tate, M. L., A finite element analysis for the prediction of load-induced fluid flow and mechanochemical transduction in bone. *J. Theor. Biol.* 2003, 220:249-259.

Stock, U. A. and Vacanti, J. P., Tissue engineering: current state and prospects. *Annu. Rev. Med.* 2001, 52:443-451.

Strait, D. S., Wang, Q., Dechow, P. C., Ross, C. F., Richmond, B. G., Spencer, M. A., and Patel, B. A., Modeling elastic properties in finite-element analysis: how much precision is needed to produce an accurate model? *Anat. Rec. A Discov. Mol. Cell Evol. Biol.* 2005, 283:275-287.

Su, R., Campbell, G. M., and Boyd, S. K., Establishment of an architecture-specific experimental validation approach for finite element modeling of bone by rapid prototyping and high resolution computed tomography. *Med. Eng Phys.* 2006,

Sun, W., Starly, B., Darling, A., and Gomez, C., Computer-aided tissue engineering: application to biomimetic modelling and design of tissue scaffolds. *Biotechnol. Appl. Biochem.* 2004, 39:49-58.

Swieszkowski, W., Tuan, B. H., Kurzydlowski, K. J., and Hutmacher, D. W., Repair and regeneration of osteochondral defects in the articular joints. *Biomol. Eng* 2007, 24:489-495.

Szivek, J. A. and Magee, F. P., A long-term in vivo bone strain measurement device. *J. Invest Surg.* 1989, 2:195-206.

Taboas, J. M., Maddox, R. D., Krebsbach, P. H., and Hollister, S. J., Indirect solid free form fabrication of local and global porous, biomimetic and composite 3D polymer-ceramic scaffolds. *Biomaterials* 2003, 24:181-194.

Takagishi, Y., Kawakami, T., Hara, Y., Shinkai, M., Takezawa, T., and Nagamune, T., Bone-like tissue formation by three-dimensional culture of MG63 osteosarcoma cells in gelatin hydrogels using calcium-enriched medium. *Tissue Eng* 2006, 12:927-937.

Tan, K. H., Chua, C. K., Leong, K. F., Cheah, C. M., Gui, W. S., Tan, W. S., and Wiria, F. E., Selective laser sintering of biocompatible polymers for applications in tissue engineering. *Biomed. Mater. Eng* 2005a, 15:113-124.

Tan, K. H., Chua, C. K., Leong, K. F., Naing, M. W., and Cheah, C. M., Fabrication and characterization of three-dimensional poly(ether- ether- ketone)/-hydroxyapatite biocomposite scaffolds using laser sintering. *Proc. Inst. Mech. Eng [H.]* 2005b, 219:183-194.

Tanaka, S. M., A new mechanical stimulator for cultured bone cells using piezoelectric actuator. *J. Biomech.* 1999, 32:427-430.

Taylor, A. F., Saunders, M. M., Shingle, D. L., Cimbala, J. M., Zhou, Z., and Donahue, H. J., Mechanically stimulated osteocytes regulate osteoblastic activity via gap junctions. *Am J. Physiol Cell Physiol* 2007, 292:C545-C552.

Taylor, G. I., Disintegration of Water Drops in an Electric Field. *Proc. Roy. Soc. London* 1964, 280:383-397.

Temenoff, J. S., Park, H., Jabbari, E., Sheffield, T. L., LeBaron, R. G., Ambrose, C. G., and Mikos, A. G., In vitro osteogenic differentiation of marrow stromal cells encapsulated in biodegradable hydrogels. *J. Biomed. Mater. Res. A* 2004, 70:235-244.

Tencer, A. F., Woodard, P. L., Swenson, J., and Brown, K. L., Bone ingrowth into polymer coated porous synthetic coralline hydroxyapatite. *J. Orthop. Res.* 1987, 5:275-282.

Tencer, A. F., Woodard, P. L., Swenson, J., and Brown, K. L., Mechanical and bone ingrowth properties of a polymer-coated, porous, synthetic, coralline hydroxyapatite bone-graft material. *Ann. N. Y. Acad. Sci.* 1988, 523:157-172.

Thevendran, V., Chen, S., Shanmugam, N. E., and Richard Liew, J. Y., Nonlinear analysis of steel-concrete composite beams curved in plan. *Finite Elements in Analysis and Design* 1999, 32:125-139.

Thomas, V., Jose, M. V., Chowdhury, S., Sullivan, J. F., Dean, D. R., and Vohra, Y. K., Mechano-morphological studies of aligned nanofibrous scaffolds of polycaprolactone fabricated by electrospinning. *J. Biomater. Sci. Polym. Ed* 2006, 17:969-984.

Thomas, V., Zhang, X., Catledge, S. A., and Vohra, Y. K., Functionally graded electrospun scaffolds with tunable mechanical properties for vascular tissue regeneration. *Biomed. Mater.* 2007, 2:224-232.

Throckmorton, G. S. and Dechow, P. C., In vitro strain measurements in the condylar process of the human mandible. *Arch. Oral Biol.* 1994, 39:853-867.

Toffaletti, J. and Kirvan, K., Spectrophotometric micro method for measurement of dialyzable calcium by use of cresolphthalein complexone and continuous-flow analysis. *Clin. Chem.* 1980, 26:1562-1565.

Torzilli, P. A., Grigiene, R., Huang, C., Friedman, S. M., Doty, S. B., Boskey, A. L., and Lust, G., Characterization of cartilage metabolic response to static and dynamic stress using a mechanical explant test system. *J. Biomech.* 1997, 30:1-9.

Tremoleda, J. L., Forsyth, N. R., Khan, N. S., Wojtacha, D., Christodoulou, I., Tye, B. J., Racey, S. N., Collishaw, S., Sottile, V., Thomson, A. J., Simpson, A. H., Noble, B. S., and McWhir, J., Bone tissue formation from human embryonic stem cells in vivo. *Cloning Stem Cells* 2008, 10:119-132.

Turner, C. H. and Forwood, M. R., What role does the osteocyte network play in bone adaptation? *Bone* 1995, 16:283-285.

Turner, C. H., Owan, I., Alvey, T., Hulman, J., and Hock, J. M., Recruitment and proliferative responses of osteoblasts after mechanical loading in vivo determined using sustained-release bromodeoxyuridine. *Bone* 1998, 22:463-469.

Turner, C. H. and Pavalko, F. M., Mechanotransduction and functional response of the skeleton to physical stress: the mechanisms and mechanics of bone adaptation. *J. Orthop. Sci.* 1998, 3:346-355.

Turner, C. H., Takano, Y., Owan, I., and Murrell, G. A., Nitric oxide inhibitor L-NAME suppresses mechanically induced bone formation in rats. *Am J. Physiol* 1996, 270:E634-E639.

Turner, M. J, Clough, R. W, Martin, H. C., and Topp, L. J, Stiffness and deflection analysis of complex structures. *Journal of aeronautical Sciences* 1956, 23:805-824.

Vacanti, J. P., Morse, M. A., Saltzman, W. M., Domb, A. J., Perez-Atayde, A., and Langer, R., Selective cell transplantation using bioabsorbable artificial polymers as matrices. *J. Pediatr. Surg.* 1988, 23:3-9.

van Grondelle, A., Worthen, G. S., Ellis, D., Mathias, M. M., Murphy, R. C., Strife, R. J., Reeves, J. T., and Voelkel, N. F., Altering hydrodynamic variables influences PGI2 production by isolated lungs and endothelial cells. *J. Appl. Physiol* 1984, 57:388-395.

van Kampen, G. P., Veldhuijzen, J. P., Kuijer, R., van de Stadt, R. J., and Schipper, C. A., Cartilage response to mechanical force in high-density chondrocyte cultures. *Arthritis Rheum.* 1985, 28:419-424.

Vance, J., Galley, S., Liu, D. F., and Donahue, S. W., Mechanical stimulation of MC3T3 osteoblastic cells in a bone tissue-engineering bioreactor enhances prostaglandin E2 release. *Tissue Eng* 2005, 11:1832-1839.

Vandamme, T. F. and Legras, R., Physico-mechanical properties of poly (epsilon-caprolactone) for the construction of rumino-reticulum devices for grazing animals. *Biomaterials* 1995, 16:1395-1400.

Veldhuijzen, J. P., Bourret, L. A., and Rodan, G. A., In vitro studies of the effect of intermittent compressive forces on cartilage cell proliferation. *J. Cell Physiol* 1979, 98:299-306.

Venugopal, J. R., Low, S., Choon, A. T., Kumar, A. B., and Ramakrishna, S., Nanobioengineered electrospun composite nanofibers and osteoblasts for bone regeneration. *Artif. Organs* 2008, 32:388-397.

Verrue, V., Dermaut, L., and Verhegghe, B., Three-dimensional finite element modelling of a dog skull for the simulation of initial orthopaedic displacements. *Eur. J. Orthod.* 2001, 23:517-527.

Vico, L., Chappard, D., Alexandre, C., Palle, S., Minaire, P., Riffat, G., Novikov, V. E., and Bakulin, A. V., Effects of weightlessness on bone mass and osteoclast number in pregnant rats after a five-day spaceflight (COSMOS 1514). *Bone* 1987, 8:95-103.

Vodna, L., Bubenikova, S., and Bakos, D., Chitosan based hydrogel microspheres as drug carriers. *Macromol. Biosci.* 2007, 7:629-634.

Vogel, J. M. and Whittle, M. W., Bone mineral changes: the second manned Skylab mission. *Aviat. Space Environ. Med.* 1976, 47:396-400.

Wagner, A., Sachse, A., Keller, M., Aurich, M., Wetzel, W. D., Hortschansky, P., Schmuck, K., Lohmann, M., Reime, B., Metge, J., Arfelli, F., Menk, R., Rigon, L., Muehleman, C., Bravin, A., Coan, P., and Mollenhauer, J., Qualitative evaluation of titanium implant integration into bone by diffraction enhanced imaging. *Phys. Med. Biol.* 2006, 51:1313-1324.

Waldman, S. D., Couto, D. C., Omelon, S. J., and Kandel, R. A., Effect of sodium bicarbonate on extracellular pH, matrix accumulation, and morphology of cultured articular chondrocytes. *Tissue Eng* 2004, 10:1633-1640.

Wang, F., Shor, L., Darling, A., Khalil, S., Sun, W., Guceri, S., and Lau, A., Precision extruding deposition and characterization of cellular poly-e-caprolactone tissue scaffold. *Rapid Prototyping Journal* 2004, 10:42-49.

Wang, L., Shelton, R. M., Cooper, P. R., Lawson, M., Triffitt, J. T., and Barralet, J. E., Evaluation of sodium alginate for bone marrow cell tissue engineering. *Biomaterials* 2003b, 24:3475-3481.

Wang, L., Shelton, R. M., Cooper, P. R., Lawson, M., Triffitt, J. T., and Barralet, J. E., Evaluation of sodium alginate for bone marrow cell tissue engineering. *Biomaterials* 2003a, 24:3475-3481.

Wee, S. and Gombotz, W. R., Protein release from alginate matrices. *Adv. Drug Deliv. Rev.* 1998, 31:267-285.

Weinbaum, S., Cowin, S. C., and Zeng, Y., A model for the excitation of osteocytes by mechanical loading-induced bone fluid shear stresses. *J. Biomech.* 1994, 27:339-360.

Wettergreen, M. A., Bucklen, B. S., Starly, B., Yuksel, E., Sun, W., and Liebschner, M. A. K., Creation of a unit block library of architectures for use in assembled scaffold engineering. *Computer-Aided Design* 2005, 37:1141-1149.

Wible, J. H., Jr. and Hynes, M. R., Measurement of serum calcium concentration after administration of gadoversetamide in dogs. *Radiology* 2004, 233:158-164.

Williams, J. M., Adewunmi, A., Schek, R. M., Flanagan, C. L., Krebsbach, P. H., Feinberg, S. E., Hollister, S. J., and Das, S., Bone tissue engineering using polycaprolactone scaffolds fabricated via selective laser sintering. *Biomaterials* 2005, 26:4817-4827.

Williamson, M. R. and Coombes, A. G., Gravity spinning of polycaprolactone fibres for applications in tissue engineering. *Biomaterials* 2004, 25:459-465.

Wissemann, K. W. and Jacobson, B. S., Pure Gelatin Microcarriers - Synthesis and Use in Cell Attachment and Growth of Fibroblast and Endothelial-Cells. *In Vitro Cellular & Developmental Biology* 1985, 21:391-401.

Wolff, j, The Law of bone remodelling (Das gesetz der transformation der knochen). 1892, DM 188:126-

Woo, S. L., Kuei, S. C., Amiel, D., Gomez, M. A., Hayes, W. C., White, F. C., and Akeson, W. H., The effect of prolonged physical training on the properties of long bone: a study of Wolff's Law. *J. Bone Joint Surg. Am* 1981, 63:780-787.

Woodfield, T. B., Malda, J., de, Wijn J., Peters, F., Riesle, J., and van Blitterswijk, C. A., Design of porous scaffolds for cartilage tissue engineering using a three-dimensional fiber-deposition technique. *Biomaterials* 2004, 25:4149-4161.

Wronski, T. J. and Morey, E. R., Effect of spaceflight on periosteal bone formation in rats. *Am J. Physiol* 1983, 244:R305-R309.

Wu, M. J., Gu, Z. Y., and Sun, W., Effects of hydrostatic pressure on cytoskeleton and BMP-2, TGF-beta, SOX-9 production in rat temporomandibular synovial fibroblasts. *Osteoarthritis. Cartilage.* 2007,

www.uktransplant.org.uk, Transplant activity in the UK. *www. uktransplant. org. uk* 2006,

Xia, W., Liu, W., Cui, L., Liu, Y., Zhong, W., Liu, D., Wu, J., Chua, K., and Cao, Y., Tissue engineering of cartilage with the use of chitosan-gelatin complex scaffolds. *J. Biomed. Mater. Res. B Appl. Biomater.* 2004, 71:373-380.

Xu, C. Y., Inai, R., Kotaki, M., and Ramakrishna, S., Aligned biodegradable nanofibrous structure: a potential scaffold for blood vessel engineering. *Biomaterials* 2004, 25:877-886.

Yang, J.-G., Murray, T. M., and Plaut, R. H., Three-dimensional finite element analysis of double angle connections under tension and shear. *Journal of Constructional Steel Research* 2000, 54:227-244.

Yang, L. J. and Ou, Y. C., The micro patterning of glutaraldehyde (GA)-crosslinked gelatin and its application to cell-culture. *Lab Chip.* 2005, 5:979-984.

Yong, C. S., Li, D. X., Oh, D. H., Kim, J. A., Yoo, B. K., Woo, J. S., Rhee, J. D., and Choi, H. G., Retarded dissolution of ibuprofen in gelatin microcapsule by cross-linking with glutaradehyde. *Arch. Pharm. Res* 2006, 29:520-524.

Yousefian, J., Firouzian, F., Shanfeld, J., Ngan, P., Lanese, R., and Davidovitch, Z., A new experimental model for studying the response of periodontal ligament cells to hydrostatic pressure. *Am. J. Orthod. Dentofacial Orthop.* 1995, 108:402-409.

Yung, C. W., Wu, L. Q., Tullman, J. A., Payne, G. F., Bentley, W. E., and Barbari, T. A., Transglutaminase crosslinked gelatin as a tissue engineering scaffold. *J. Biomed. Mater. Res. A* 2007, 83:1039-1046.

Zar, J., Biostatical Analysis. 1984, Second Edition:

Zaslansky, P., Currey, J. D., Friesem, A. A., and Weiner, S., Phase shifting speckle interferometry for determination of strain and Young's modulus of mineralized biological materials: a study of tooth dentin compression in water. *J. Biomed. Opt.* 2005, 10:024020-

Zein, I., Hutmacher, D. W., Tan, K. C., and Teoh, S. H., Fused deposition modeling of novel scaffold architectures for tissue engineering applications. *Biomaterials* 2002, 23:1169-1185.

Zhang, H., Alsarra, I. A., and Neau, S. H., An in vitro evaluation of a chitosan-containing multiparticulate system for macromolecule delivery to the colon. *Int. J. Pharm.* 2002, 239:197-205.

Zhang, Y. and Zhang, M., Synthesis and characterization of macroporous chitosan/calcium phosphate composite scaffolds for tissue engineering. *J. Biomed. Mater. Res* 2001, 55:304-312.

Zhu, H., Ji, J., Tan, Q., Barbosa, M. A., and Shen, J., Surface engineering of poly(DL-lactide) via electrostatic self-assembly of extracellular matrix-like molecules. *Biomacromolecules.* 2003, 4:378-386.

Zhu, X., Beuerman, R. W., Chan-Park, M. B., Cheng, Z., Ang, L. P., and Tan, D. T., Enhancement of the mechanical and biological properties of a biomembrane for tissue engineering the ocular surface. *Ann. Acad. Med. Singapore* 2006, 35:210-214.

Zienkiewicz, O. C. and Cheung, Y. K., The finite element method in structural and continuum mechanics. 1967,

Zigler, J. S., Lepe-Zuniga, J. L., Vistica, B., and Gery, I., Analysis of the cytotoxic effects of light-exposed HEPES-containing culture medium. *In Vitro Cell Dev. Biol.* 1985, 21:282-287.

Appendix A

Technovit 9100 Process

1a. ‘Pre-infiltration 1’ solution was prepared on the day by a mixing a 1:1 concentration of xylene and stabilised Technovit 9100.

1b. ‘Pre-infiltration 2’ solution was made up in the following proportions: 200ml of stabilised Technovit 9100 solution and 1g of ‘hardener 1’ (dibenzoyl peroxide), which was prepared on the day.

1c. ‘Pre-infiltration 3’ solution was prepared with 200ml of Technovit 9100 destabilised solution and 1g of ‘hardener 1’, the solution was stored at room temperature.

2. ‘Infiltration solution’ was prepared by adding 20g of polymethylmethacrelate (PMMA) powder, 1g of ‘hardener 1’ (dibenzoyl peroxide) to 250ml of destabilised basic solution.

3a. ‘Stock solution A’ was prepared by adding 80g of PMMA stepwise to approximately 400ml of destabilised basic solution. When fully in solution 3g of ‘hardener 1’ was added with continuous stirring. Finally the basic solution is added until the 500ml graduation mark has been reached.

3b. ‘Stock solution B’ was prepared by adding 4ml of ‘hardener 2’ (N,N-3,5-tetramethylaniline) and 2ml of ‘regulator’ (decane-1-thiol) to 50 ml of destabilised basis solution.

The pre-infiltration, infiltration and stock solutions were kept a 4°C.

Before embedding, the samples were dehydrated in increasing concentrations of alcohol, starting at 70%, 80%, 96% and finally 100% ethanol for one hour in each concentration. The samples were then immersed in xylene for 48 hours with a change of xylene at 24 hours. Samples are then transferred to ‘pre-infiltration 1’ for 12 hours at room temperature. Samples then are placed in ‘pre-infiltration 2’ for 12 hours at room temperature. The final pre-

infiltration step involves ‘pre-infiltration 3’ solution in which the sample stayed immersed for 2 days at 4°C. The samples were then ready to undergo the infiltration step by leaving them in the ‘infiltration solution’ for 2 days at 4°C.

Polymerisation of the samples was achieved by mixing the cooled stock solution A with cooled stock solution B in the proportions of 9:1 directly before use. This step was performed in a beaker using a glass stirring rod to stir the mixture. Samples were then positioned in containers and completely covered with the polymerisation mixture and left to stand at 4°C for ten minutes to allow any air bubbles to escape. The resulting blocks were then placed in a sealed container with no air above the specimen and left to polymerise at -20°C for 24 hours. Once polymerisation had occurred, the samples were transferred to 4°C for at least an hour before being allowed to come slowly to room temperature. The samples were not exposed to the atmosphere before they had reached equilibrium with room temperature. The samples were then mounted and sections were cut using a microtome. When cutting the specimens, 30% ethanol was used as the cutting fluid and the sections mounted on superfrost plus slides with 50% ethanol and covered with PVC-foil. The excess fluid was removed with filter paper and then sections loaded into a section press.

Prior to staining, the polymer was removed by washing the slides twice in xylene for 20 minutes then once for 20 minutes in 2-methoxyethylacetate (2-MEA) followed by two washes in 100% acetone for 5 minutes with a final three washes in 2-MEA for 20 minutes.

Appendix B

Title:-	**MSC culture**
SOP Number:-	MTEC/068
Laboratories:-	GU 501
Personnel to carry out procedure:-	This protocol must be carried out by appropriately trained staff
See References:-	
S.O.P.:-	
Equipment:-	
COSHH:-	
Manual Handling:-	
SOP prepared by:-	Christine Huber, MTEC
Date:-	27/09/07

Medium

DMEM (Sigma D5671) complete with

10% FBS (Gibco)

5% L-Glu (Gibco)

5% Pen/Strep (Gibco)

Dressing packs (Vernaid small, obtained from University pharmacy, £3.15/pack)

Bone cutters

Universals

PROCEDURE

1) Open an new sterile dressing pack
2) Use clean bone cutters
3) From the femoral head scoop as much of the trabecular bone as possible into a universal.
4) Add 7mls of complete DMEM to universal and stir vigorously for ~1 min
5) Remove medium into a new universal
6) Repeat step 4 twice more until the bone chips become "white". Transfer medium (total of 14 mls) into the universal.
7) Transfer medium (total of 21mls) to a T75 flask*.
8) Number the flask according to the numbering and fill in the rest of the details in the purple folder (TC room).
9) Put Presept in the pot and leave it in the cold room to get cleaned.

- When transferring the medium from the universal to the T75 flask try to avoid the fat layer.
- The size of the flask and the volume of the medium varies according to the amount of bone obtained from each femoral head.

10) Leave the flask in the incubator for 5 days without touching it or moving it.
11) On the 5^{th} day wash the surface with media and add fresh media
12) Change the media again on the 6^{th} day
13) Keep feeding them until they become ~80% confluent.
14) Split them (1:2)

Appendix C

Musculo-Skeletal Research Unit, The University of Edinburgh

Standard Operating Procedure

Title: Bioplotter and scaffold manufacture

SOP number:

Personnel to carry out procedure: Must be carried out by appropriately trained staff

See references: Bioplotter manual

SOP:

Equipment:

COSHH: Read COSHH forms for all reagents used

Manual Handling:

SOP prepared by: Phil Vadillo

Date: 20/05/2008

Musculo-Skeletal Research Unit, The University of Edinburgh

Standard Operating Procedure

Bioplotter and scaffold manufacture

Method:

Open hood

Connect nitrogen cylinder via yellow tubing to regulator

Connect PC to Bioplotter via SCSI cable

Switch on computer (username: phil, password: mtec)

Double click on shortcut to 'PrimCAM.exe' on desktop

Open a 'Data set', i.e. Dispensing Data.DAT

Click on the 'magnifying glass' icon then on a line of the subset to alter plotting parameters and notes can be added to remind the operator (i.e. name, layer thickness, strand distance, speed, offset, layer orientation). Click on 'OK' when all alterations have been made.

Click on 'CAM' icon ('IMPORT' will come up when pointer is hovered over icon) and select an appropriate STL file with dimensions of extruded scaffold in title. Alternatively the scaffold dimensions and geometry can be created in 'SolidWorks' (shortcut also present on desktop). File should then be saved in the .STL format in the folder c:\bioplotter-backup\cad-data.

Select the data subset where changes were made

Click on 'NC' icon and confirm

Click on 'Start dispensing machine' icon which is situated below the 'NC' icon

Load the barrel of the syringe, fasten needle via luer lock and place in holder on Bioplotter. Fasten pressure outlet (orange bung connected to tubing) to the top of the syringe barrel.

Turn valve at the top of the nitrogen cylinder anticlockwise, turn the regulator attached to the nitrogen cylinder clockwise until pressure reaches approximately 1.5 bar. Switch on

Bioplotter via red switch on right hand side and press green button marked ‘Steuerung EIN’, then extruding pressure can be accurately controlled with dial marked ‘Druck’ at the front.

Click on the ‘REF’ icon which moves the Bioplotter to it starting position

Initial dispensing height can be altered with icon ‘parameters’

Place plotting bath in position

Press ‘spulen’ to extrude some material this prevents any material that might have dried up in the needle tip to be removed and allow smooth flow during extrusion.

Click the ‘RUN’ icon when satisfied that everything is correctly connected and in place. Make sure the working area of the Bioplotter is clear of any bottles and tubes as these may hinder the movement of the arms.

IMPORTANT: Emergency stop button is at the front of the Bioplotter and marked ‘NOT AUS’

The programme will then prompt for the needle length which is 30mm

Once the scaffold has been manufactured the arms will automatically move back to their starting position and the scaffold may be removed. However if the operator wishes to stop the plotting process prematurely, the ‘STOP’ icon should be pressed followed by the ‘REF’ icon to move the arms back to their starting position.

At this stage the operator may wish to change some parameters which can be accomplished by pressing the ‘EXIT’ icon (Top right) which will return the operator to the data subset screen. N.B. if parameters are altered, a new NC code has to be created before plotting is restarted.

Before exiting the programme which can be accomplished by pressing the ‘EXIT’ icon at the top right of the screen, the nitrogen cylinder regulator should be turn anti clockwise to close and the valve at the top closed before pressing ‘Spulen’ to evacuate the remaining gas in the system. The operator should remove the syringe, the plotting bath and clean for future use.

The Bioplotter should be switched off and the SCSI cable carefully removed and the yellow tubing removed from the Bioplotter regulator. Close the hood and switch off computer.